



UNIVERSITY OF
KWAZULU-NATAL

INYUVESI
YAKWAZULU-NATALI

**Synthesis and physiochemical
characterization of new siderophore-
inspired peptide-chelators with 1-
hydroxypridine-2-one (1,2-HOPO)**

Thesis Submitted in fulfilment of the requirements for the degree of
Doctor of Philosophy

by

Danah Mahdi AlShaer

2020

Supervisor: Prof. Beatriz Garcia de la Torre

Co-supervisor: Prof. Fernando Albericio

Synthesis and physiochemical characterization of new siderophore-inspired peptide-chelators with 1-hydroxypridine-2-one (1,2-HOPO)

217078895


Danah Mahdi AlShaer

A thesis submitted to the School of Health Sciences, College of Health Sciences, University of KwaZulu-Natal, Westville, for the degree of Doctor of Philosophy by research in Pharmaceutical Chemistry.

This is the thesis in which the chapters are written as a set of discrete research publications that have followed each journal's format with an overall introduction and final summary. These chapters have been published in internationally recognized, peer-reviewed journals.

This is to certify that the contents of this thesis are the original research work of **Mrs Danah Mahdi AlShaer**, carried out under our supervision at the Peptide Sciences Laboratory, Westville campus, University of KwaZulu-Natal, Durban, South Africa.


Supervisor:

Signed: 

Name: **Prof. Beatriz. G. de la Torre**

Date: **8th December 2020**

Co-Supervisor:

Signed: 

Name: **Prof. Fernando. Albericio**

Date: **8th December 2020**

As the candidate's supervisors we agree to the submission of this thesis

Table of Contents

Abstract.....	1
Declaration 1: Plagiarism.....	2
Declaration 2: Publications	3
Acknowledgment.....	5
Aim and objectives.....	6
Chapter 1: (Introduction) Hydroxamate Siderophores: Natural Occurrence, Chemical Synthesis, Iron Binding Affinity and Use as Trojan Horses Against	7
Reprint.....	8
Chapter 2: Solid-phase synthesis of peptides containing 1-Hydroxypyridine-2-one (1,2-HOPO)	39
Reprint.....	40
Chapter 3: Protocol for efficient solid-phase synthesis of peptides containing 1-hydroxypyridine-2-one (1,2-HOPO)	44
Reprint.....	45
Chapter 4: Chapter 4. Synthesis of new peptide-based Ligands with 1,2-HOPO pendant chelators and the thermodynamic evaluation of their iron (III) complexes	53
1. Introduction	53
2. Results and discussion.....	55
2.1 Synthesis of Ligands.....	55
2.2 Physicochemical characterization of ligands and their Fe(III) complexes.....	57
2.2.1 Ligand-Fe (III) complex stoichiometry determination	57
2.2.2 Determination of pKa values.....	59
2.2.3 Iron (III) complexation.....	61
3. Conclusion.....	63
4. Experimental.....	63
5. References	66

Chapter 5: 2019 FDA TIDES (Peptides and Oligonucleotides) Harvest	68
Reprint.....	69
Chapter 6: 2018 FDA TIDES Harvest	85
Reprint.....	86
Chapter 7: 2017 FDA peptide Harvest	92
Reprint.....	93
Chapter 8: Conclusion and future perspectives.....	103
Supplementary information	

Abstract

Compounds containing hydroxamate moieties (N-hydroxyl amides) in their structure have found a vast range of therapeutic applications such as antibacterial, anti-tumour, anti-immune suppressor, and for iron overloading treatment. Hydroxamate chelators binds to Fe (III) tightly through its electron donating oxygens. The binding strength is maximized in compounds containing three hydroxamic moieties due to the so called “chelate effect”. As all microorganisms require iron for surviving, they develop endogenous siderophores to acquire iron from the surroundings. Siderophores contain hydroxamate, catecholates, α -hydroxy carboxylates groups, among others, in their structures. The acquisition of iron by siderophores in microorganisms goes through specific cycles that includes sequestration of Fe(III), recognition and uptake of the ferri-siderophore through the cell membrane, and then release of the iron in the cytoplasm.

Many natural hydroxamate siderophores contain a peptidyl backbone. In this work, peptides containing one or more units of 1,2-hydroxypyridine-N-oxide (1,2-HOPO) have been synthesized. The introduction of these units on the peptides has been done by means of 4-carboxy-1-hydroxypyridil-2-one (1,2-HOPO-4-COOH) using solid-phase peptides synthesis (SPPS) protocols. The obtention of the new “siderophores” containing three 1,2-HOPO units have been done by two different approaches, sequential and convergent. The compounds have been evaluated as potential iron chelators. Thus, the pKa values and the thermodynamic constants of all ligands have been spectrophotometrically determined. The Fe(III) affinities of the two hexadentate ligands (ligand B and ligand C) have been determined by competition experiments against EDTA. The results showed that the iron complex ligand B is stronger than the iron complex EDTA since the last is not able to replace it. Hence, this new siderophore could be a promising candidate to be used in further therapeutic applications.

Declaration 1- Plagiarism

I, Danah Mahdi AlShaer, declare that,

1. The research report in this thesis, except where otherwise indicated, is my original work.
2. This thesis has not been submitted for any degree or examination at any other university.
3. This thesis does not contain other person's data, pictures, graphs, or other information, unless specifically acknowledged as being sourced from other persons.
4. This thesis does not contain other person's writing, unless specifically acknowledged as being sourced from other researchers. Where other written sources have been quoted, then:
 - a. Their words have been re-written, but the general information attributed to them has been referenced.
 - b. Where their exact words have been used, then their writing has been placed in italics and inside quotation marks and referenced.
5. This thesis does not contain text, graphics or tables copied and pasted from the internet, unless specifically acknowledged, and the source being detailed in the thesis and in the references sections.

Signed



Declaration 2- Publication

List of publications originated from this Thesis

1. **Al Shaer, D.**; Al Musaimi, O.; de la Torre, B, G.; Albericio, F. Hydroxamate siderophores: Natural occurrence, chemical synthesis, iron binding affinity and use as Trojan horses against pathogens. *Eur. J.Med.Chem.* **2020**, *208*. 10.1016/j.ejmech.2020.112791.

(**Al Shaer D.**, and Al Musaimi, O. contributed to searching for information and in writing the manuscript, the remaining authors are supervisors).

2. **Al Shaer, D.** ; Albericio, F.; de la Torre, B, G. Solid-phase synthesis of peptides containing 1-Hydroxypyridine-2-one (1,2-HOPO). *Tetrahedron Lett.* **2020**, *61*. 10.1016/j.tetlet.2020.152299.

(**Al Shaer, D.** contributed in the synthesis, analysis, characterization of all compounds in this work, the remaining authors are supervisors).

3. **Al Shaer, D.**; de la Torre, B, G.; Albericio, F. Protocol for efficient solid-phase synthesis of peptides containing 1-hydroxypyridine-2-one (1,2-HOPO). *MethodsX* **2020**, *7*. 10.1016/j.mex.2020.101082. (**Al Shaer, D.** contributed in the synthesis, analysis, characterization of all compounds in this work, also in writing the manuscript, the remaining authors are supervisors).

4. **Al Shaer, D.** ; Albericio, F.; de la Torre, B, G. Synthesis of new peptide-based Ligands with 1,2-HOPO pendant chelators and the thermodynamic evaluation of their iron (III) complexes (**submitted manuscript**).

(**Al Shaer, D.** contributed to the synthesis, analysis, characterization of all compounds in this work, the remaining authors are supervisors).

5. **Al Shaer, D.**; Al Musaimi, O.; Albericio, F.; de la Torre, B, G. 2019 FDA TIDES (Peptides and Oligonucleotides) Harvest. *Pharmaceuticals (Basel)*. **2020**, *13*, doi:10.3390/ph13030040.

(**Al Shaer D.**, and Al Musaimi, O. contributed equally to searching for information and in writing the manuscript, the remaining authors are supervisors).

6. **Al Shaer, D.**; Al Musaimi, O.; Albericio, F.; de la Torre, B, G. 2018 FDA Harvest. *Pharmaceuticals (Basel)*. **2019**, *12*, doi: 10.3390/ph12020052.

(**Al Shaer D.**, and Al Musaimi, O. contributed equally to searching for information and in writing the manuscript, the remaining authors are supervisors).

7. Al Musaimi, O.; **Al Shaer, D.**; de la Torre, B.G.; Albericio, F. 2017 FDA peptide harvest. *Pharmaceuticals (Basel)* **2018**, *11*. 10.3390/ph11020042.

(**Al Shaer D.**, and Al Musaimi, O. contributed equally to searching for information and in writing the manuscript, the remaining authors are supervisors).

Acknowledgements

My heartfelt thanks and praises to almighty God “Allah” for giving me the health, patience and strength to move on in life, and for all his blessings.

Then, special thanks to my supervisors Prof. Beatriz de la Torre and Prof. Fernando Albericio for their continuous support, guidance, inspiration, and motivation all throughout my PhD study, my gratitude cannot be expressed by words, THANK YOU BOTH.

Next, many thanks and appreciation go to my colleague and husband Dr. Othman Al Musaimi, and all my group mates Dr. Anamika, Dr. Ashish, Dr. Edikarlos, Dr. Al Hassan, Dr. Srinivas, Nandhini, Amit, Amanda, Jessica, Shaveer, Sine, Noki, Rotimi, Hlobi, Talia, Estelle in the laboratory of peptide sciences. It was precious knowing and working together with you all, THANK YOU.

My sincere gratitude goes for my supportive family in Jordan, my father, mother, sisters, and brother.

Special thanks and love to my wonderful kids Lamar, Yazan, Sewar. Thanks for being in my life, I LOVE YOU.

The final appreciation goes to the University of KwaZulu-Natal, College of Health Sciences, for the opportunity they granted me to undertake my PhD study and the National Research Foundation (NRF, SA) for financial support, I say a big thank you.

Aim and objectives

The aim of this work is to develop a simple method to obtain peptides bearing hydroxamic acid through the linkage of 1,2-hydroxypyridine-N-oxide (1,2-HOPO) moieties to be used as iron chelators (ligands). To achieve this aim, the following objectives have been proposed:

1. Study the best conditions to introduce 4-carboxy-1-hydroxypyridil-2-one (1,2-HOPO-4-COOH) in a peptide sequence using solid-phase peptide synthesis (SPPS) protocols.
 - 1.a. Unprotected strategy.
 - 1.b. Benzyl protection of *N*-hydroxyl function. Removal of the protecting group at the end of the synthesis
2. Optimization of the synthesis of peptides with multiple HOPO containing moieties: sequential *vs* convergent approaches.
3. Spectrophotometric determination of the pKa's of the new bidentate and hexadentate ligands. Comparison with the unconjugated moieties: 1,2-HOPO-4-CONH₂.
4. Study of iron complexation of the different ligands: stoichiometric ratios and stability constants determination (β_{MLH}).
5. Determination of the Fe-ligand affinity (pFe^{3+}) by competition experiments against EDTA.

Thesis outline

An introduction to the use of hydroxamate siderophores as trojan horses is provided in Chapter 1. An efficient method for synthesis of HOPO-containing peptides on solid phase support is introduced in Chapter 2. A detailed protocol for the SPPS method used to prepare HOPO-containing peptides is included in Chapter 3. A thermodynamic evaluation of four new ligands and their Fe (III) complexes using spectrophotometric methods is reported and discussed in Chapter 4. FDA-approved “Tides” (peptides and oligonucleotides) in the last three years are discussed in Chapters 5-7. Two of the drugs approved ($[^{177}\text{Lu}]$ Lu-DOTATATE in 2018 and $[^{68}\text{Ga}]$ Ga-DOTATOC in 2019) were based on peptides holding metal chelators.

Chapter I. Hydroxamate Siderophores: Natural Occurrence, Chemical Synthesis, Iron Binding Affinity and Use as Trojan Horses Against Pathogens

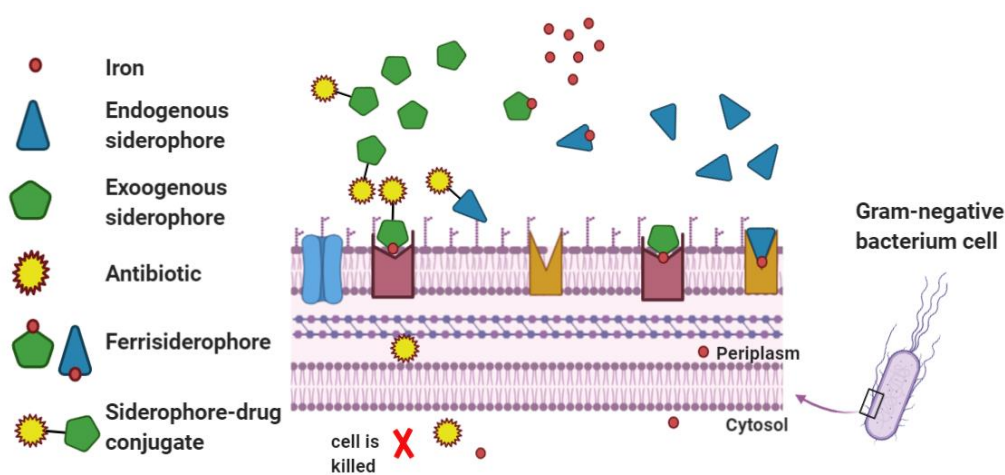
Danah Al Shaer^{1,2}, Othman Al Musaimi^{1,2}, Beatriz G. de la Torre^{1*}, Fernando Albericio^{2,3,4*}

1 KRISP, School of Laboratory of Medicine and Medical Science, College of Health Sciences, University of KwaZulu-Natal, Durban 4001, South Africa.

2 School of Chemistry and Physics, University of KwaZulu-Natal, Durban 4001, South Africa

3 Institute for Advanced Chemistry of Catalonia (IQAC-CSIC), Jordi Girona 18-26, 08034 Barcelona, Spain.

4 CIBER-BBN, Networking Centre on Bioengineering, Biomaterials and Nanomedicine and Department of Organic Chemistry, University of Barcelona, 08028 Barcelona, Spain.



Siderophore-antibiotic conjugates as trojan horses against Gram-negative bacteria



Review article

Hydroxamate siderophores: Natural occurrence, chemical synthesis, iron binding affinity and use as Trojan horses against pathogens

Danah Al Shaer^{a, b}, Othman Al Musaimi^{a, b}, Beatriz G. de la Torre^{a, **},
Fernando Albericio^{b, c, d, *}

^a KRISP, School of Laboratory of Medicine and Medical Science, College of Health Sciences, University of KwaZulu-Natal, Durban, 4001, South Africa

^b School of Chemistry and Physics, University of KwaZulu-Natal, Durban, 4001, South Africa

^c Institute for Advanced Chemistry of Catalonia (IQAC-CSIC), Jordi Girona 18-26, 08034, Barcelona, Spain

^d CIBER-BBN, Networking Centre on Bioengineering, Biomaterials and Nanomedicine and Department of Organic Chemistry, University of Barcelona, 08028, Barcelona, Spain

ARTICLE INFO

Article history:

Received 1 August 2020

Received in revised form

23 August 2020

Accepted 24 August 2020

Available online 5 September 2020

Keywords:

Siderophore

Hydroxamate

Trojan horse

Siderophore-drug conjugate

Fe (III) binding affinity

Sideromycins

ABSTRACT

Hydroxamic acids are an important class of molecules, in particular because of their metal-chelating ability. Microorganisms, including pathogenic bacteria, use hydroxamate-based entities (siderophores), among others, to acquire Fe (III). The “Trojan horse” strategy exploits the need of bacteria for this metal by using Fe (III) active transporters to carry antibacterial or bactericidal moieties into the bacterial cell. Many natural Trojan horses (sideromycins) are derived from hydroxamic acids, thereby reflecting their potency. Various artificial sideromycins and their antibacterial activities have been reported. This review discusses the structural aspects of the hydroxamate-siderophores isolated in the last two decades, the chemical synthesis of their building blocks, their binding affinity towards Fe (III), and their application as Trojan horses (weaknesses and strengths).

© 2020 Elsevier Masson SAS. All rights reserved.

Contents

1. Introduction	2
2. Hydroxamate-based siderophores	2
2.1. Natural occurrence of hydroxamate siderophores	2
2.2. Chemical synthesis of hydroxamate residues in siderophores	3
2.2.1. Synthesis of δ -acyl- δ -N-Hydroxy-Orn building block	3
2.2.2. Synthesis of N-5-aminopentyl-N(hydroxy)-succinic acid building block	15
2.2.3. Synthesis of other hydroxamate building blocks	15
2.2.4. Incorporating the hydroxamate building block into the backbone	15
2.3. Binding affinity towards iron	15
2.4. Applications of hydroxamate molecules and hydroxamate siderophores	15
2.4.1. HA siderophores-antibiotic conjugates (application as Trojan horses)	16
2.4.2. Other hydroxamate siderophore conjugates	27
3. Cefiderocol (FETROJA®): the first siderophore-drug conjugate in the market	27
4. Conclusion	28
Declaration of competing interest	28
Acknowledgement	28
References	28

* Corresponding author. School of Chemistry and Physics, University of KwaZulu-Natal, Durban, 4001, South Africa.

** Corresponding author. KRISP, School of Laboratory of Medicine and Medical Science, College of Health Sciences, University of KwaZulu-Natal, Durban, 4001, South Africa.
E-mail addresses: garciaadelatorreg@ukzn.ac.za (B.G. de la Torre), albericio@ukzn.ac.za (F. Albericio).

1. Introduction

Iron is an essential nutrient for most living organisms [1]. Although accounting for about 35% of Earth's mass [2], its bioavailability to microorganisms is limited. This is attributed to the fact that under anaerobic conditions, iron is present as Fe (III), which in aqueous media is either precipitated out (trapped) as insoluble hydroxides ($K_{sp} = 10^{-18}$ M) or is bound to host proteins such as transferrin, ferritin and lactoferrin leaving the free Fe (III) at concentrations as low as 1×10^{-24} M [1,3].

To acquire iron in iron-deficient environments, microorganisms (such as bacteria and fungi) produce "Siderophores" [1,4], the Greek term meaning iron carriers. Siderophores have specific and high affinity towards iron, thus allowing microorganisms to scavenge this coveted nutrient from their environment and ensure their survival.

Fe (III) forms octahedral complexes with six electron-donating atoms symmetrically spatially distributed around the central iron. Maximum binding affinity is achieved when all six atoms interacting with iron are present in the same molecule, thus emphasizing the "chelate effect" in the multiple denticity. Natural siderophores are mostly hexadentates, in which the binding units vary between catecholates, α -hydroxy carboxylates, hydroxamates and a mixture of these functional groups [5] (Fig. 1).

The microbial iron uptake cycle starts with the production and secretion of "endogenous" siderophores (those produced by the cell itself) into the surroundings. These siderophores solubilize Fe(III) from its hydroxide or capture it from host proteins [6]. Ferrisiderophores (siderophore-Fe(III) complexes) are usually more than 500 Da, which means that they require certain transport systems to transfer them into the cell. Specific membrane (outer membrane in gram-negative bacteria) protein receptors recognize the complex via key features [6,7]. Recognition triggers the transport system and subsequent uptake occurs. Some outer membrane protein receptors are binding unit-specific and can recognize a wide spectrum of siderophores with same type of chelating units, such as FhuA (ferric hydroxamate outer membrane receptor) and FecA (ferric citrate). This capacity allows some species to use the siderophores produced by other organisms (xenosiderophores) [8]. Other receptors are specific for only a given siderophore, such as FptA (ferric pyochelin transport) and FpvA (ferric pyoverdine) [9].

Although outer membrane receptors for ferrisiderophore mediate the nourishment (feeding) of the cell, they can also poison it. Some microorganisms hybridize the siderophore with a bactericidal moiety (sideromycin = siderophore + antibiotic) to attack other species and kill them. This microbial strategy (Trojan horse) has inspired the research community to develop a new approach to increase the permeability of the drug into the multi-drug resistant cell [10–12]. In this regard, increasing bacterial resistance to almost all known antibiotics has come about from the overuse of antibiotics for the treatment of bacterial infections [13,14]. The discovery of only a handful of novel antibiotics over the last few decades has made it necessary to devise innovative strategies to combat pathogenic bacteria [15], the Trojan horse strategy emerging as a promising approach.

Among the five known families of natural sideromycins, three—albomycins, ferrimycins and salmycins—use the hydroxamate binding moiety (the other two families are salmochelins and microcins). Albomycins (3, Fig. 2) are the most widely known natural sideromycins and they have a proven efficiency against many organisms with the FhuA receptor in their outer membrane (see section 2.4.1.1). This activity emphasises the role of this family of chelators in overcoming the permeability barriers of the microbial

cell wall [16].

In this review we discuss hydroxamate siderophores in terms of their natural occurrence, chemical synthesis, binding affinity towards Fe(III) and potency as antimicrobial drug conjugates.

2. Hydroxamate-based siderophores

Hydroxamic acids have the general formula $RC(O)N(OH)R'$. They can be defined as *N*-hydroxy amides. This structure gives the proton of the hydroxyl some acidic properties depending on the solvent, with pKa values of about 9 [17]. When deprotonated, hydroxamate ion can strongly bind to various positively charged metal ions (Fig. 2). In a wide spectrum of natural siderophores, the chelating unit of hydroxamic acid is found either within the backbone or as pendants (Fig. 2).

2.1. Natural occurrence of hydroxamate siderophores

Hydroxamate siderophores are produced mainly by fungi and some strains of bacteria. The first known families were ferrichrome (1, Fig. 2), which was isolated from smut fungus *Ustilago sphaerogana* [18], and coprogen (5) [19], both isolated and reported in 1952. The structure of ferrichrome was characterized later in 1960 [20]. Another hydroxamate siderophore is desferrioxamine B (DFO B, 6), the most famous member of the ferrioxamine family. Nobel laureate Vladimir Prelog and co-workers isolated DFO B from *Streptomyces pilosus* and first reported it in 1960 [21]. Ciba-Geigy (now Novartis) introduced DFO B to the market as a strong metal chelator and this compound was later approved by US Food and Drug Administration (FDA) in 1968 as "Desferal" for the treatment of iron poisoning (iron overloading) [22].

Albomycins are hydroxamate sideromycins. They were reported previously as grisein [23] and were first isolated in 1947, but their structures were not fully characterized till 1982 [24] (see section 2.4.1.1).

Many other hydroxamate siderophores have since been isolated and reported [25]. In the last two decades (2000-to date), more than 135 new members have been added to the family (entries 10–61, Table 1), many extracted mainly from bacterial species collected from the Atlantic Ocean [26]. Most hydroxamate siderophores are hydrophilic. In contrast, most marine siderophores are amphiphilic, having both hydrophilic and hydrophobic parts in their structure, the latter enabling the siderophore to form micelles when complexed to Fe(III), thereby increasing the availability of the complex to the cell in the seawater environment [27]. Ferrioxamine E and G are among the most soluble marine siderophores [26]. Table 1 shows most of the hydroxamate siderophores isolated in the period 2000–2020, their structures and the species that produce them.

From a structural point of view, all the siderophores in Table 1 contain the hydroxamate chelating unit, either alone as in entries 10–29 and 34–38, or mixed with other binding units as in entries 30–33 and 39–61. The hydroxamate parts are derived from Orn, Lys, or *N*-hydroxydiaminoalkane [17]. In Orn-derived hydroxamates, the δ -N of the Orn is hydroxylated and acylated. The acylation moieties vary between formyl, as in 13, 17, 23–26, 30, 31, and 33, acetyl as in 10–12 and 14–15, malonyl as in 16, or anhydromevalonyl as in 20–22 and 28, 3-hydroxy-butanoyl as in 27, 3-methyl-glutaconyl as in 29 (this acyl is an intermediate in leucine metabolism [84]), fatty acid as in 56–57, α -COOH of the Orn itself forming a six membered cycle as in 23–26, or the α -COOH of another amino acid within the backbone (Arg, Asn, or Ser) as in 17–19 and 24–26. Some siderophores show two or more different

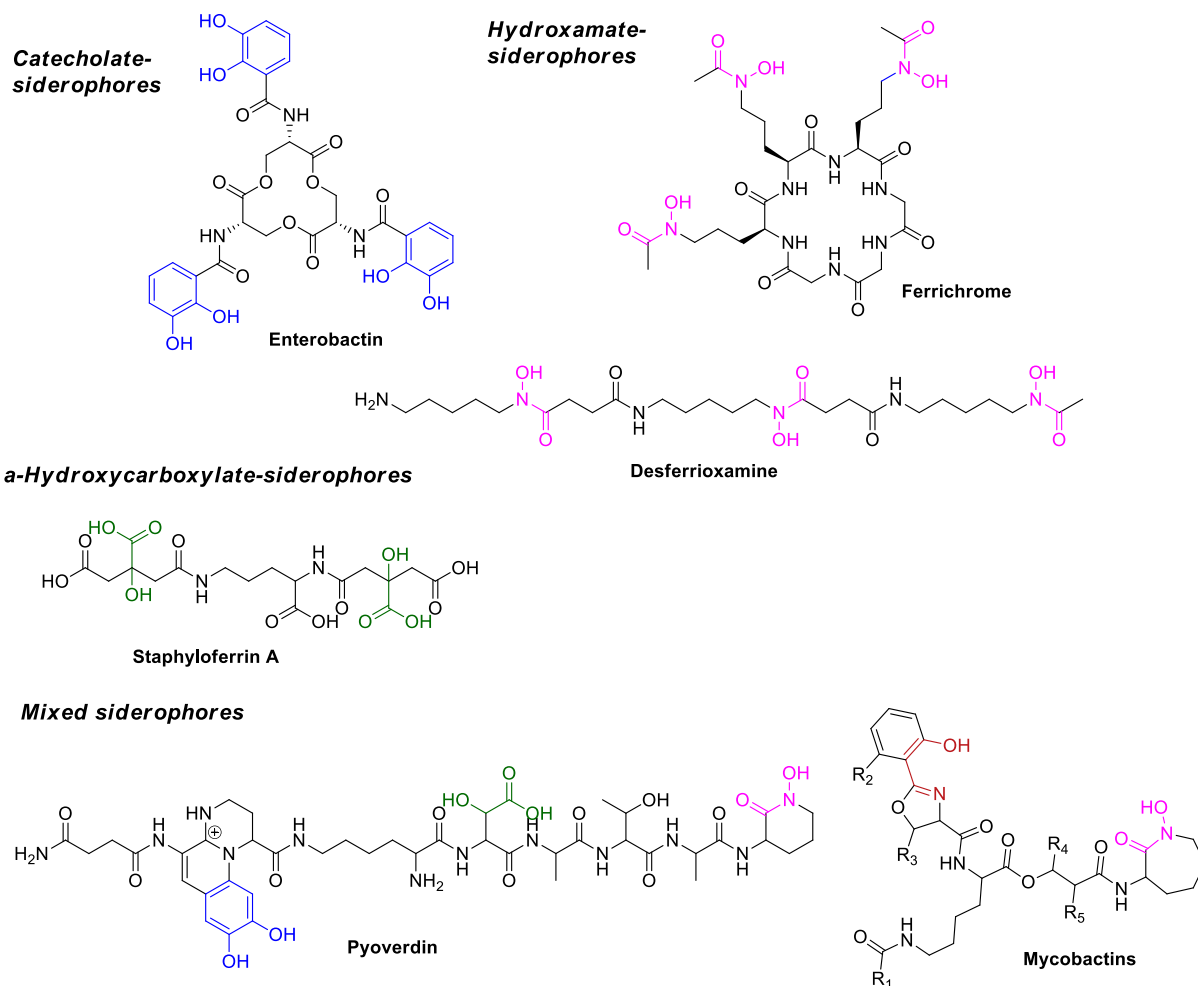


Fig. 1. Representative natural siderophores with different binding units (hydroxamic groups are shown in purple, catechol in blue, α -hydroxy carboxylic acid in green, and other groups in maroon). (For interpretation of the references to colour in this figure legend, the reader is referred to the Web version of this article.)

acylating moieties for the distinct hydroxamate groups within the same molecule as in **17–19** and **23–26**.

Also, ϵ -hydroxamate Lys residues are found in amamistatins (**30**), brasilibactin (**31**), nocardimicins (**32** and **33**), with the acylating moieties varying as in the Orn siderophores.

Other hydroxamate siderophores are derived from N-hydroxy-1,5-diaminopentane as in **34–38** and are usually acylated with a succinic moiety. N-hydroxy-1,5-diaminobutane is found in **38**.

Many of these hydroxamate siderophores are peptides. They show a variety of structures. In agreement with the previously known representative siderophores, siderophores **10–13** are linear with hydroxamate appendages, as in albomycin (**3**) (although **11** has a cyclic part but the chelating unit is linear). Siderophores **14–16** are cyclic peptides (lactams) with exocyclic hydroxamate appendages as in ferrichrome **1**.

Entries **17–22** resemble coprogen (**5**), a tris hydroxamate siderophore with a cyclic di-Orn part with hydroxamate side chains. The denticity is extended to hexadentate through the acyl (peptidyl) part of the hydroxamate moieties to include an additional functionalized Orn as in **17–19**, or other hydroxamate containing acyl as in **20–22**.

The hydroxamate in the non-peptidyl siderophores are found only with the backbone (not as appendages) and the backbones are either linear as in **35–37** or cyclic (endo cyclic hydroxamate) as in **38–39**.

2.2. Chemical synthesis of hydroxamate residues in siderophores

Several synthetic pathways can be used to prepare hydroxamic acids. In this regard, these acids can be synthesized from carboxylic acids [85], esters [86], aldehydes [87], alkyl halides [86], amines [88,89], and nitro compounds [90,91]. All reported methods can be briefly outlined as one of the five possible routes (either full or sub-route) shown in Scheme 1, which illustrates the most general approaches for the synthesis of hydroxamic acids from alkyl amines, hydroxyl amine or simple amides.

2.2.1. Synthesis of δ -acyl- δ -N-Hydroxy-Orn building block

To prepare the δ -acyl- δ -N-hydroxy-ornithine building unit, most of the reported procedures involved the conversion of the alkylamine (in this case the Orn side chain) to N-hydroxyl alkylamine and then to N-acyl-N-hydroxyl alkylamine (the red route in Scheme 1). The hydroxylation of the primary amine (δ -NH₂) is the crucial step in the synthesis, and various approaches for this reaction have been reported in the literature. The syntheses start with Orn, with suitable protecting groups for the α -NH₂ and COOH. Next, δ -N is hydroxylated mostly with benzoyl peroxide in a biphasic mixture at pH = 10.5 [88,89,92] (Scheme 2). Although this is the most widely used protocol, it is hampered by low yield and requires critical purification due to the formation of the δ -benzamide by-product. Another peroxide, dimethyl dioxirane (DMD) with

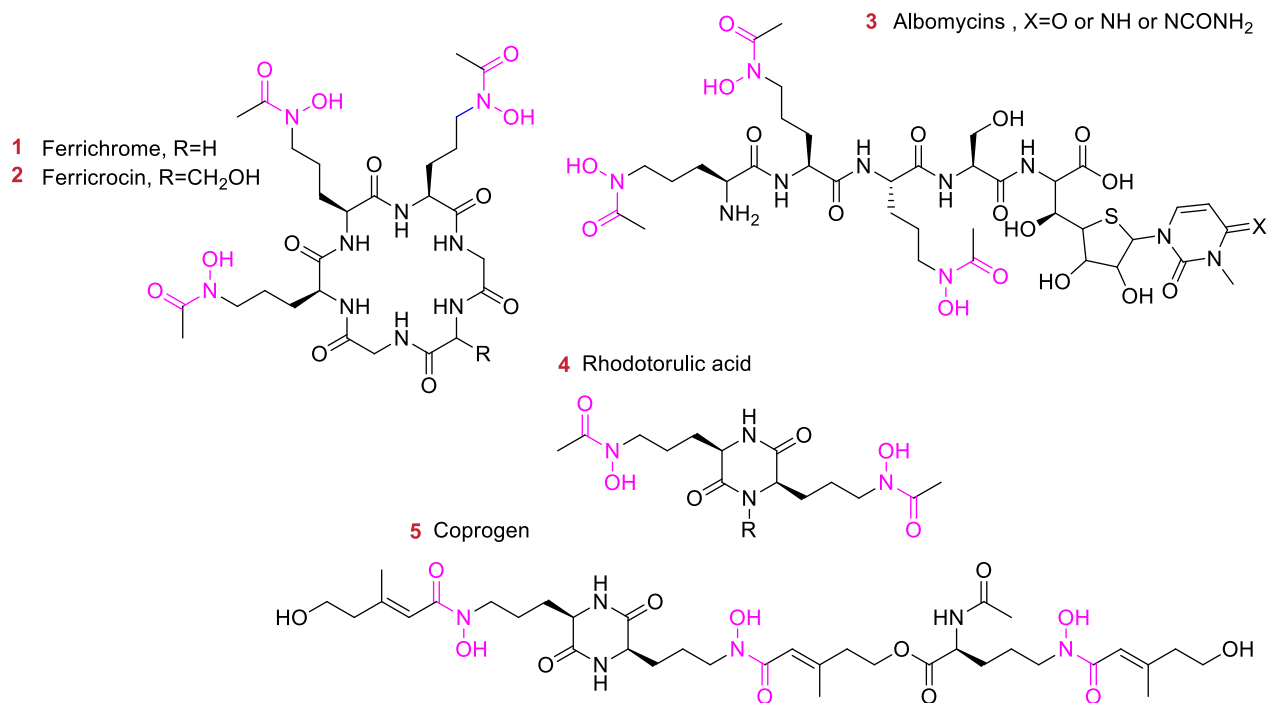
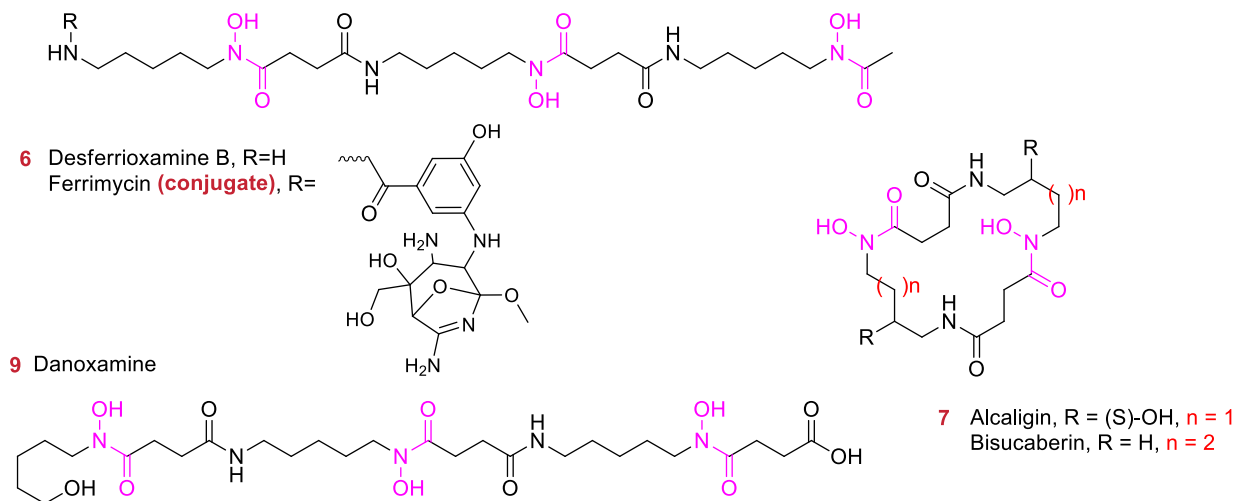
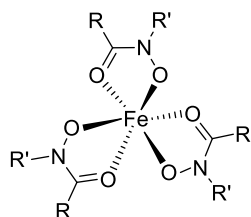
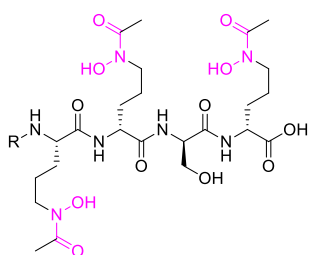
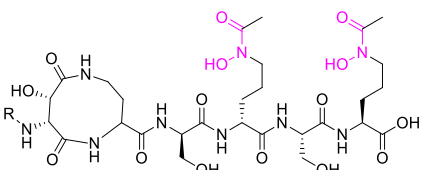
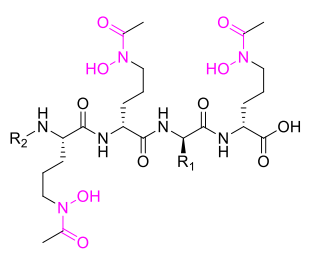
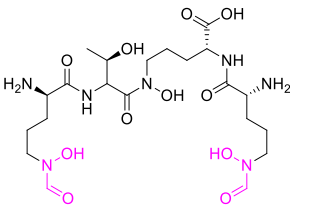
Siderophores with hydroxamate pendants:**Siderophores with backbone hydroxamate:****Representative Hydroxamate-Fe(III) complex**

Fig. 2. Representative hydroxamate-derived siderophores.

Table 1
Hydroxamate siderophores isolated and reported in 2000–2020.

# Siderophore	Structure	Secreted by	Ref
Ornithine-derived siderophores 10 Amphibactins B-I, S, and T	 <p style="text-align: center;">Amphibactins</p> <p> $R = \text{---} \left(\text{---} \right)_m \text{---} \text{C}(=\text{O})\text{---}$, $R = \text{---} \left(\text{---} \right)_m \text{---} \text{C}(=\text{O})\text{---}$ $R = \text{---} \left(\text{---} \right)_m \text{---} \text{C}(=\text{O})\text{---}$, $R = \text{---} \left(\text{---} \right)_m \text{---} \text{C}(=\text{O})\text{---}$ </p> <p> B, m=10, X=OH C, m=5, n=5, X=OH D, m=10, X=H E, m=5, n=5, X=H F, m=12, X=OH G, m=7, n=5, X=OH H, m=12, X=H I, m=7, n=5, X=H T, m=8, X=H S, m=5, n=3, X=H </p>	Amphibactin B-I: <i>Proteobacteriu, Vibrio sp. R-10</i> Amphibactin S and T: <i>Vibrio sp. HC0601C5</i>	[28,29]
11 Marinobactins A, B, C, D1, D2, E, and F	 <p style="text-align: center;">Marinobactins</p> <p> $R = \text{---} \left(\text{---} \right)_m \text{---} \text{C}(=\text{O})\text{---}$, $R = \text{---} \left(\text{---} \right)_m \text{---} \text{C}(=\text{O})\text{---}$ $R = \text{---} \left(\text{---} \right)_m \text{---} \text{C}(=\text{O})\text{---}$, $R = \text{---} \left(\text{---} \right)_m \text{---} \text{C}(=\text{O})\text{---}$ </p> <p> A, m=10 B, m=5, n=5 C, m=12 D1, m=5, n=7 E, m=14 D2, m=7, n=5 F, m+n=14 </p>	<i>Marinobacter sp. strains DS40M6 and DS40M8</i>	[30,31]
12 Moanachelins	 <p style="text-align: center;">Moanachelins</p> <p> $R2 = \text{---} \left(\text{---} \right)_m \text{---} \text{C}(=\text{O})\text{---}$, $R2 = \text{---} \left(\text{---} \right)_m \text{---} \text{C}(=\text{O})\text{---}$ $R2 = \text{---} \left(\text{---} \right)_m \text{---} \text{C}(=\text{O})\text{---}$, $R2 = \text{---} \left(\text{---} \right)_m \text{---} \text{C}(=\text{O})\text{---}$ </p> <p> Ala-B, R₁=CH₃, m=10 Gly-C, R₁=H, m+n=10 Ala-D, R₁=CH₃, m=12 Gly-E, R₁=H, m=7, n=5 Gly-B, R₁=H, m=10 Gly-D, R₁=H, m=12 </p>	<i>Marine bacterial isolate Vibrio sp. Nt1</i>	[32]
13 Coelichelin	 <p style="text-align: center;">Coelichelin</p>	<i>Nocardia tenerifensis NBRC 101015</i>	[33]

(continued on next page)

Table 1 (continued)

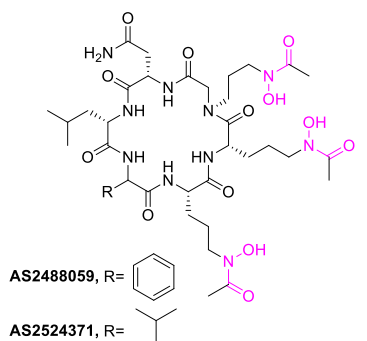
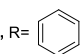
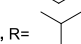
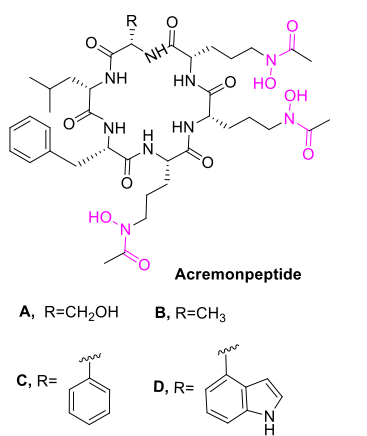
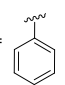
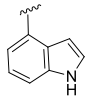
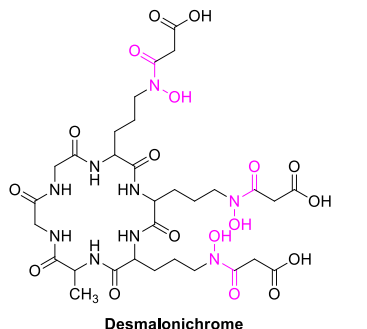
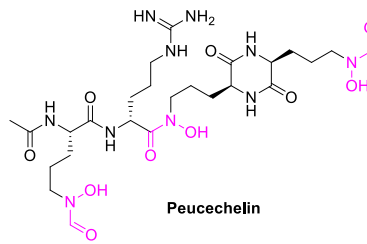
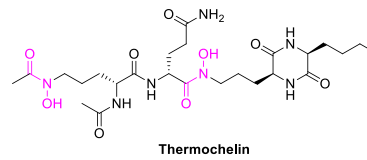
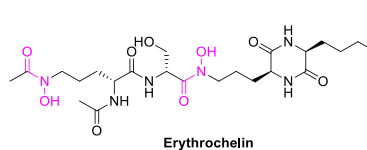
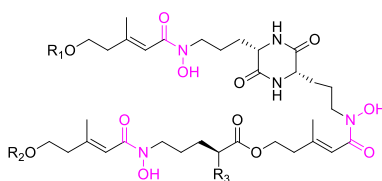
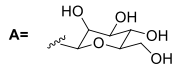
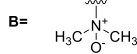
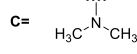
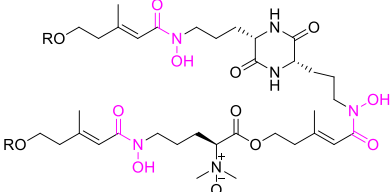
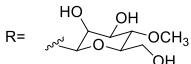
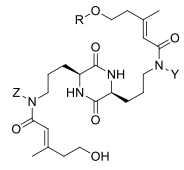
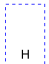
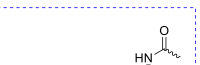

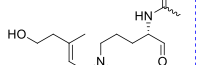


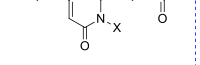

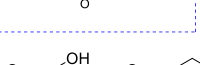
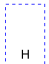
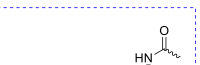

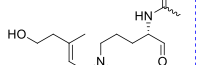


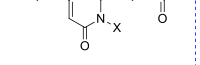

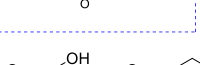
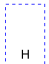
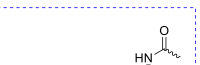

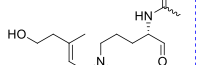


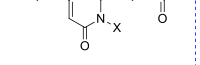

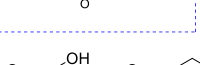
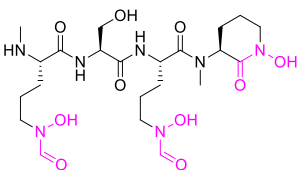
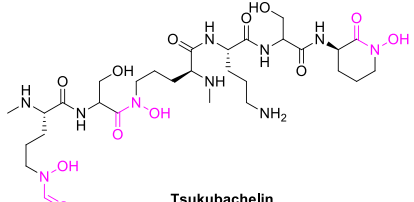
# Siderophore	Structure	Secreted by	Ref
14 AS2524371, and AS2488059	 <p>AS2488059, R= </p> <p>AS2524371, R= </p>	<i>Acremonium persicinum</i> MF-347833	[34]
15 Acremonpeptides A– D	 <p>Acremonpeptide</p> <p>A, R=CH₂OH B, R=CH₃</p> <p>C, R=  D, R= </p>	Marine-Derived <i>Acremonium persicinum</i> SCSIO 115	[35]
16 Desmalonichrome	 <p>Desmalonichrome</p>	Fungus <i>Fusarium oxysporum</i>	[36]
17 Peucechelin	 <p>Peucechelin</p>	<i>Streptomyces. peucetius</i>	[37]
18 Thermoachelin	 <p>Thermoachelin</p>	<i>Thermocrispum agreste</i> DSM 44070	[38]
19 Erythrochelin	 <p>Erythrochelin</p>	Strain <i>S. erythraea</i>	[39]

Table 1 (continued)

# Siderophore	Structure	Secreted by	Ref																														
20 Metachelins 1, 2, and 3	 <p>Metachelin 1, R₁=R₂=A, R₃=B 2, R₁=R₂=A, R₃=C 3, R₁=R₂=H, R₃=B</p> <p>A=  B=  C= </p>	<i>Metarhizium robertsii</i>	[40]																														
21 Beauverichelin A	 <p>Beauverichelin A R= </p>	<i>Beauveria bassiana</i>	[41]																														
22 Talarazines A–E	 <p>Talarazine</p> <table border="1"> <thead> <tr> <th></th> <th>R</th> <th>X</th> <th>Y</th> <th>Z</th> </tr> </thead> <tbody> <tr> <td>A</td> <td>H</td> <td>-</td> <td>OH</td> <td></td> </tr> <tr> <td>B</td> <td></td> <td>H</td> <td></td> <td>H</td> </tr> <tr> <td>C</td> <td></td> <td></td> <td>H</td> <td></td> </tr> <tr> <td>D</td> <td></td> <td>OH</td> <td></td> <td>OH</td> </tr> <tr> <td>E</td> <td></td> <td>OH</td> <td>OH</td> <td>H</td> </tr> </tbody> </table>		R	X	Y	Z	A	H	-	OH		B		H		H	C			H		D		OH		OH	E		OH	OH	H	Fungus, <i>Talaromyces</i> sp. (CMB-W045)	[42]
	R	X	Y	Z																													
A	H	-	OH																														
B		H		H																													
C			H																														
D		OH		OH																													
E		OH	OH	H																													
23 Albisporachelin	 <p>Albisporachelin</p>	<i>Amycolatopsis</i>	[43]																														
24 Tsukubachelin	 <p>Tsukubachelin</p>	<i>Streptomyces</i> sp. TM-74	[44]																														

(continued on next page)

Table 1 (continued)

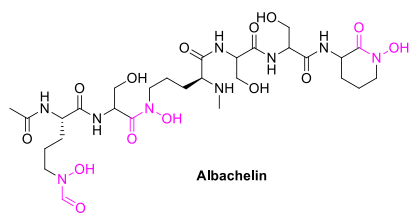
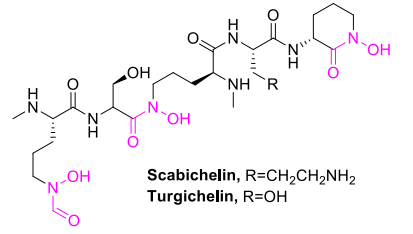
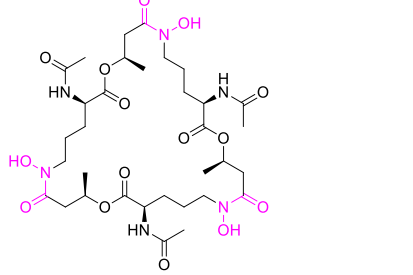
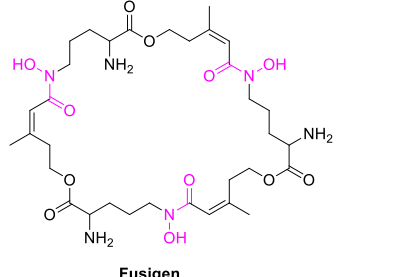
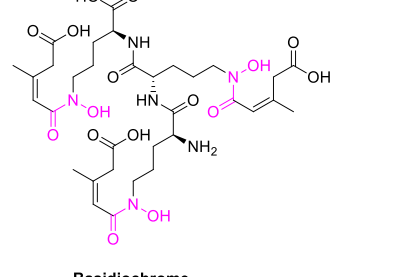
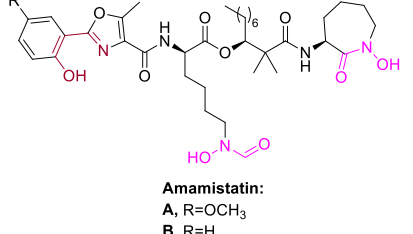
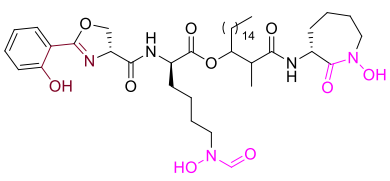
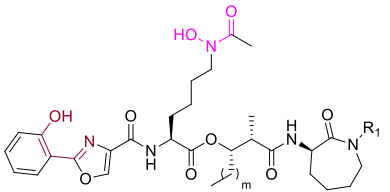
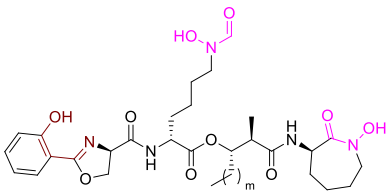
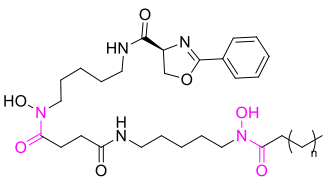
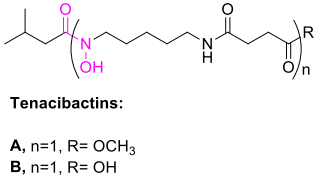
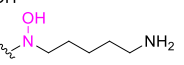
# Siderophore	Structure	Secreted by	Ref
25 Albachelin	 Albachelin	<i>Amycolatopsis alba</i>	[45]
26 Scabichelin and Turgichelin	 Scabichelin, R=CH ₂ CH ₂ NH ₂ Turgichelin, R=OH	Scabichelin: <i>Streptomyces antibioticus</i> NBRC 13838/ <i>Streptomyces scabies</i> JCM 7914 Turgichelin: <i>Streptomyces turgidiscabies</i> JCM 10429	[46]
27 Vicibactin	 Vicibactin	<i>Rhizobium leguminosarum</i> ATCC 14479 bv. <i>Trifolii</i>	[47]
28 Fusigen	 Fusigen	<i>Aureobasidium pullulans</i> HN6.2	[48]
29 Basidiochrome	 Basidiochrome	Mycorrhizal fungi <i>Ceratobasidium</i> and <i>Rhizoctonia</i> spp.	[49]
Lysine-derived hydroxamate siderophores			
30 Amamistatins A, and B	 Amamistatin: A, R=OCH ₃ B, R=H	Actinomycete <i>Nocardia asteroides</i> SCRC-A2359	[50,51]

Table 1 (continued)

# Siderophore	Structure	Secreted by	Ref
31 Brasilibactin A	 <p>Brasilibactin A Brasilibactin A is a stereoisomer of Nocardimicin H (#33)</p>	Actinomycete <i>Nocardia brasiliensis</i> IFM 0995	[52]
32 Nocardimicins A-F	 <p>Nocardimicin A: R₁=OH, m=8 B: R₁=OH, m=10 C: R₁=O, m=10 D: R₁=OH, m=12 E: R₁=H, m=12 F: R₁=OH, m=14</p>	<i>Nocardia</i> sp. TP-A0674	[53]
33 Nocardimicins G-I	 <p>Nocardimicin G: m=12 H: m=14 I: m=16</p> <p>Nocardimicin H is a stereoisomer of Brasilibactin A (#31)</p>	<i>Nocardia nova</i> JCM 6044	[54]
N-Hydroxy-diaminoalkane-derived hydroxamate siderophores			
34 Nocardichelins A and, B	 <p>Nocardichelin A, n=12 B, n=10</p>	<i>Nocardia</i> Strain Acta 3026	[55]
35 Tenacibactins A, and B	 <p>Tenacibactins: A, n=1, R= OCH₃ B, n=1, R= OH C, n=2, R=OH D, n=2, R= </p>	Marine-derived bacterium <i>Tenacibaculum</i> sp. A4K-17	[56]

(continued on next page)

Table 1 (continued)

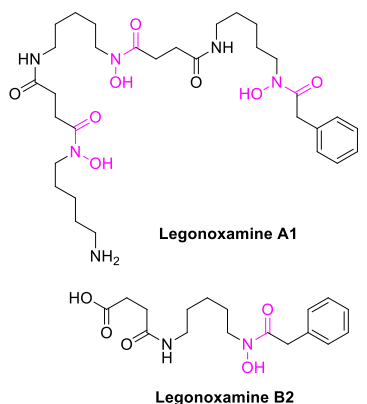
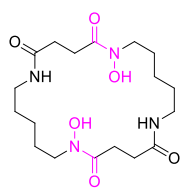
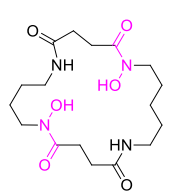
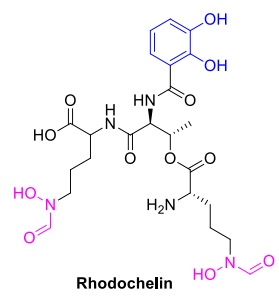
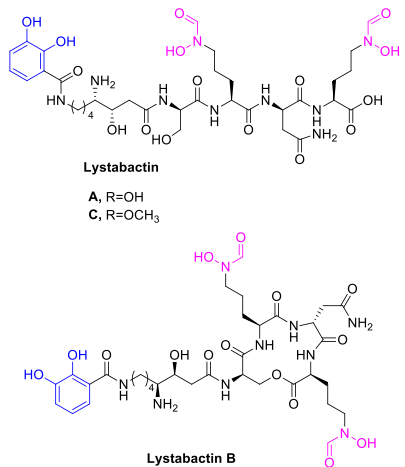
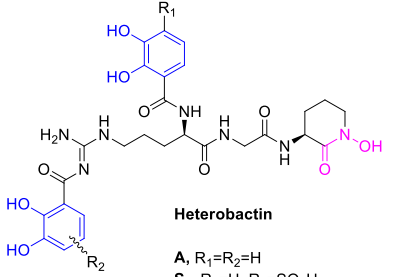
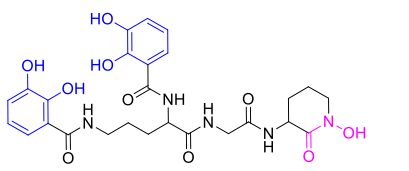
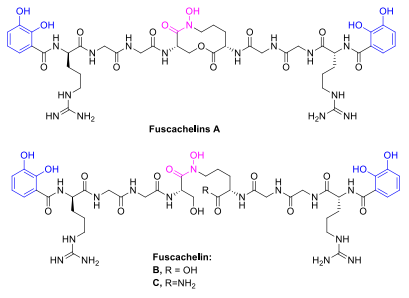
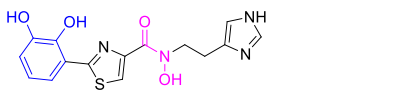
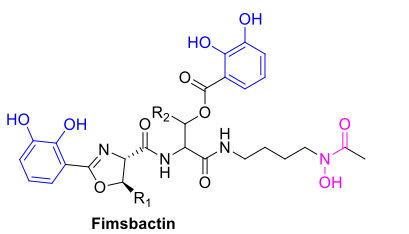
# Siderophore	Structure	Secreted by	Ref
36 Legonoxamine A1, and B2	 <p>Legonoxamine A1</p> <p>Legonoxamine B2</p>	The soil bacterium, <i>Streptomyces</i> sp. MA37	[57]
37 Bisucaberin	 <p>Bisucaberin</p>	<i>Salmonicida</i>	[58]
38 Avaroferrin	 <p>Avaroferrin</p>	<i>Shewanella algae</i> B516	[59]
Mixed 39 Rhodochelin	 <p>Rhodochelin</p>	<i>Rhodococcus jostii</i> RHA1	[60]
40 Lystabactins A, B, and C	 <p>Lystabactin</p> <p>A, R=OH C, R=OCH₃</p> <p>Lystabactin B</p>	Marine <i>Pseudoalteromonas</i> sp	[61]

Table 1 (continued)

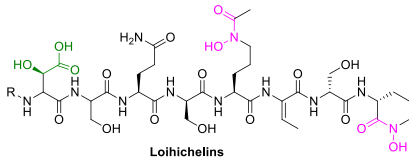
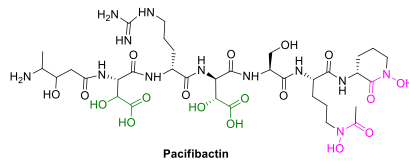
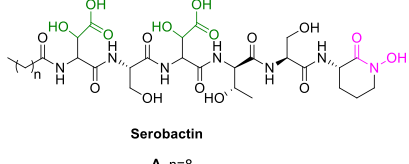
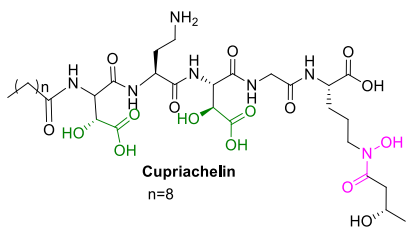
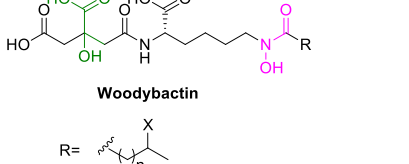
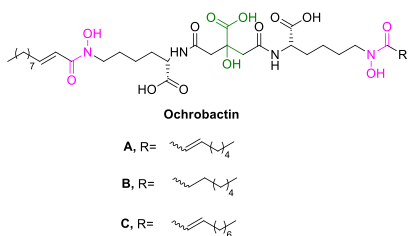
# Siderophore	Structure	Secreted by	Ref
41 Rhodobactin	 Rhodobactin	<i>Rhodococcus erythropolis</i> PR4	[62]
42 Heterobactins A, S ₁ , and S ₂	 Heterobactin A, R ₁ =R ₂ =H S ₁ , R ₁ =H, R ₂ =SO ₃ H S ₂ , R ₁ =SO ₃ H, R ₂ =H	<i>Rhodococcus erythropolis</i> PR4	[63]
43 JBIR-16	 JBIR-16	<i>Nocardia tenerifensis</i> NBRC 101015	[64]
44 Fuscachelins A-C	 Fuscachelins A Fuscachelin: B, R = OH C, R = NH ₂	<i>Thermobifida fusca</i>	[65]
45 Anguibactin	 Anguibactin	<i>Vibrio</i> sp. DS40M4	[66]
46 Fimsbactins A-C	 Fimsbactin A : R ₁ = H, R ₂ = H B : R ₁ = CH ₃ , R ₂ = H C : R ₁ = CH ₃ , R ₂ = CH ₃	<i>Acinetobacter baumannii</i> and <i>Acinetobacter baylyi</i>	[67]

(continued on next page)

Table 1 (continued)

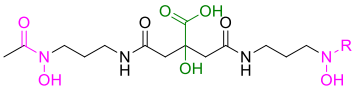
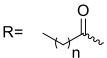
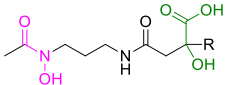
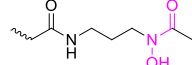
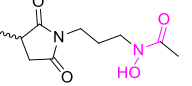
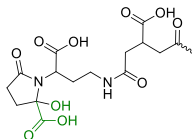
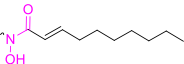
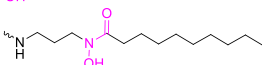
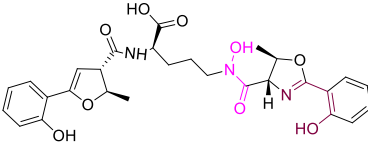
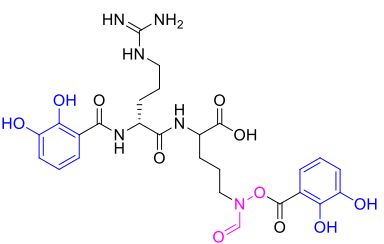
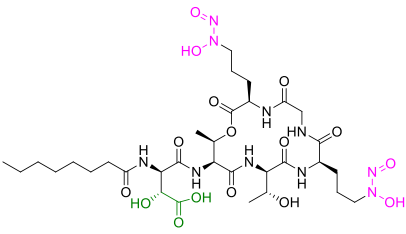
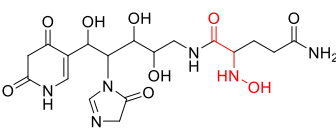
# Siderophore	Structure	Secreted by	Ref
47 Aquachelins A, B, C, D, I, and J	<p>Aquachelins</p> <p>R = , R = </p> <p>B, X=H, m=8 D, X=H, m=10 I, X=OH, m=8 J, X=H, m=6</p> <p>A, m=5, n=3 C, m=5, n=5</p>	<p>For A-D: <i>Halomonas aquamarina</i> strain DS40M3</p> <p>For I, J: <i>Halomonas meridiana</i> str. HC4321C1</p>	[30]
48 Variochelins A, and B	<p>Variochelins</p> <p>A, n=10 B, n=12</p>	<i>Variovorax boronicumulans</i>	[68]
49 Imaqobactin	<p>Imaqobactin</p>	Arctic Marine Bacterium <i>Variovorax</i> Species RKJM285	[69]
50 Variobactins A, and B	<p>Variobactins</p> <p>A, n=11 B, n=9</p>	<i>Variovorax paradoxus</i> P4B	[70]
51 Vacidobactins A, and B	<p>Vacidobactin</p> <p>A, R=OH B, R=H</p>	<i>Variovorax</i>	[70]

Table 1 (continued)

#	Siderophore	Structure	Secreted by	Ref
52	Loihichelins A-F	 <p style="text-align: center;">Loihichelins</p> <p style="text-align: center;"> $R = \text{---} \left[\text{---} \text{CH}_2 \text{---} \text{CH}(\text{X}) \text{---} \text{CH}_2 \text{---} \right]_m \text{---} \text{CH}_2 \text{---} \text{COOH}$ </p> <p style="text-align: center;"> $R = \text{---} \left[\text{---} \text{CH}_2 \text{---} \text{CH}(\text{X}) \text{---} \text{CH}_2 \text{---} \right]_m \text{---} \text{CH}_2 \text{---} \text{CH}(\text{X}) \text{---} \text{CH}_2 \text{---} \text{COOH}$ </p> <p style="text-align: center;"> A, X=H, m=6 B, X=OH, m=8 D, X=H, m=9 F, X=H, m=10 </p> <p style="text-align: center;"> C, m=5, n=3 E, m=5, n=5 </p>	Marine bacterium <i>Halomonas</i> sp. LOB-5	[71]
53	Pacifibactin	 <p style="text-align: center;">Pacifibactin</p>	<i>Alcanivorax pacificus</i>	[72]
54	Serobactins (A-C)	 <p style="text-align: center;">Serobactin</p> <p style="text-align: center;"> A, n=8 B, n=10 C, n=12 </p>	Grass endophyte <i>Herbaspirillum seropedicae</i>	[73]
55	Cupriachelin	 <p style="text-align: center;">Cupriachelin n=8</p>	Bioplastic Producer <i>Cupriavidus necator</i> H16	[74]
56	Woodybactins A-D	 <p style="text-align: center;">Woodybactin</p> <p style="text-align: center;"> $R = \text{---} \left[\text{---} \text{CH}_2 \text{---} \text{CH}(\text{X}) \text{---} \text{CH}_2 \text{---} \right]_n \text{---} \text{CH}_2 \text{---} \text{COOH}$ </p> <p style="text-align: center;"> A, X=H, n=5 B, X=CH₃, n=5 C, X=H, n=6 D, X=H, n=7 </p>	A marine <i>Shewanella</i>	[75]
57	Ochrobactins A, B, and C	 <p style="text-align: center;">Ochrobactin</p> <p style="text-align: center;"> A, R= $\text{---} \left[\text{---} \text{CH}_2 \text{---} \text{CH}(\text{X}) \text{---} \text{CH}_2 \text{---} \right]_4 \text{---} \text{CH}_2 \text{---} \text{COOH}$ B, R= $\text{---} \left[\text{---} \text{CH}_2 \text{---} \text{CH}(\text{X}) \text{---} \text{CH}_2 \text{---} \right]_4 \text{---} \text{CH}_2 \text{---} \text{COOH}$ C, R= $\text{---} \left[\text{---} \text{CH}_2 \text{---} \text{CH}(\text{X}) \text{---} \text{CH}_2 \text{---} \right]_6 \text{---} \text{CH}_2 \text{---} \text{COOH}$ </p>	Coastal α -proteobacterium <i>Ochrobactrum</i> sp. SP18	[76]

(continued on next page)

Table 1 (continued)

# Siderophore	Structure	Secreted by	Ref
58 Synechobactins A, B, and C	 <p style="text-align: center;">Synechobactin</p> <p style="text-align: center;">R= </p> <p style="text-align: center;">A, n=10 B, n=8 C, n=6</p>	Coastal marine cyanobacterium <i>Synechococcus</i> sp. PCC 7002	[77]
59 Schizokinen, and Schizokinen A	 <p style="text-align: center;">Schizokinen, R= </p> <p style="text-align: center;">Schizokinen A, R= </p>	<i>Rhizobium leguminosarum</i> IARI 917	[78]
60 Baumannoferrins A and B	 <p style="text-align: center;">Baumannoferrin A </p> <p style="text-align: center;">Baumannoferrin B </p>	<i>Acinetobacter baumannii</i>	[79]
61 Catenulobactins B		<i>Catenuloplanes</i> sp. RD067331	[80]
Other Interesting			
62 Mirubactin	 <p style="text-align: center;">Mirubactin</p>	<i>Actinosynnema mirum</i>	[81]
63 Gramibactin	 <p style="text-align: center;">Gramibactin</p>	<i>Rhizosphere bacteria (Paraburkholderia graminis)</i>	[82]
64 Strepturidin	 <p style="text-align: center;">Strepturidin</p>	<i>Streptomyces albus</i> DSM 40763	[83]

acetone, was used for the oxidation of the amine to provide the nitron (the N-oxide of the imine) and then the hydroxamic acid in two steps [87] (Scheme 3). In other cases, and following the same imine-nitron approach, the hydroxylation step was done by reacting the δ -N of Orn with benzaldehyde in basic medium, followed by the addition of an oxidizing agent (m-CPBA) and then a treatment with acid to obtain N-OH. The advantage of this functionalization is that it can be done either to the building block (Scheme 3) or to the Orn residue side chains after the peptide has been built [87].

Once the δ -NH₂ has been hydroxylated, the acylation step is carried out using strong amide formation strategies, such as acyl halides [89,92], acyl anhydrides [87] and HATU [88], due to lower nucleophilicity of the hydroxylated amine compared to the free amine.

Other syntheses reported the preparation of the hydroxamate Orn starting from different amino acids. A full synthesis of ferrichrome in 1969 described the conversion of δ -nitro norvaline (non-branched Val) into δ -N-hydroxy ornithine by reducing the nitro group with zinc in an aqueous ammonium chloride solution [90,91] (Scheme 4). Another protocol included the conversion of the COOH side chain of glutamic acid to OH then its attachment to a protected simple hydroxamic acid (blue route in Scheme 1) using diisopropyl azodicarboxylate and triphenyl phosphine [85] (Scheme 4).

2.2.2. Synthesis of N-5-aminopentyl-N(hydroxy)-succinic acid building block

Reported syntheses of N-5-aminopentyl-N(hydroxy)-succinic acid building unit started with the protected hydroxylamine, followed by an alkylation step with a cyano aldehyde (4-cyanobutanal) as in the preparation of desferrioxamine B [93], or a haloalkane nitrile (5-chloro valeronitrile) as in the synthesis of bisucaberin [94] (see Scheme 5). The prepared cyanoalkylhydroxylamine is divided into two parts, the nitrile group in one of them is reduced to an amine group and acylation is done using succinic anhydride (the route followed is shown by green dashed lines, Scheme 1). The same route was reported for the synthesis of alcaligin but with a shorter alkyl part to prepare the N-5-aminobutyl-N(hydroxy)-succinic acid [95].

2.2.3. Synthesis of other hydroxamate building blocks

In some artificial siderophores, the hydroxamate moiety was embedded in the backbone through α -N-hydroxy amino acids prepared indirectly from other closely related acids. For example, α -benzyloxyglycine was obtained by reacting bromoacetic acid tert-butyl ester and O-benzylhydroxylamine [96]. N-benzyloxyalanine (or N-benzyloxyphenylalanine) was prepared starting from D-lactic acid (or D-phenyllactic) acid *t*-butyl ester by converting the α -OH to

a triflate intermediate, followed by the reaction with O-benzylhydroxylamine [97]. The S_N2 attack of the benzyloxyamine resulted with inverted configuration of α -carbon. The amide bond was then formed by condensing the hydroxylated α -N with an α -COOH of another amino acid using an effective form of activated acid [96,98]. All these methods followed the green route of Scheme 1 by introducing the alkyl part into a previously prepared benzyl protected-hydroxylamine (Scheme 6).

A more recent study hydroxylated the α -N of the amino acid with m-CPBA after alkylating it with bromoacetonitrile (converting it temporarily into a secondary amine prior to hydroxylation, making the latter much more efficient) [99] (Scheme 6).

2.2.4. Incorporating the hydroxamate building block into the backbone

In literature, the synthesized hydroxamate building blocks were incorporated into the siderophore molecule through various strategies. Some were done on solid phase, the others in solution phase (see Table 2).

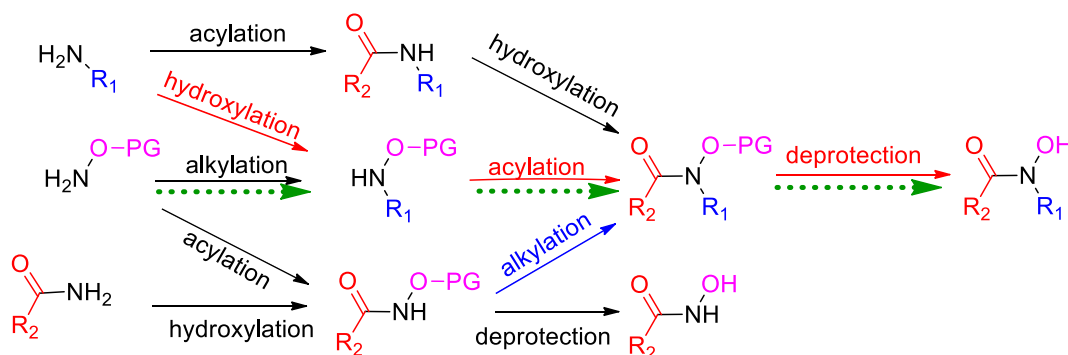
2.3. Binding affinity towards iron

Siderophores, in general, form strong complexes with Fe (III), with thermodynamic formation constants β up to 10⁴⁹ for the tris-catecholate enterobactin (Fig. 1), compared to 10²⁵ for EDTA, a widely used complexing agent for metal ions. Tris hydroxamate siderophores also show high formation constants of \sim 10³⁰. In the fully deprotonated forms of ligands (at highly basic conditions), catecholate siderophores show greater binding to Fe(III) than hydroxamates (the difference in log β values can go up to 19 units, which means that the concentration of the catecholate-Fe complex is 10¹⁹ times that of hydroxamate-Fe under same conditions). However, at physiological pH (pH = 7.4), the binding affinity (reflected by pFe³⁺, which equals $-\log[\text{Fe}^{3+}]_{\text{free}}$ at pH = 7.4, [Fe³⁺] total = 10⁻⁶ M and [Ligand]_{total} = 10⁻⁵ M) of the two siderophores is comparable (the difference in binding affinities is much lower). This observation is attributed to the acidic character of the hydroxamates, a feature that increases the proportion of deprotonated molecules (ready to bind to Fe(III)) of hydroxamate compared to catecholate.

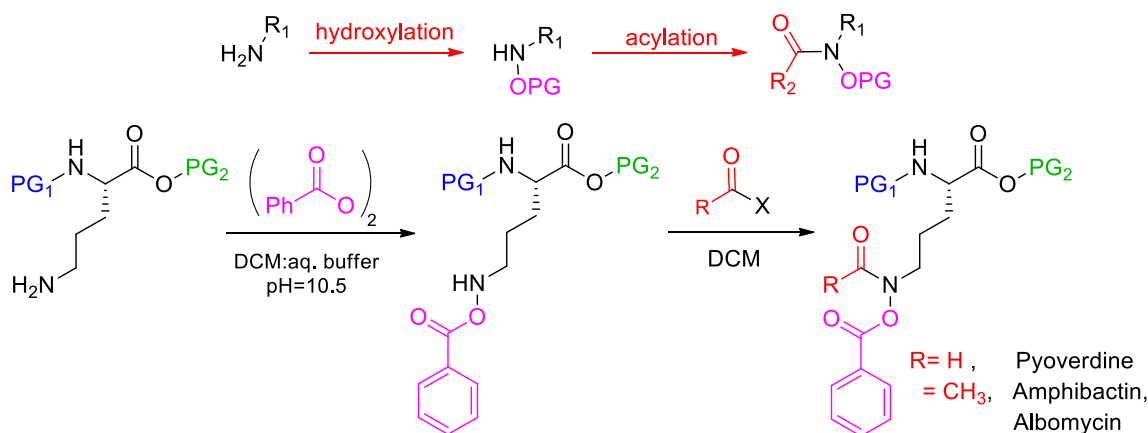
For comparative purposes, Table 3 shows the formation constants and iron affinity for several siderophores with different chelating groups.

2.4. Applications of hydroxamate molecules and hydroxamate siderophores

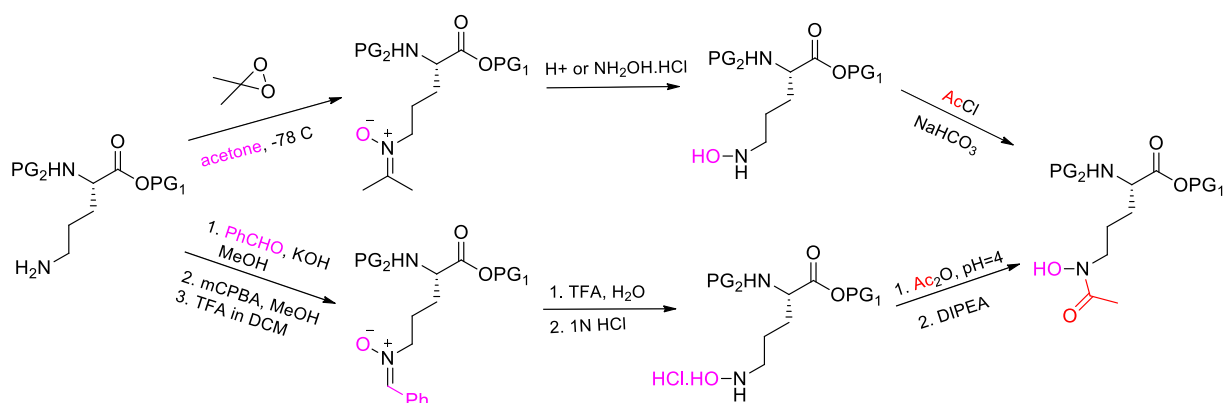
Hydroxamic acids have found many applications in medical and



Scheme 1. Possible routes for the preparation of hydroxamic acid from different starting compounds (coloured arrows represent routes reported for siderophore synthesis, all arrows (black and coloured represent reported routes for hydroxamic acid preparation in general).



Scheme 2. Synthesis of 'PG₁-Orn(acyl,OBz)-OPG₂' building block, using benzoyl peroxide (for the hydroxylation step). (R = H, X = EDC active ester) in pyoverdin D. [88], (R = CH₃, X = Cl) in amphibactin-T [92] and albomycin [89].



Scheme 3. Synthesis of 'PG₁-Orn(acyl,OBz)-OPG₂' building block through the imine-nitron intermediates and using DMD or PhCHO [87].

agricultural practices [109] and as probes [1,3]. Their medical use can be therapeutic or diagnostic [110]. The presence of hydroxy substituents on the amide bonds of an active peptide enhances its stability against enzymatic degradation [96]. Furthermore, hydroxamic acids inhibit methionine aminopeptidase (MetAP), an essential enzyme in protein synthesis in a variety of organisms. This inhibition enables the use of hydroxamic acids as potent antibacterial or antitumor agents [96,111]. Also, these acids have the potential to inhibit metalloproteases and HIV protease, and they show activity in immune suppression [96].

As metal chelators, Desferal, the brand name of desferrioxamine B (**6**), was the first drug used for the treatment of metal poisoning, namely iron overloading [22,112]. Also, the hydroxamate groups have shown unprecedented activity against the growth of *P. aeruginosa* biofilms (which confer cells extra resistance to antibiotics by adhering in the form of a film) when they were combined with glycol motifs in a bifunctional molecule, in which the glycol targeted the adhesion of cells and hydroxamate deprived cells of iron [113].

In this review, we focus on and discuss the use of hydroxamate siderophores as Trojan horses to overcome bacterial resistance to antibiotics.

2.4.1. HA siderophores-antibiotic conjugates (application as Trojan horses)

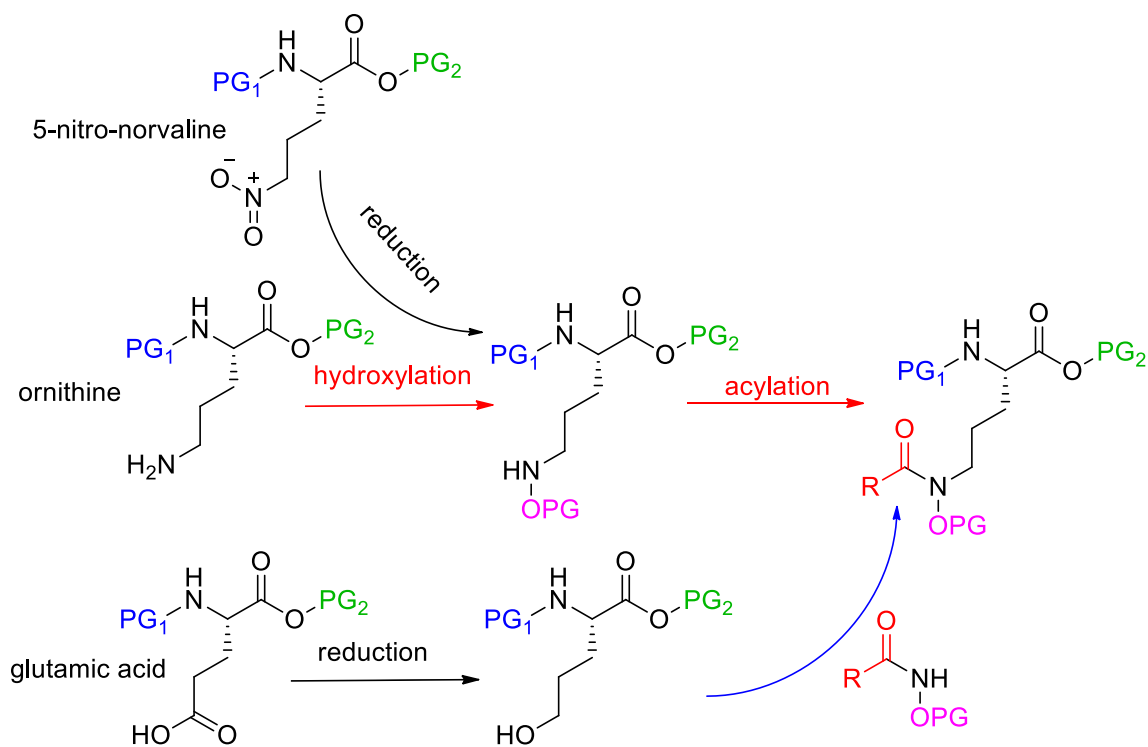
After being excreted and complexed to Fe(III), the loaded siderophores are recognized by specific protein receptors present on

the microbial cell membrane. They are then transferred through specified cycles to their target inside the cell (cytoplasm or sometimes periplasm in some gram-negative bacteria). Fe(III) is then released from the siderophore through certain mechanisms [11,12], reduced to Fe(II) and metabolized [8].

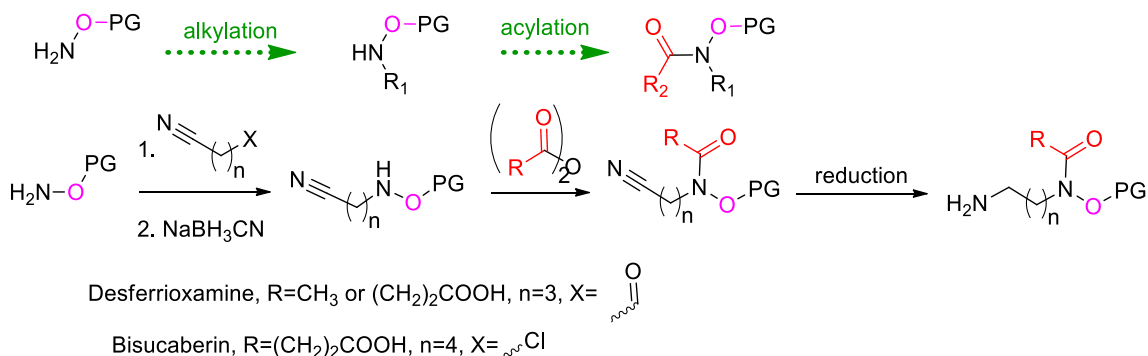
The microorganisms that produce hydroxamate siderophores have a special protein receptor, FhuA, embedded in their membranes to recognize and mediate the uptake of the iron-siderophore complex [11,16,114]. FhuA may also be present in the membrane of other microorganisms that do not produce endogenous hydroxamate siderophores yet can take up the hydroxamate siderophores produced by other organisms [13].

Some studies have suggested that the protein receptors recognize and identify key points in the siderophore backbone. Others propose that recognition occurs via identification of the steric configuration of the e-donating atoms around the central iron in the inner coordination sphere [13,17]. The latter notion may explain how some species can take up iron from **xenosiderophore** complexes. A study by Shanzer's group suggested that the recognition takes place in two domains: first, the configuration of the complex around iron; and second, the spatial orientation of the functional groups (C=O) with respect to the inner coordination sphere [115,116]. It is likely that microorganisms have two types of receptors—specific ones to identify endogenous siderophore-iron complexes and more general ones that identify the core of the xenosiderophore-iron complexes.

Some bacterial strains exploit the greed for theft of other species



Scheme 4. Synthesis of 'PG₁-Orn(acyl,OBn)-OPG₂' starting from 3 different amino acids.



Scheme 5. Synthesis of N-5-aminopentyl-N(hydroxy)-succinic acid building block in desferrioxamine B [93] and bisucaberin [94].

by producing and attaching a siderophore chelator to a **microbiocidal** moiety. The resulting conjugate is called a "sideromycin". These molecules are then released into the matrix as Trojan horses to poison competing opponent cells.

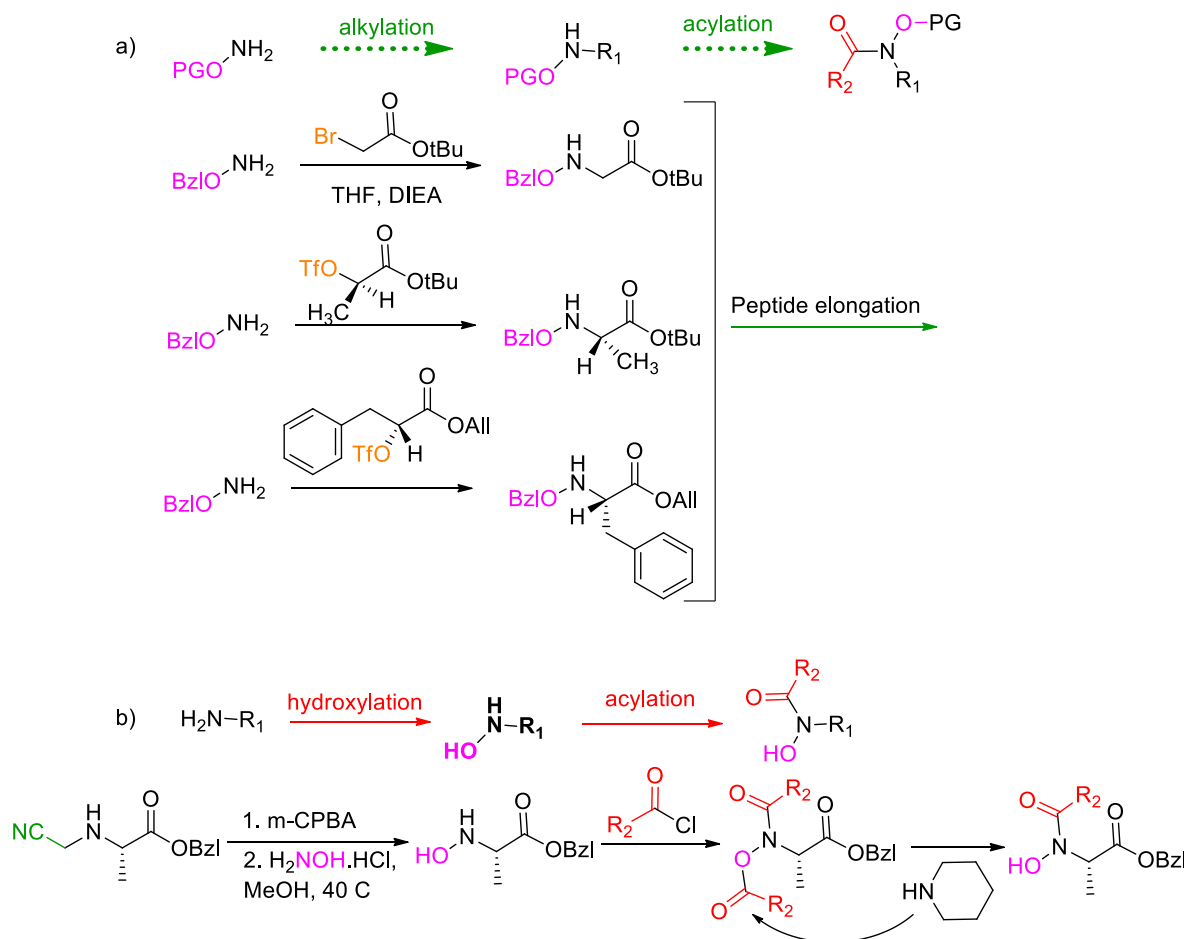
2.4.1.1. Natural conjugates (sideromycins). Natural sideromycins are highly specific against certain types of bacteria and are taken up through the same pathway as the corresponding type of siderophores with respect to the binding unit.

The first reported sideromycin was grisein, discovered by Waksman's group in 1947 [23]. It was isolated from a strain of *Streptomyces griseus*. It showed antimicrobial activity against many strains of bacteria but its structure was not elucidated then and was partially characterized in 1951 [117]. Grisein was later reported as albomycin (3) [112]. Albomycins are the most widely known natural sideromycins. In 1951, Gause and Brazhnikova isolated an albomycin from *Actinomyces suibtropicus*, a species of streptomycetes [118]. It was found to strongly inhibit the growth of some gram-positive bacteria, such as *S. aureus*, *S. pneumoniae* and

B. subtilis, as well as some gram-negative bacteria [112]. The activity of this albomycin was found to be ten times stronger than that of penicillin [118], and it was used in the Soviet Union as an antibiotic. Its structure was firmly established by Benz and coworkers in 1982 [24]. Similarities between grisein and albomycin that led to conclude that they are the same compound have been discussed in the literature [119]. Other examples of hydroxamate sideromycins are salmycins and ferrimycins (Table 4).

All bacteria susceptible to the microbicidal activity of these hydroxamate sideromycins were found to have the FhuA receptor in their membranes. These sideromycins function better under iron starvation conditions than under conditions of sufficiency [3]. Iron starvation can be achieved by using biostatic agents (strong chelators that bind iron tightly).

In addition to these sideromycins, another seryl tRNA synthetase inhibitor, SB-217452 [122], was isolated from a *Streptomyces* species. Although structural characterization showed that SB-217452 contains the same nucleoside moiety present in albomycin, it showed very weak antibacterial activity compared to the



Scheme 6. Reported syntheses of α -N-benzyloxy amino acids through two routes: a) alkylation of hydroxylamine [97] and b) hydroxylation of alkylamine [99].

Table 2
Reported strategies used for the incorporation of hydroxamate building blocks into the siderophore backbone.

Hydroxamate Building unit	Siderophore	Entry No.	Synthetic Strategies	Ref.
Ornithine-derived hydroxamate siderophores	Pyoverdinin	Fig. 1	Fmoc/tBu	Super acid-labile Rink acid resin (solid phase) [88]
	Amphibactin-T	10	Fmoc/tBu	CTC-polystyrene resin (solid phase) [92]
	Albomycin	3	Fmoc/tBu	Solution phase [89]
	Ferrichrome	1	Boc/Bzl	Solution phase [90]
	DIG-siderophore (conj.)	–	Functionalizing the Orn as building block or its tripeptide with free side chains	Solution phase [87]
N-hydroxy diaminoalkane derived siderophores	Desferrioxamine	6	Metal-templated Cyclic Trimerization	Solution phase [100]
	Bisucaberin	37	Boc/Bzl	Solution phase [101]
	Alcaligin	7	Diphenylphosphoryl azide (DPPA) + triethyl amine	Solution phase [95]

latter. This can be explained by the fact that SB-217452 does not contain the chelator moiety that mediates the uptake of albomycin [13,122]. This example and many others clearly demonstrate the role played by the chelator moiety in overcoming the low permeability of the pathogenic cell wall towards the bactericidal moiety alone.

Albomycin (**3**) consists of a linear Orn-derived tri hydroxamate. The tri peptide is linked through its C-terminus to a glycoside entity by a di-seryl linker. When the competing bacteria internalize the conjugate-iron complex, peptidases release the warhead, thus inducing bacterial death [13] (Fig. 3-A). Ferrimycin (**66**) resembles the ferrioxamine family in its chelating unit, which is a linear non-

peptidyl tris-hydroxamate derived from alternative N-hydroxy-diaminopentane and succinic acid with a 4-amino-5-hydroxybenzamide linkage to an iminoester-substituted lactam antibiotic [112]. Salmoglycin consists of danoxamine siderophore (**9**) attached to an aminoglycoside through a succinic linker [121]. When the hydroxamate moieties are engaged with iron complexation, the payload remains attached to the conjugate. Once the reductase of the cell frees the iron, the protonated hydroxamate attacks the ester group causing a cyclization reaction that results in the release of the antibiotic. This only happens after the competing cell obtains the iron from the stolen complex [13,123]. The mechanism of drug release is shown in Fig. 3-B [123].

Table 3

Comparison of the thermodynamic constants for various representative tris-hydroxamate siderophores and their Fe(III) complexes with that of enterobactin.

Siderophores	Entry no.	pKa	Log β_{110}	$^a pFe^{3+}$	Ref
Enterobactin (triscatecholate)	Fig. 1	6.00 7.50 8.55	49	34.3	[102,103]
Ferrichrome	1	8.11 9.00 9.83	29.07	25.2	[104,105]
Ferricrocin	2	8.14 9.01 9.92	30.4	26.5	[106]
Ferrioxamine B	6	8.39 9.03 9.70	30.6	26.6	[104–106]
Basidiochrome	30	Not evaluated	27.8	25	[107]
Aquachelin-C (bi-hydroxamate)	40	3.79 (COOH) 8.73 (CONOH) 9.52 (CONOH)	31.4	–	[108]
Marinobactin-D (bi-hydroxamate)	11	3.75 (COOH) 8.47 (CONOH) 9.40 (CONOH)	Not evaluated	–	[108]
Marinobactin-E (bi-hydroxamate)	11	3.85 (COOH) 8.89 (CONOH) 9.52 (CONOH)	31.8	–	[108]

^a $pFe^{3+} = -\log[Fe^{3+}]_{free}$ at pH = 7.4, $[Fe^{3+}]_{total} = 10^{-6}$ M, $[Ligand]_{total} = 10^{-5}$ M.

Of note, the sideromycin-producing organism itself is not affected by the conjugate because it does not have a target for the warhead or the related enzyme that causes drug release [13]. Also, vulnerable bacteria can readily develop resistance against these sideromycins through the deletion of the hydroxamate membrane receptor [14].

2.4.1.2. Artificial conjugates mimicking the natural ones. The activity of the natural sideromycins opened the door for research into new conjugates. In this regard, attention was turned to tuning the structure of the chelators and varying the antimicrobial moiety, thereby providing promising tools for tackling fatal multidrug-resistant bacteria.

The first synthetic conjugate **85** was reported by Zahner in 1977 [13]. He hybridized DFO B with a sulfonamide directly through an amide bond (no linker) between the available primary amine of the chelator moiety and the carboxyl of the sulfonamide. Many artificial hybrids containing hydroxamate chelators have been reported to date (Table 5), with cargos varying between cephalosporines, fluoroquinolones and others. However, none of the hydroxamate-drug hybrids have yet been approved as a drug. Cefiderocol (S-649266) is the first and only siderophore-drug conjugate to be authorized by the FDA (November 2019) [124]. This drug consists of a catechol chelating unit and a cephalosporin antibiotic cargo [125] (see section 3).

In summary, conjugates **68–73** are semi synthetic sideromycins that share the same chelator moiety as albomycin (**3**) which is a linear Orn-derived tri hydroxamate. The antibiotic moieties in these conjugates varies between β -lactams as in **68** and **69**, and fluoroquinolones as in **70**, attached to the C-terminal of the chelating peptide backbone. In conjugates **71–73**, the antibiotics digoxigenin, biotin and virgimycin, respectively, are attached to the tripeptide backbone via different linkers through its N-terminals.

Conjugates **74–77** are totally synthetic; the chelator moiety is an iso cyanuric acid-based tri Orn hydroxamate, inspired by the natural bi hydroxamate siderophore rhodotorulic (**4**). The antibiotic is directly attached to the acyl part of the hydroxamate, enabling the preparation of multi-warhead conjugates [142].

Conjugates **78–82** were synthesized to illustrate the effect of linker on overall activity. All are containing the same chelator moiety, desferrioxamine B, and ciprofloxacin antibiotic. The linkers vary from stable uncleavable succinic moiety **78** to esterase-cleavable **79**, phosphatase-cleavable **80** and reductase-cleavable **81**, ending with thiol-maleimide linker **82**. The mechanisms of drug release are shown in Fig. 4 [132]. Conjugates **82–84** share the same desferrioxamine B chelator, the same linker (thiol maleimide) and three different antibiotics.

Conjugates **86–88** contain danoxamine analogue chelators with differing denticity (mono, bi and tri hydroxamate) and three different antibiotics attached through a stable linker.

Conjugates **89–102** contain mixed chelators. Compounds **89–98** are biscatecholate-mono hydroxamate, with various antibiotic warheads, while **99–102** are pyoverdine-derived (bis hydroxamate, mono catecholate) chelators attached to a range of drugs through different linkers at distinct positions of the pyoverdine scaffold.

Conjugate **106** is mycobactin chelator (employing lysine residue as the hydroxamate-bearing moiety) attached to the antibiotic artemisinin.


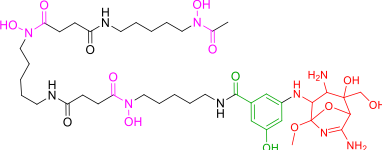
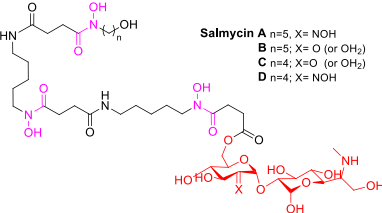
2.4.1.2.1. Summary of the antibacterial activity of these conjugates. Most of these conjugates had moderate to low antibacterial activity. Conjugates with β -lactams showed better performance than those with non β -lactams [14]. The activity of the conjugates under iron-deficient conditions was enhanced but was lower than that of the parent antibiotic alone in most cases. This observation may be attributable to premature release, non-suitable substrates for enzymatic cleavage, or readily developed resistance [135]. The modification of linkers (trimethyl lock) in **79–80** did not achieve better results.

Here are some examples with the main conclusions learned from their study:

Conjugates **86–88** showed that the denticity of the chelator is crucial, where it should form a 1:1 complex with Fe(III) to actively transport the conjugate [134,135].

Conjugate **92** employs a bis catecholate-mono hydroxamate chelator that is analogous to fimsbactin (a siderophore produced by

Table 4
Natural hydroxamate sideromycins, chelator moieties are shown in black and purple, linkers in green and antibiotic moiety in red.

#	Sideromycin	Structure	Produced naturally by	Year/ref.
	General structure	 <p>Chelator → Linker → Antibiotic</p> <p>the driving moiety the toxic drug</p>		
65 3	Grisein Albomycin	Structure not fully elucidated Albomycin ϵ_1 , X=O Albomycin δ_1 , X=NH Albomycin δ_2 , X=NC(=O)NH ₂	<i>Streptomyces griseus</i> <i>Actinomyces substrictus</i>	1947 [23,120] 1951 [118]
66	Ferrimycin	Ferrimycin A ₁ 		1960 [112]
67	Salmycin	Salmycin A n=5, X=NOH B n=5; X=O (or OH ₂) C n=4; X=O (or OH ₂) D n=4; X=NOH 	<i>Streptomyces violaceus</i>	1995 [121]

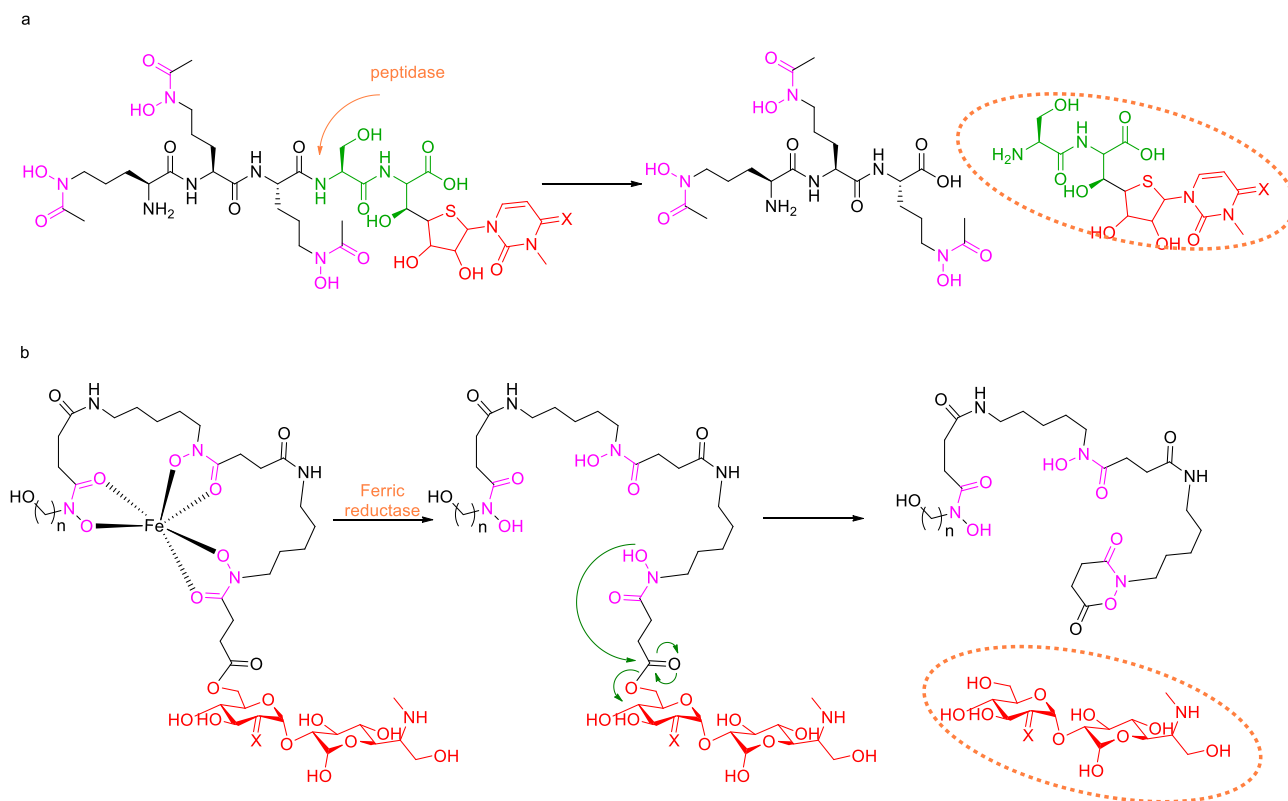
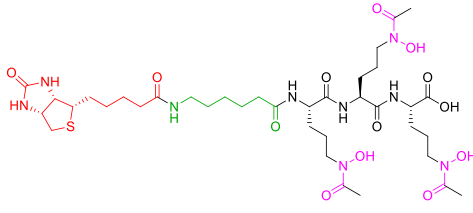


Fig. 3. Possible mechanisms for drug release from sideromycin: a) albomycin and b) salmycin.

Table 5

Artificial hydroxamate siderophore-drug (SD) conjugates, chelator moieties are shown in black and purple, linkers in green and antibiotic moiety in red.

#	Structure	Antibiotic	ref.
68		Loracarbef	[126,127]
69		Oxamazin	[128]
70		Flouroquinoline	[129]
71		Digoxigenin	[87]
72		Biotin	[87]
73		Virgimycin	[130]

(continued on next page)

Table 5 (continued)

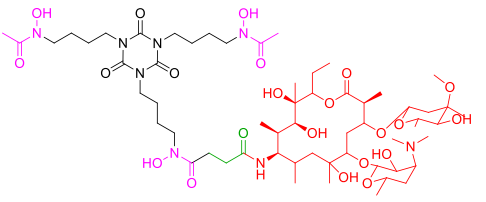
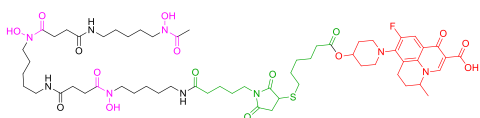
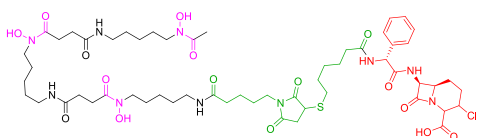
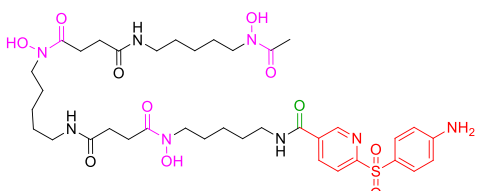
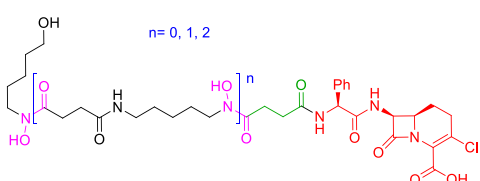
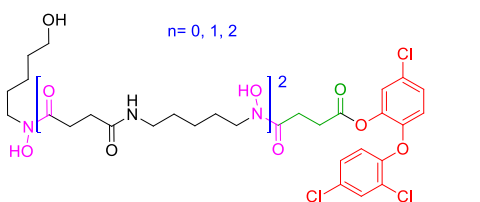
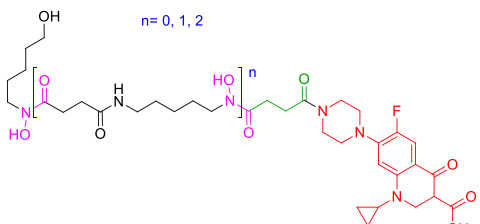
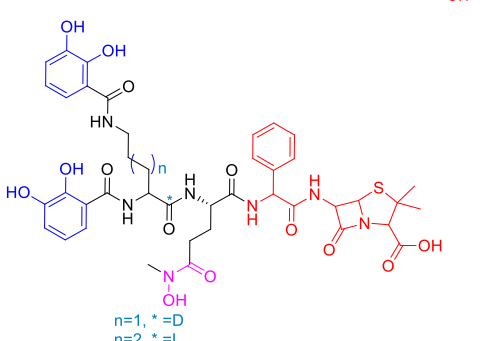
#	Structure	Antibiotic	ref.
74			[131]
75			[131]
76		Nucleoside	[14]
77		Macrolide	[14]
78			[132]
79		Esterase release	[132]
80		Phosphatase release	[132]
81		Reductase cleave	[112]
82			[133]

Table 5 (continued)

#	Structure	Antibiotic	ref.
83			[133]
84			[133]
85		Sulfonamide	[112]
86		β -Lactam Lorabide	[134]
87		Triclosan	[135]
88		Fluroquinoline Ciprofloxacin	[134]
89		Ampicillin	[136]

(continued on next page)

Table 5 (continued)

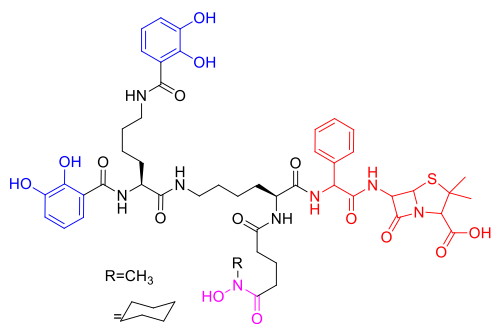
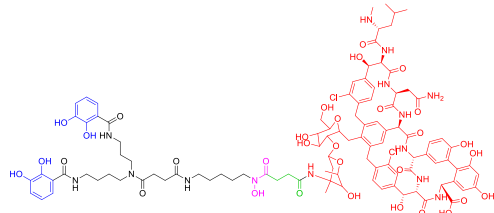
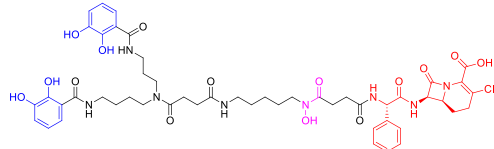
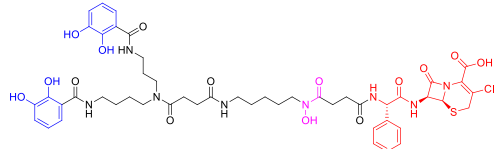
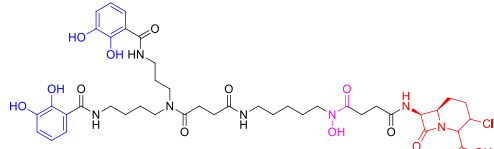
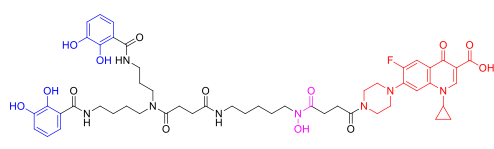
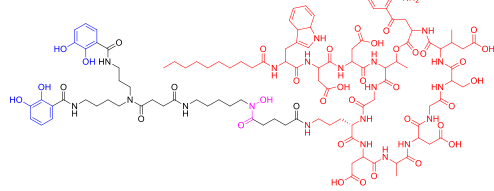
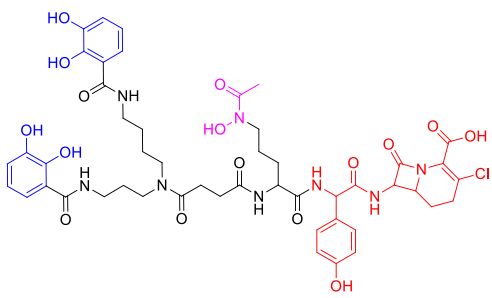
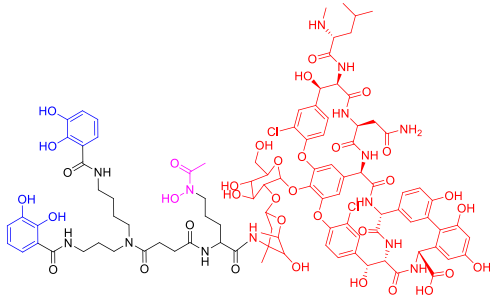
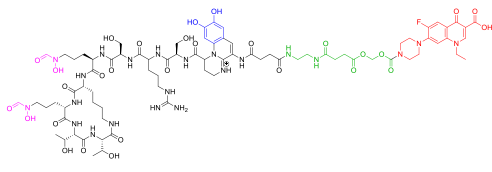
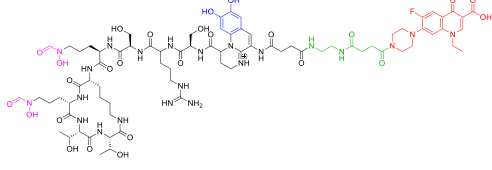
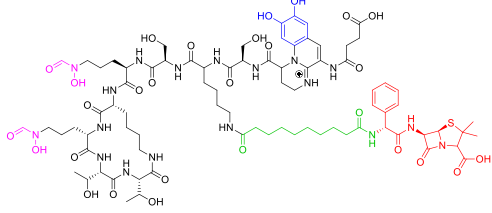
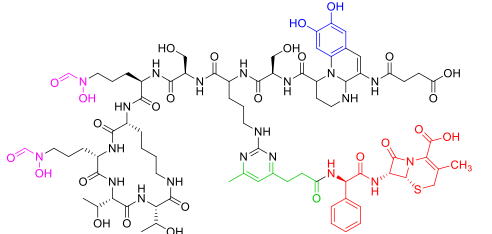
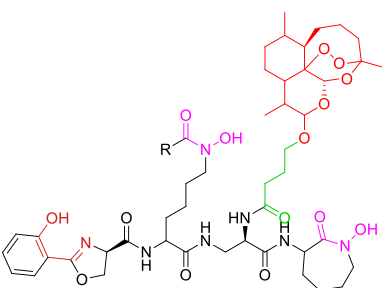
#	Structure	Antibiotic	ref.
90			[136]
91		Glycopeptide Vancomycin	[14,112]
92		Loracarbef	[13,112,137,138]
93		Cephalosporin	[13]
94			[137]
95			[112,138]
96		Daptomycin	[112,139]

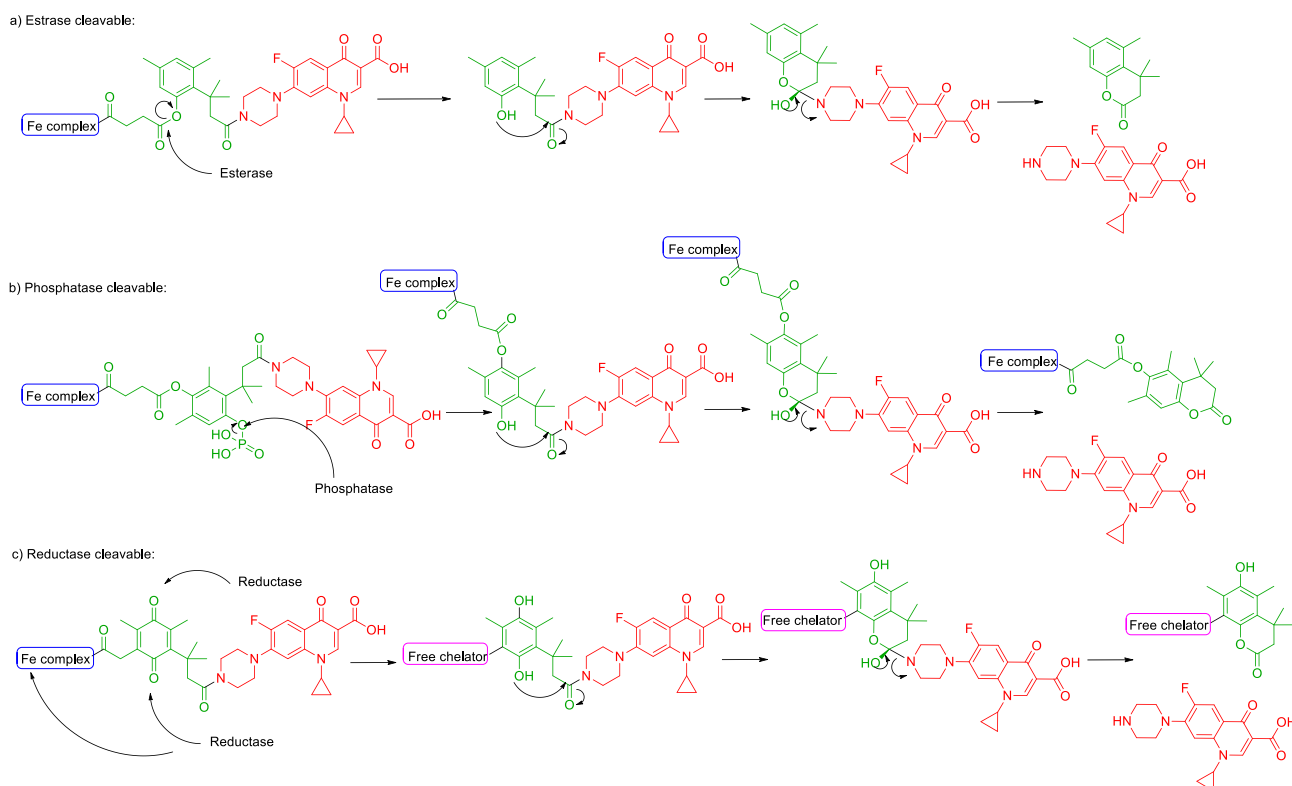
Table 5 (continued)

#	Structure	Antibiotic	ref.
97		Cephem	[13,14]
98		Vancomycin	[13]
99		Norofloxacin cleavable	[112]
100		Norofloxacin non cleavable	[112]
101		Ampicillin	[112,140]
102			[141]

(continued on next page)

Table 5 (continued)

#	Structure	Antibiotic	ref.
103		Artemisinin	[13]

Fig. 4. "Trimethyl lock" mechanism of drug release in conjugates: a) **79** b) **80** [132] and c) **81** [13].

A. baumannii), the chelator is conjugated to loracarbef. It shows high activity against *A. baumannii*, again demonstrating the vulnerability of a bacterium against a hybrid of its own siderophore (advantage of endogenous over xenogenous siderophores). Furthermore, **92** mediates uptake through two receptors in *E. coli*, namely Cir (for the catechol) and FhuA (for the hydroxamate) [14,112].

The same mixed bis-catecholate mono-hydroxamate chelator hybridized with a ciprofloxacin warhead as in **95**, shows no activity against *A. baumannii* [112,134], emphasizing the importance of harmony between the uptake cycle of the chelator and the target of the antibiotic. The cycle of this conjugate ends in the periplasm, while the target of ciprofloxacin (unlike the loracarbef in **92**) is the cytoplasm, thereby explaining the lack of activity of **95**.

A strong promising example is conjugate **96**, which conferred the gram-positive antibiotic daptomycin activity against some gram-negative bacteria [138,139]. This conjugate revealed that that large molecules (such as daptomycin >500 Da which cannot diffuse

into the cell like the smaller molecules) can also be transported into the cell through specific iron-mediated receptors [112].

Conjugate **103** was highly specific to *M. tuberculosis*. The chelating moiety in conjugate **103** resembles mycobactin, the siderophore produced by *M. tuberculosis*. However, **103** did not attack other gram-positive or -negative bacteria [13,112]. Again, this observation indicates that the use of the pathogen's own siderophore may be useful. The same conclusion was drawn from pyoverdine-derived conjugate **101** against the pyoverdine producer *P. aeruginosa* [140].

2.4.1.3. Rational design for choice of artificial siderophore-drug conjugates. Traditional antibiotics are classified into four groups on the basis of their cellular targets. The targets are cell wall assembly (as for β -lactams and glycopeptides), protein synthesis (as for aminoglycosides and macrolides), DNA/RNA replication (as for fluoroquinolones and sulfonamides) and membrane disruption (as for lipopeptides; daptomycin) [112]. Small antibiotics (<500 Da)

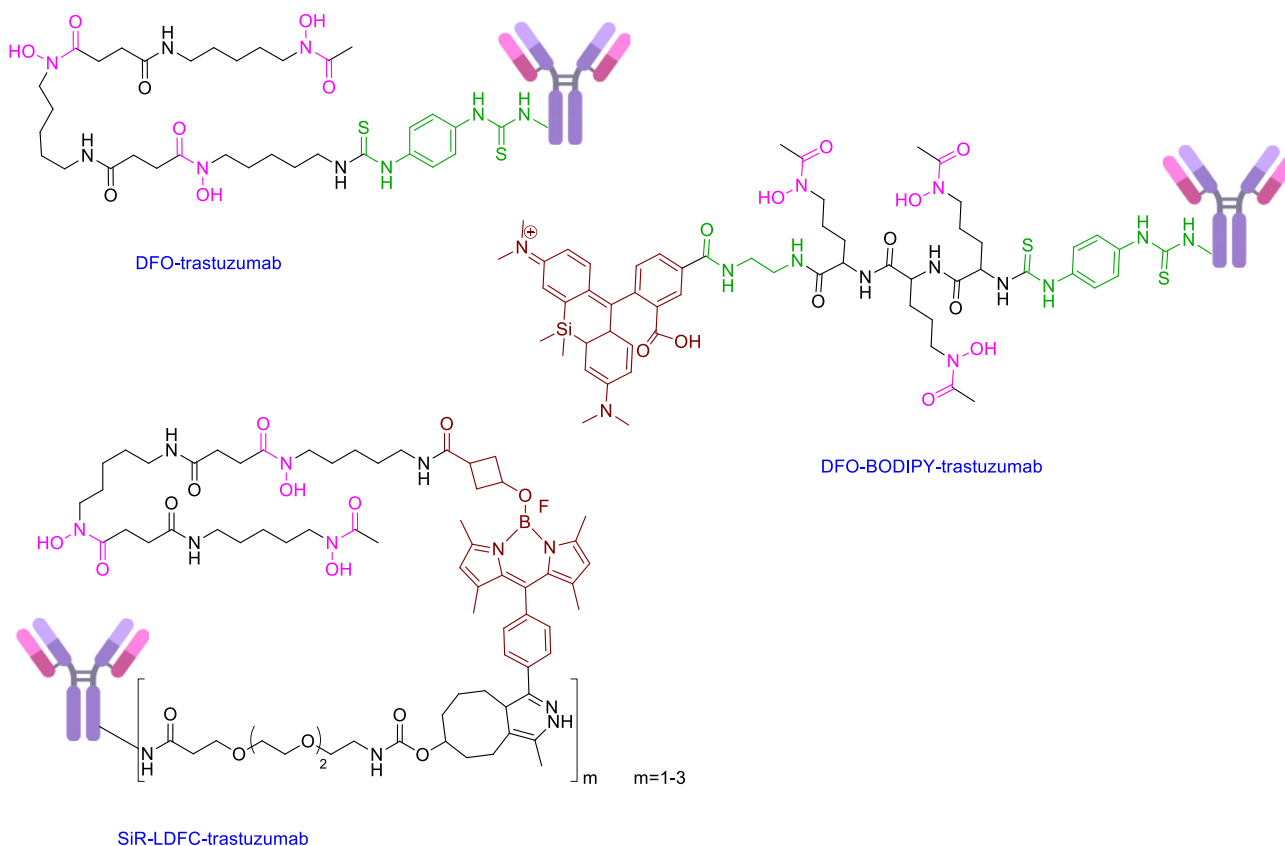


Fig. 5. Hydroxamate chelator-antibody conjugates for imaging applications.

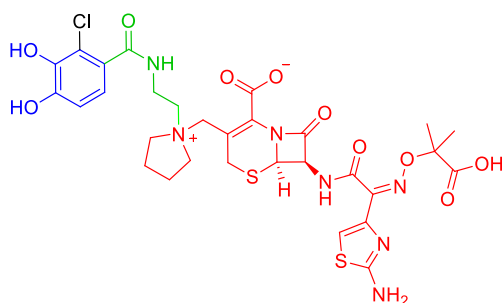


Fig. 6. Chemical structure of Cefiderocol.

enter the cell by passive diffusion through the porins in the cell wall of gram-negative bacteria and they are usually broad spectrum. On the other hand, glycopeptides and daptomycin are active only against gram-positive bacteria, with targets present on the outer part of the cell [112]. Hybridizing these antibiotics with siderophores can broaden or narrow the spectrum of activity of the antibiotic warhead.

2.4.1.3.1. Choosing the chelator. The chelator of choice depends on the pathogen targeted, its outer membrane protein receptors (what types of siderophores it can recognize), and the iron cycle (where Fe(III) is released—in the cytoplasm or periplasm) [135]. For example, trihydroxamate is suitable to drive cytoplasmic drugs while biscatechol-hydroxamate is suitable for periplasmic drugs for gram-negative bacteria.

2.4.1.3.2. Role played by the linker. Linkers play a critical role in determining the efficiency of the conjugate. Premature release of the warhead or halting it back from attacking the target may fail the

whole process. The choice of linker depends on the above-mentioned factors. Several types have been reported, some of which have been mentioned before. Another kind of chelator is β -lactam as a linker attached to any type of antibiotic. The release mechanism depends on the attack of β -lactamase to free the other antibiotic payload [13].

2.4.1.3.3. Choosing the antibiotic. The antibiotic warhead target determines where the release takes place, and, consequently, the type of linker to be used. Even when taking all factors carefully into consideration, the bacterial fast development of resistance remains the biggest challenge.

2.4.2. Other hydroxamate siderophore conjugates

In all the previous conjugates mentioned, the chelating units are the moiety that drives them towards the target and the payloads are the antibiotics. Hydroxamate chelators can also be used in other conjugates in which an antibody is the driving moiety and a radiolabelled metal-chelator complex is the cargo used for imaging [113,143] (Fig. 5).

3. Cefiderocol (FETROJA®): the first siderophore-drug conjugate in the market

Cefiderocol (previously known S-649266) is a novel catechol-based siderophore that targets gram-negative bacteria, including strains with carbapenem resistance, via a Trojan horse active transport mechanism [125,144]. The aminoacyl catechol moiety is attached with a di-methylene linker to the pyrrolidine ring of the antibiotic [144,145] (Fig. 6).

The structure of the payload in cefiderocol combines the features of the antibiotics ceftazidime and cefepime, thereby boosting

activity against gram-negative bacteria, as well as stability. The quaternized N-methyl-pyrrolidine and the carboxylate moieties of cefiderocol form a zwitterion that enhances water solubility, degradation resistance, and capacity to rapidly penetrate the outer cell membrane of gram-negative bacteria [146]. GR69153 (cefetecol), M – 14659 and S-9096 are other catechol-cephalosporine conjugates that showed strong antibacterial activity *in vitro*, but were not successful *in vivo* [145].

Cefiderocol was approved by the FDA on November 14, 2019 [124]. It is used for the treatment of complicated urinary tract infections (cUTI), including pyelonephritis caused by susceptible gram-negative microorganisms. It is administered intravenously. It has some reported adverse effects, including diarrhea, infusion site reactions, constipation, rash, candidiasis, cough, elevations in liver tests, headache, hypokalemia, nausea, and vomiting [147].

4. Conclusion

Forty years of research have been devoted to the synthesis and use of sideromycins to tackle pathogens. Among these conjugates, only one has reached the market, namely Cefiderocol, which was approved by the FDA in 2019. Although Cefiderocol contains a catechol (not a hydroxamic) binding unit—the field remains open for the development of others. No other reported artificial conjugates have been commercialized to date, but they have all contributed to bringing the pieces of the puzzle together. Inspired by albomycins, ferrimycins and salmycins, hydroxamate-based siderophores are well positioned to achieve success. While the full picture of successful conjugate design and development is gaining clarity, more research efforts are required to optimize the technology.

Declaration of competing interest

Developing Multi-drug resistance in bacteria threatens human health when entering the post-antibiotic era. Iron acquiring gates supply bacteria with its nutrient, iron (III) by iron carrying molecules (Siderophores). Using this strategy, siderophore-antibiotic conjugates (sideromycins) internalize the drug into the bacterial cell through iron gates, release the drug inside the cell and kill it. The most famous natural sideromycins (Albomycin, Salmycin, Ferrimycin) chelate iron (III) through their hydroxamate moieties, which also mediate the recognition and up take. An insisting need to understand the full picture behind their potency lead to the writing of this review. Most recent natural hydroxamate siderophore, chemical synthesis of building blocks, conclusions from the artificial sideromycins trials are all discussed thoroughly in this review.

In our opinion, this is a fully transversal review, which should be of interest to a broad scientific audience. Thus, synthetic chemists can find rich information about natural siderophores and comprehensive synthetic source for building blocks syntheses.

Microbiologists will have access to the detailed structure and producing species for almost all hydroxamate siderophores isolated in the last two decades. It also helps biochemists with the rational relation between the choice of each of the bacteria, chelator, linker, antibiotic and the antibacterial activity, concluded from literature. Finally, drug hunters could find inspiration for the development of new drug discovery programs.

Acknowledgement

The work carried out in the laboratory was funded in part by the following: the National Research Foundation (NRF) (# 105892 and Blue Sky's Research Programme # 120386) and the University of

KwaZulu-Natal (South Africa); and Marató TV3 foundation 2018 (#20183530). We thank Professor Miquel Viñas (University of Barcelona) for fruitful discussions.

References

- [1] T.C. Johnstone, E.M. Nolan, Beyond iron: non-classical biological functions of bacterial siderophores, *Dalton Trans.* 44 (2015) 6320–6339, <https://doi.org/10.1039/c4dt03559c>.
- [2] Iron is the Future – Part One: everything you want to know about iron!, <https://newsroom.posco.com/en/iron-future-part-one-everything-want-know-iron/#:~:text=Atomic%20number%2026%20Fe%2C%20a.k.a.,even%20in%20the%20human%20body>. (Accessed 22 August 2020).
- [3] G. Tonziello, E. Caraffa, B. Pinchera, G. Granata, N. Petrosillo, Present and future of siderophore-based therapeutic and diagnostic approaches in infectious diseases, *Infect. Dis. Rep.* 11 (2019) 8208, <https://doi.org/10.4081/idr.2019.8208>.
- [4] H. Drechsel, G. Jung, Peptide siderophores, *J. Pept. Sci.* 4 (1998) 147–181. DOI: 1075-2617/98/030147-35.
- [5] D.J. Raines, T.J. Sanderson, E.J. Wilde, A.K. Duhme-Klair, Siderophores, in: *Reference Module in Chemistry, Molecular Sciences and Chemical Engineering*, Elsevier, Waltham, 2015.
- [6] K.D. Krewulak, H.J. Vogel, Structural biology of bacterial iron uptake, *Biochim. Biophys. Acta* 1778 (2008) 1781–1804, <https://doi.org/10.1016/j.bbame.2007.07.026>.
- [7] E. Clément, P.J. Mesini, F. Pattus, I.J. Schalk, The binding mechanism of pyoverdinin with the outer membrane receptor FpvA in *Pseudomonas aeruginosa* is dependent on its iron-loaded status, *Biochemistry* 43 (2004) 7954–7965, <https://doi.org/10.1021/bi049768c>.
- [8] I.J. Schalk, G.L.A. Mislin, Bacterial iron uptake pathways: gates for the import of bactericide compounds, *J. Med. Chem.* 60 (2017) 4573–4576, <https://doi.org/10.1021/acs.jmedchem.7b00554>.
- [9] M. Sandy, A. Butler, Microbial iron acquisition: marine and terrestrial siderophores, *Chem. Rev.* 109 (2009) 4580–4595, <https://doi.org/10.1021/cr9002787>.
- [10] G.S. Tillotson, Trojan horse antibiotics—A novel way to circumvent gram-negative bacterial resistance? *Infect. Dis. Res. Treat.* 9 (2016) 45–52, <https://doi.org/10.4137/IDRT.S31567>.
- [11] K. Dhusia, A. Bajpai, P.W. Ramteke, Overcoming antibiotic resistance: is siderophore Trojan horse conjugation an answer to evolving resistance in microbial pathogens? *J. Contr. Release* 269 (2018) 63–87, <https://doi.org/10.1016/j.jconrel.2017.11.001>.
- [12] A. Gorska, A. Sloderbach, M.P. Marszall, Siderophore-drug complexes: potential medicinal applications of the 'Trojan horse' strategy, *Trends Pharmacol. Sci.* 35 (2014) 442–449, <https://doi.org/10.1016/j.tips.2014.06.007>.
- [13] Y.M. Lin, M. Ghosh, P.A. Miller, U. Mollmann, M.J. Miller, Synthetic sideromycins (skepticism and optimism): selective generation of either broad or narrow spectrum Gram-negative antibiotics, *Biometals* 32 (2019) 425–451, <https://doi.org/10.1007/s10534-019-00192-6>.
- [14] M.G. Page, Siderophore conjugates, *Ann. N. Y. Acad. Sci.* 1277 (2013) 115–126, <https://doi.org/10.1111/nyas.12024>.
- [15] E.D. Brown, G.D. Wright, Antibacterial drug discovery in the resistance era, *Nature* 529 (2016) 336–343, <https://doi.org/10.1038/nature17042>.
- [16] A. Pramanik, V. Braun, Albomycin uptake via a ferric hydroxamate transport system of *Streptococcus pneumoniae* R6, *J. Bacteriol.* 188 (2006) 3878–3886, <https://doi.org/10.1128/JB.00205-06>.
- [17] A. Shazer, C.E. Felder, Y. Barda, Natural and biomimetic hydroxamic acid based siderophores, in: *PATAI'S Chemistry of Functional Groups*, 2010.
- [18] J.B. Neilands, A crystalline organo-iron pigment from a rust fungus (*Ustilago sphaerogena*), *J. Am. Chem. Soc.* 74 (1952) 4846, <https://doi.org/10.1021/ja01139a033>.
- [19] C.W. Hesseltine, C. Pidacks, A.R. Whitehill, N. Bohonos, B.L. Hutchings, J.H. William, Coprogen, a new growth factor for Coprophilic Fungi, *Communications to the editor* 74 (1952) 1362, <https://doi.org/10.1021/ja01125a525>.
- [20] T. Emery, J.B. Neilands, Contribution to the structure of the ferrichrome compounds: characterization of the acyl moieties of the hydroxamate functions, *J. Am. Chem. Soc.* 82 (1960) 3658–3662, <https://doi.org/10.1021/ja01499a047>.
- [21] H. Bickel, G.E. Hall, W. Keller-Schierlein, V. Prelog, E. Vischer, A. Wettstein, 261. Stoffwechselprodukte von Actinomyceten über die Konstitution von Ferrioxamin B 27. Mitteilung, *Helv. Chim. Acta* XLIII (1960) 2129–2138, <https://doi.org/10.1002/hlca.19600430732>.
- [22] H. Heli, S. Mirtorabi, K. Karimian, Advances in iron chelation: an update, *Expert Opin. Ther. Pat.* 21 (2011) 819–856, <https://doi.org/10.1517/13543776.2011.569493>.
- [23] D.M. Reynolds, A. Schatz, S. Waksman, Grisein, a new antibiotic produced by a strain of *Streptomyces griseus*, *Proc. Soc. Exp. Biol. Med.* 64 (1947) 50–54, <https://doi.org/10.3181/00379727-64-15695>.
- [24] G. Benz, L. Schroder, J. Kurz, C. Wiinsche, W. Karl, G. Steffens, J. Pfitzner, D. Schmidt, Constitution of the deferrirform of the albomycins δ 1, δ 2 and ϵ , *Angew. Chem. Int. Ed. Engl.* 21 (1982) 527–528, <https://doi.org/10.1002/anie.198205271>.

- [25] J.M. Roosenberg II, Y. Lin, Y. Lu, M.J. Miller, Studies and syntheses of siderophores, microbial iron chelators, and analogs as potential drug delivery agents, *Curr. Med. Chem.* 7 (2000) 159–197, <https://doi.org/10.2174/0929867003375353>.
- [26] E. Mawji, M. Gledhill, J.A. Milton, G.A. Tarran, S. Ussher, A. Thompson, G.A. Wolff, P.J. Worsfold, E.P. Achterberg, Hydroxamate siderophores: occurrence and importance in the Atlantic Ocean, *Environ. Sci. Technol.* 42 (2008) 8675–8680, <https://doi.org/10.1021/es801884r>.
- [27] A. Butler, R.M. Theisen, Iron(III)-siderophore coordination chemistry: reactivity of marine siderophores, *Coord. Chem. Rev.* 254 (2010) 288–296, <https://doi.org/10.1016/j.ccr.2009.09.010>.
- [28] J.S. Martinez, J.N. Carter-Franklin, E.L. Mann, J.D. Martin, M.G. Haygood, A. Butler, Structure and membrane affinity of a suite of amphiphilic siderophores produced by a marine bacterium, *Proc. Natl. Acad. Sci.* 100 (2003) 3754–3759, <https://doi.org/10.1073/pnas.0637444100>.
- [29] J.M. Vraspir, P.D. Holt, A. Butler, Identification of new members within suites of amphiphilic marine siderophores, *Biometals* 24 (2011) 85–92, <https://doi.org/10.1007/s10534-010-9378-1>.
- [30] J.S. Martinez, G.P. Zhang, P.D. Holt, H.T. Jung, C.J. Carrano, M.G. Haygood, A. Butler, Self-assembling amphiphilic siderophores from marine bacteria, *Science* 287 (2000) 1245–1247, <https://doi.org/10.1126/science.287.5456.1245>.
- [31] J.S. Martinez, A. Butler, Marine amphiphilic siderophores: marinobactin structure, uptake, and microbial partitioning, *J. Inorg. Biochem.* 101 (2007) 1692–1698, <https://doi.org/10.1016/j.jinorgbio.2007.07.007>.
- [32] J.M. Gauglitz, A. Butler, Amino acid variability in the peptide composition of a suite of amphiphilic peptide siderophores from an open ocean *Vibrio* species, *J. Biol. Inorg. Chem.* 18 (2013) 489–497, <https://doi.org/10.1007/s00775-013-0995-3>.
- [33] S. Lautru, R.J. Deeth, L.M. Bailey, G.L. Challis, Discovery of a new peptide natural product by *Streptomyces coelicolor* genome mining, *Nat. Chem. Biol.* 1 (2005) 265–269, <https://doi.org/10.1038/nchembio731>.
- [34] I. Nakamura, S. Yoshimura, T. Masaki, S. Takase, K. Ohsumi, M. Hashimoto, S. Furukawa, A. Fujie, ASP2397: a novel antifungal agent produced by *Acremonium persicinum* MF-347833, *J. Antibiot.* 70 (2017) 45–51, <https://doi.org/10.1038/ja.2016.107>.
- [35] M. Luo, R. Zang, X. Wang, Z. Chen, X. Song, J. Ju, H. Huang, Natural hydroxamate-containing siderophore acremonpeptides A–D and an aluminum complex of acremonpeptide D from the marine-derived *Acremonium persicinum* SCSIO 115, *J. Nat. Prod.* 82 (2019) 2594–2600, <https://doi.org/10.1021/acs.jnatprod.9b00545>.
- [36] K.-F. Mo, Z. Dai, D.S. Wunschel, Production and characterization of desmalo-chrome relative binding affinity for uranyl ions in relation to other siderophores, *J. Nat. Prod.* 79 (2016) 1492–1499, <https://doi.org/10.1021/acs.jnatprod.5b00933>.
- [37] S. Kodani, H. Komaki, M. Suzuki, F. Kobayakawa, H. Hemmi, Structure determination of a siderophore peucechelins from *Streptomyces peucetius*, *Biometals* 28 (2015) 791–801, <https://doi.org/10.1007/s10534-015-9866-4>.
- [38] T. Heine, M. Mehnert, R. Schwabe, D. Tischler, Thermochelin, a hydroxamate siderophore from *Thermocristum agreste* DSM 44070, *Solid State Phenom.* 262 (2017) 501–504, <https://doi.org/10.4028/www.scientific.net/SSP.262.501>.
- [39] L. Robbel, T.A. Knappe, U. Linne, X. Xie, M.A. Marahiel, Erythrochelin–a hydroxamate-type siderophore predicted from the genome of *Saccharopolyspora erythraea*, *FEBS J.* 277 (2010) 663–676, <https://doi.org/10.1111/j.1742-4658.2009.07512.x>.
- [40] S.B. Krasnoff, I. Keresztes, B.G.G. Donzelli, D.M. Gibson, Metachelins, mannosylated and N-oxidized coprogen-type siderophores from *Metarhizium robertsii*, *J. Nat. Prod.* 77 (2014) 1685–1692, <https://doi.org/10.1021/np500300s>.
- [41] S.B. Krasnoff, K.J. Howe, M.L. Heck, B.G.G. Donzelli, Siderophores from the entomopathogenic fungus *Beauveria bassiana*, *J. Nat. Prod.* 83 (2020) 296–304, <https://doi.org/10.1021/acs.jnatprod.9b00698>.
- [42] P. Kalansuriya, M. Quezada, B.P. Espósito, R.J. Capon, Talarazines A–E: non-cytotoxic iron(III) chelators from an Australian mud dauber wasp-associated fungus, *Talaromyces* sp. (CMB-W045), *J. Nat. Prod.* 80 (2017) 609–615, <https://doi.org/10.1021/acs.jnatprod.6b00889>.
- [43] Q. Wu, R.W. Deering, G. Zhang, B. Wang, X. Li, J. Sun, J. Chen, H. Zhang, D.C. Rowley, H. Wang, Albisporachelin, a new hydroxamate type siderophore from the deep ocean sediment-derived actinomycete *amycolatopsisalbispora* WP1(T), *Mar. Drugs* 16 (2018) 199, <https://doi.org/10.3390/md16060199>.
- [44] S. Kodani, F. Kobayakawa, M. Hidaki, Isolation and structure determination of new siderophore tsukubachelin B from *Streptomyces* sp. TM-74, *Nat. Prod. Res.* 27 (2013) 775–781, <https://doi.org/10.1080/14786419.2012.698412>.
- [45] S. Kodani, H. Komaki, M. Suzuki, H. Hemmi, M. Ohnishi-Kameyama, Isolation and structure determination of new siderophore albachelin from *Amycolatopsis alba*, *Biometals* 28 (2015) 381–389, <https://doi.org/10.1007/s10534-015-9842-z>.
- [46] S. Kodani, J. Bicz, L. Song, R.J. Deeth, M. Ohnishi-Kameyama, M. Yoshida, K. Ochi, G.L. Challis, Structure and biosynthesis of scabichelin, a novel tris-hydroxamate siderophore produced by the plant pathogen *Streptomyces scabies* 87.22, *Org. Biomol. Chem.* 11 (2013) 4686–4694, <https://doi.org/10.1039/c3ob40536b>.
- [47] W. Wright, J. Little, F. Liu, R. Chakraborty, Isolation and structural identification of the trihydroxamate siderophore vicibactin and its degradative products from *Rhizobium leguminosarum* ATCC 14479 bv, *trifolii*, *BioMetals* 26 (2013) 271–283, <https://doi.org/10.1007/s10534-013-9609-3>.
- [48] W. Wang, Z. Chi, G. Liu, M.A. Buzdar, Z. Chi, Q. Gu, Chemical and biological characterization of siderophore produced by the marine-derived *Aureobasidium pullulans* HN6.2 and its antibacterial activity, *Biometals* 22 (2009) 965, <https://doi.org/10.1007/s10534-009-9248-x>.
- [49] K. Haselwandter, V. Passler, S. Reiter, D.G. Schmid, G. Nicholson, P. Hentschel, K. Albert, G. Winkelmann, Basidiochrome – a novel siderophore of the orchidaceous mycorrhizal fungi *ceratobasidium* and *rhizoctonia* spp, *Biometals* 19 (2006) 335–343, <https://doi.org/10.1007/s10534-006-6986-x>.
- [50] S. Kokubo, K. Suenaga, C. Shinohara, T. Tsuji, D. Uemura, Structures of amamistatins A and B, novel growth inhibitors of human tumor cell lines from an actinomycete, *Tetrahedron Lett.* 40 (1999) 1945–1948, [https://doi.org/10.1016/S0040-4039\(99\)00050-7](https://doi.org/10.1016/S0040-4039(99)00050-7).
- [51] S. Kokubo, K. Suenaga, C. Shinohara, T. Tsujib, D. Uemura, Structures of amamistatins A and B, novel growth inhibitors of human tumor cell lines from *Nocardia asteroides*, *Tetrahedron* 56 (2000) 6435–6440, [https://doi.org/10.1016/S0040-4020\(00\)00591-3](https://doi.org/10.1016/S0040-4020(00)00591-3).
- [52] M. Tsuda, M. Yamakawa, S. Oka, Y. Tanaka, Y. Hoshino, Y. Mikami, A. Sato, H. Fujiwara, Y. Ohizumi, J. Kobayashi, Brasilibactin A, a cytotoxic compound from actinomycete *Nocardia brasiliensis*, *J. Nat. Prod.* 68 (2005) 462–464, <https://doi.org/10.1021/np0496385>.
- [53] Y. Ikeda, H. Nonaka, T. Furumai, H. Onaka, Y. Igarashi, Nocardimicins A, B, C, D, E, and F, siderophores with muscarinic M3 receptor inhibiting activity from *Nocardia* sp. TP-a0674, *J. Nat. Prod.* 68 (2005) 1061–1065, <https://doi.org/10.1021/np050091j>.
- [54] Y. Ikeda, T. Furumai, Y. Igarashi, Nocardimicins G, H and I, siderophores with muscarinic M3 receptor binding inhibitory activity from *Nocardia nova* JCM 6044, *J. Antibiot.* 58 (2005) 566–572, <https://doi.org/10.1038/ja.2005.77>.
- [55] K. Schneider, I. Rose, S. Vinkeswary, A.L. Jones, M. Goodfellow, G. Nicholson, W. Beil, R.D. Süßmuth, H.-P. Fiedler, Nocardichelins A and B, siderophores from *Nocardia* strain acta 3026, *J. Nat. Prod.* 70 (2007) 932–935, <https://doi.org/10.1021/np060612i>.
- [56] J.-H. Jang, K. Kanoh, K. Adachi, S. Matsuda, Y. Shizuri, Tenacibactins A–D, hydroxamate siderophores from a marine-derived bacterium, *tenacibaculum* sp. A4K-17, *J. Nat. Prod.* 70 (2007) 563–566, <https://doi.org/10.1021/np060502b>.
- [57] F. Maglangit, M.H. Tong, M. Jaspars, K. Kyeremeh, H. Deng, Legonoxamines A–B, two new hydroxamate siderophores from the soil bacterium, *Streptomyces* sp. MA37, *Tetrahedron Lett.* 60 (2019) 75–79, <https://doi.org/10.1016/j.tetlet.2018.11.063>.
- [58] G. Winkelmann, D.G. Schmid, G. Nicholson, G. Jung, D.J. Colquhoun, Bisuca-berin – a dihydroxamate siderophore isolated from *Vibrio salmonicida*, an important pathogen of farmed *Atlantic salmon* (*Salmo salar*), *Biometals* 15 (2002) 153–160, <https://doi.org/10.1023/A:1015206419613>.
- [59] T. Böttcher, J. Clardy, A chimeric siderophore halts swarming *Vibrio*, *Angew. Chem. Int. Ed.* 53 (2014) 3510–3513, <https://doi.org/10.1002/anie.201310729>.
- [60] M. Bosello, L. Robbel, U. Linne, X. Xie, M.A. Marahiel, Biosynthesis of the siderophore rhodochelin requires the coordinated expression of three independent gene clusters in *Rhodococcus jostii* RHA1, *J. Am. Chem. Soc.* 133 (2011) 4587–4595, <https://doi.org/10.1021/ja1109453>.
- [61] H.K. Zane, A. Butler, Isolation, structure elucidation, and iron-binding properties of lystabactins, siderophores isolated from a marine *pseudoalteromonas* sp., *J. Nat. Prod.* 76 (2013) 648–654, <https://doi.org/10.1021/np3008655>.
- [62] S. Dhungana, R. Michalczyk, H. Boukhalfa, J.G. Lack, A.T. Koppisch, J.M. Fairlee, M.T. Johnson, C.E. Ruggiero, S.G. John, M.M. Cox, C.C. Browder, J.H. Forsythe, L.A. Vanderberg, M.P. Neu, L.E. Hersman, Purification and characterization of rhodobactin: a mixed ligand siderophore from *Rhodococcus rhodochrous* strain OFS, *Biometals* 20 (2007) 853–867, <https://doi.org/10.1007/s10534-006-9079-y>.
- [63] M. Bosello, M. Zeyadi, F.I. Kraas, U. Linne, X. Xie, M.A. Marahiel, Structural characterization of the heterobactin siderophores from *Rhodococcus erythropolis* PR4 and elucidation of their biosynthetic machinery, *J. Nat. Prod.* 76 (2013) 2282–2290, <https://doi.org/10.1021/np4006579>.
- [64] A. Mukai, H. Komaki, M. Takagi, K. Shin-ya, Novel siderophore, JBIR-16, isolated from *Nocardia tenerifensis* NBRC 101015, *J. Antibiot.* 62 (2009) 601–603, <https://doi.org/10.1038/ja.2009.84>.
- [65] E.J. Dimise, P.F. Widboom, S.D. Bruner, Structure elucidation and biosynthesis of fuscachelins, peptide siderophores from the moderate thermophile *Thermobifida fusca*, *Proc. Natl. Acad. Sci.* 105 (2008) 15311–15316, <https://doi.org/10.1073/pnas.0805451105>.
- [66] M. Sandy, A. Han, J. Blunt, M. Munro, M. Haygood, A. Butler, Vanchrobactin and anguibactin siderophores produced by *Vibrio* sp. DS40M4, *J. Nat. Prod.* 73 (2010) 1038–1043, <https://doi.org/10.1021/np900750g>.
- [67] A. Proschak, P. Lubuta, P. Grun, F. Lohr, G. Wilharm, V. De Berardinis, H.B. Bode, Structure and biosynthesis of fimsbactins A–F, siderophores from *Acinetobacter baumannii* and *Acinetobacter baylyi*, *ChemBioChem* 14 (2013) 633–638, <https://doi.org/10.1002/cbic.201200764>.
- [68] C. Kurth, S. Schieferdecker, K. Athanasopoulou, I. Seccareccia, M. Nett, Vari-ochelins, lipopeptide siderophores from *Variovorax boronicumulans* discovered by genome mining, *J. Nat. Prod.* 79 (2016) 865–872, <https://doi.org/10.1021/acs.jnatprod.5b00932>.
- [69] A.W. Robertson, N.G. McCarville, L.W. MacIntyre, H. Correa, B. Haulti,

- D.H. Marchbank, R.G. Kerr, Isolation of imaobactin, an amphiphilic siderophore from the arctic marine bacterium *variovorax* species RKM285, *J. Nat. Prod.* 81 (2018) 858–865, <https://doi.org/10.1021/acs.jnatprod.7b00943>.
- [70] C.W. Johnston, M.A. Skinner, M.A. Wyatt, X. Li, M.R.M. Ranieri, L. Yang, D.L. Zechel, B. Ma, N.A. Magarvey, An automated Genomes-to-Natural Products platform (GNP) for the discovery of modular natural products, *Nat. Commun.* 6 (2015) 8421, <https://doi.org/10.1038/ncomms9421>.
- [71] V.V. Homann, M. Sandy, J.A. Tincu, A.S. Templeton, B.M. Tebo, A. Butler, Loihichelins A–F, a suite of amphiphilic siderophores produced by the marine bacterium H. LOB-5, *J. Nat. Prod.* 72 (2009) 884–888, <https://doi.org/10.1021/np800640h>.
- [72] C.D. Hardy, A. Butler, Ambiguity of NRPS structure predictions: four bidentate chelating groups in the siderophore pacifibactin, *J. Nat. Prod.* 82 (2019) 990–997, <https://doi.org/10.1021/acs.jnatprod.8b01073>.
- [73] F. Rosconi, D. Davy, V. Martinez, M. Martinez, J.A. Abin-Carriquiry, H. Zane, A. Butler, E.M. de Souza, E. Fabiano, Identification and structural characterization of serobactins, a suite of lipopeptide siderophores produced by the grass endophyte *Herbaspirillum seropedicae*, *Environ. Microbiol.* 15 (2013) 916–927, <https://doi.org/10.1111/1462-2920.12075>.
- [74] M.F. Kreuzer, H. Kage, M. Nett, Structure and biosynthetic assembly of cupriachelin, a photoreactive siderophore from the bioplastic producer *Cupriavidus necator* H16, *J. Am. Chem. Soc.* 134 (2012) 5415–5422, <https://doi.org/10.1021/ja300620z>.
- [75] J.R. Carmichael, H. Zhou, A. Butler, A suite of asymmetric citrate siderophores isolated from a marine *Shewanella* species, *J. Inorg. Biochem.* 198 (2019) 110736, <https://doi.org/10.1016/j.jinorgbio.2019.110736>.
- [76] J.D. Martin, Y. Ito, V.V. Homann, M.G. Haygood, A. Butler, Structure and membrane affinity of new amphiphilic siderophores produced by *Ochrobactrum* sp. SP18, *J. Biol. Inorg. Chem.* 11 (2006) 633–641, <https://doi.org/10.1007/s00775-006-0112-y>.
- [77] Y. Ito, A. Butler, Structure of synechobactins, new siderophores of the marine cyanobacterium *Synechococcus* sp. PCC 7002, *Limnol. Oceanogr.* 50 (2005) 1918–1923, <https://doi.org/10.4319/lo.2005.50.6.1918>.
- [78] E.P. Storey, R. Boghazian, J.L. Little, D.W. Lowman, R. Chakraborty, Characterization of 'Schizokinen', a dihydroxamate-type siderophore produced by *Rhizobium leguminosarum* IARI 917, *Biometals* 19 (2006) 637–649, <https://doi.org/10.1007/s10534-006-9001-7>.
- [79] W.F. Penwell, N. DeGrace, S. Tentarelli, L. Gauthier, C.M. Gilbert, B.A. Arivett, A.A. Miller, T.F. Durand-Reville, C. Joubnan, L.A. Actis, Discovery and characterization of new hydroxamate siderophores, baumannoferrin A and B, produced by *Acinetobacter baumannii*, *ChemBioChem* 16 (2015) 1896–1904, <https://doi.org/10.1002/cbic.201500147>.
- [80] S. Hoshino, M. Ozeki, T. Awakawa, H. Morita, H. Onaka, I. Abe, Catenulobactins A and B, heterocyclic peptides from culturing *catenuloplanes* sp. with a mycolic acid-containing bacterium, *J. Nat. Prod.* 81 (2018) 2106–2110, <https://doi.org/10.1021/acs.jnatprod.8b00261>.
- [81] T.W. Giessen, K.B. Franke, T.A. Knappe, F.I. Kraas, M. Bosello, X. Xie, U. Linne, M.A. Marahiel, Isolation, structure elucidation, and biosynthesis of an unusual hydroxamic acid ester-containing siderophore from *Actinosynnema mirum*, *J. Nat. Prod.* 75 (2012) 905–914, <https://doi.org/10.1021/np300046k>.
- [82] R. Hermenau, K. Ishida, S. Gama, B. Hoffmann, M. Pfeifer-Leeg, W. Plass, J.F. Mohr, T. Wichard, H.-P. Saluz, C. Hertweck, Gramibactin is a bacterial siderophore with a diazeniumdiolate ligand system, *Nat. Chem. Biol.* 14 (2018) 841–843, <https://doi.org/10.1038/s41589-018-0101-9>.
- [83] A. Pesic, B. Steinhaus, S. Kemper, J. Nachtigall, H.J. Kutzner, G. Höfle, R.D. Süßmuth, Isolation and structure elucidation of the nucleoside antibiotic strepturidin from *Streptomyces albus* DSM 40763, *J. Antibiot.* 67 (2014) 471–477, <https://doi.org/10.1038/ja.2014.16>.
- [84] B. Winterberg, S. Uhlmann, U. Linne, F. Lessing, M.A. Marahiel, R. Eichhorn, R. Kahmann, J. Schirawski, Elucidation of the complete ferrichrome A biosynthetic pathway in *Ustilago maydis*, *Mol. Microbiol.* 75 (2010) 1260–1271, <https://doi.org/10.1111/j.1365-2958.2010.07048.x>.
- [85] E.K. Dolence, C.-E. Lin, M.J. Miller, Synthesis and siderophore activity of albomycin-like peptides derived from N5-acetyl-N5-hydroxy-L-ornithine, *J. Med. Chem.* 34 (1991) 956–968, <https://doi.org/10.1021/jm00107a013>.
- [86] A. Ganeshpurkar, D. Kumar, S.K. Singh, Strategies for the synthesis of hydroxamic acids, *Curr. Org. Synth.* 15 (2018) 154–165, <https://doi.org/10.2174/1570179414666170614123508>.
- [87] Y. Lin, M.J. Miller, Practical synthesis of hydroxamate-derived siderophore components by an indirect oxidation method and syntheses of a DIG-siderophore conjugate and a biotin-siderophore conjugate, *J. Org. Chem.* 64 (1999) 7451–7458, <https://doi.org/10.1021/jo990769y>.
- [88] R. Mashiach, M.M. Meijler, Total synthesis of pyoverdinin D, *Org. Lett.* 15 (2013) 1702–1705, <https://doi.org/10.1021/ol400490s>.
- [89] Z. Lin, X. Xu, S. Zhao, X. Yang, J. Guo, Q. Zhang, C. Jing, S. Chen, Y. He, Total synthesis and antimicrobial evaluation of natural albomycins against clinical pathogens, *Nat. Commun.* 9 (2018) 3445, <https://doi.org/10.1038/s41467-018-05821-1>.
- [90] Y. Isowa, M. Ohmori, H. Kurita, Total synthesis of ferrichrome, *Bull. Chem. Soc. Jpn.* 47 (1974) 215–220, <https://doi.org/10.1246/bcsj.47.215>.
- [91] W. Keller - Schierlein, B. Maurer, 67. Metabolic products of microorganisms Synthesis of ferrichrome; Part 2, *Helv. Chim. Acta* 52 (1969) 603–610, <https://doi.org/10.1002/hlca.19690520307>.
- [92] P. Cherkupally, S. Ramesh, T. Govender, H.G. Kruger, B.G. de la Torre, F. Albericio, An efficient solid-phase strategy for total synthesis of naturally occurring amphiphilic marine siderophores: amphibactin-T and moanachelin ala-B, *Org. Biomol. Chem.* 13 (2015) 4760–4768, <https://doi.org/10.1039/c5ob000100e>.
- [93] R.J. Bergeron, J.J. Pegram, An efficient total synthesis of desferrioxamine B, *J. Org. Chem.* 53 (1988) 555–558, <https://doi.org/10.1021/jo00249a001>.
- [94] R. Bergem, J. McManis, The total synthesis of Bisucaberin, *Tetrahedron* 45 (1989) 4939–4944, [https://doi.org/10.1016/S0040-4020\(01\)81074-7](https://doi.org/10.1016/S0040-4020(01)81074-7).
- [95] R. Bergeron, J. McManis, P. Perumal, S. Algee, The total synthesis of alcaligin, *J. Org. Chem.* 56 (1991) 5560–5563, <https://doi.org/10.1021/jo00019a017>.
- [96] S. Zhang, L.M. De Leon Rodriguez, R. Huang, I.K.H. Leung, P.W.R. Harris, M.A. Brimble, Total synthesis of the proposed structure of talarolide A, *Org. Biomol. Chem.* 16 (2018) 5286–5293, <https://doi.org/10.1039/c8ob01230j>.
- [97] Y. Ye, M. Liu, J. Kao, G.R. Marshall, Peptide-bond modification for metal coordination: peptides containing two hydroxamate groups, *Biopolymers* 71 (2003) 489–515, <https://doi.org/10.1002/bip.10471>.
- [98] Y. Ye, M. Liu, J.L. Kao, G.R. Marshall, Novel trihydroxamate-containing peptides: design, synthesis, and metal coordination, *Biopolymers* 84 (2006) 472–489, <https://doi.org/10.1002/bip.20532>.
- [99] M.P. Sarnowski, J. Del Valle, N-Hydroxy peptides: solid-phase synthesis and β -sheet propensity, *Org. Biomol. Chem.* (2020) 3690–3696, <https://doi.org/10.1039/d0ob00664e>.
- [100] R. Kachadourian, S. Chuilon, C. Mérienne, G. Kunesch, A. Deroussent, A new total synthesis of ferrioxamine E through metal-templated cyclic trimerization, *Supramol. Chem.* 8 (1997) 301–308, <https://doi.org/10.1080/10610279708034949>.
- [101] J.M. Roosenberg, M.J. Miller, Total synthesis of the siderophore danoxamine, *J. Org. Chem.* 65 (2000) 4833–4838, <https://doi.org/10.1021/jo000050m>.
- [102] A.L. Crumbliss, J.M. Harrington, Iron Sequestration by Small Molecules: Thermodynamic and Kinetic Studies of Natural Siderophores and Synthetic Model Compounds, 2009, pp. 179–250.
- [103] R.C. Scarrow, D.J. Ecker, C. Ng, S. Liu, K.N. Raymond, Iron(III) coordination chemistry of linear dihydroxyserine compounds derived from enterobactin, *Inorg. Chem.* 30 (1991) 900–906, <https://doi.org/10.1021/ic00005a007>.
- [104] G. Anderegg, F.L. Eplattener, G. Schwarzenbach, 156. Hydroxamatkomplexe (III). Eisen(III)-Austausch zwischen Sideraminen und Komplexonen Diskussion der Bildungskonstanten der Hydroxamatkomplexe, *Helv. Chim. Acta* 156 (1963) 1409–1422, <https://doi.org/10.1002/hlca.19630460436>.
- [105] S. Dhungana, S. Heggemann, P. Gebhardt, U. Mollmann, A.L. Crumbliss, Fe(III) coordination properties of a new saccharide-based exocyclic trihydroxamate analogue of ferrichrome, *Inorg. Chem.* 42 (2003) 42–50, <https://doi.org/10.1021/ic025647u>.
- [106] S. Dhungana, J.M. Harrington, P. Gebhardt, U. Mollmann, A.L. Crumbliss, Iron chelation equilibria, redox, and siderophore activity of a saccharide platform ferrichrome analogue, *Inorg. Chem.* 46 (2007) 8362–8371, <https://doi.org/10.1021/ic070158l>.
- [107] J.M. Harrington, G. Winkelmann, K. Haselwandter, A.L. Crumbliss, Fe(III)-complexes of the tripodal trihydroxamate siderophore basidiochrome: potential biological implications, *J. Inorg. Biochem.* 105 (2011) 1670–1674, <https://doi.org/10.1016/j.jinorgbio.2011.08.010>.
- [108] G. Zhang, S.A. Amin, F.C. Kupper, P.D. Holt, C.J. Carrano, A. Butler, Ferric stability constants of representative marine siderophores: marinobactins, aquachelins, and petrobactin, *Inorg. Chem.* 48 (2009) 11466–11473, <https://doi.org/10.1021/ic901739m>.
- [109] S.S. Ali, N.N. Vidhale, Bacterial siderophore and their application: a review, *Int. J. Curr. Microbiol. Appl. Sci.* 2 (2013) 303–312.
- [110] M. Petrik, C. Zhai, H. Haas, C. Decristoforo, Siderophores for molecular imaging applications, *Clin. Transl. Imag.* 5 (2017) 15–27, <https://doi.org/10.1007/s40336-016-0211-x>.
- [111] X. Hu, J. Zhu, S. Srivathsan, D. Pei, Peptidyl hydroxamic acids as methionine aminopeptidase inhibitors, *Biorg. Med. Chem. Lett.* 14 (2004) 77–79, <https://doi.org/10.1016/j.bmcl.2003.10.031>.
- [112] T.A. Wenczewicz, M.J. Miller, Sideromycins as pathogen-targeted antibiotics, *Int. Antibacterials*, 2017, pp. 151–183.
- [113] M. Taouai, K. Chakroun, R. Sommer, G. Michaud, D. Giacalone, M.A. Ben Maouia, A. Vallin-Butruille, D. Mathiron, R. Abidi, T. Darbre, P.J. Cragg, C. Mullie, J.L. Reymond, G.A. O'Toole, M. Benazza, Glycocluster tetrahydroxamic acids exhibiting unprecedented inhibition of *Pseudomonas aeruginosa* biofilms, *J. Med. Chem.* 62 (2019) 7722–7738, <https://doi.org/10.1021/acs.jmedchem.9b00481>.
- [114] M. Hannauer, Y. Barda, G.L. Mislin, A. Shanzer, I.J. Schalk, The ferrichrome uptake pathway in *Pseudomonas aeruginosa* involves an iron release mechanism with acylation of the siderophore and recycling of the modified desferrichrome, *J. Bacteriol.* 192 (2010) 1212–1220, <https://doi.org/10.1128/JB.01539-09>.
- [115] R. Nudelman, O. Ardon, Y. Hadar, Y. Chen, J. Libman, A. Shanzer, Modular fluorescent-labeled siderophore analogues, *J. Med. Chem.* 41 (1998) 1671–1678, <https://doi.org/10.1021/jm970581b>.
- [116] I. Dayan, J. Libman, Y. Agi, A. Shanzer, Chiral siderophore analogs: ferrichrome, *Inorg. Chem.* 32 (1993) 1467–1475, <https://doi.org/10.1021/ic00060a024>.
- [117] F.A. Kuehl, M.N. Bishop, L. Chaiet, K. Folkers, Isolation and some chemical properties of grisein, *J. Am. Chem. Soc.* 73 (1951) 1770–1773, <https://doi.org/10.1021/ja01148a099>.
- [118] G.F. Gause, Recent studies on Albomycin, a new antibiotic, *Br. Med. J.* 2 (1955) 1177–1179, <https://doi.org/10.1136/bmj.2.4949.1177>.

- [119] E.O. Stapley, R.E. Ormond, Similarity of albomycin and grisein, *Science* 125 (1957) 587–589, <https://doi.org/10.1126/science.125.3248.587>.
- [120] A. Hartmann, H. Fiedler, V. Braun, Uptake and conversion of the antibiotic albomycin *Escherichia coli* K-12, *Eur. J. Biochem.* 99 (1979) 517–524, <https://doi.org/10.1111/j.1432-1033.1979.tb13283.x>.
- [121] L. Vertesy, W. Aretz, H.-W. Fehlhaber, H. Kogler, 3. Salmycin A-D, Antibiotika aus *Streptomyces violaceus*, DSM 8286, mit Siderophor-Aminoglycosid-Struktur, *Helv. Chim. Acta* 78 (1995) 46–60, <https://doi.org/10.1002/hlca.19950780105>.
- [122] A.L. Stefanska, M. Fulston, C. Houge-Frydrych, J. Jones, S.R. Warr, A potent seryl tRNA synthetase inhibitor SB-217452 isolated from a *Streptomyces* species, *J. Antibiot.* 53 (2000) 1346–1353, <https://doi.org/10.7164/antibiotics.53.1346>.
- [123] P. Ding, C.E. Schous, M.J. Miller, Design and synthesis of a novel protected mixed ligand siderophore, *Tetrahedron Lett.* 49 (2008) 2306–2310, <https://doi.org/10.1016/j.tetlet.2008.02.007>.
- [124] Cefiderocol approval letter. https://www.accessdata.fda.gov/drugsatfda_docs/nda/2019/209445Orig1s000ltr.pdf. (Accessed 22 August 2020).
- [125] Y. Saisho, T. Katsube, S. White, H. Fukase, J. Shimada, Pharmacokinetics, safety, and tolerability of cefiderocol, a novel siderophore cephalosporin for gram-negative bacteria, in healthy subjects, *Antimicrob. Agents Chemother.* (2018) 62, <https://doi.org/10.1128/AAC.02163-17>.
- [126] E.K. Dolence, A.A. Minnick, M.J. Miller, N5-Acetyl-N5-hydroxy-L-ornithine-Derived siderophore-carbacephalosporin & lactam conjugates: iron transport mediated drug delivery, *J. Med. Chem.* 33 (1990) 464–479, <https://doi.org/10.1021/jm00164a001>.
- [127] A. Brochu, N. Brochu, T.J. Nicas, T.R. Parr Jr., A.A. Minnick Jr., E.K. Dolence, J.A. McKee, M.J. Miller, M.C. Lavoie, F. Malouin, Modes of action and inhibitory activities of new siderophore-beta-lactam conjugates that use specific iron uptake pathways for entry into bacteria, *Antimicrob. Agents Chemother.* 36 (1992) 2166–2175, <https://doi.org/10.1128/aac.36.10.2166>.
- [128] E.K. Dolence, A.A. Minnick, C.-E. Lin, M.J. Miller, Synthesis and siderophore and antibacterial activity of N5-acetyl-N5-hydroxy-L-ornithine-Derived siderophore-lactam conjugates: iron-transport-mediated drug delivery, *J. Med. Chem.* 34 (1991) 968–978, <https://doi.org/10.1021/jm00107a014>.
- [129] A. Pandey, C. Savino, S.H. Ahn, Z. Yang, S.G. Van Lanen, E. Boros, Theranostic gallium siderophore ciprofloxacin conjugate with broad spectrum antibiotic potency, *J. Med. Chem.* 62 (2019) 9947–9960, <https://doi.org/10.1021/acs.jmedchem.9b01388>.
- [130] Y.-M. Lin, P. Helquist, M.J. Miller, Synthesis and biological evaluation of a siderophore-virginiamicin conjugate, *Synthesis* S1 (1999) 1510–1514, <https://doi.org/10.1055/s-1999-3655>.
- [131] M. Ghosh, M.J. Miller, Iron transport-mediated drug delivery: synthesis and biological evaluation of cyanuric acid-based siderophore analogs and -Lactam conjugates, *J. Org. Chem.* 59 (1994) 1020–1026, <https://doi.org/10.1021/jo00084a018>.
- [132] C. Ji, M.J. Miller, Chemical syntheses and in vitro antibacterial activity of two desferrioxamine B-ciprofloxacin conjugates with potential esterase and phosphatase triggered drug release linkers, *Bioorg. Med. Chem.* 20 (2012) 3828–3836, <https://doi.org/10.1016/j.bmc.2012.04.034>.
- [133] R.E. Juarez-Hernandez, P.A. Miller, M.J. Miller, Syntheses of siderophore-drug conjugates using a convergent thiol-maleimide system, *ACS Med. Chem. Lett.* 3 (2012) 799–803, <https://doi.org/10.1021/ml300150y>.
- [134] T.A. Wencewicz, T.E. Long, U. Mollmann, M.J. Miller, Trihydroxamate siderophore-fluoroquinolone conjugates are selective sideromycin antibiotics that target *Staphylococcus aureus*, *Bioconjugate Chem.* 24 (2013) 473–486, <https://doi.org/10.1021/bc300610f>.
- [135] T.A. Wencewicz, U. Mollmann, T.E. Long, M.J. Miller, Is drug release necessary for antimicrobial activity of siderophore-drug conjugates? Syntheses and biological studies of the naturally occurring salmycin “Trojan Horse” antibiotics and synthetic desferrioxamine-antibiotic conjugates, *Biomaterials* 22 (2009) 633–648, <https://doi.org/10.1007/s10534-009-9218-3>.
- [136] S. Wittmann, M. Schnabelrauch, I. Scherlitz-Hofmann, U. Möllmann, D. Ankel-Fuchs, L. Heinisch, New synthetic siderophores and their β -lactam conjugates based on diamino acids and dipeptides, *Bioorg. Med. Chem.* 10 (2002), [https://doi.org/10.1016/s0968-0896\(02\)00044-5](https://doi.org/10.1016/s0968-0896(02)00044-5), 1695–1670.
- [137] A. Ghosh, M. Ghosh, C. Niu, F. Malouin, U. Moellmann, M.J. Miller, Iron transport-mediated drug delivery using mixed-ligand siderophore- β -Lactam conjugates, *Chem. Biol.* 3 (1996) 1011–1019, [https://doi.org/10.1016/S1074-5521\(96\)90167-2](https://doi.org/10.1016/S1074-5521(96)90167-2).
- [138] T.A. Wencewicz, M.J. Miller, Biscatecholate-monohydroxamate mixed ligand siderophore-carbacephalosporin conjugates are selective sideromycin antibiotics that target *Acinetobacter baumannii*, *J. Med. Chem.* 56 (2013) 4044–4052, <https://doi.org/10.1021/jm400265k>.
- [139] M. Ghosh, P.A. Miller, U. Mollmann, W.D. Claypool, V.A. Schroeder, W.R. Wolter, M. Suckow, H. Yu, S. Li, W. Huang, J. Zajicek, M.J. Miller, Targeted antibiotic delivery: selective siderophore conjugation with daptomycin confers potent activity against multidrug resistant *acinetobacter baumannii* both in vitro and in vivo, *J. Med. Chem.* 60 (2017) 4577–4583, <https://doi.org/10.1021/acs.jmedchem.7b00102>.
- [140] O. Kinzel, R. Tappe, I. Gerus, H. Budzikiewicz, The synthesis and antibacterial activity of two pyoverdinin-ampicillin conjugates, entering *Pseudomonas aeruginosa* via the pyoverdinin-mediated iron uptake pathway, *J. Antibiot.* 51 (1998) 499–507, <https://doi.org/10.7164/antibiotics.51.499>.
- [141] O. Kinzel, H. Budzikiewicz, Synthesis and biological evaluation of a pyoverdinin-blactam conjugate: a new type of arginine-specific crosslinking in aqueous solution, *J. Pept. Res.* 53 (1999) 618–625, <https://doi.org/10.1034/j.1399-3011.1999.00053.x>.
- [142] A.P. Murray, M.J. Miller, The preparation of a fully differentiated “multi-warhead” siderophore precursor, *J. Org. Chem.* 68 (2003) 191–194, <https://doi.org/10.1021/jo026391c>.
- [143] S.H. Ahn, D. Thach, B.A. Vaughn, V.M. Alford, A.N. Preston, S.T. Laughlin, E. Boros, Linear desferrioxamine-linked silicon-rhodamine antibody conjugate enables targeted multimodal imaging of HER2 in vitro and in vivo, *Mol. Pharm.* 16 (2019) 1412–1420, <https://doi.org/10.1021/acs.molpharmaceut.8b01278>.
- [144] J.Y. Wu, P. Srinivas, J.M. Pogue, Cefiderocol: a novel agent for the management of multidrug-resistant gram-negative organisms, *Infect. Dis. Ther.* 9 (2020) 17–40, <https://doi.org/10.1007/s40121-020-00286-6>.
- [145] T. Sato, K. Yamawaki, Cefiderocol: discovery, chemistry, and in vivo profiles of a novel siderophore cephalosporin, *Clin. Infect. Dis.* 69 (2019) S538–S543, <https://doi.org/10.1093/cid/ciz826>.
- [146] R.M. El-Lababidi, J.G. Rizk, Cefiderocol: a siderophore cephalosporin, *Ann. Pharmacother.* (2020), 1060028020929988, <https://doi.org/10.1177/1060028020929988>.
- [147] Cefiderocol drug label. https://www.accessdata.fda.gov/drugsatfda_docs/nda/2019/209445Orig1s000lbl.pdf. (Accessed 22 August 2020).

Chapter 2. Solid-phase synthesis of peptides containing 1-Hydroxypyridine-2-one (1,2-HOPO)

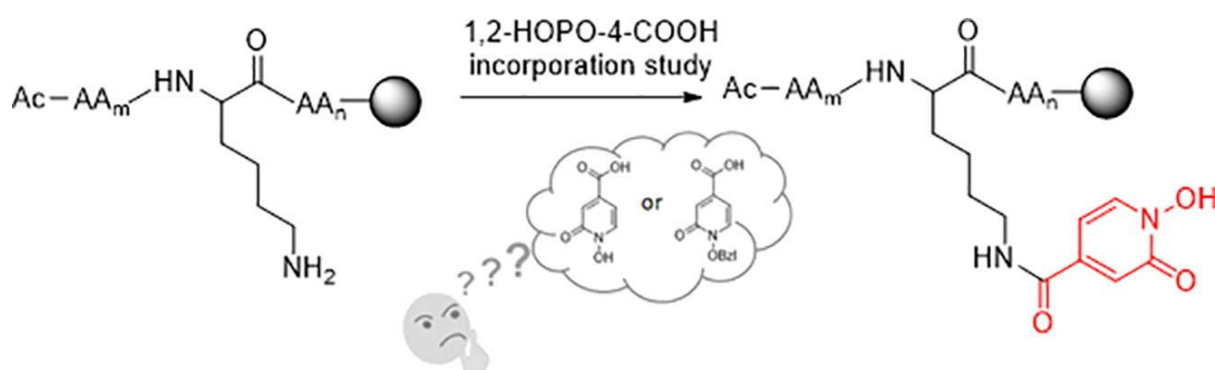
Danah Al Shaer ^{a,b}, Fernando Albericio ^{b,c,d,*}, Beatriz G. de la Torre ^{a,*}

^a KwaZulu-Natal Research Innovation and Sequencing Platform (KRISP), School of Laboratory Medicine and Medical Sciences, College of Health Sciences, University of KwaZulu-Natal, Durban 4041, South Africa

^b Peptide Science Laboratory, School of Chemistry and Physics, University of KwaZulu-Natal, Durban 4001, South Africa

^c Institute for Advanced Chemistry of Catalonia (IQAC-CSIC), 08034 Barcelona, Spain

^d CIBER-BBN, Networking Centre on Bioengineering, Biomaterials and Nanomedicine, and Department of Organic Chemistry, University of Barcelona, 08028 Barcelona, Spain



Investigating the possibility of incorporating the unprotected N-OH of HOPO in SPPS



Solid-phase synthesis of peptides containing 1-Hydroxypyridine-2-one (1,2-HOPO)

Danah Al Shaer^{a,b}, Fernando Albericio^{b,c,d,*}, Beatriz G. de la Torre^{a,*}

^a KwaZulu-Natal Research Innovation and Sequencing Platform (KRISP), School of Laboratory Medicine and Medical Sciences, College of Health Sciences, University of KwaZulu-Natal, Durban 4041, South Africa

^b Peptide Science Laboratory, School of Chemistry and Physics, University of KwaZulu-Natal, Durban 4001, South Africa

^c Institute for Advanced Chemistry of Catalonia (IQAC-CSIC), 08034 Barcelona, Spain

^d CIBER-BBN, Networking Centre on Bioengineering, Biomaterials and Nanomedicine, and Department of Organic Chemistry, University of Barcelona, 08028 Barcelona, Spain

ARTICLE INFO

Article history:

Received 22 June 2020

Revised 23 July 2020

Accepted 25 July 2020

Available online 3 August 2020

Keywords:

Siderophores

Fe(III) chelating compounds

Solid-phase peptide synthesis

Trifluoromethanesulfonic acid

Bzl protecting group

ABSTRACT

Herein a friendly method for the preparation of 1-hydroxypyridine-2-one (1,2-HOPO)-containing peptides is described. The elongation of the peptide is carried out on a solid support, using a protecting group for the ϵ -amino of the Lys that is removable in very mild conditions and that does not provoke cleavage of the peptide from the resin. Once the ϵ -amino of the Lys is released, HOPO can be incorporated using a commercially available derivative (1,2-HOPO-4-COOH), which has a carboxylic acid at position 4 of the aromatic ring. 1,2-HOPO-4-COOH can be introduced with the free *N*-hydroxyl or protected with the benzyl group. The former is recommended in many cases. If the protected derivative is to be used, the benzyl group can be removed during global deprotection and cleavage from the resin by adding trifluoromethanesulfonic acid to the cleavage cocktail.

© 2020 Elsevier Ltd. All rights reserved.

Introduction

Metals play pivotal roles in living organisms and their imbalance can cause disorders in the form of diseases.[1,2] However, metal sequestration can enhance therapy and diagnostics. In this regard, chelators are key moieties in many medicinal chemistry programs.[3] Siderophores (iron carriers in Greek) are an important class of natural chelators.[4] As their name indicates, siderophores are secreted by microorganisms to acquire nutrient Fe(III) from the surroundings under conditions of iron starvation. In nature, a large number of bidentate molecules can complex Fe(III), and a combination of three of these molecules are present in most natural siderophores. The most common bidentate moieties are catechols, α -hydroxy carboxylic derivatives, and hydroxamic acids. Thus, in some natural peptide siderophores, the hydroxamic acid structure is present into the *N*^δ-acetyl, *N*^δ-hydroxy ornithine resi-

dues. However, little attention has been paid to 1-hydroxypyridin-2-one (**1**) (1,2-HOPO) derivatives, which have found application as additives in carbodiimide-mediated peptide bond formation.[5] These 1,2-HOPO moieties are isoelectronic to both the ones found into the hydroxamic peptide siderophores and the catechols.[6–7] Furthermore, two commercially available carboxylic acid derivatives of 1,2-HOPO, in position 4 and 6 [4/6-carboxy-1-hydroxypyridin-2-one (1,2-HOPO-4-COOH (**2**)) /1,2-HOPO-6-COOH (**3**)] (Fig. 1), can facilitate its incorporation into an organic scaffold or other biological molecule of interest.

The literature provides only a few examples, mainly by Raymond [6,8–9], and Tetard[7,10] groups, in which the 1,2-HOPO-6-COOH (**3**) has been introduced into triamine-based cores in solution. In all, the *N*-hydroxyl of the 1,2-HOPO was masked with a benzyl group (Bzl) prior to the incorporation. Herein, and due to the importance of having chelator moieties to be incorporated onto different biological interesting structures such as peptides, a friendly strategy for the preparation of 1,2-HOPO-4-COOH-containing peptides is described. The method is based on the use of the conveniently Solid-Phase Peptide Synthesis strategy, paying special attention to the need of using a protecting group for the *N*-OH of the HOPO moiety. Thus, comparison of masked and unmasked *N*-OH was investigated. The presence of peptides in the chelator can be important for modulating the solubility of these

* Corresponding authors at: Peptide Science Laboratory, School of Chemistry and Physics, University of KwaZulu-Natal, Durban 4001, South Africa (F. Albericio). KwaZulu-Natal Research Innovation and Sequencing Platform (KRISP), School of Laboratory Medicine and Medical Sciences, College of Health Sciences, University of KwaZulu-Natal, Durban 4041, South Africa (B.G. de la Torre).

E-mail addresses: albericio@ukzn.ac.za (F. Albericio), garciaadelatorreb@ukzn.ac.za (B.G. de la Torre).

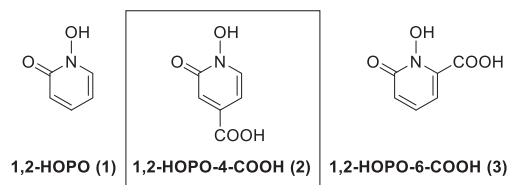


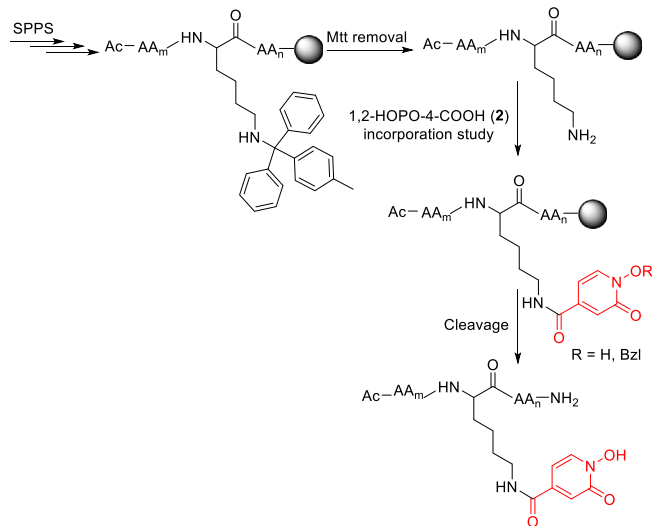
Fig. 1. Structures of 1,2-HOPO derivatives.

compounds, and, possibly, their selectivity and affinity in front of the metals, as well.

Results and discussion

The first strategy consists of building a Lys-containing peptide in solid-phase using a Rink-amide resin. The methyltrityl (Mtt) group is used to protect the ϵ -amino of the Lys and is later removed by means of 2% trifluoroacetic acid (TFA) when the peptide is still anchored to the resin. Then, the 1,2-HOPO-4-COOH derivative is incorporated, followed by final global deprotection and cleavage of the peptide from the resin (Scheme 1).

In addition to the carboxylic group, 1,2-HOPO-4-COOH (2) contains a reactive *N*-hydroxy moiety (Fig. 1). *N*-Hydroxy derivatives, such as HOPO,[5] ethyl cyanohydroxyiminoacetate (OxymaPure[®]) [11], 1-hydroxy-benzotriazole (HOBt)[12], and *N*-hydroxysuccinimide (HOSu)[13], are additives used in carbodiimide-based coupling reagents[5]. These derivatives react with the *O*-acylisourea formed by the reaction of the carboxylic group with the carbodiimide to render the active ester, which is the main acylating species. Thus, the presence of this *N*-hydroxy in 1,2-HOPO-4-COOH (2) could interfere with the activation of the carboxylic group and posterior acylation. However, it could also act as an internal additive favoring this reaction. Therefore, the first question to be addressed is whether 1,2-HOPO-4-COOH (2) can be used without masking the *N*-hydroxy group and whether it is necessary to use an extra amount of additive such as OxymaPure[®] to enhance coupling, as the *N*-hydroxy of 1,2-HOPO-4-COOH (2) could be autoconsumed, forming a kind of 1,2-HOPO-4-COOH (2) oligomer anchored to the peptide resin. These oligomers should not appear as impurities in the final peptide because the bond between the different monomers should be an active ester, which can be broken by treatment with piperidine. However, the infertile consumption of 1,2-HOPO-4-COOH (2) will be translated into poor incorporation.



Scheme 1. Synthetic strategy for the preparation of 1,2-HOPO containing peptides.

The synthetic strategy for the introduction of 1,2-HOPO-4-COOH (2) showed in Scheme 1 was applied, first, to the simple model Ac-F-K-A-resin, (for characterization of the initial peptide, see S1, S2, SI). 1,2-HOPO-4-COOH (2) (1.5 eq.) was introduced with only *N,N'*-diisopropylcarbodiimide (DIC) (1.5 equiv) in DMF for 90 min, followed by piperidine treatment before cleavage the free peptide (4, Fig. 2) from the resin. HPLC showed a conversion of 92% (Fig. 2, A, the peak at 4.1 min corresponded to the unreacted peptide). The reaction was then repeated, but in the presence of OxymaPure[®] (2 eq.). Surprisingly, the conversion was lower, only 81% (Fig. 2, B). The reaction in the presence of OxymaPure[®] was then repeated, but a re-coupling step was carried out, with just half the reagents, and without the final piperidine treatment. As expected, the conversion was superior, but a small peak (5.7%) with a higher retention time (5.8 min), which tentatively could be assigned to an extra incorporation of the HOPO derivative on the HOPO residue, was observed (Fig. 2, C). Finally, this experiment was repeated (re-coupling), but the piperidine treatment was again introduced into the synthetic process, resulting in the highest purity (95%) of the whole series, with the disappearance of the peak at 5.8 min (Fig. 2, D) (for characterization Fig. S3, SI). The first conclusion from this simple model is that 1,2-HOPO-4-COOH (2) can be incorporated without masking the *N*-hydroxy group. Given the cost of the HOPO derivative and although the re-coupling renders a better result, a single coupling could be appropriate for simple models. Furthermore, the use of piperidine treatment is recommended as an extra step in the synthetic process for removing the over incorporation of the HOPO derivative.

The Ac-K-K-K-S(tBu)-S(tBu)-resin, which has three Lys residues in a row and mimics the sequence of natural siderophores, alboxymycins,[14] was used in this study (for characterization of the initial peptide S4-S5, SI). In this case, using similar conditions to those of the experiment shown in Fig. 2A (single coupling using 1.5 eq., but for 3 h instead of 90 min), HPLC showed that all the starting product (2.1 min; see S6, SI) had been consumed and that coupling over the three ϵ -amino groups (5, Fig. 3) took place with a yield of 39% (Fig. 3, A; for characterization Figure S7-S9, SI). Peaks at 4.5–5.0 and 5.5–6.0 min corresponded to coupling over one and two ϵ -amino groups, respectively (for characterization Figure S7 and S8, SI). A second coupling for 3 h was then performed using 0.33 eq. of reagents. The purity achieved with this approach was slightly greater (44%, Fig. 3, B). Finally, a double coupling protocol with 1.5 eq. for the first and 0.75 equiv. for the second was done,

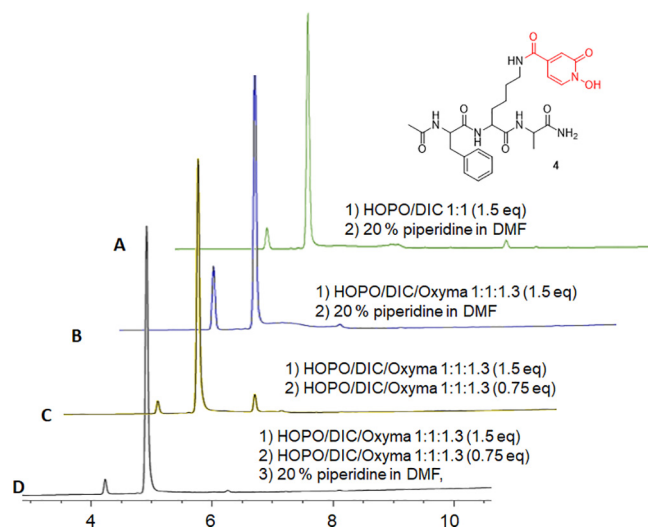


Fig. 2. Comparison of the HPLC crudes after the incorporation of unprotected 1,2-HOPO-4-COOH to the Ac-F-K-A-resin. Method 5–95% B in A over 15 min. See experimental part and SI for full HPLC conditions and characterization.

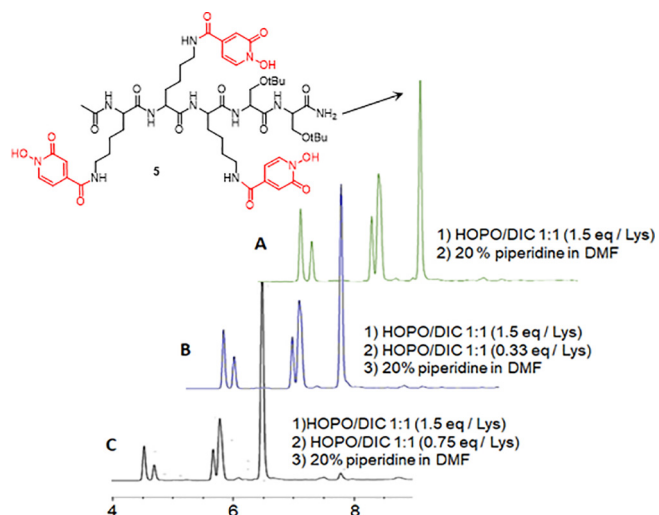


Fig. 3. Comparison of the HPLC crudes after the incorporation of unprotected 1,2-HOPO-4-COOH to Ac-K-K-K-S(tBu)-S(tBu)-resin. Method 0–50% B in A over 15 min. See experimental part for full HPLC conditions and SI for characterization.

which rendered a purity of 60% (Fig. 3, C). Of note, although the results were not outstanding, the target product can be easily purified as the impurities were far away from the main peak, as shown by HPLC.

Attempts to optimize this reaction at different temperatures were made, as well as using a mixture of DMF and CH_3CN as solvent. However, these approaches did not give better results than those reported above (Figure S10, SI).

Finally, the use of *N*-hydroxy protected 1,2-HOPO-4-COOH was explored. In the literature, only Raymond's[15] and Tetard's [7,10] laboratories have described synthetic procedures involving protected 1,2-HOPO, the benzyl (Bzl) group being the only one used for this purpose. However, the conditions reported for the removal of Bzl were not friendly (in solid-phase: 0.1 M BBr_3 in DCM for 60 min,[16] 10% HBr in AcOH for 14 h;[17] in solution: 1 M BCl_3 in DCM for 2 d,[18] 50% HCl in AcOH for 4 d,[10]). Therefore, the synthesis of other protected derivatives such as phenacyl and tetrahydropyranyl was attempted but resulted unsuccessful in our hands.

Then, the use of the Bzl as protecting group was investigated. Thus, 1,2-HOPO-4-COOH was reacted with BzlBr in the presence of K_2CO_3 in MeOH as previously reported[17] and the product was obtained in a 68% yield. The 1,2-HOPO(Bzl)-4-COOH (6) (1.5 eq.) was reacted with the Ac-K-K-K-S(tBu)-S(tBu)-resin, in DMF for 90 min using DIC (1.5 eq.). The cleavage carried out with TFA-triisopropylsilane (TIS)- H_2O (95:2.5:2.5), which kept the HOPO residue protected, showed that total conversion of the starting product and the purity of the protected HOPO(Bzl) peptide (7) was 69% (Fig. 4, A). Finally, the unprotected HOPO peptide (5) was obtained with a purity of 62% by cleavage with trifluoromethanesulfonic (TFMSA)-TFA-TIS (3:8:1) at room temperature for 70 min (Fig. 4, B) –conditions used as an alternative to anh. HF in the *tert*-butoxycarbonyl (Boc)-Bzl SPPS strategy to release the unprotected peptides[19–20]. By comparison with the chromatogram of Fig. 3, the peaks at 4.5–5 and 5.5–6 min were tentatively assigned to those derivatives containing one or two residues of 1,2-HOPO, respectively.

Although the purity of the final product obtained from the Bzl protected 1,2-HOPO-4-COOH was slightly greater than that prepared from the unprotected HOPO derivative (62% vs 60%) (Fig. 4-B vs. 3-C), the use of the former could be most cost effective, because it avoids a protection step involving an expensive raw material. Furthermore, some care should be taken when using TFMSA in the laboratory to unmask the HOPO derivative.

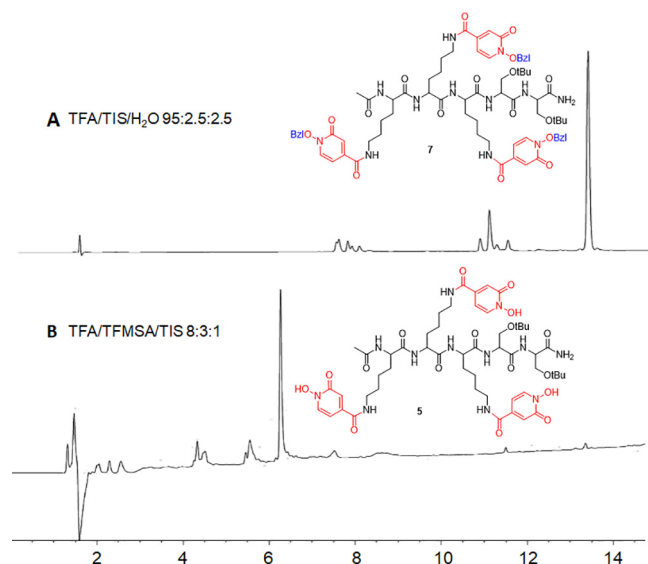


Fig. 4. HPLC analysis of A) the crude product (7) after acylation of the Ac-K-K-K-S(tBu)-S(tBu)-resin with Bzl *N*-hydroxy protected 1,2-HOPO-4-COOH (6) and cleavage from the resin with TFA-TIS- H_2O (95:2.5:2.5), method 5–95% B in A over 15 min.; B) the same but after the cleavage with TFMSA-TFA-TIS (3:8:1), to obtain 5, method 0–50% B in A over 15 min. See experimental part and SI for the full HPLC conditions and characterization.

Conclusions

The chelating effect in most of the metal-chelators, which show applications in therapy and diagnostics, is achieved because of the presence of three units of catechols, α -hydroxy carboxylic derivatives, and/or hydroxamic acids. The chelators offer the “hard” electron donating oxygen atoms to strongly bind with “hard” metal cation, such as Fe^{3+} . 1,2-HOPO-4-COOH (2) is a commercially available compound that fulfils these characteristics, by having the *N*-hydroxyl and the adjacent carbonyl as the binding moiety. Here, we have described two friendly strategies for the Solid-Phase Peptide Synthesis of 1,2-HOPO-containing peptide chelators. The first involves the use of unprotected 1,2-HOPO-4-COOH (2), while that the second uses the protected Bzl *N*-hydroxy (6). The use of unprotected HOPO could be useful for the synthesis of most molecules, which is beneficial due to the high cost of the building block. On the other hand, if a Bzl protected HOPO derivative is being used, we propose a friendlier protocol for removing the protecting group than those reported in the literature,[10,16–19] namely the addition of TFMSA to the cocktail used for global deprotection and cleavage of the peptide from the resin. The convenient SPPS strategies described herein for the preparation of peptide chelators should fuel further investigation in the field.

Experimental part

Materials

All reagents and solvents were from commercial suppliers and used without further purification. Fmoc amino acids and Fmoc-Rink Amide AM PS resin (loading 0.74 mmol/g) were purchased from Iris Biotech GmbH (Marktredwitz, Germany). DIC and Oxy-maPure[®] were a gift from Luxembourg Biotech. (Ness Ziona, Israel), and *N,N*-diisopropylethylamine (DIEA) and piperidine were supplied by Sigma-Aldrich (St. Louis, Missouri, USA). Organic solvents [DMF, CH_2Cl_2 (DCM)] and HPLC quality acetonitrile (CH_3CN) were purchased from SRL (CRD-SRL, India). Milli-Q water was used for RP-HPLC analyses. Analytical HPLC was performed on an Agilent 1100 system using a Phenomenex AerisTMC18 (3.6 μm ,

4.6 × 150 mm) column, with flow rate of 1.0 mL/min and UV detection at 220 nm. Chemstation software was used for data processing. Buffer A: 0.1% TFA in H₂O; buffer B: 0.1% TFA in CH₃CN. LC-MS were performed on two systems: Shimadzu 2020 UFLC-MS, column YMC-Triart C₁₈ (5 μm, 4.6 × 1150 mm) column, 30 °C (system 1), an Ultimate™ 3000, Aeris™ 3.6 μm Wide pore column, Phenomenex C₁₈ (4.6 mm × 150) column (system 2). In both systems were used Buffer A: 0.1% formic acid in H₂O; buffer B: 0.1% formic acid in CH₃CN, flow 1.0 mL/min, UV detection 220 nm.

Solid-Phase peptide synthesis

Peptides were synthesized manually using a syringe fitted with a porous polyethylene disc and attached to a vacuum trap for easy filtration. Fmoc-Rink-amide-PS resin (100 mg, 0.74 mmol/g loading) was taken and swelled in DMF (1 mL) for 15 min. Washings before and after Fmoc removal and coupling were carried out with DMF (1 mL). Fmoc removal was carried out with piperidine-DMF (2:8) (3 mL 1 min + 7 min). Couplings were achieved by dissolving the Fmoc-aa-OH (3 eq.) in the minimum amount of DMF. OxymaPure® (3 eq.) and DIC (3 eq.) were then added sequentially, and the mixture was left to pre-activate for 3 min. The resulting solution was added to the resin in the syringe and allowed to couple for 1 h with sporadic stirring. Acetylation of the N-termini was achieved by adding DIEA (20 equiv.) to the swelled peptide resin, followed by addition of acetic anhydride (Ac₂O) (10 equiv.). The resin was then allowed to react for 30 min. with occasional stirring. Mtt deprotection was done using TFA-TIS-DCM (2:5:93) (3 mL for 2 × 2 min. + 1 × 15 min.).

1,2-HOPO-4-COOH incorporation: After removal of the Mtt group, the resin was treated with DIEA-DCM (1:19) (3 mL, 3 × 1 min) and then washed with DMF. The corresponding equiv. of **2** or **6**, and OxymaPure (1 equiv. respect **2**), if required, were dissolved in the minimum amount of DMF and added to the peptide resin. Then, DIC (1 eq with respect to **2**) was added to the mixture and left to react for 90 min. The resin was washed with DMF.

Global deprotection and cleavage was performed by adding TFA-TIS-H₂O (95:2.5:2.5) or TFMSA-TFA-TIS (3:8:1) (500 μL) per 50 mg of the peptide resin for 70 min. at RT. In the first case, the crude peptide was precipitated with diethylether, isolated by centrifugation, dried under vacuum and then dissolved in H₂O, and lyophilized. While after the TFMSA cleavage, the filtrate was collected over H₂O (2.0 mL) and the precipitate was isolated by centrifugation, washed with diethyl ether, dissolved in H₂O, and lyophilized.

Declaration of Competing Interest

The authors declare that they have no known competing financial interests or personal relationships that could have appeared to influence the work reported in this paper.

Acknowledgements

The work was funded in part by the following: the National Research Foundation, South Africa (NRF) (# 105892 and Blue Sky's Research Programme # 120386) and the University of KwaZulu-Natal (South Africa); and the Spanish Ministry of Science, Innovation, and Universities (RTI2018-093831-B-I00), the Generalitat de Catalunya (2017 SGR 1439) (Spain), and Marató TV3 foundation 2018 (#20183530). We thank Professor Miquel Viñas (University of Barcelona) for fruitful discussions.

Appendix A. Supplementary data

Supplementary data to this article can be found online at <https://doi.org/10.1016/j.tetlet.2020.152299>.

References

- [1] A. Cilibrizzi, V. Abbate, Y.L. Chen, Y. Ma, T. Zhou, R.C. Hider, Chem. Rev. 118 (2018) 7657–7701, <https://doi.org/10.1021/acs.chemrev.8b00254>.
- [2] L.E. Scott, C. Orvig, Chem. Rev. 109 (2009) 4885–4910, <https://doi.org/10.1021/cr9000176>.
- [3] S.J. Flora, V. Pachauri, Int. J. Environ. Res. Public Health. 7 (2010) 2745–2788, <https://doi.org/10.3390/ijerph7072745>.
- [4] G. Tonziello, E. Caraffa, B. Pinchera, G. Granata, N. Petrosillo, Infect. Dis. Rep. 11 (2019) 8208, <https://doi.org/10.4081/idr.2019.8208>.
- [5] A. El-Faham, F. Albericio, Chem. Rev. 111 (2011) 6557–6602, <https://doi.org/10.1021/cr100048w>.
- [6] T.M. Hoette, R.J. Abergel, J. Xu, R.K. Strong, K.N. Raymond, J. Am. Chem. Soc. 130 (2008) 17584–17592, <https://doi.org/10.1021/ja8074665>.
- [7] D.G. Workman, M. Hunter, S. Wang, J. Brandel, V. Hubscher, L.G. Dover, T.D. Bioorg, and references cited therein from the same group, Chem. 95 (2020), <https://doi.org/10.1016/j.bioorg.2019.103465>.
- [8] E.J. Werner, J. Kozhukh, M. Botta, E.G. Moore, S. Avedano, S. Aime, K.N. Raymond, Inorg. Chem. 48 (2009) 277–286, <https://doi.org/10.1021/ic801730u>.
- [9] C. Jocher, E. Moore, J. Xu, S. Avedano, M. Botta, S. Aime, K.N. Raymond, Inorg. Chem. 46 (2007) 9182–9191, <https://doi.org/10.1021/ic700985j>.
- [10] D.G. Workman, M. Hunter, L.G. Dover, D. Tetard, J. Inorg. Biochem. 160 (2016) 49–58, <https://doi.org/10.1016/j.jinorgbio.2016.04.018>.
- [11] R. Subiros-Funosas, R. Prohens, R. Barbas, A. El-Faham, F. Albericio, Chem., Eur. J. 15 (2009) 9394–9403, <https://doi.org/10.1002/chem.200900614>.
- [12] W. König, R. Geiger, Ber. Dtsch. Chem. Ges. 103 (1970) 788–798, <https://doi.org/10.1002/cber.19701030319>.
- [13] G. Anderson, J.E. Zimmerman, F.M. Callahan, J. Am. Chem. Soc. 89 (1963) 178, <https://doi.org/10.1021/ja00977a054>.
- [14] A. Hartmann, H. Fiedler, V. Braun, Eur. J. Biochem. 99 (1979) 517–524, <https://doi.org/10.1111/j.1432-1033.1979.tb13283.x>.
- [15] J. Xu, P.W. Durbin, B. Kullgren, S.N. Ebbe, L.C. Uhlir, K.N. Raymond, J. Med. Chem. 45 (2002) 3963–3971, <https://doi.org/10.1021/jm010564t>.
- [16] A. Ricano, I. Captain, K.P. Carter, B.P. Nell, G.J.P. Deblonde, R. Abergel, J. Chem. Sci. 10 (2019) 6834–6843, <https://doi.org/10.1039/c9sc01068h>.
- [17] W. Yantasee, G.E. Fryxell, Y. Lin, H. Wu, K.N. Raymond, J. Xu, J. Nansci Nanotechno. 5 (2005) 527–529, <https://doi.org/10.1166/jnn.2005.096>.
- [18] T. Zhou, X.L. Kong, R.C. Hider, Dalton Trans. 48 (10) (2019) 3459–3466, <https://doi.org/10.1039/c8dt05014g>.
- [19] J.P. Tam, W.F. Heath, R.B. Merrifield, J. Am. Chem. Soc. 108 (1986) 5242–5251, <https://doi.org/10.1021/ja00277a031>.
- [20] B.G. de la Torre, D. Andreu, J. Pept. Sci. 14 (2008) 360–363, <https://doi.org/10.1002/psc.956>.

Chapter 3: Protocol for efficient solid-phase synthesis of peptides containing 1-hydroxypyridine-2-one (1,2-HOPO)

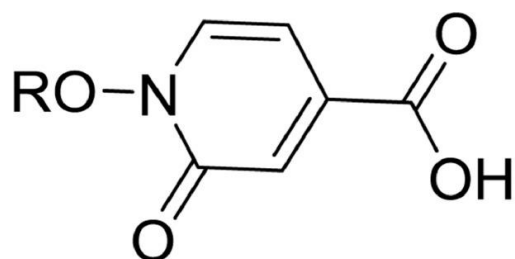
Danah Al Shaer ^{a,b}, Beatriz G. de la Torre ^{a,*}, Fernando Albericio ^{b,c,d,*}

^a *KwaZulu-Natal Research Innovation and Sequencing Platform (KRISP), School of Laboratory Medicine and Medical Sciences, College of Health Sciences, University of KwaZulu-Natal, Durban 4041, South Africa*

^b *Peptide Science Laboratory, School of Chemistry and Physics, University of KwaZulu-Natal, Durban 4001, South Africa*

^c *Institute for Advanced Chemistry of Catalonia (IQAC-CSIC), 08034 Barcelona, Spain*

^d *CIBER-BBN, Networking Centre on Bioengineering, Biomaterials and Nanomedicine and Department of Organic Chemistry, University of Barcelona, 08028 Barcelona, Spain*



R = H, Bzl

An efficient protocol for synthesizing HOPO containing peptides on SPPS is described in detail



ELSEVIER

Contents lists available at ScienceDirect

MethodsX

journal homepage: www.elsevier.com/locate/mex

Method Article

Protocol for efficient solid-phase synthesis of peptides containing 1-hydroxypyridine-2-one (1,2-HOPO)[☆]

Danah Al Shaer^{a,b}, Beatriz G. de la Torre^{a,*}, Fernando Albericio^{b,c,d,*}^a KwaZulu-Natal Research Innovation and Sequencing Platform (KRISP), School of Laboratory Medicine and Medical Sciences, College of Health Sciences, University of KwaZulu-Natal, Durban 4041, South Africa^b Peptide Science Laboratory, School of Chemistry and Physics, University of KwaZulu-Natal, Durban 4001, South Africa^c Institute for Advanced Chemistry of Catalonia (IQAC-CSIC), 08034 Barcelona, Spain^d CIBER-BBN, Networking Centre on Bioengineering, Biomaterials and Nanomedicine and Department of Organic Chemistry, University of Barcelona, 08028 Barcelona, Spain

ARTICLE INFO

Method name: -

Keywords: Fe (III) chelators, Siderophores, Solid phase peptide synthesis, 1-Hydroxypyridine-2-one, Trifluoromethanesulfonic acid (TFMSA)

Article history: Received 8 August 2020; Accepted 24 September 2020; Available online 28 September 2020

Specifications table

Subject Area	Chemistry
More specific subject area	Peptide Synthesis
Method name	-
Name and reference of original method	D. Al Shaer, F. Albericio, B.G. de la Torre. Solid-Phase Synthesis of Peptides Containing 1-Hydroxypyridine-2-one (1,2-HOPO). Tetrahedron Lett., (2020), https://doi.org/10.1016/j.tetlet.2020.152299
Resource availability	-

[☆] **Direct Submission or Co-Submission:** Co-submissions are papers that have been submitted alongside an original research paper accepted for publication by another Elsevier journal Co-Submission Solid-Phase Synthesis of Peptides Containing 1-Hydroxypyridine-2-one (1,2-HOPO) <https://doi.org/10.1016/j.tetlet.2020.152299> Journal title: Tetrahedron Letters Article Number: 152299

DOI of original article: [10.1016/j.tetlet.2020.152299](https://doi.org/10.1016/j.tetlet.2020.152299)

* Corresponding authors.

E-mail addresses: garciaelatorreb@ukzn.ac.za (B.G. de la Torre), albericio@ukzn.ac.za (F. Albericio).<https://doi.org/10.1016/j.mex.2020.101082>

2215-0161/© 2020 The Authors. Published by Elsevier B.V. This is an open access article under the CC BY license

<http://creativecommons.org/licenses/by/4.0/>

Method details

1,2-HOPO containing peptides were synthesized on solid-phase by derivatization of Lys side chain residues once the peptide chain was fully elongated. This derivatization was done in two different routes, the first route uses the free form (no N-OH protection) of 1,2-HOPO-4-COOH (peptides 1 and 2, Fig. 2). The second route uses the Bzl protected N-OH form of 1,2-HOPO-4-COOH as it is commonly reported in the literature (peptide 3, Fig. 2). Peptide 1 was obtained in a very good purity, while peptide 2 was obtained in lower but acceptable purity and, very importantly, very easy to be purified. This is due because the main impurities containing only two or one incorporation of 1,2-HOPO-4-COOH moieties, appeared in the HPLC far away of the target peak. In peptide 3, the removal of the Bzl groups is carried out during the global deprotection and cleavage of the peptide from the resin using a friendlier condition [TFA- TFMSA-H₂O (8:3:1)] than those reported in the literature. Scheme 1 describes all the synthetic steps of both routes for the synthesis of the peptides.

The different steps are:

(I) Peptide backbone elongation on solid support

(This step was performed following a standard Fmoc/tBu strategy protocol. 0.1 mmol of the peptide will be prepared following these steps:

Chemicals and apparatus

Caution: You should perform steps I-IV in a fume hood wearing a protective coat, goggles, and gloves. Fmoc-Rink-amide-AM-PS-resin (Loading: 0.7 mmol/g, Iris Biotech, 200-400 mesh)

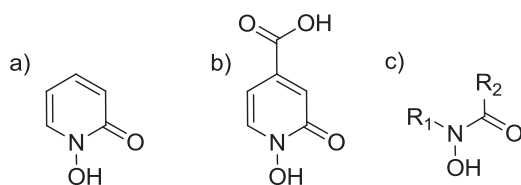


Fig. 1. (a) 1,2-HOPO (b) 1,2-HOPO-4-COOH (c) General structure of a hydroxamic acid.

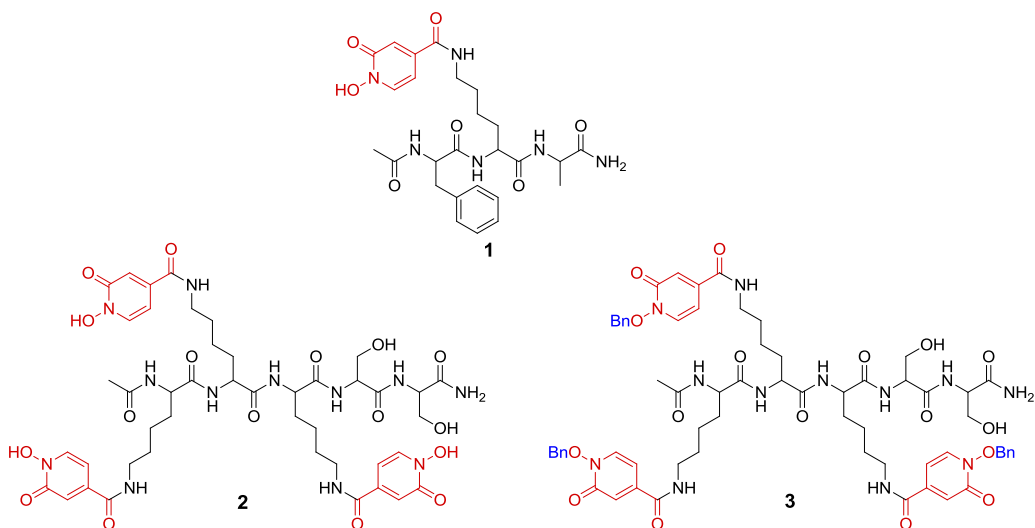


Fig. 2. Peptides synthesized containing 1,2-HOPO moieties.

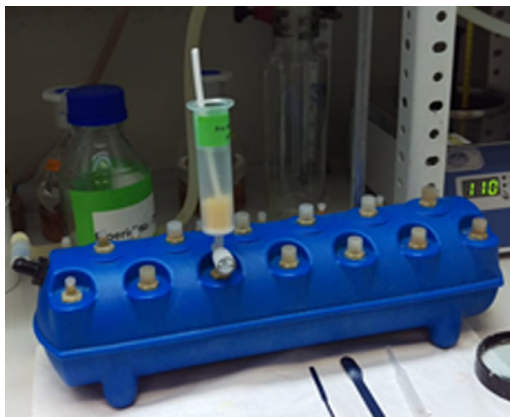


Fig. 3. Set up for solid phase peptide synthesis (manifold + syringe + Teflon rod + Teflon stopcock).

N^α -(9-Fluorenylmethoxycarbonyl) amino acids: Fmoc-Ala-OH, Fmoc-Lys(Mtt)-OH, Fmoc-Phe-OH (for peptide 1), and Fmoc-Ser(tBu)-OH, Fmoc-Lys(Mtt)-OH for peptide 2 and 3. Mtt: methyltrityl, tBu: tert-butyl, Iris Biotech.

N,N' -Diisopropylcarbodiimide (DIC) (Luxembourg Bio Technologies. **Be careful!!**, it is flammable and irritant)

OxymaPure (Luxembourg Bio Technologies)

Acetyl chloride (AcCl) Sigma-Aldrich, **Be careful!!**, it is flammable and corrosive)

N,N' -Diisopropylethylamine (DIEA) (reagent grade 99%, Sigma-Aldrich, **Be careful!!**, it is flammable and corrosive)

Piperidine (reagent grade 99%, Sigma-Aldrich, **Be careful!!**, it is flammable, corrosive and toxic)

N,N' -Dimethyl formamide (DMF) (extra pure AR grade, SRL, **Be careful!!**, it is flammable, harmful and health hazard)

Analytical balance (Mettler Toledo)

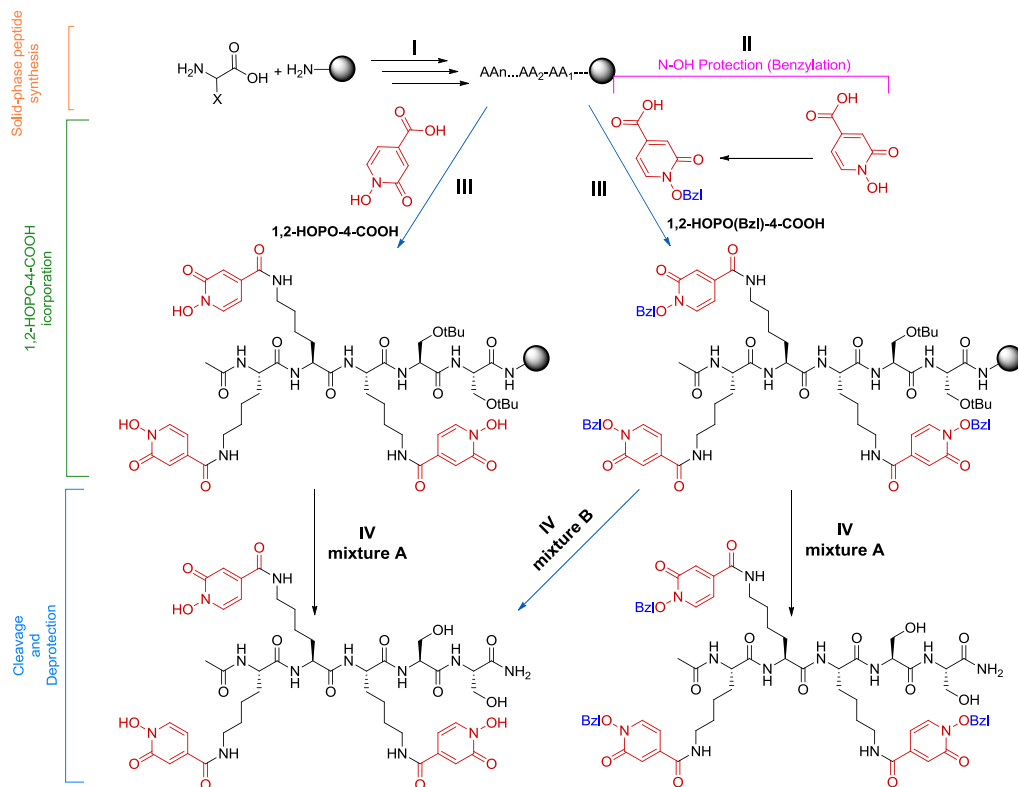
5 mL polypropylene syringe fitted with a polypropylene preinserted frit (20 μ m).

Vacuum manifold (Vac-Man® Laboratory Vacuum Manifold, Promega) (Fig. 3)

Vacuum pump

Procedure

1. Prepare the syringe fitted with a polypropylene filter.
2. Weigh Fmoc-rink-amide-AM-PS-resin (143 mg for 0.1 mmol synthesis scale) and place it in the syringe.
3. Place the syringe on the manifold (as in Fig. 3) and adjust the suction (you only need a gentle suction).
4. Wash the resin with DMF (1 min, 1 mL) and drain the solvent over gentle vacuum, repeat it twice.
5. Add DMF (3 mL) and allow it to swell the resin for about 15 min. *This step will make the active sites of the resin to be accessible for the reactants in the following steps.*
6. Meanwhile, in separate glass vials, weigh 0.3 mmol (3 eq. with respect to the resin). of each the Fmoc-AA-OH required to build the peptide chain. [To prepare peptide 1, Fmoc-Ala-OH: 93.4 mg, Fmoc-Lys(Mtt)-OH:187.4 mg, and Fmoc-Phe-OH:116.2 mg. To prepare peptides 2 and 3, 2x Fmoc-Ser(tBu)-OH:115 mg, and of 3x Fmoc-Lys(Mtt)-OH:187.4 mg, for each peptide].
7. Add (43 mg, 0.3 mmol) of OxymaPure to each Fmoc-AA-OH vial. *This additive will form the corresponding active ester after that the Fmoc-amino acid has been activated with DIC see step #12, modulating the reactivity to minimize early hydrolysis and/or side-reaction formation. See ref [7] for a better understanding of the mechanism of the reaction.*



Scheme 1. Synthesis of 1,2-HOPO-containing peptides using both strategies. Blue arrows represent the steps that were introduced and/or optimized.

8. To remove the Fmoc protecting group, prepare a 20% solution of piperidine in DMF. *It is not necessary to prepare freshly this solution. Once per week is advisable, keep it a dark glass bottle.*
9. Once the resin is well swollen, filter off the solvent and start the synthesis.
10. Add the piperidine solution (1 mL) to the resin, stir for 1 min and drain the solution off. Add again 1 mL of the piperidine solution and stir for 7 min, then filter and wash with DMF (3 × 1 ml).
11. Dissolve the mixture of Fmoc-AA-OH/OxymaPure corresponding to the residue to be incorporate (be aware that the peptide synthesis starts by the C-terminal end of the sequence). It is advisable to use the minimum amount of DMF for dissolving the mixture but should be enough to cover the swollen resin (for 143 mg of this kind of resin, approx. 600 μ L are needed).
12. To the previous mixture solution, add the coupling reagent, DIC (47 μ L, 0.3 mmol) and allow the activation for 2 min. *The active ester is formed. More time could conduct to the hydrolysis of the ester and/or epimerization.*
13. Transfer the solution to the drained resin in the syringe (after Step 10), make sure all resin beads are covered with the solution, add few more drops of DMF if needed.
14. Leave the slurry to react for 40-60 minutes with occasional stirring. The course of the reaction could be confirmed by the ninhydrin test.
- 15 Drain the solution, wash with DMF (1 mL, 30 sec.) with stirring, drain it, and repeat the washing for two more times.
16. Repeat Steps 8–15 for each amino acid in the sequence.
17. Proceed to Step 10 to remove the last Fmoc protecting group.

18. To acetylate the N-terminal of the prepared peptide, add DIEA (345 μ L, 20 mmol), then AcCl (95 μ L, 10 mmol), shake it for 30 min., drain the solution and wash with DMF (3 \times 1 mL).
- (II) **Protecting the N-OH of 1,2-HOPO-4-COOH [1,2-HOPO(Bzl)-4-COOH]**

This step was done following with slight modifications the procedure reported in literature for other 1,2-HOPO derivative [8].

Chemicals and apparatus

4-Carboxy-1-hydroxypyridin-2-one (1,2-HOPO-4-COOH) (ChemSpace)

Benzyl bromide (BzlBr) (Sigma-Aldrich)

Potassium carbonate (K_2CO_3) (Sigma-Aldrich)

Methanol (MeOH) (Laboratory reagent >99.6%, Sigma-Aldrich)

6 M HCl

Ice

Round bottom flask

Condenser

Oil bath

Hotplate and stirrer

Rotatory evaporator

Procedure

1. In a round bottom flask with a magnetic stirrer, weigh 1,2-HOPO-4-COOH (155 mg, 1 mmol) and K_2CO_3 (268 mg, 2 mmol).
 2. Add 10 mL of MeOH and place the round bottom flask in an oil bath.
 3. Stir the suspension and add BzlBr (143 μ L, 1.2 mmol) drop wise over 1 min.
 4. Attach the condenser, and reflux the mixture at 65–70 $^{\circ}C$ for 16 h.
 5. Remove the MeOH under reduced pressure in a rotatory evaporator.
 6. Dissolve the residue with H_2O (5 mL). If does not readily dissolve add few drops of 1M NaOH.
 7. Acidify the aqueous solution with HCl (6 M) dropwise to pH 2, a white precipitate should heavily form.
 8. Filter the precipitate, wash it with ice-cold water, and dry it under vacuum.
 9. Characterize the product using NMR, analytical HPLC and LCMS. The yield is about 70%.
- (III) **Incorporation of HOPO (protected and unprotected) to the peptide**

Chemicals and apparatus

Peptidyl resins prepared in part I (Ac-F-K(Mtt)-A-NH-Rink-amide-resin and Ac-K(Mtt)-K(Mtt)-K(Mtt)-S(tBu)-S(tBu)-NH- Rink-amide-resin)

1,2-HOPO-4-COOH (ChemSpace).

1,2-HOPO(Bzl)-4-COOH (prepared in II)

N,N-Diisopropylcarbodiimide (DIC) (Luxembourg Bio Technologies. **Be careful!!**, it is flammable and irritant)

N,N-Dimethyl formamide (DMF) (extra pure AR grade, SRL, **Be careful!!**, it is flammable, harmful and health hazard)

Trifluoroacetic acid (TFA) (reagent grade 98%, Sigma-Aldrich. **Be careful!!**, it is corrosive and harmful)

Triisopropyl silane (TIS) (Reagent grade 98%, Sigma-Aldrich. **Be careful!!**, it is flammable).

Dichloromethane (DCM) (ACS reagent >99.9%, Honeywell. **Be careful!!**, it is harmful and health hazard).

Diisopropylethylamine (DIEA) (reagent grade 99%, Sigma-Aldrich. **Be careful!!**, it is flammable and corrosive)

5 mL polypropylene syringe fitted with a polyethylene filter

The solid phase peptide set up mentioned in section I (Fig. 3).

Procedure

1. Place the peptide resin in the syringe, place it on the manifold and wash it with DCM (3 \times 1 mL)

2. To remove Mtt protecting, prepare a solution of TFA-TIS-DCM (3:5:92) (300 μ L TFA, 500 μ L TIS, 9.2 mL DCM).
 3. Add 2 ml of the TFA solution to the peptide resin and shake it for 15 min. *Evolution and disappearance of yellow color is detected, which indicates the release of the Mtt carbocations and its posterior scavenging.*
 4. Filter off the solution. Wash the resin with DCM (3 \times 3 mL) for 30 sec.
 5. Repeat Steps 3 and 4 for one more time.
 6. Wash the resin with 5% DIEA in DCM solution (3 \times 1 mL). *The DIEA treatments is to liberate the free amine of the Lys.*
 7. Wash the resin with DCM (3 \times 1 ml), then with DMF (2 \times 1 mL), the peptide resin is now ready for the incorporation of 1,2-HOPO-4-COOH, unprotected and protected.
 8. a) Unprotected: dissolve 24 mg (0.15 mmol) of 1,2-HOPO-4-COOH per each Lys to be derivatized, in 600 μ L of DMF;
 - b) Protected: dissolve 37 mg (0.15 mmol) of Bzl protected 1,2-HOPO-4-COOH per each Lys to be derivatized, in 600 μ L of DMF.
1. Transfer the HOPO solution to the resin, then add DIC (24 μ L, 0.15 mmol per Lys), shake for 90 min, drain the solution off, then wash with DMF (3 \times 1 mL).
 2. An optional second coupling can be done using less equivalents of HOPO and DIC to increase the yield (as in Table 1). But as 1,2-HOPO-4-COOH is rather expensive, this step can be avoided.
 3. In case of using the unprotected HOPO (in peptides 1 and 2), treat the peptidyl resin with 1 mL of 20% piperidine in DMF solution for 10 min. *(To remove any ester oligomers that may have formed through the N-OH).* Wash the resin with DMF (3 \times 1 mL)
 4. Wash the resin with DCM (3 \times 1 mL).

(IV) **Cleaving the peptide from the resin**

Chemicals and apparatus

Peptide resins prepared in part III (Ac-F-K(HOPO)-A-NH-resin, Ac-K(HOPO)-K(HOPO)-K(HOPO)-S(tBu)-S(tBu)-NH-Rink-amide-resin and Ac-K(HOPO-Bzl)-K(HOPO-Bzl)-K(HOPO-Bzl)-S(tBu)-S(tBu)-NH-Rink-amide-resin)

Trifluoromethanesulfonic (TFMSA) (reagent grade 98%, Sigma-Aldrich. Be careful!!, it is corrosive and harmful)

Trifluoroacetic acid (TFA) (reagent grade 98%, Sigma-Aldrich. **Be careful!!**, it is corrosive and harmful)

Triisopropyl silane (TIS) (Reagent grade 98%, Sigma-Aldrich. **Be careful!!**, it is flammable).

Dichloromethane (DCM) (ACS reagent >99.9%, Honeywell. **Be careful!!**, it is harmful and health hazard).

Diethylether (DEE)

Methanol

Milli-Q water

5 mL polypropylene syringe fitted with a polyethylene filter

Falcon tube

Two cleavage mixtures were used:

Mixture A (TFA-TIS-H₂O, 95:2.5:2.5) to cleave peptide from resin and to remove the acid labile protecting groups, namely, tBu from the Ser side chain (and leaving the Bzl unaffected if it is present) (this mixture was used for all peptides).

Mixture B (TFA-TFMSA-TIS, 8:3:1) to cleave the peptide from the resin and to remove all other protecting groups including the Bzl (this mixture was used to get peptide 2 from **peptide resin** 3).

Procedure

1. Place the peptide resin in the syringe and wash it with MeOH and dry under gentle suction.
2. Weigh the resin and transfer it into a falcon tube fitted with a cap.

Table 1
Purities and yields for the prepared peptides, 1-3.

Peptide	Form of HOPO incorporated	Cleavage solution used	Purity	% Yield
1	Free N-OH	Mixture A	92% for single coupling (1.5 eq) 97% for double coupling (1.5 eq, then 0.75 eq)	88% crude peptide
2	Free N-OH	Mixture A	39% for single coupling (1.5 eq per Lys) 60% for double coupling (1.5 eq per Lys, then 0.75 eq per Lys)	87 % crude peptide
3	N-OBn	Mixture A	69%	71 % crude peptide
2 from 3	N-OBn	Mixture B	62%	63 % crude peptide

Note: HPLC and MS-LC chromatograms can be found in the original report [9].

3. Add the cleavage mixture (1 mL/100 mg peptidyl resin), close the cap and shake the tube for 70 min.

For **mixture A**:

1. Add ice-cold diethyl ether (5 mL/1 mL cleavage mixture), shake well (the peptide will precipitate), centrifuge the mixture and decant the supernatant, repeat the ether washing for two more times. *Do not discard the diethyl ether washing till you get your peptide at the end.*
2. Dry the residue under reduced pressure, add water (3 mL) to dissolve the peptide.
3. Filter off the resin beads and keep the filtrate.
4. Wash the resin beads two more times with (1 mL) water each, filter and combine all filtrates.
5. Lyophilize the peptide solution.

For **mixture B**

1. Add water (5 mL/1 mL cleavage mixture).
2. Wash the aqueous layer with diethyl ether (5 mL).
3. Remove the ether layer and repeat the washing 2 more times.
4. Filter off the resin beads.
5. Lyophilize the aqueous filtrate.

(V) **Purification and Characterization**

All peptides were purified using reversed phase semi preparative HPLC, the pure fractions were lyophilized and stored at 4 °C. All peptides were obtained in good yields. They were characterized using analytical HPLC and LCMS techniques. Purities of peptides were determined by comparison of peak area for each peptide in the HPLC chromatogram at 220 nm. Yields were determined from the mass of the lyophilized peptide in relation with the theoretical mass (see [Table 1](#)).

Acknowledgements

The work was funded in part by the following: the National Research Foundation (NRF) (# 105892 and Blue Sky's Research Programme # 120386) and the University of KwaZulu-Natal (South Africa); and the Spanish Ministry of Science, Innovation, and Universities (RTI2018-093831-B-100), the Generalitat de Catalunya (2017 SGR 1439) (Spain), and Marató TV3 foundation 2018 (#20183530). We thank Professor Miquel Viñas (University of Barcelona) for fruitful discussions.

XX The authors declare that they have no known competing financial interests or personal relationships that could have appeared to influence the work reported in this paper.

References

- [1] M.S. Thomas, Iron acquisition mechanisms of the Burkholderia cepacia complex, *Biometals* 20 (2007) 431–452, doi:[10.1007/s10534-006-9065-4](https://doi.org/10.1007/s10534-006-9065-4).
- [2] A. Ricano, et al., Combinatorial design of multimeric chelating peptoids for selective metal coordination, *Chem. Sci.* (2019), doi:[10.1039/c9sc01068h](https://doi.org/10.1039/c9sc01068h).
- [3] W. Yantasee, et al., Hydroxypyridinone functionalized self-assembled monolayers on nanoporous silica for sequestering lanthanide cations, *J. Nanosci. Nanotechnol.* 5 (2005) 527–529, doi:[10.1166/jnn.2005.096](https://doi.org/10.1166/jnn.2005.096).
- [4] T. Zhou, X.L. Kong, R.C. Hider, Synthesis and iron chelating properties of hydroxypyridinone and hydroxypyranone hexadentate ligands, *Dalton Trans* 48 (2019) 3459–3466, doi:[10.1039/c8dt05014g](https://doi.org/10.1039/c8dt05014g).
- [5] D.G. Workman, et al., Synthesis of novel Iron(III) chelators based on triaza macrocycle backbone and 1-hydroxy-2(H)-pyridin-2-one coordinating groups and their evaluation as antimicrobial agents, *J. Inorg. Biochem.* 160 (2016) 49–58, doi:[10.1016/j.jinorgbio.2016.04.018](https://doi.org/10.1016/j.jinorgbio.2016.04.018).
- [6] R. Mashlach, M.M. Meijler, Total synthesis of pyoverdine D, *Org. Lett.* 15 (2013) 1702–1705, doi:[10.1021/ol400490s](https://doi.org/10.1021/ol400490s).
- [7] A. El-Faham, F. Albericio, Peptide coupling reagents, more than a letter soup, *Chem Rev* 111 (2011) 6557–6602, doi:[10.1021/cr100048w](https://doi.org/10.1021/cr100048w).
- [8] J. Xu, et al., Synthesis and initial evaluation for in vivo chelation of pu(IV) of a mixed octadentate spermine-based ligand containing 4-carbamoyl-3-hydroxy-1-methyl-2(1H)-pyridinone and 6-carbamoyl-1-hydroxy-2(1H)-pyridinone, *J. Med. Chem.* 45 (2002) 3963–3971, doi:[10.1021/jm010564t](https://doi.org/10.1021/jm010564t).
- [9] D. Al Shaer, F. Albericio, B.G. de la Torre, Solid-phase synthesis of peptides containing 1-Hydroxypyridine-2-one (1,2-HOPO), *Tetrahedron Lett.* 61 (2020), doi:[10.1016/j.tetlet.2020.152299](https://doi.org/10.1016/j.tetlet.2020.152299).

Chapter 4. Synthesis of new peptide-based Ligands with 1,2-HOPO pendant chelators.

The thermodynamic evaluation of their iron (III) complexes

Danah Al Shaer^{a,b}, Fernando Albericio^{b,c,d,*} and Beatriz G. de la Torre^{a,*}

^a*KwaZulu-Natal Research Innovation and Sequencing Platform (KRISP), School of Laboratory Medicine and Medical Sciences, College of Health Sciences, University of KwaZulu-Natal, Durban 4041, South Africa*

^b*Peptide Science Laboratory, School of Chemistry and Physics, University of KwaZulu-Natal, Durban 4001, South Africa*

^c*Institute for Advanced Chemistry of Catalonia (IQAC-CSIC), 08034 Barcelona, Spain*

^d*CIBER-BBN, Networking Centre on Bioengineering, Biomaterials and Nanomedicine, and Department of Organic Chemistry, University of Barcelona, 08028 Barcelona, Spain*

Abstract:

Hydroxypyridones (HOPO) are an important class of chelating compounds. They bind strongly to hard metal ions such as Fe (III). Here we present the solid-phase synthesis of peptides containing 1,2-HOPO moieties linked through a carboxylic acid placed at 4-position of the ring. A total of four ligands have been studied, two bidentate and two hexadentate. The last have been synthesized by two different strategies, stepwise and convergent. The Physiochemical characterization of ligands and their complexes have been carried out. The determined pK_a values for all ligands showed their total deprotonation at pH lower than the physiological. The determined formation constant of the Fe(III) complex ($\log \beta$) were from 23.66, corresponding to ligand A, to 27.63 corresponding to ligand C. When the pFe^{3+} at pH=7.4 were calculated the result showed that ligands B and C had a strong iron affinity (26.91 and 28.58, respectively) which make them suitable for further investigation in therapeutic applications.

1. Introduction:

Iron is essential for almost all living organisms to transport oxygen, to produce energy, as a nutrient, and as part of the metabolic process. To address their iron needs, microorganisms such as bacteria and fungi produce siderophores, which in Greek means iron carriers. The main characteristic of the siderophores is its high affinity towards Fe(III) [1, 2]. Through this mechanism, microorganisms scavenge Fe(III) from the environment and assures their survival. From a chemical point of view, most part of the siderophores contain *O,O'* bidentate chelate, which can be mostly derived from catechols, α -hydroxy carboxylic acids, or hydroxamic acids [3, 4]. Most of the natural siderophores contains three of these bidentate chelate making them hexadentate chelators. In some of them, there are only one class of the chelate, while very often mixture of them is present [4, 5].

In addition of Fe(III), hydroxamic acids also show high binding affinities in front of a broad range of transition metals. This capacity has fuelled its further application in another scientific areas such as metal scavenging or as radiopharmaceuticals [6-8] .

Many reported synthetic Fe (III) chelators are based on hydroxypyridinones (HOPO), a pyridine heterocycle with carbonyl and hydroxy substituents [9-12]. For siderophore purposes, they can exist in the forms of 1-hydroxypyridine-2-one (1,2-HOPO), 3-hydroxypyridine-2-one (3,2-HOPO), and 3-hydroxypyridine-4-one (3,4-HOPO) (Figure 1). 1,2-HOPO is the only one that is a hydroxamic acid, and therefore has the lower pKa among this family (Figure 1) [13]. 1,2-HOPO is deprotonated at physiological pH, which could be an advantage thinking in medicinal chemistry terms. This does not happen in the aliphatic hydroxamic acid derivatives, which are present in the natural siderophores.

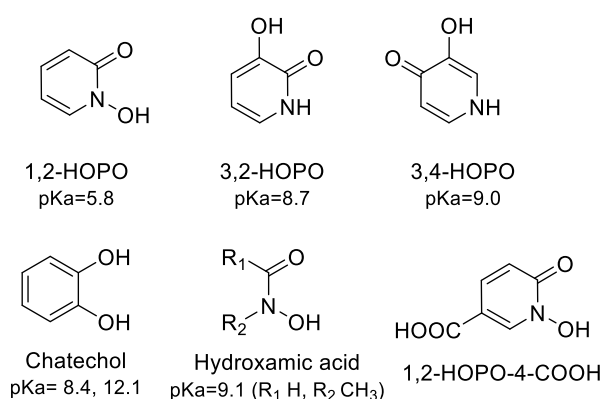


Figure 1. Representative structures of different HOPOs, n-Hydroxypyridine-m-one, n:1, 3, m:2, 4.

To incorporate these moieties in an organic scaffold, an additional functionality is needed. In this regard, two commercially available carboxylic acid derivatives of 1,2-HOPO, in position 4 and 6 [4/6-carboxy-1-hydroxypyridin-2-one (1,2-HOPO-4-COOH/1,2-HOPO-6-COOH)], can facilitate its incorporation into an organic scaffold or other biological molecule of interest.

To facilitate the preparation of HOPO containing peptides and study their Fe(III) binding, we have previously reported a method to synthesize these molecules on solid phase support using 1,2-HOPO-4-COOH (Figure 1), which is incorporated with the OH unmasked to the ϵ -amino function of the Lys, resulting in a very convenient synthetic strategy [14, 15].

In this work we describe three ligands (A, B, and C) containing 1,2-HOPO binding units anchored to peptide through 1,2-HOPO-4-COOH. Furthermore, the carboxamide derivative of the binding unit 1,2-HOPO-4-COOH (Y) has been also included in the study (Figure 2). The ligands vary in denticity, two bidentates (A, Y) and two linear hexadentate (B, C) chelators. The solution thermodynamic properties of the four ligands (A, B, C, Y), as well as their Fe (III) complexes based on spectrophotometric methods are described herein. This will give an indication of their potential application as therapeutic agents.

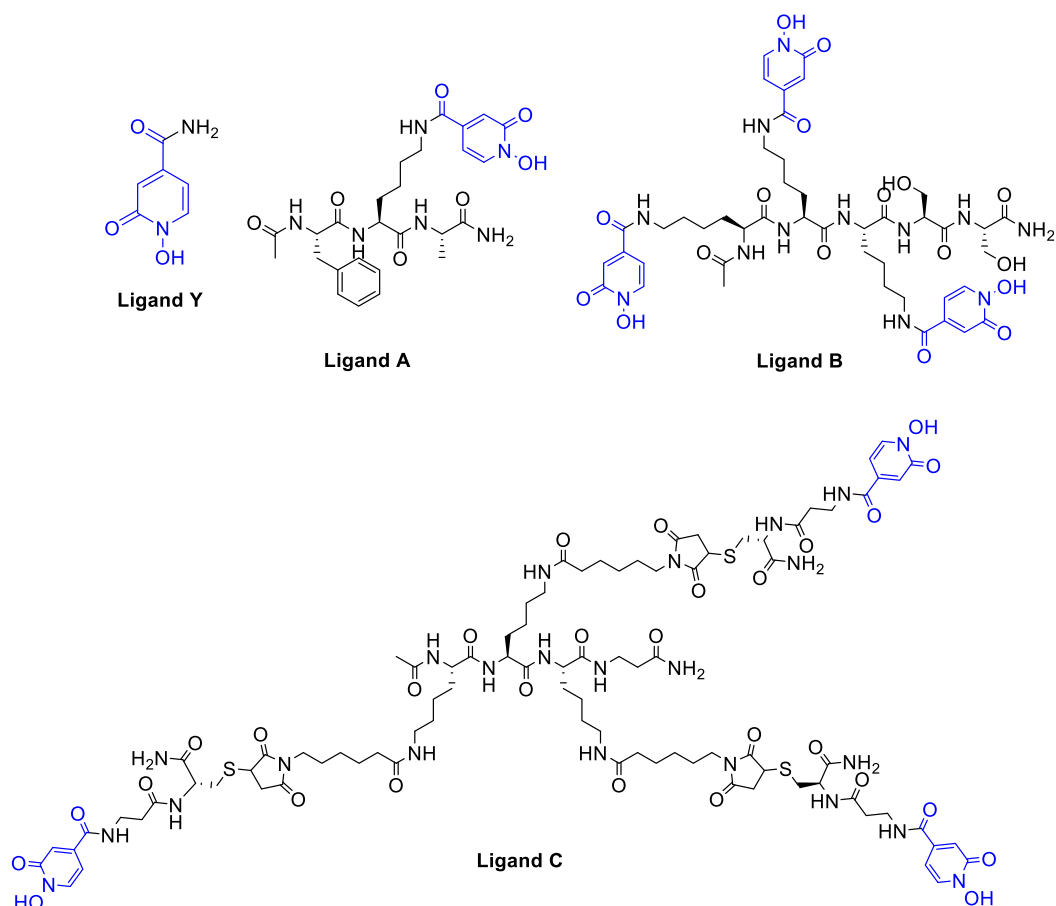


Figure 2. HOPO-containing ligands A, B, C and Y.

2. Results and discussion

2.1 Synthesis of the ligands

Syntheses of A and B have been previously described in our earlier publication [14]. Their syntheses were carried out in a stepwise manner by incorporation of 1,2-HOPO-4-COOH to the peptide chain anchored to the resin after the selective deprotection of the ϵ -amino of the Lys. Y was obtained by amidation of 1,2-HOPO-4-COOH.

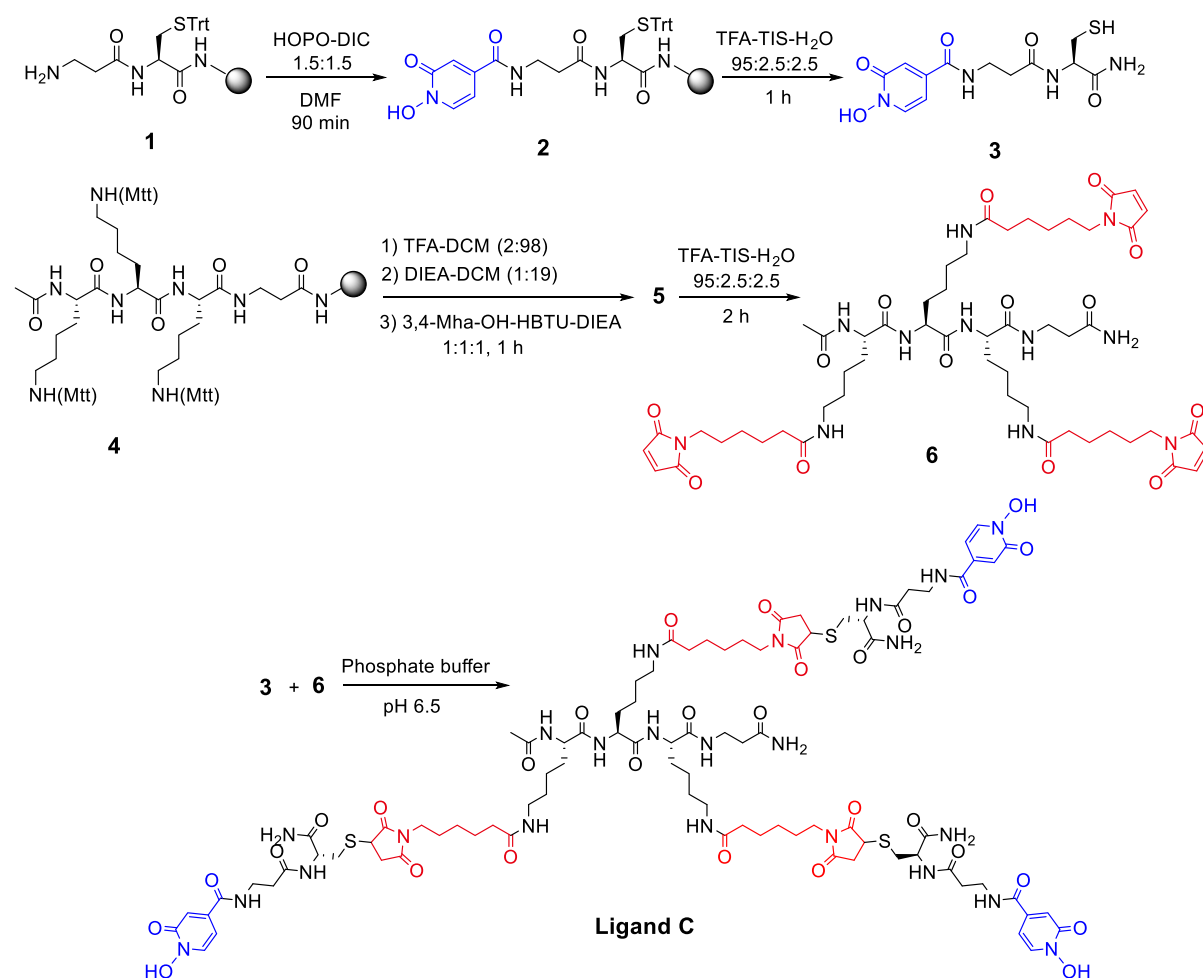
Ligand C is prepared by a convergent approach where a small unit of β -Ala-Cys having the 1,2-HOPO at the N-terminal and the free thiol of the Cys is incorporated in solution to the peptide having maleimido moieties anchored to the three Lys of the peptides (Scheme 1). Ligand A, B, and C have their N-terminus acetylated to prevent any possible interference in Fe(III) chelation.

Units **3** and **6** have been prepared on Rink-amide-resin using Fmoc/tBu based SPPS techniques. Thus, 1,2-HOPO-4-COOH was incorporated to the H- β Ala-Cys(Trt)-NH-Rink-amide-resin (**2**) using N,N'-diisopropylcarbodiimide (DIC) as activating agent, without protection of the N-OH as previously described by our group [14] (Scheme 1). After the cleavage of the resin with trifluoroacetic acid (TFA)-

triisopropylsilane (TIS)-H₂O (95:2.5:2.5), which also remove the Trt (trityl) of the Cys side-chain, the free thiol peptide (**3**) was purified by semi-preparative HPLC.

Using the same strategy, Ac-Lys(Mtt)-Lys(Mtt)-Lys(Mtt)-βAla-NH-Rink-amide resin (**4**) was prepared. The Mtt (methyltrityl) of the ε-amino of the Lys was selectively removed using 2% trifluoroacetic acid (TFA) in dichloromethane (DCM). Treatment with 5% N,N-diisopropylethylamine (DIEA) in DCM liberates the free amines, which were acylated with 6-maleimidohexanoic acid with HBTU and DIEA. Peptide **6** was cleaved from the resin as before and purified by semi-preparative HPLC.

Conjugation of peptides **3** and **6** was smoothly performed through a thiol-ene Michael addition of peptide **3** containing the free thiol on the maleimido moieties of peptide **6** at pH 6.5 which avoid the dimerization on the thiol-peptide (Scheme 1). Although this kind of reactions renders high purity products and usually desalting is only required, Ligand C was purified by semi-preparative HPLC for ensuring the highest purity for the subsequent physico-chemical determination.



Scheme 1. Preparation of Ligand C.

2.2 Physicochemical characterization of ligands and their complexes

The calculation of the ligand's affinity towards Fe (III) requires the determination of the acid dissociation constants of all ligands (pKa) as well as the formation constants of their complexes with Fe (III) ($\log \beta_{MLH}$). The pKa's were determined by spectrophotometric titrations and the $\log \beta_{MLH}$ by solution competition with the well-known strong metal chelator ethylenediaminetetraacetic acid (EDTA).

Bidentate ligands are expected to form an FeL_3 complexes, and FeL for hexadentate. Since our ligands are peptide-based and they contain other functional groups (acetylated N-terminals as well as hydroxyl groups of the Ser in ligand B), we first performed an experiment to determine the stoichiometry of each ligand's complex.

2.2.1 Ligand-Fe (III) complex stoichiometry determination

The stoichiometry of Fe(III) complexes of each ligand was determined by UV-absorption. A serial solutions (methanol as solvent) in which the ligand concentration was constant with increasing concentration of Fe(III) were prepared. To ensure full deprotonation of the ligands (and consequently maximum complexation) a mild base 2,6-Lutidine was added in a small excess with respect to the ligand. In all cases, the range of Fe(III) concentration added was from 0 to the double amount required to form complexes 1:3 (bidentate ligands) and 1:1 (hexadentate ligands). All mixtures gave pale yellow colour corresponding to the Fe-HOPO complexes. First, the spectra of the solutions containing only Fe(III), only the ligand, and the mixture of both were recorded in a range of 280-700 nm. These spectra, allowed to select the best wavelength to study the complex formation. All the complexes showed a weak broad absorption peak in the range of 400-550 nm with no interferences because the absorption of the free ligand or Fe(III) solution (Fig.3). For further plots, absorbances at 460 nm for ligand Y, 480 nm for ligands A and B and 450 nm for ligand C were chosen.

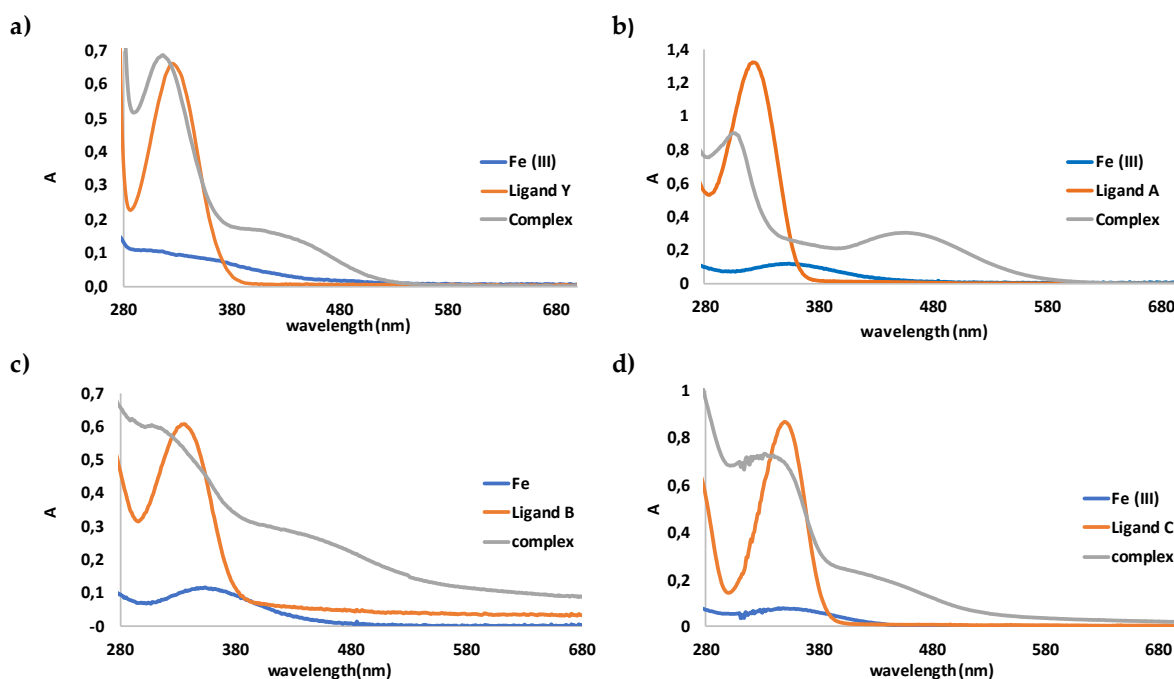


Figure 3. Comparison of UV-visible spectra of Fe (III), and: a) Ligand Y b) Ligand A c) Ligand B d) ligand C, and one representative L-Fe mixture.

The complexes stoichiometry can be easily determined by plotting the absorbance at the selected wavelengths of the previously described solutions vs the different ratio concentration Fe/L (Fig. 4). The plots showed that initially there is an increase in the absorbance as the Fe(III) concentration is increasing. Then, a plateau is reached, no absorbance changes by adding Fe(III), which means that all the ligand is now forming the complex. The obtained ratios were, as expected, around 0.33 for the bidentate ligands Y and A (complex formula FeL_3) and around 1 for the hexadentate ligands B and C (complex formula FeL). On base of these results, the rest of experiments as well as the evaluation of the thermodynamic constants were done using these ratios.

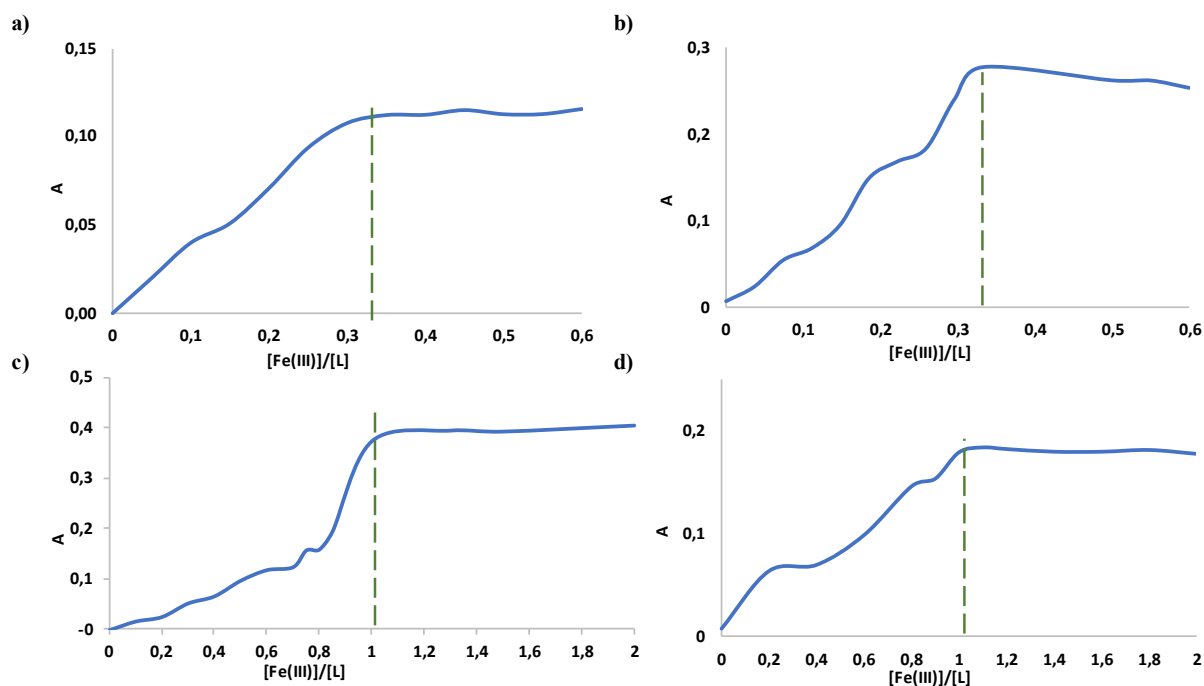


Figure 4. Plot of Absorbance vs [Fe (III)]/[Ligand X]. a) Ligand Y at 460 nm. b) Ligand A at 480 nm. c) Ligand B at 480 nm d) Ligand C at 450 nm.

2.2.2 Determination of pK_a values

The determination of pK_a values of the ligands were carried out by spectrophotometrical titration. The UV spectra were recorded from 200 to 800 nm in a pH range from 2 to 11. In all cases a shift of λ_{\max} from values around 315 to values around 340 (depending on the ligand) were observed (Fig. 5). The data were analysed and refined using the program KEV [16].

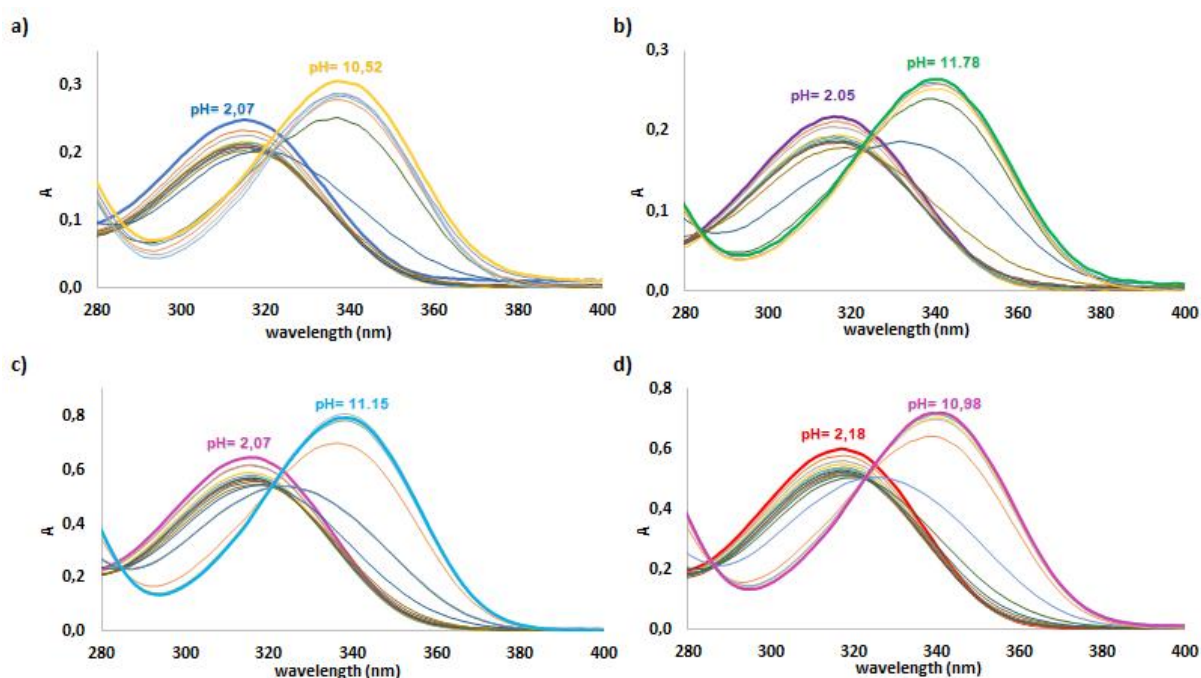


Figure 5. Dependence of UV spectra on pH ($I=0.1$ M KCl) of 5.2×10^{-5} M solutions of a) Ligand Y, b) Ligand A, c) Ligand B, and d) Ligand C. The highlighted spectra correspond to starting solution and end of each titration. Full spectra (200-800 nm) are shown in the SI-Fig.8

The pK_a values obtained from non-linear least square regression analysis are shown in Table 1. These pK_a values are consistent with values reported in the literature for similar compounds [9, 11, 17, 18]. The bidentate ligands Y and A have very close pK_a values (5.29 and 5.25 respectively), being a little bit higher than the pK_a value of 1,2-HOPO-6-COOH (5.17) [12], and lower than 1,2-HOPO (5.8) [13]. For the hexadentate ligands B and C, the respective pK_a values also are very close. The low pK_a values showed by all the ligands indicates that at physiological pH would be mainly in a deprotonated form, hence the competition of the protons for the iron complexation would be low.

Table 1. Proton dissociation constants for HOPO moieties in Ligands Y, A, B, and C.

	Ligand Y	Ligand A	Ligand B	Ligand C
pK_{a1}	-----	-----	4.46	3.75
$(\log \beta_{13})$			(15.79)	(15.18)
pK_{a2}	-----	-----	5.03	5.05
$(\log \beta_{12})$			(11.33)	(11.43)
pK_{a3}	5.29	5.25	6.30	6.38
$(\log \beta_{11})$			(6.30)	(6.38)

2.2.3 Iron (III) complexation

The stability constants ($\log \beta$) were determined by Fe (III) binding competition between the ligands and EDTA. To this end, solutions containing a fix amount of Fe(III) and the corresponding stoichiometric amount of ligand were prepared. Then, EDTA from 0 to 10 times the Fe(III) concentration was added and the solutions were equilibrating for 48 h. After that time the UV spectra were recorded (Fig.10). The spectra showed clearly the different behaviour of the bidentate ligands respect the hexadentate ligands. Whilst, the addition of EDTA made disappear the UV peak corresponding to the complex FeL_3 in case of ligand Y and A, the peak corresponding to FeL remained unaltered for ligands B and C.

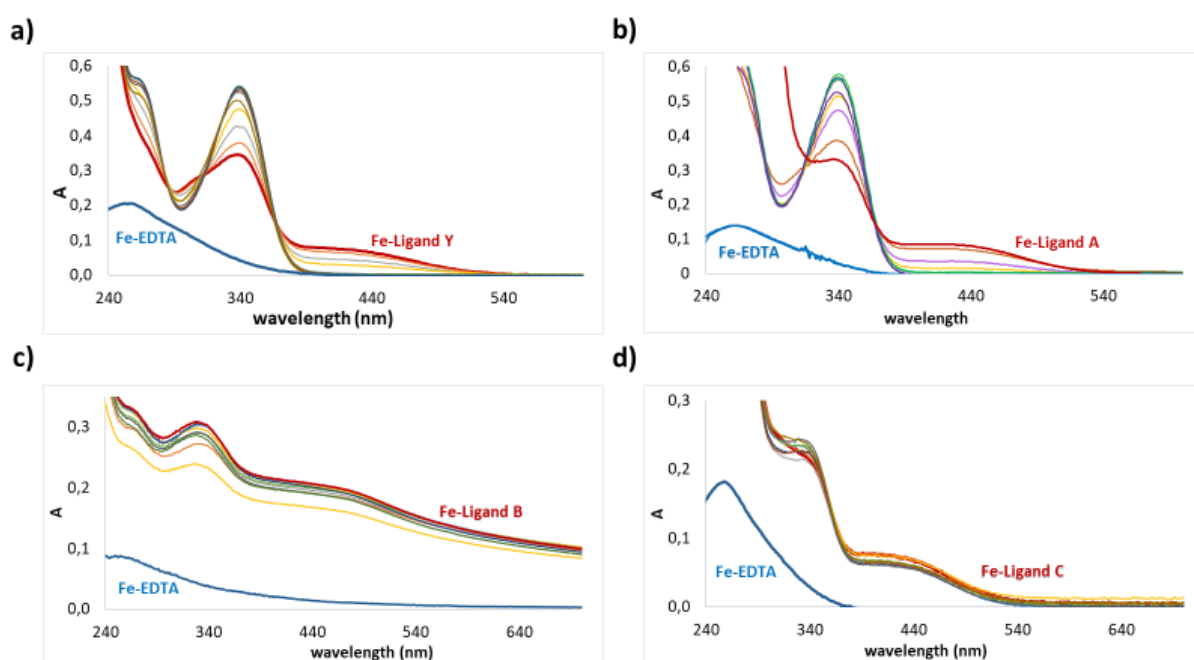


Figure 6. UV-visible spectra of EDTA competition with a) Ligand A b) Ligand Y c) Ligand B d) Ligand C. where $[Fe^{3+}] = 3.0 \times 10^{-5} M$, $[L]_{B,C} = 3.1 \times 10^{-5} M$, $[L]_{A,Y} = 9.3 \times 10^{-5} M$, $[EDTA^{2-}]$ from $6.2 \times 10^{-6} M$ to $3.1 \times 10^{-4} M$.

The spectral data were processed using the software KEV. For the calculations, the absorbance at $\lambda = 470$ nm for ligands Y, A, and B, and $\lambda = 420$ nm for ligand C were used. Additionally, the pK_a values of ligands obtained before, pK_a value of EDTA, the reported formation constants values of $FeEDTA^{2-}$ [12], and the measured pH of each solution were used. Thus, the complexes formation constants β_3 and β_{110} were determined.

Table 2. Complex formation constants and pFe³⁺ values for Ligands Y, A, B, and C

Complex	Log β_{13}	pFe
Fe(L _Y) ₃	24.05	14.59
Fe(L _A) ₃	23.66	14.19
Log β_{110}		pFe
Fe(L _B)	25,99	26,91
Fe(L _C)	27,63	28.58

*this work, pFe³⁺ values were calculated at pH=7.4, [L]=10⁻⁵, [Fe³⁺]=10⁻⁶M

The log β values determined are in the expected range compared with the reported value for their parent compound, 1,2-HOPO (log β_3 =26.9) [12]. When the pFe³⁺ values were calculated clearly the highest affinity corresponds to hexadentate ligands (C and D) in contrast to bidentate, due to the chelate effect. Iron complexes of ligands B and C showed affinities close to similar compounds reported in literature [11].

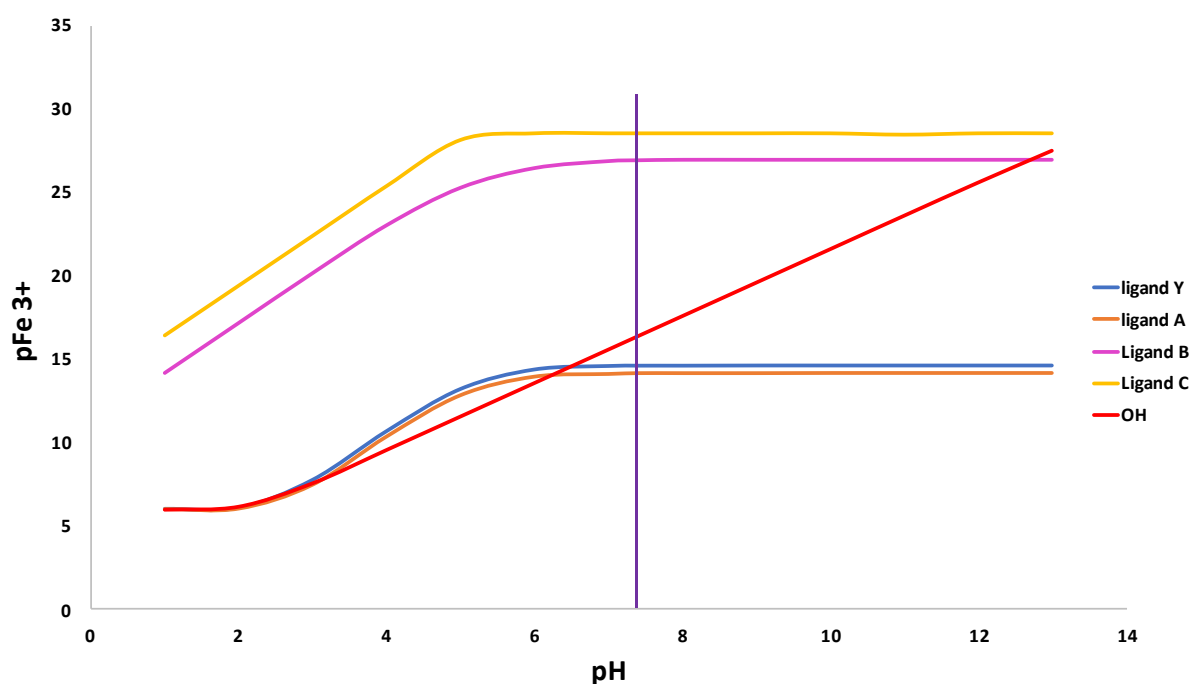


Figure 7. pH dependence of calculated pFe³⁺ values for ligands A,B,C and Y, under the conditions [chelator]=10⁻⁵M, [Fe³⁺]=10⁻⁶ M, compared to OH⁻ (red thick line, the formation constants used for the calculations for the iron hydroxides are, log β_{11} =11.2, log β_{12} =22.3, log β_{13} =-38.8, log β_{14} =34.4) [13].

3. Conclusion

Fe (III) chelators are important class of molecules that have found a vast range of applications in different fields, such as imaging, probes, or chelation therapy. 1,2-HOPO as Fe (III) chelating moiety, through 1,2-HOPO-4-COOH has been safely incorporated to peptide backbones. We have demonstrated that 1,2-HOPO-4-COOH could be incorporated to the peptide through a SPPS scheme without protecting the N-OH. Two routes have been developed. The first one involves a direct acylation of side-chains of Lys, named stepwise strategy (ligand B) and the second one, convergent strategy (ligand C), involves the conjugation of two pre-synthesized moieties, one which contain the 1,2-HOPO unit as well as a thiol function and a core bearing maleimide derivatives. From a synthetic point of view, both routes show pros and cons but allowed the preparation of 1,2-HOPO-peptides. The four ligands included in this study, two bidentate (Y and A) and two hexadentate (B and C) form iron complexes, however the former ones showed low pFe^{3+} whilst ligands B and C showed a strong pFe^{3+} . These results highlight the importance of being hexadentates ligands supported by a scaffold, in this case peptides which can improve the solubility or can be designed to facilitate the uptake. Thus, we can conclude that this new family of 1,2-HOPO containing peptides are promising candidates to be explored further as therapeutic agents and diagnostic applications.

4. Experimental:

General

All reagents and solvents were from commercial suppliers and used without further purification. Fmoc-Rink-amide polystyrene resin and Fmoc-amino acids from Iris Biotech GMBH (Marktredwitz, Germany). OxymaPure was a generous gift of Luxembourg Bio Technologies (Ness Ziona, Israel). 1,2-HOPO-4-COOH was purchased from Chemspace US Inc. (Monmouth Junction, New Jersey, USA). N,N-diisopropylethylamine (DIEA) and piperidine were supplied by Sigma-Aldrich (St. Louis, Missouri, USA). Organic solvents [DMF, DCM] and HPLC quality acetonitrile (CH_3CN) were purchased from SRL (CRD-SRL, India). All other chemicals were purchased from Merck-Millipore (Burlington, Massachusetts, USA).

Analytical HPLC was performed on an Agilent 1100 system using a Phenomenex AerisTMC18 (3.6 μm , 4.6 x 150 mm) column, with flow rate of 1.0 mL/min and UV detection at 220 nm. Chemstation software was used for data processing. Buffer A: 0.1% TFA in H_2O ; buffer B: 0.1% TFA in CH_3CN . LCMS were performed on a Thermo Scientific™ UltiMate™ 3000 Standard Binary System, ISQ™ EC Single Quadrupole. Buffer A: 0.1% formic acid in H_2O ; buffer B: 0.1% formic acid in CH_3CN , Flow: 1.0 mL/min., UV detection=220 nm, Column: Phenomenex Luna C18 3.6 μm , 4.6 x 150 mm column,

30 °C. UV spectra were recorded on two systems: 1) Impelen NP80 UV nano-drop spectrophotometer, 2) Shimadzu UV-3600 using cuvettes with 10 mm path length. pH-measurements were done using Insmark pH-meter. Milli-Q water was used for RP-HPLC analyses as well as all physiochemical characterization experiments.

Solid-Phase peptide synthesis

Ligands A and B were synthesised as previously reported by our group [14]. Peptides were synthesized manually following the SPPS Fmoc/tBu strategy using a syringe fitted with a porous polyethylene disc and attached to a vacuum trap for easy filtration as follows. Fmoc-Rink-amide-resin (0.74 mmol/g) was placed in the syringe, swollen with 3 mL DMF for 15 minutes. The solvent was drained and 2 mL of piperidine-DMF (2:8) (3 mL 1 min + 7 min) drained and washed with DMF (x 3). To a premixed solution of the Fmoc-amino acid (3 eq.) and OxymaPure (3 eq.) in 600 μ L DMF, DIC (3 eq.) was added and the solution was left to pre-activate for 2 minutes. The resulting solution was added to the resin in the syringe and allowed to react for 30 min. with sporadic stirring. The Fmoc removal, Fmoc-amino acid coupling steps were repeated for all amino acids in the sequence.

Cleavage of the peptides from the resin was carried out with TFA-TIS-DCM (95:2.5:2.5, 500 μ L/50 mg resin) for 1 hr. The filtrates were added over cold ether and the precipitated was isolated by centrifugation. Crude peptides were purified by semi-preparative HPLC and lyophilized purified.

Synthesis of ligand C:

HOPO- β Ala-Cys-NH₂ (3)

The dipeptidyl resin H- β Ala-Cys(Trt)-NH-resin (**1**) was prepared as described above. Then, 1,2-HOPO-4-COOH (1.5 equiv.) and DIC (1.5 equiv.) in DMF were added, and the mixture was left for 90 min. with occasional stirring. The resin was washed with DMF(3x). After cleavage peptide **3** was obtained. (ESI-MS (m/z): 329.1 [M+H]⁺), and calculated 328.08 g/mol. See SI for HPLC chromatograms.

Ac-Lys(Mha)-Lys(Mha)-Lys(Mha)- β Ala-NH₂ (6)

Acetylation of the last Lys residue was carried out by adding Ac₂O (10 equiv.) and DIEA (20 equiv.) in DMF to the resin and left to react for 30 min with occasional stirring, and finally washed with DMF (3x).

Mtt side-chain protecting group was removed from peptide resin (**4**) by TFA-TIS- DCM (2:5:93) (3 mL for 2 x 2 min. + 1 x 15 min), then it was washed with DCM, and with 5% DIEA in DCM to neutralize the ϵ -amine side chain. The resin was then washed with DCM and DMF before adding a solution of 6-maleimidohexanoic acid (Mha, 9 equiv., 3 equiv. per Lys) in DMF followed by 3-[bis(dimethylamino)methylumyl]-3H-benzotriazol-1-oxide hexafluorophosphate (HBTU, 9 equiv.)

and DIEA (18 equiv.) coupling reagent, the mixture was stirred for 60 min. before being washed with DMF. After cleavage, the crude was purified by semi-preparative HPLC and lyophilized to yield peptide **6**. (ESI-MS (m/z): 548.13 [M+2H]²⁺), and calculated 1094.26 g/mol. See SI for HPLC chromatograms.

Ligand C

Peptide **6** was dissolved in 1 mL of ACN and 4 mL of phosphate buffer (pH= 6.5) were added. Then, peptide **4** (3 equiv., 1 equiv. per each Mha group) was added to the solution. The overall mixture was shaken vigorously for 2 min to yield the target peptide. which was purified using semi-preparative HPLC and lyophilized to yield Ligand C. ESI-MS (m/z): 694.04 [M+3H]³⁺. And calculated 2077.83 g/mol. See SI for HPLC chromatograms.

Physiochemical characterization of the ligands and their Fe(III) complexes

General solutions preparation:

For all titrations, deionized milli-Q water was used. A carbonate-free 0.1 M KOH solutions were freshly prepared and standardized against KHP (potassium hydrogen phthalate) primary standard before each experiment to find the exact concentration of KOH. HCl solutions (0.1 M) of were freshly prepared. EDTA²⁻ solutions were prepared from EDTA.2Na salt and pre-standardized against MgSO₄ standard solution at pH=10 to Eriochrome black T endpoint. Fe (III) solutions were freshly prepared using Fe(NO₃)₃.9H₂O either in MeOH (for stoichiometric experiments) or in deionized water for the rest of experiments, and standardized against EDTA²⁻ solution at pH=4 using salicylic acid as an indicator. UV-visible spectra were recorded over the range of 200-800 nm (unless other range is specified) against blank solutions of the same solvent and ionic strength of each sample. All physiochemical characterization experiments were done at room temperature.

Ligand-Fe (III) complex stoichiometry determination

A series of 13 solutions all containing 0.15 mM of Ligand A or Y in MeOH (0.05 mM in case of Ligands B and C), various volumes of standard Fe(III) solution in MeOH were added to each solution with Fe(III) to ligand ratios ranging between 0 and 0.6 for ligand A and Y, while ratios were ranging between 0 and 2 for ligands B and C. 1.1 equivalents of 2,6-lutidine per ligand were added to all solutions. All solutions were made up to the same volume with methanol. UV-visible spectra for each solution were recorded.

Determination of Ligand's protonation constants (pKa)

For each ligand, a 50.0 mL solution of 5.2 x 10⁻⁵ M at ionic strength equals 0.1 M of KCl was acidified with HCl standard solution to pH about 2. The solution was then stirred vigorously through the experiment and titrated against KOH solution over the pH range 2-11. Small additions of KOH could

raise the pH by around 0.3 unit, when the pH reading changed by <0.01 unit over 3 seconds, and equilibrium period for 1 minute started. Then pH reading, as well as UV-visible spectra, were recorded after each addition with a total of 20 addition. All titration data were analysed by KEV software and species diagrams were generated using Hyss software.

Competition with EDTA

A series of 10 solutions, all containing a constant amount of the corresponding Ligand (3.1×10^{-5} M, and 9.3×10^{-5} M for ligand A) and Fe(III) (3.0×10^{-5} M) in 0.5 % DMSO-water. Ionic strength in all was adjusted to be 0.1 M KCl, and various volumes of standard EDTA²⁻ solution were added to each solution to make [EDTA²⁻] / [Fe³⁺] ratios ranging between 0 and 10. All solutions were made up to the same volume with water, shaken vigorously for 48 hrs. pH readings and UV-visible spectra for each solution were recorded after the equilibration time.

Conflicts of interest

Authors declare no conflict of interests.

Acknowledgment

The work was funded in part by the following: the National Research Foundation (NRF) (# 105892 and Blue Sky's Research Programme # 120386) and the University of KwaZulu-Natal (South Africa); and the Spanish Ministry of Science, Innovation, and Universities (RTI2018-093831-B-100), the Generalitat de Catalunya (2017 SGR 1439) (Spain), and Marató TV3 foundation 2018 (#20183530). We thank Professor Miquel Viñas (University of Barcelona) for fruitful discussions.

5. Notes and References:

- [1] A. Chao, P.J. Sieminski, C.P. Owens, C.W. Goulding, Iron Acquisition in Mycobacterium tuberculosis, *Chem Rev*, 119 (2019) 1193-1220. DOI: 10.1021/acs.chemrev.8b00285.
- [2] R. Saha, N. Saha, R.S. Donofrio, L.L. Bestervelt, Microbial siderophores: a mini review, *J Basic Microbiol*, 53 (2013) 303-317. DOI: 10.1002/jobm.201100552.
- [3] H. Drechsel, G. Jung, Peptide Siderophores, *J. Pept. Sci.*, 4 (1998) 147-181. DOI: 1075-2617/98/030147-35.
- [4] J.M. Roosenberg II, Y. Lin, Y. Lu, M.J. Miller, Studies and Syntheses of Siderophores, Microbial Iron Chelators, and Analogs as Potential Drug Delivery Agents, *Curr. Med. Chem.*, 7 (2000) 159-197. DOI: 10.2174/0929867003375353.
- [5] D. Al Shaer, O. Al Musaimi, B.G. de la Torre, F. Albericio, Hydroxamate Siderophores: Natural Occurrence, Chemical Synthesis, Iron Binding Affinity and Use as Trojan Horses Against Pathogens, *European Journal of Medicinal Chemistry*, (2020). DOI: 10.1016/j.ejmech.2020.112791.
- [6] G. Tonziello, E. Caraffa, B. Pinchera, G. Granata, N. Petrosillo, Present and future of siderophore-based therapeutic and diagnostic approaches in infectious diseases, *Infect. Dis. Rep.*, 11 (2019) 8208. DOI: 10.4081/idr.2019.8208.
- [7] A. Pandey, C. Savino, S.H. Ahn, Z. Yang, S.G. Van Lanen, E. Boros, Theranostic Gallium Siderophore Ciprofloxacin Conjugate with Broad Spectrum Antibiotic Potency, *J. Med. Chem.*, 62 (2019) 9947-9960. DOI: 10.1021/acs.jmedchem.9b01388.

- [8] T.C. Johnstone, E.M. Nolan, Beyond iron: non-classical biological functions of bacterial siderophores, *Dalton Trans.*, 44 (2015) 6320-6339. DOI: 10.1039/c4dt03559c.
- [9] D.G. Workman, M. Hunter, S. Wang, J. Brandel, V. Hubscher, L.G. Dover, D. Tetard, The influence of linkages between 1-hydroxy-2(1H)-pyridinone coordinating groups and a tris(2-aminoethyl)amine core in a novel series of synthetic hexadentate iron(III) chelators on antimicrobial activity, *Bioorg Chem*, 95 (2020) 103465. DOI: 10.1016/j.bioorg.2019.103465.
- [10] D.G. Workman, M. Hunter, L.G. Dover, D. Tetard, Synthesis of novel Iron(III) chelators based on triaza macrocycle backbone and 1-hydroxy-2(H)-pyridin-2-one coordinating groups and their evaluation as antimicrobial agents, *J Inorg Biochem*, 160 (2016) 49-58. DOI: 10.1016/j.jinorgbio.2016.04.018.
- [11] T. Zhou, X.L. Kong, R.C. Hider, Synthesis and iron chelating properties of hydroxypyridinone and hydroxypyranone hexadentate ligands, *Dalton Trans*, 48 (2019) 3459-3466. DOI: 10.1039/c8dt05014g.
- [12] R.C. Scarrow, P.E. Riley, K. Abu-Dari, L.D. White, K.N. Raymond, Ferric Ion Sequestering Agents. 13. Synthesis, Structures, and Thermodynamics of Complexation of Cobalt (111) and Iron(III) Tris Complexes of Several Chelating Hydroxy pyridinones, *Inorg. Chem.*, 24 (1985).
- [13] A. Cilibrizzi, V. Abbate, Y.L. Chen, Y. Ma, T. Zhou, R.C. Hider, Hydroxypyridinone Journey into Metal Chelation, *Chem Rev*, 118 (2018) 7657-7701. DOI: 10.1021/acs.chemrev.8b00254.
- [14] D. Al Shaer, F. Albericio, B.G. de la Torre, Solid-phase synthesis of peptides containing 1-Hydroxypyridine-2-one (1,2-HOPO), *Tetrahedron Letters*, 61 (2020). DOI: 10.1016/j.tetlet.2020.152299.
- [15] D. Al Shaer, B.G. de la Torre, F. Albericio, Protocol for efficient solid-phase synthesis of peptides containing 1-hydroxypyridine-2-one (1,2-HOPO), *MethodsX*, 7 (2020) 101082. DOI: 10.1016/j.mex.2020.101082.
- [16] A.N. Meshkova, G.A. Gamov, KEV: A free software for calculating the equilibrium composition and determining the equilibrium constants using UV-Vis and potentiometric data, *Talanta*, 198 (2019) 200-205. DOI: 10.1016/j.talanta.2019.01.107.
- [17] T.M. Hoette, R.J. Abergel, J. Xu, R.K. Strong, K.N. Raymond, The Role of Electrostatics in Siderophore Recognition by the Immunoprotein Siderocalin, *J. AM. CHEM. SOC.*, 130 (2008) 17584-17592. DOI: 10.1021/ja8074665.
- [18] E.J. Werner, J. Kozhukh, M. Botta, E.G. Moore, S. Avedano, S. Aime, K.N. Raymond, 1,2-Hydroxypyridonate/Terephthalamide Complexes of Gadolinium(III): Synthesis, Stability, Relaxivity, and Water Exchange Properties, *Inorg Chem*, 48 (2009) 277-286. DOI: 10.1021/ic801730u.

Chapter 5. 2019 FDA TIDES (Peptides and Oligonucleotides) Harvest

Danah Al Shaer^{1,2,†}, **Othman Al Musaimi**^{1,2,†}, **Fernando Albericio**^{2,3,*} and **Beatriz G. de la Torre**^{1,*}

1 KRISP, School of Laboratory of Medicine and Medical Science, College of Health Sciences, University of KwaZulu-Natal, Durban 4001, Africa; 217078895@stuukznac.onmicrosoft.com (D.A.S.); 217078894@stuukznac.onmicrosoft.com (O.A.M.)

2 School of Chemistry and Physics, University of KwaZulu-Natal, Durban 4001, Africa

3 CIBER-BBN, Networking Centre on Bioengineering, Biomaterials and Nanomedicine and Department of Organic Chemistry, University of Barcelona, 08028 Barcelona, Spain

** Correspondence: albericio@ukzn.ac.za (F.A.); garciadelatorreb@ukzn.ac.za (B.G.d.l.T.); Tel.: +27-614-009-144 (F.A.); Tel.: +27614047528 (B.G.d.l.T.)*

† These authors contributed equally to this work.



Review

2019 FDA TIDES (Peptides and Oligonucleotides) Harvest

Danah Al Shaer ^{1,2,†}, Othman Al Musaimi ^{1,2,†}, Fernando Albericio ^{2,3,*}
and Beatriz G. de la Torre ^{1,*}

¹ KRISP, School of Laboratory of Medicine and Medical Science, College of Health Sciences, University of KwaZulu-Natal, Durban 4001, South Africa; 217078895@stuukznac.onmicrosoft.com (D.A.S.); 217078894@stuukznac.onmicrosoft.com (O.A.M.)

² School of Chemistry and Physics, University of KwaZulu-Natal, Durban 4001, South Africa

³ CIBER-BBN, Networking Centre on Bioengineering, Biomaterials and Nanomedicine and Department of Organic Chemistry, University of Barcelona, 08028 Barcelona, Spain

* Correspondence: albericio@ukzn.ac.za (F.A.); garciadelatorreb@ukzn.ac.za (B.G.d.l.T.); Tel.: +27-614-009-144 (F.A.); Tel.: +27614047528 (B.G.d.l.T.)

† These authors contributed equally to this work.

Received: 11 February 2020; Accepted: 3 March 2020; Published: 5 March 2020

Abstract: 2019 has been an excellent year in terms of peptides and oligonucleotides (TIDES) approved by the FDA. Despite the drop in the number of total drugs approved by the FDA in 2019 in comparison with 2018 (48 vs. 59), the total number of TIDES authorized increased (seven vs. three). Year after year, TIDES are increasingly present in therapy, as imaging agents, theragnostic and constituent moieties of other complex drugs, such as antibody drug conjugates. This means a consolidation of these kinds of drugs in the pharmaceutical arena, paving the way in the coming years for the approval of others for diverse medical indications. Here the TIDES approved in 2019 are analyzed in terms of chemical structure, medical target, mode of action, and adverse effects.

Keywords: afamelanotide; bremelanotide; DOTATOC; drugs; ⁶⁸Ga-DOTATOC; enfortumab vedotin; golodirsen; givosiran; polatuzumab vedotin; oligonucleotides; peptides; pharmaceutical market

1. Introduction

Drug discovery is a multifactorial activity involving the private and public sectors and, more importantly, society as a whole, which is represented by patients. From 2016 to 2019, the United States Food and Drug Administration (FDA) approved a total of 175 new drugs for commercialization (Figure 1) [1–4]. Forty-eight drugs were approved in 2019 [4], 10 of which were biologics and the remaining 38 new chemical entities (NCEs). The peptides and oligonucleotides (TIDES) class is manufactured chemically and thus belongs to NCEs; however, these molecules have a clear biological structure and could; therefore, be considered a transition between the two subclasses. In 2019, five TIDES (three peptides and two oligonucleotides) were authorized (Table 1). This figure accounts for approximately 10% of the total drugs approved and agrees with the total number approved in the period 2016–2019 (18 TIDES: 11 peptides and seven oligonucleotides, vs. 175). Furthermore, three antibody drug conjugates (ADCs) were approved. In two of these, namely enfortumab vedotin-ejfv and polatuzumab vedotin-piiq, the payload is the peptide monomethyl auristatin E (MMAE), derived from the marine mollusk dolastatin. Finally, peptides serve as linkers between the payload and the antibody in all three ADCs. Thus, TIDES are present in eight of the 48 drugs approved in 2019. These figures reflect the high relevance of such molecules for biomedical applications.

Here, TIDES from the 2019 harvest are discussed from a molecular perspective, application as a drug, mode of action, and adverse effects.

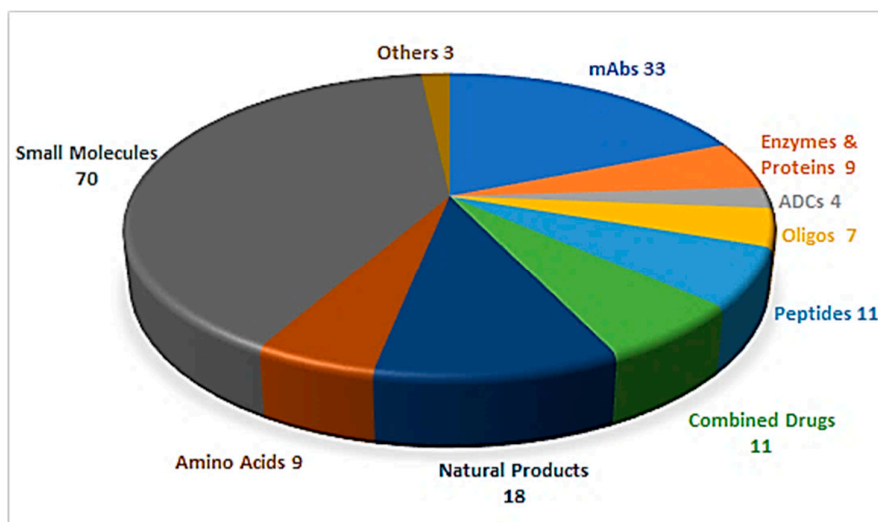


Figure 1. A total of 175 new drugs approved by the FDA from 2016 to 2019 [1–4]. mAbs; Monoclonal antibodies, ADCs; antibody drug conjugates, Oligos; oligonucleotides

Table 1. Summary of the 2019 FDA peptides & oligonucleotides (TIDES) harvest [5].

#	Active Ingredient Trade Name	Type	Indication	Target	Route
1	Golodirsén Vyondys 53™	Antisense oligonucleotide	Duchenne’s Muscular Dystrophy (DMD)	Exon 53 in dystrophin gene	Intravenous
2	Givosiran Givlaari™	Antisense oligonucleotide	Acute Hepatic Porphyria (AHP)	Aminolevulinatase synthase 1 (ALAS1) mRNA	Subcutaneous
3	⁶⁸ Ga-DOTATOC	Peptide	Scintigraphic imaging	Somatostatin receptor	Intravenous
4	Afamelanotide Scenesse™	Peptide	Erythropoietic protoporphyria (EPP)	Melanocyte-stimulating hormone receptor	Subcutaneous
5	Bremelanotide Vyleesi™	Peptide	Hypoactive sexual desire disorder	Melanocyte-stimulating hormone receptor	Subcutaneous
6	Enfortumab vedotin-ejfv Padcev™	ADC with peptide payload and linker	Urothelial cancers	Nectin-4 receptor	Intravenous
7	Polatuzumab vedotin-piiq Polivy™	ADC with peptide payload and linker	Refractory diffuse large B-cell lymphoma	CD79b receptor expressed in mature B-cells	Intravenous
8	Fam-trastuzumab deruxtecan-nxki Enhertu™	ADC with a peptide linker	Unresectable or metastatic HER2-positive breast cancer	Human epidermal growth factor receptor-2 (HER2)	Intravenous

ADC; antibody drug conjugate.

2. Oligonucleotides

2.1. Golodirsén (Vyondys 53™)

Golodirsén is an antisense oligonucleotide with a single strand of 25 monomers [6]. The subunits are linked through a synthetic neutral phosphorodiamidate morpholino oligomer (PMO) backbone. This neutral backbone confers greater stability to the strand than the natural negatively-charged

phosphodiester linkage. The nitrogenous bases are incorporated on a morpholine six-membered heterocycle instead of the natural five-membered ribose (or deoxyribose) ring. The strand ends with a small hydrophilic triethylene glycol chain. Golodirsen has a molecular weight of 8647.4 Da (Figure 2).

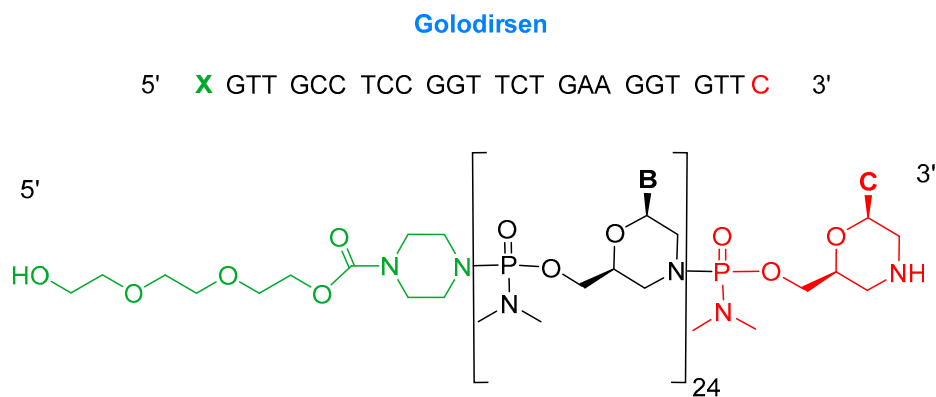


Figure 2. Chemical structure of golodirsin (Vyondys 53™).

Golodirsin was developed for the treatment of Duchenne’s muscular dystrophy (DMD), which is a progressive muscle deterioration that starts in early childhood and in most cases ends up crippling patients before adolescence. After several years, patients die mainly from heart failure [7,8]. This disorder is caused by a deletion mutation in the dystrophin gene, which transcribes for the production of dystrophin, a huge protein that covers muscular fibers, protecting them from damage upon contraction and enhancing muscle performance. The genetic disorder causes the production of a non-functioning dystrophin protein and consequently muscle wasting. This gene is linked to the X chromosome, thus making DMD disorder more noticeable in male infants [7,9].

The dystrophin gene consists of 79 exons. Some genetic mutations cause the deletion of exon 52, which blocks the translation process [7]. Golodirsin conceals exon 53, allowing translation to take place and producing a protein with some missing parts but still functional [9,10]. A similar previous drug, eteplirsin (Exondys 51), was the first FDA-approved antisense (in 2016) therapy for the treatment of the same disorder by exon 51 skipping [10].

Golodirsin is administered intravenously [10]. Some adverse effects include headache, pyrexia, fall, abdominal pain, nasopharyngitis, cough, vomiting, and nausea [11].

Both golodirsin and eteplirsin were developed by Sarepta Therapeutics. Golodirsin was approved by the FDA on 12 December 2019 [12], and there are some concerns about its renal toxicity [10,11].

2.2. Givosiran (Givlaari™)

Givosiran is the second small interfering RNA (siRNA) drug to be approved by FDA [13] (the first one was patisiran (Onpattro™), which was authorized in 2018 for the treatment of hereditary transthyretin-mediated amyloidosis and targets hepatic cells [14,15]). Additionally, givosiran is the first approved drug that demonstrates the enhanced stabilization chemistry (ESC)-GalNAc-siRNA conjugate technology. This technology involves several synthetic RNA stabilization chemistries. The 2'-OH of the ribose in some monomers are methylated (forming 2'-O-methyl-ribonucleoside), while in others they are substituted by the highly electronegative fluorine atom (2'-F-ribonucleoside) in order to boost the stability of the double strands against the nuclease [16]. In addition, the hepatocyte-targeting ligand that is attached to the 3' terminal of the sense strand has three N-acetylgalactosamine moieties. The other three terminals (5' of the sense strand, and 3',5' of the antisense strand) have thiophosphate linkages in the last two subunits for each side. This conjugation (ESC-GalNAc-siRNA) confers enhanced stability upon subcutaneous administration of the siRNA and offers a 10-fold increased potency of the drug over the standard template chemistry (STC) [13,17]. Givosiran is

prepared as the sodium salt of a double-strand oligonucleotide (sense and antisense strands) (Figure 3) and it has a molecular weight of 17,245.56 Da.

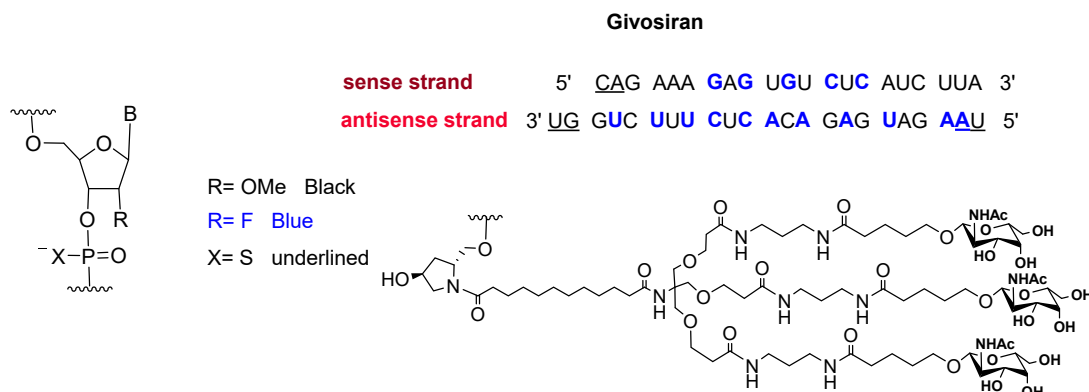


Figure 3. Chemical structure of givosiran (Givlaari™) [13].

Givosiran was developed for the treatment of acute hepatic porphyria in adults, which is a genetic disorder that results in the accumulation of the neurotoxic intermediates aminolevulinic acid (ALA) and porphobilinogen (PBG) during the hemes production cycle (the hemoglobin oxygen binding site) in hepatic cells. This disorder causes severe abdominal pain, nausea, vomiting, and constipation and it can be triggered by several factors, such as certain drugs, low sugar intake due to fasting, smoking, and stress [18,19].

The N-acetylgalactosamine ligand bound to the sense strand facilitates the uptake into liver cells [19]. After entering hepatocytes, it binds to and silences aminolevulinic acid synthase 1 (ALAS1) mRNA, thereby halting ALA production and consequently preventing the accumulation of the toxic intermediates in body tissues [18].

Givosiran is administered subcutaneously and is well-tolerated. However, regular check-ups for liver and kidney function are highly recommended [19]. It was developed by Alnylam Pharmaceuticals Inc. (Cambridge, Massachusetts, United States) (the same company that developed patisiran) and approved by the FDA on 20 November 2019 [20].

3. Peptide-Based Drugs

3.1. [⁶⁸Ga]Ga-DOTATOC ([⁶⁸Ga]Ga-DOTA, Tyr³)-Octreotide)

⁶⁸Ga-DOTATOC belongs to the peptide receptor radionuclide therapy (PRRT) class and it is used for scintigraphic imaging [21]. It is composed of ⁶⁸Ga, which has a half-life of 68 min and a high positron abundance [22,23], as radionuclide, which is chelated by DOTA that in turn is attached to [Tyr³]-octreotide (Figure 4). It is used mainly in positron imaging therapy (PET) for the detection of somatostatin receptor-positive neuroendocrine tumors (NETs).

⁶⁸Ga-DOTATOC is related to ⁶⁸Ga-DOTATATE, which was approved in 2016. Both share almost the same affinity towards the somatostatin receptor (sstr). The in vitro affinity of ⁶⁸Ga-DOTATATE towards sstr subtype 2 (sstr2) is about 10-fold that of ⁶⁸Ga-DOTATOC [24]. Nevertheless, ⁶⁸Ga-DOTATOC is able to detect more NET lesions than the DOTATATE analogue with highly reproducible imaging efficiency [22]. Furthermore, the higher in vitro affinity of the DOTATATE analogue has not proven to be relevant clinically. These studies showed that ⁶⁸Ga-DOTATOC has a higher affinity towards sstr2 receptor than the ⁶⁸Ga-DOTATATE as demonstrated by higher tumor uptake values. This could explain the superiority of ⁶⁸Ga-DOTATOC for more lesion detection [24].

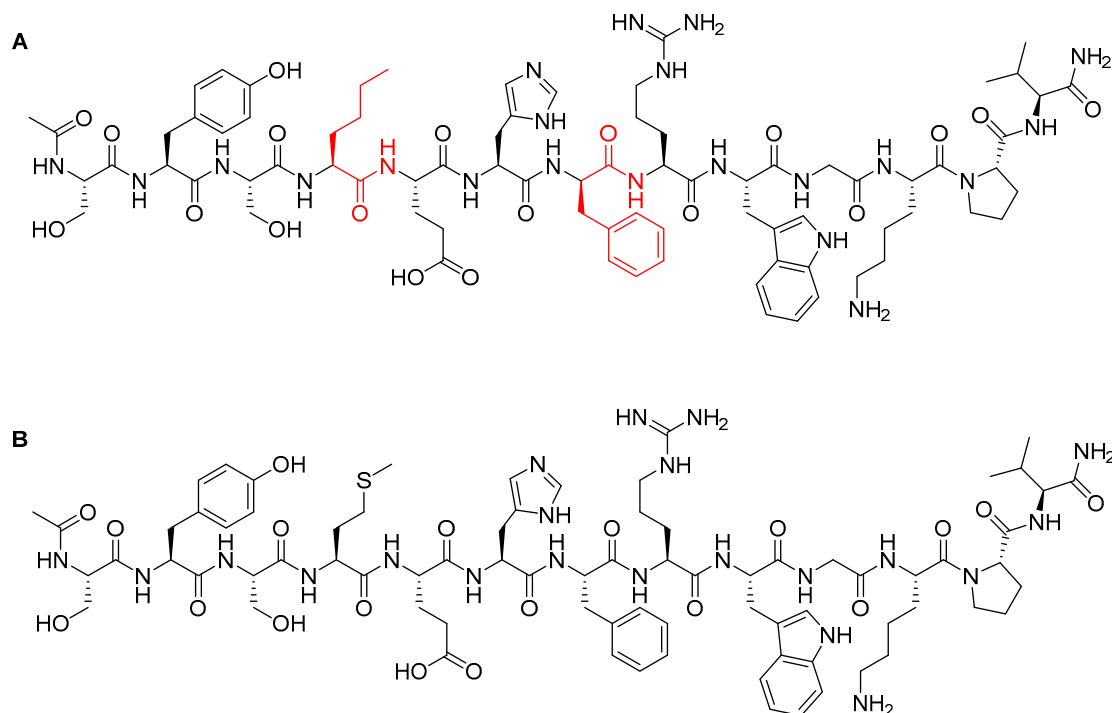


Figure 5. Chemical structure of: (A) Afamelanotide (Scenesse™); (B) α -melanocyte stimulating hormone (α -MSH). Differences are shown in red.

Afamelanotide is used for the treatment of erythropoietic protoporphyria (EPP) [29]. It provides photoprotection upon exposure to direct sunlight by increasing the density of eumelanin in the skin—this is called the skin tanning process [34]. It works like α -MSH, binding to the G-protein-coupled MC1R in dermal cells and stimulating the production of melanin, along with consecutive biological processes [35]. Despite stimulating melanin synthesis in the same way, afamelanotide is considered a preventive therapy. In which, unlike α -MSH natural analogue, afamelanotide induces eumelanin synthesis in advance and independently of having UV-damaged skin cells [32].

Afamelanotide is administered subcutaneously [36] through a poly(lactic-co-glycolic acid) (PLGA) biodegradable polymer [34]. It has a half-life of 30 to 50 min, after which it is hydrolyzed into shorter peptides and amino acid residues [30,32]. Most of the active materials are excreted within two days, and by 10 days its plasma levels are below the limit of quantification [30,32].

Afamelanotide has some adverse effects, including, but not limited to, nausea, vomiting, flushing, headache, cough, fatigue, and dizziness [36].

Its development was started in the 1980s by Tomi Sawyer and Victor Hruby at the University of Arizona [29], then Clinuvel Inc. performed the required clinical studies and brought the product to the market. It has been sold in Switzerland and Italy since 2013 [35], but was only approved by FDA on 8 October 2019 [37].

3.3. Bremelanotide (VYLEESI™)

Bremelanotide is a homodetic side-chain to tail cyclic heptapeptide with the sequence of Ac-Nle-cyclo[Asp-His-DPhe-Arg-Trp-Lys]-OH [38]. The cycle through an amide bond is between the β carboxylic acid of Asp ϵ amino of the Lys, which is the C-terminal residue. The exocyclic Nle is acetylated. It has a molecular weight of 1025.182 Da. The structure is shown in Figure 6.

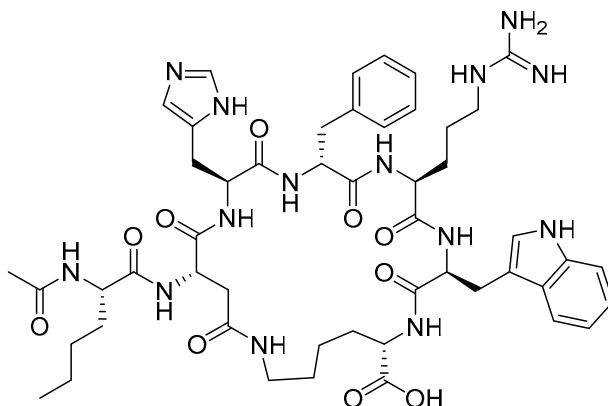


Figure 6. Chemical structure of brexelanotide (Vyleesi™).

Brexelanotide is an analogue of the natural α -MSH [39]. It works as an agonist of melanocortin receptors and is used to treat hypoactive sexual desire (HSDD) in women of fertile age. This disorder results in a low sex drive that is not caused by other factors such as medications or any medical or psychiatric condition [40,41].

The drug is administered subcutaneously and possible adverse effects include nausea, flushing, injection site reactions, headache, and vomiting [42,43].

Brexelanotide was first studied by Arizona Cancer Research Centre as a self-tanning inducer. However, increased sexual desire in patients was observed as a side effect [44]. Later on, it was developed by Palatin technology as a treatment for HSDD [44] and then out-licensed to AMAG PHARMS and approved by the FDA on 21 June 2019 [45].

Although brexelanotide and afamelanotide belong to the same α -MSH hormone-analogous family, their structures show some differences. Brexelanotide resembles the middle section of afamelanotide with the absence of the first three residues Ser-Tyr-Ser at the N-terminus and the last two residues Pro-Val at the C-terminus, in addition to the Gly, the tenth residue. Additionally, brexelanotide comprises a side-to-side amide bond that forms the cycle.

4. Peptides as Payloads in ADCs

4.1. Enfortumab Vedotin-Ejfv (PADCEV™)

Enfortumab vedotin-ejfv is an ADC therapy [46], which is an emerging therapeutic strategy for transporting cytotoxic chemotherapeutic agents to certain tumors [47]. This drug has three main components: payload/cytotoxic drug, mAb, and linker [47]. The antibody comprises human monoclonal antibody (enfortumab) and targets nectin-4 (also known as poliovirus receptor-related protein 4 (PVL4)), which is highly expressed in NETs [46]. Enfortumab is derived either from a Chinese hamster cell ovary line [ASG-22CE] or can be prepared via murine hybridoma technology (AGS-22M6E (or ASG-22ME)) [48]. Enfortumab is conjugated to MMAE (vedotin) via a cathepsin-cleavable linker (Figure 7) [46].

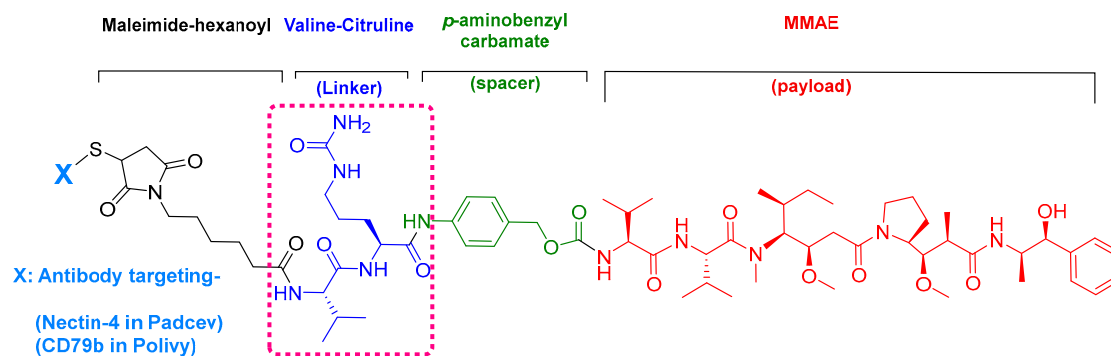


Figure 7. Chemical structure of enfortumab vedotin-ejfv (Padcev™) and polatuzumab vedotin-piiq (Polivy™). MMAE; monomethyl auristatin E

MMAE, the cytotoxic component [49], is a synthetic pentapeptide (717.99 Da) that works as a potent microtubule-disrupting agent [48]. It is a structurally-modified analogue of the natural dolastatin 10 [50], a potent antineoplastic pentapeptide (785.1 Da) isolated from the marine mollusk *dolabella auricularia* by Pettit et al. in 1987 [51]. MMAE comprises the following four amino acid residues: dolavaline (Dov), Val, dolaisoleuine (Dil), dolaproine (Dap), and the C-terminal amine dolaphenine (Doe) [52]. Figure 8 shows the structural differences between the synthetic MMAE analogue (A) and the natural pentapeptide dolastatin 10 (B).

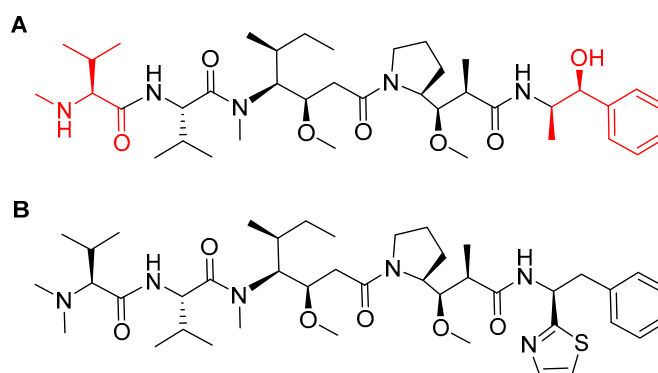


Figure 8. Chemical structure of: (A) Synthetic monomethyl auristatin E (MMAE) analogue; (B) natural dolastatin 10. Differences are shown in red [50].

Given that MMAE is a peptide, it is metabolized into smaller non-toxic amino acid fragments and then recycled or excreted by the body [53].

Nectin-4 is a 66 kDa protein that is expressed in several cancer tissues (breast, lung, bladder, among others) and highly expressed in urothelial cancer [54]. Among other nectins, it is considered a potential target due to its distinguished sequence in its family (1, 2, or 3) with low degree of similarity with other family members [55]. Furthermore, the limited expression of nectin-4 in normal tissues minimizes the possibility of these tissues being targeted during the course of the treatment [46].

Enfortumab vedotin-ejfv is a pan-fibroblast growth factor receptor (FGFR) suppressor [56]. It is indicated for the treatment of adult patients with locally advanced or metastatic urothelial cancer who previously received immune checkpoint therapy [programmed death receptor-1 (PD-1) or programmed death-ligand 1 (PD-L1) inhibitor] [56]. After platinum-based chemotherapy, enfortumab vedotin-ejfv is prescribed as a second line treatment for patients with susceptible FGFR2 or FGFR3 [48,56].

The drug binds to nectin-4-expressing cells. The resulting complex is internalized into the cell and then the valine-citruline (Val-Cit) dipeptide linker is recognized and cleaved by cathepsin-B in the tumor cell [57]. Consequently, the cytotoxic MMAE is selectively released, thereby leading to apoptosis [46].

It is administered intravenously. Common adverse effects include fatigue, peripheral neuropathy, decreased appetite, rash, alopecia, nausea, dysgeusia, diarrhea, dry eye, pruritus, and dry skin [58].

It was developed by Astellas Pharma and granted accelerated approval by the FDA on 18 December 2019 [59].

4.2. Polatuzumab Vedotin-Piiq (Polivy™)

Polatuzumab vedotin-piiq is an ADC therapy [60]. It comprises the same linker and payload as in the previous drug (enfortumab vedotin-ejfv), but a different antibody (Figure 9). It is prescribed as a combination with bendamustine and rituximab (BR combination) [5] and is used for the treatment of adults with relapsed or refractory diffuse large B-cell lymphoma [61].

It selectively binds to CD79b that is overexpressed in mature B-cells [61]. Following the same mechanism in enfortumab vedotin-ejfv which ends by cell apoptosis.

Of note, the tolerability and safety profile of this drug was accepted for non-Hodgkin's lymphoma (NHL) patients but not for those with chronic lymphocytic leukemia (CLL) [61].

It is administered intravenously. Common adverse effects include neutropenia, thrombocytopenia, anemia, peripheral neuropathy, fatigue, diarrhea, pyrexia, decreased appetite, and pneumonia [62].

It was developed by Roche and granted accelerated approval by the FDA on 10 June 2019 [63].

5. Peptides as Linkers in ADCs

5.1. Val-Cit

The choice of a suitable linker is a highly sensitive step in ADC manufacturing. First, the conjugate should be stable enough during its circulation in blood serum to avoid damaging body tissues. Second, the programmable release of cargo should be easily triggered once the conjugate reaches its target. Thus, a suitable linker should successfully combine serum stability and in-target lability without adversely affecting the stability of the antibody itself upon conjugation [64,65].

Among the four known types of linkers, namely hydrazones, disulfides, peptides, and thioethers [57], short peptidyl linkers, such as Val-Cit dipeptide, fulfill the requirements for this critical function and even outperform the tetra-peptidyl linkers (Gly-Phe-Leu-Gly and Ala-Leu-Ala-Leu) previously used and that showed some aggregation issues upon conjugation [57,64,65]. The premature release of the payload in the case of hydrazone (due to pH changes) and disulfide linkers (due to exchange with other thiols, such as glutathione) may influence the potency of the treatment, while the delayed release of cargo in the case of thioether linkers (payload is released only after total degradation of the antibody) may cause the loss of anticancer activity [65,66]. In Padcev™ and Polivy™, a maleimidocarbonyl moiety is added to the N-terminal of the dipeptide Val-Cit to facilitate conjugation to the antibody. The amide bond formed by the C-carboxyl group of the Cit, which is linked to a self-immolative p-amino benzyl carbamate (PABC) spacer, is stable in serum and can be rapidly hydrolyzed by lysosomal cathepsin-B releasing the PABC-MMAE moiety. This undergoes self-elimination liberating the payload MMAE [57]. The mechanism of drug release is shown in Figure 9.

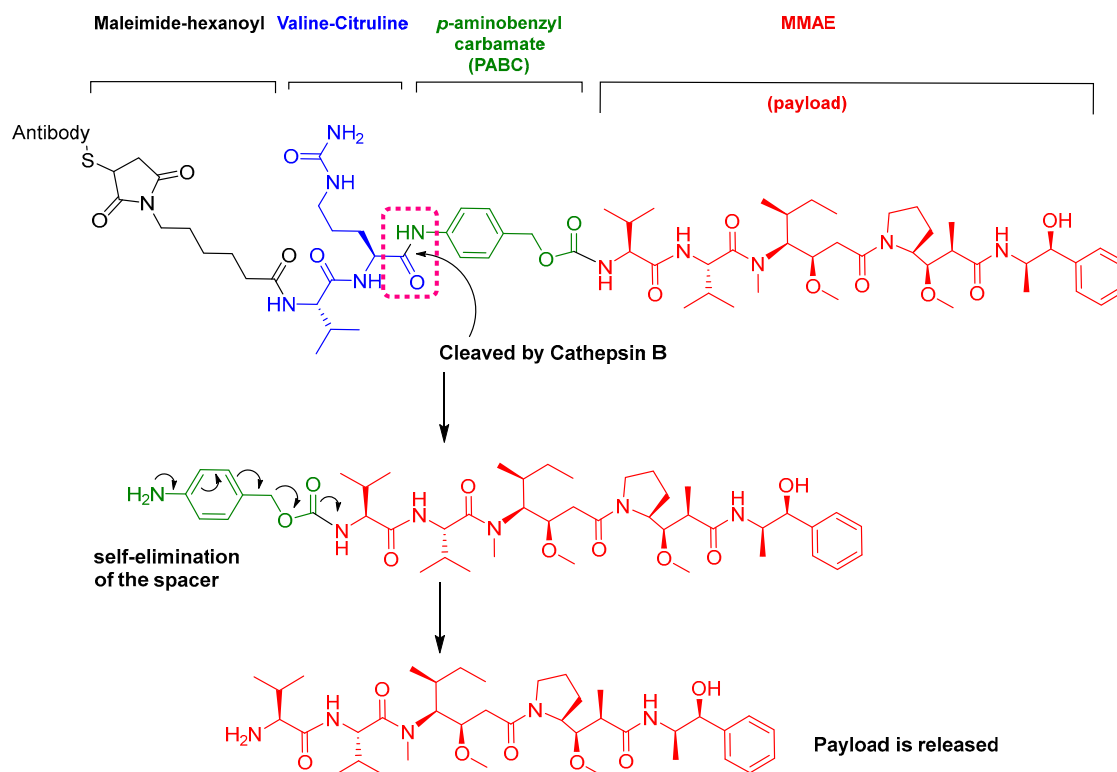


Figure 9. Mechanism of payload release in ADCs with Val-Cit linker and p-aminobenzyl carbamate as a spacer [67]. MMAE; monomethyl auristatin E

5.2. Gly-Gly-Phe-Gly

The ADC fam-trastuzumab deruxtecan-nxki (Enhertu™) targets human epidermal growth factor receptor-2 (HER2) [66]. It is used for the treatment of adult patients with unresectable or metastatic HER2-positive breast cancer [68].

Trastuzumab is conjugated to the antibody via a tetrapeptide linker, Gly-Gly-Phe-Gly (Figure 10), which is cleavable by lysozymes [69]. The linker is connected to a Cys residue of the mAb through a maleimidocarbonyl component [66] and to a self-immolative amino methylene (AM) spacer [70].

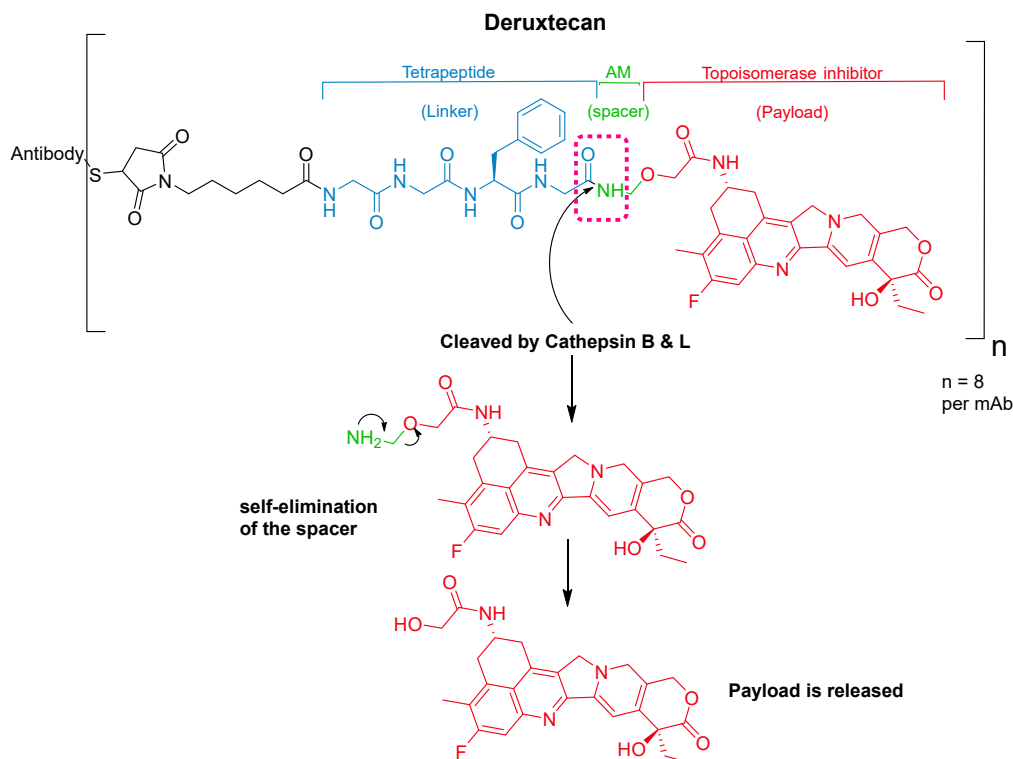


Figure 10. Chemical structure of fam-trastuzumab deruxtecan-nxki (Enhertu™) showing the tetrapeptide linker and amino methylene cleavage in the payload-release process. AM; aminomethyl

It was developed by Daiichi Sankyo and approved by the FDA on 20 December 2019 [71].

4. Conclusions

The 2019 year has been very successful regarding the role of TIDES in the drug arena. Thus, in addition to approving two oligonucleotides and three peptide APIs, the FDA authorized two ADCs with a peptide as payload. Finally, three ADCs (including the former two) have a peptide-based linker. Therefore, eight of the 48 drugs (more than 15%) approved this year were or contained TIDES. While the peptide market is already consolidated through the large number of authorized peptides, the seven oligonucleotides recently (2017–2019) given the green light pave the way for the approval of others for diverse medical indications. Of note, is the presence of peptides as payloads and as a part of the linkers in the ADCs.

Author Contributions: All authors participated in the search for information and in writing the manuscript and have approved the final version.

Funding: This work was funded in part by the following: the National Research Foundation (NRF) and the University of KwaZulu-Natal (South Africa); MINECO, (RTI2018-093831-B-100), and the Generalitat de Catalunya (2017 SGR 1439) (Spain).

Conflicts of Interest: The authors declare no conflicts of interest.

References

- de la Torre, B.G.; Albericio, F. The pharmaceutical industry in 2016. An analysis of FDA drug approvals from a perspective of the molecule type. *Molecules* **2017**, *22*. 10.3390/molecules22030368
- de la Torre, B.G.; Albericio, F. The pharmaceutical industry in 2017. An analysis of FDA drug approvals from the perspective of molecules. *Molecules* **2018**, *23*. 10.3390/molecules23030533

3. de la Torre, B.G.; Albericio, F. The pharmaceutical industry in 2018. An analysis of FDA drug approvals from the perspective of molecules. *Molecules* **2019**, *24*. 10.3390/molecules24040809
4. de la Torre, B.G.; Albericio, F. The pharmaceutical industry in 2019. An analysis of FDA drug approvals from the perspective of molecules. *Molecules* **2020**, *25*, 745. 10.3390/molecules25030745
5. New drug therapy approvals 2019. **2019**. <https://www.fda.gov/media/134493/download>, (accessed on 27 February 2020)
6. Heo, Y.A. Golodirsen: First approval. *Drugs* **2020**, *80*, 329-333. 10.1007/s40265-020-01267-2
7. D'Amario, D.; Gowran, A.; Canonico, F.; Castiglioni, E.; Rovina, D.; Santoro, R.; Spinelli, P.; Adorasio, R.; Amodio, A.; Perrucci, G.L.; Borovac, J.A.; Pompilio, G.; Crea, F. Dystrophin cardiomyopathies: Clinical management, molecular pathogenesis and evolution towards precision medicine. *J. Clin. Med.* **2018**, *7*. 10.3390/jcm7090291
8. Farini, A.; Gowran, A.; Bella, P.; Sitzia, C.; Scopece, A.; Castiglioni, E.; Rovina, D.; Nigro, P.; Villa, C.; Fortunato, F.; Comi, G.P.; Milano, G.; Pompilio, G.; Torrente, Y. Fibrosis rescue improves cardiac function in dystrophin-deficient mice and duchenne patient-specific cardiomyocytes by immunoproteasome modulation. *Am. J. Pathol.* **2019**, *189*, 339-353. 10.1016/j.ajpath.2018.10.010
9. Echevarria, L.; Aupy, P.; Goyenvalle, A. Exon-skipping advances for duchenne muscular dystrophy. *Hum. Mol. Genet.* **2018**, *27*, R163-R172. 10.1093/hmg/ddy171
10. Rodrigues, M.; Yokota, T. An overview of recent advances and clinical applications of exon skipping and splice modulation for muscular dystrophy and various genetic diseases. *Methods Mol. Biol.* **2018**, *1828*, 31-55. 10.1007/978-1-4939-8651-4_2
11. Vyondys 53 drug label. **2019**. https://www.accessdata.fda.gov/drugsatfda_docs/label/2019/211970s000lbl.pdf, (accessed on 27 February 2020)
12. Vyondys 53 approval letter. **2019**. https://www.accessdata.fda.gov/drugsatfda_docs/applletter/2019/211970Orig1s000ltr.pdf, (accessed on 27 February 2020)
13. Janas, M.M.; Harbison, C.E.; Perry, V.K.; Carito, B.; Sutherland, J.E.; Vaishnav, A.K.; Keirstead, N.D.; Warner, G. The nonclinical safety profile of GalNAc-conjugated i therapeutics in subacute studies. *Toxicol. Pathol.* **2018**, *46*, 735-745. 10.1177/0192rna623318792537
14. Zhang, X.; Goel, V.; Robbie, G.J. Pharmacokinetics of patisiran, the first approved RNA interference therapy in patients with hereditary transthyretin-mediated amyloidosis. *J. Clin. Pharmacol.* **2019**, *00*, 1-13. 10.1002/jcph.1553
15. Akinc, A.; Maier, M.A.; Manoharan, M.; Fitzgerald, K.; Jayaraman, M.; Barros, S.; Ansell, S.; Du, X.; Hope, M.J.; Madden, T.D.; Mui, B.L.; Semple, S.C.; Tam, Y.K.; Ciufolini, M.; Witzigmann, D.; Kulkarni, J.A.; van der Meel, R.; Cullis, P.R. The Onpattro story and the clinical translation of nanomedicines containing nucleic acid-based drugs. *Nature Nanotechnology* **2019**, *14*, 1084-1087. 10.1038/s41565-019-0591-y
16. Allerson, C.R.; Sioufi, N.; Jarres, R.; Prakash, T.P.; Naik, N.; Berdeja, A.; Wanders, L.; Griffey, R.H.; Swayze, E.E.; Bhat, B. Fully 2'-modified oligonucleotide duplexes with improved in vitro potency and stability compared to unmodified small interfering RNA. *J. Med. Chem.* **2005**, *48*, 901-904. 10.1021/jm049167j
17. Shen, X.; Corey, D.R. Chemistry, mechanism and clinical status of antisense oligonucleotides and duplex RNAs. *Nucleic Acids Res.* **2018**, *46*, 1584-1600. 10.1093/nar/gkx1239

18. Vita, G.; Vita, G.L.; Stancanelli, C.; Gentile, L.; Russo, M.; Mazzeo, A. Genetic neuromuscular disorders: Living the era of a therapeutic revolution. Part 1: Peripheral neuropathies. *Neurol. Sci.* **2019**, *40*, 661-669. 10.1007/s10072-019-03778-7
19. de Paula Brandao, P.R.; Titze-de-Almeida, S.S.; Titze-de-Almeida, R. Leading RNA interference therapeutics part 2: Silencing delta-aminolevulinic acid synthase 1, with a focus on givosiran. *Mol. Diagn. Ther.* **2020**, *24*, 61-68, 10.1007/s40291-019-00438-6
20. Givlaari approval letter. **2019**. https://www.accessdata.fda.gov/drugsatfda_docs/label/2019/0212194s000lbl.pdf, (accessed on 27 February 2020)
21. Graham, M.M.; Gu, X.; Ginader, T.; Breheny, P.; Sunderland, J.J. ⁶⁸Ga-dotatoc imaging of neuroendocrine tumors: A systematic review and metaanalysis. *J. Nucl. Med.* **2017**, *58*, 1452-1458. 10.2967/jnumed.117.191197
22. Menda, Y.; Ponto, L.L.B.; Schultz, M.K.; Zamba, G.K.D.; Watkins, G.L.; Bushnell, D.L.; Madsen, M.T.; Sunderland, J.J.; Graham, M.M.; O'Dorisio, T.M.; O'Dorisio, M.S. Repeatability of gallium-68 dotatoc positron emission tomographic imaging in neuroendocrine tumors. *Pancreas* **2013**, *42*, 937-943. 10.1097/MPA.0b013e318287ce21
23. Le, V.S. (68)Ga generator integrated system: Elution-purification-concentration integration. *Recent Results Cancer Res.* **2013**, *194*, 43-75. 10.1007/978-3-642-27994-2_4
24. Poeppel, T.D.; Binse, I.; Petersenn, S.; Lahner, H.; Schott, M.; Antoch, G.; Brandau, W.; Bockisch, A.; Boy, C. ⁶⁸Ga-dotatoc versus ⁶⁸Ga-dotatate pet/ct in functional imaging of neuroendocrine tumors. *J. Nucl. Med.* **2011**, *52*, 1864-1870. 10.2967/jnumed.111.091165
25. Khor, L.K.; Loi, H.Y.; Sinha, A.K.; Tong, K.T.; Goh, B.C.; Loh, K.S.; Lu, S.J. ⁶⁸Ga-dota-peptide: A novel molecular biomarker for nasopharyngeal carcinoma. *Head Neck* **2016**, *38*, E76-80. 10.1002/hed.24164
26. ⁶⁸Ga-dotatoc drug label. **2019**. https://www.accessdata.fda.gov/drugsatfda_docs/label/2019/210828s000lbl.pdf, (accessed on 27 February 2020)
27. ⁶⁸Ga-dotatoc approval letter. **2019**. https://www.accessdata.fda.gov/drugsatfda_docs/applletter/2019/210828Orig1s000ltr.pdf, (accessed on 27 February 2020)
28. Al Shaer, D.; Al Musaimi, O.; Albericio, F.; de la Torre, B.G. 2018 FDA tides harvest. *Pharmaceuticals (Basel)* **2019**, *12*, 52. 10.3390/ph12020052
29. Sawyer, T.K.; Sanfilippo, P.J.; Hruby, V.J.; Engel, M.H.; Heward, C.B.; Burnett, J.B.; Hadley, M.E. 4-Norleucine, 7-D-phenylalanine- α -melanocyte-stimulating hormone: A highly potent α -melanotropin with ultralong biological activity. *Proc. Natl. Acad. Sci. USA* **1980**, *77*, 5754-5758. 10.1073/pnas.77.10.5754
30. Lane, A.M.; McKay, J.T.; Bonkovsky, H.L. Advances in the management of erythropoietic protoporphyria - role of afamelanotide. *Appl. Clin. Genet.* **2016**, *9*, 179-189. 10.2147/TACG.S122030
31. Spichty, R.; Balimann, M.; Barman, J.; Minder, E.I. A bioassay for the detection of neutralizing antibodies against the alpha-melanocyte stimulating hormone analog afamelanotide in patients with erythropoietic protoporphyria. *J. Pharm. Biomed. Anal.* **2013**, *75*, 192-198. 10.1016/j.jpba.2012.11.040
32. Kim, E.S.; Garnock-Jones, K.P. Afamelanotide: A review in erythropoietic protoporphyria. *Am. J. Clin. Dermatol.* **2016**, *17*, 179-185. 10.1007/s40257-016-0184-6

33. Fetissov, S.O.; Harro, J.; Jaanisk, M.; Järv, A.; Podar, I.; Allik, J.; Nilsson, I.; Sakthivel, P.; Lefvert, A.K.; Hökfelt, T. Autoantibodies against neuropeptides are associated with psychological traits in eating disorders. *PNAS* **2005**, *102*, 14865-14870. 10.1073/pnas.0507204102
34. Committee for medicinal products for human use (CHMP). Scenese assessment report. **2014**. https://www.ema.europa.eu/en/documents/assessment-report/scenese-epar-public-assessment-report_en.pdf, (accessed on 27 February 2020)
35. Fabrikant, J.; Touloei, K.; Brown, S.M. A review and update on melanocyte stimulating hormone therapy: Afamelanotide. *J. Drugs Dermatol.* **2013**, *12*, 775-779. <https://www.ncbi.nlm.nih.gov/pubmed/23884489>, (accessed on 27 February 2020)
36. Scenese drug label. **2019**. https://www.accessdata.fda.gov/drugsatfda_docs/label/2019/210797s000lbl.pdf, (accessed on 27 February 2020)
37. Scenese approval letter. **2019**. https://www.accessdata.fda.gov/drugsatfda_docs/appltr/2019/210797Orig1s000ltr.pdf, (accessed on 27 February 2020)
38. Molinoff, P.B.; Shadiack, A.M.; Earle, D.; Diamond, L.E.; Quon, C.Y. Pt-141: A melanocortin agonist for the treatment of sexual dysfunction. *Ann. N. Y. Acad. Sci.* **2003**, *994*, 96-102. 10.1111/j.1749-6632.2003.tb03167.x
39. Miller, M.K.; Smith, J.R.; Norman, J.J.; Clayton, A.H. Expert opinion on existing and developing drugs to treat female sexual dysfunction. *Expert Opin. Emerg. Drugs* **2018**, *23*, 223-230. 10.1080/14728214.2018.1527901
40. Both, S. Recent developments in psychopharmaceutical approaches to treating female sexual interest and arousal disorder. *Curr. Sex Health Rep.* **2017**, *9*, 192-199. 10.1007/s11930-017-0124-3
41. Clayton, A.H.; Lucas, J.; DeRogatis, L.R.; Jordan, R. Phase I randomized placebo-controlled, double-blind study of the safety and tolerability of bremelanotide coadministered with ethanol in healthy male and female participants. *Clin. Ther.* **2017**, *39*, 514-526 e514. 10.1016/j.clinthera.2017.01.018
42. Kingsberg, S.A.; Clayton, A.H.; Portman, D.; Williams, L.A.; Krop, J.; Jordan, R.; Lucas, J.; Simon, J.A. Bremelanotide for the treatment of hypoactive sexual desire disorder: Two randomized phase 3 trials. *Obstet. Gynecol.* **2019**, *134*, 899-908. 10.1097/aog.0000000000003500
43. Vyleesi drug label. **2019**. https://www.accessdata.fda.gov/drugsatfda_docs/label/2019/210557s000lbl.pdf, (accessed on 27 February 2020)
44. Sohita, D.; Susan, J., K. *Bremelanotide: First approval. Drugs.* **2019**, *79*, 1599-1606 10.6084/m9.figshare.9409019.v1
45. Vyleesi approval letter. **2019**. https://www.accessdata.fda.gov/drugsatfda_docs/appltr/2019/210557Orig1s000ltr.pdf, (accessed on 27 February 2020)
46. Challita-Eid, P.M.; Satpayev, D.; Yang, P.; An, Z.; Morrison, K.; Shostak, Y.; Raitano, A.; Nadell, R.; Liu, W.; Lortie, D.R.; Capo, L.; Verlinsky, A.; Leavitt, M.; Malik, F.; Avina, H.; Guevara, C.I.; Dinh, N.; Karki, S.; Anand, B.S.; Pereira, D.S.; Joseph, I.B.; Donate, F.; Morrison, K.; Stover, D.R. Enfortumab vedotin antibody-drug conjugate targeting nectin-4 is a highly potent therapeutic agent in multiple preclinical cancer models. *Cancer Res.* **2016**, *76*, 3003-3013. 10.1158/0008-5472.Can-15-1313
47. Diamantis, N.; Banerji, U. Antibody-drug conjugates--an emerging class of cancer treatment. *Br. J. Cancer.* **2016**, *114*, 362-367. 10.1038/bjc.2015.435
48. McGregor, B.A.; Sonpavde, G. Enfortumab vedotin, a fully human monoclonal antibody against nectin 4 conjugated to monomethyl auristatin E for metastatic urothelial carcinoma. *Expert Opin. Investig. Drugs.* **2019**, *28*, 821-826. 10.1080/13543784.2019.1667332

49. Pettit, G.R.; Srirangam, J.K.; Barkoczy, J.; Williams, M.D.; Durkin, K.P.; Boyd, M.R.; Bai, R.; Hamel, E.; Schmidt, J.M.; Chapuis, J.C. Antineoplastic agents 337. Synthesis of dolastatin 10 structural modifications. *Anticancer Drug Des.* **1995**, *10*, 529-544. <https://www.ncbi.nlm.nih.gov/pubmed/7495477>, (accessed on 27 February 2020)
50. Bouchard, H.; Viskov, C.; Garcia-Echeverria, C. Antibody-drug conjugates-a new wave of cancer drugs. *Bioorg. Med. Chem. Lett.* **2014**, *24*, 5357-5363. 10.1016/j.bmcl.2014.10.021
51. Pettit, G.R.; Singh, S.B.; Hogan, F.; Lloyd-Williams, P.; Herald, D.L.; Burkett, D.D.; Clewlow, P.J. Antineoplastic agents. Part 189. The absolute configuration and synthesis of natural (-)-dolastatin 10. *Am. Chem. Soc.* **1989**, *111*, 5463-5465. 10.1021/ja00196a061
52. Akaiwa, M.; Martin, T.; Mendelsohn, B.A. Synthesis and evaluation of linear and macrocyclic dolastatin 10 analogues containing pyrrolidine ring modifications. *ACS Omega* **2018**, *3*, 5212-5221. 10.1021/acsomega.8b00093
53. Han, T.H.; Zhao, B. Absorption, distribution, metabolism, and excretion considerations for the development of antibody-drug conjugates. *Drug Metab. Dispos.* **2014**, *42*, 1914-1920. 10.1124/dmd.114.058586
54. Takahashi, S.; Uemura, M.; Kimura, T.; Kawasaki, Y.; Takamoto, A.; Yamaguchi, A.; Melhem-Bertrandt, A.; Gartner, E.M.; Inoue, T.; Akazawa, R.; Kadokura, T.; Tanikawa, T. A phase I study of enfortumab vedotin in Japanese patients with locally advanced or metastatic urothelial carcinoma. *Invest. New Drugs* **2019**. 10.1007/s10637-019-00844-x
55. Reymond, N.; Fabre, S.; Lecocq, E.; Adelaide, J.; Dubreuil, P.; Lopez, M. Nectin4/PRR4, a new afadin-associated member of the nectin family that trans-interacts with Nectin1/PRR1 through V domain interaction. *J. Biol. Chem.* **2001**, *276*, 43205-43215. 10.1074/jbc.M103810200
56. Hanna, K.S. Clinical overview of enfortumab vedotin in the management of locally advanced or metastatic urothelial carcinoma. *Drugs* **2019**, *80*, 1-7, 10.1007/s40265-019-01241-7
57. Bargh, J.D.; Isidro-Llobet, A.; Parker, J.S.; Spring, D.R. Cleavable linkers in antibody-drug conjugates. *Chem. Soc. Rev.* **2019**, *48*, 4361-4374. 10.1039/c8cs00676h
58. Padcev drug label. **2019**. https://www.accessdata.fda.gov/drugsatfda_docs/label/2019/761137s000lbl.pdf, (accessed on 27 February 2020)
59. Padcev approval letter. **2019**. https://www.accessdata.fda.gov/drugsatfda_docs/applletter/2019/761137Orig1s000ltr.pdf, (accessed on 27 February 2020)
60. Sehn, L.H.; Matasar, M.J.; Flowers, C.R.; Kamdar, M.; McMillan, A.K.; Hertzberg, M.; Assouline, S.; Kim, T.M.; Kim, W.S.; Ozcan, M.; Croft, B.; Hirata, J.; Cheng, J.; Ku, G.; Herrera, A.F. Polatuzumab vedotin plus bendamustine with rituximab in relapsed/refractory diffuse large B-cell lymphoma: Updated results of a phase Ib/II randomized study. *Blood* **2019**, *134*, 4081-4081. 10.1182/blood-2019-123449
61. Palanca-Wessels, M.C.A.; Czuczman, M.; Salles, G.; Assouline, S.; Sehn, L.H.; Flinn, I.; Patel, M.R.; Sangha, R.; Hagenbeek, A.; Advani, R.; Tilly, H.; Casasnovas, O.; Press, O.W.; Yalamanchili, S.; Kahn, R.; Dere, R.C.; Lu, D.; Jones, S.; Jones, C.; Chu, Y.-W.; Morschhauser, F. Safety and activity of the anti-CD79B antibody-drug conjugate polatuzumab vedotin in relapsed or refractory B-cell non-Hodgkin lymphoma and chronic lymphocytic leukaemia: A phase 1 study. *Lancet Oncol.* **2015**, *16*, 704-715. 10.1016/s1470-2045(15)70128-2
62. Polivy drug label. **2019**. https://www.accessdata.fda.gov/drugsatfda_docs/label/2019/761121s000lbl.pdf, (accessed on 27 February 2020)

63. Polivy approval letter. **2019**.
https://www.accessdata.fda.gov/drugsatfda_docs/applletter/2019/761121Orig1s000ltr.pdf, (accessed on 27 Februray 2020)
64. Dorywalska, M.; Dushin, R.; Moine, L.; Farias, S.E.; Zhou, D.; Navaratnam, T.; Lui, V.; Hasa-Moreno, A.; Casas, M.G.; Tran, T.T.; Delaria, K.; Liu, S.H.; Foletti, D.; O'Donnell, C.J.; Pons, J.; Shelton, D.L.; Rajpal, A.; Strop, P. Molecular basis of valine-citrulline-PABC linker instability in site-specific ADCs and its mitigation by linker design. *Mol. Cancer Ther.* **2016**, *15*, 958-970. 10.1158/1535-7163.MCT-15-1004
65. Dal Corso, A.; Cazzamalli, S.; Gebleux, R.; Mattarella, M.; Neri, D. Protease-cleavable linkers modulate the anticancer activity of noninternalizing antibody-drug conjugates. *Bioconjug. Chem.* **2017**, *28*, 1826-1833. 10.1021/acs.bioconjchem.7b00304
66. Xu, Z.; Guo, D.; Jiang, Z.; Tong, R.; Jiang, P.; Bai, L.; Chen, L.; Zhu, Y.; Guo, C.; Shi, J.; Yu, D. Novel HER2-targeting antibody-drug conjugates of trastuzumab beyond T-DM1 in breast cancer: Trastuzumab deruxtecan(DS-8201a) and (Vic-)trastuzumab duocarmazine (SYD985). *Eur. J. Med. Chem.* **2019**, *183*, 111682. 10.1016/j.ejmech.2019.111682
67. Jain, N.; Smith, S.W.; Ghone, S.; Tomczuk, B. Current ADC linker chemistry. *Pharm. Res.* **2015**, *32*, 3526-3540. 10.1007/s11095-015-1657-7
68. Nakada, T.; Sugihara, K.; Jikoh, T.; Abe, Y.; Agatsuma, T. The latest research and development into the antibody-drug conjugate, [fam-] trastuzumab deruxtecan (DS-8201a), for HER2 cancer therapy. *Chem. Pharm. Bull. (Tokyo)* **2019**, *67*, 173-185. 10.1248/cpb.c18-00744
69. Ogitani, Y.; Abe, Y.; Iguchi, T.; Yamaguchi, J.; Terauchi, T.; Kitamura, M.; Goto, K.; Goto, M.; Oitate, M.; Yukinaga, H.; Yabe, Y.; Nakada, T.; Masuda, T.; Morita, K.; Agatsuma, T. Wide application of a novel topoisomerase I inhibitor-based drug conjugation technology. *Bioorg. Med. Chem. Lett.* **2016**, *26*, 5069-5072. 10.1016/j.bmcl.2016.08.082
70. Ogitani, Y.; Aida, T.; Hagihara, K.; Yamaguchi, J.; Ishii, C.; Harada, N.; Soma, M.; Okamoto, H.; Oitate, M.; Arakawa, S.; Hirai, T.; Atsumi, R.; Nakada, T.; Hayakawa, I.; Abe, Y.; Agatsuma, T. DS-8201a, a novel HER2-targeting ADC with a novel DNA topoisomerase I inhibitor, demonstrates a promising antitumor efficacy with differentiation from T-DM1. *Clin. Cancer Res.* **2016**, *22*, 5097-5108. 10.1158/1078-0432.CCR-15-2822
71. Enhertu approval letter. **2019**.
https://www.accessdata.fda.gov/drugsatfda_docs/applletter/2019/761139Orig1s000ltr.pdf, (accessed on 27 Februray 2020)



© 2020 by the authors. Licensee MDPI, Basel, Switzerland. This article is an open access article distributed under the terms and conditions of the Creative Commons Attribution (CC BY) license (<http://creativecommons.org/licenses/by/4.0/>).

Chapter 6. 2018 FDA Tides Harvest

Danah Al Shaer^{1,2,†}, **Othman Al Musaimi**^{1,2,†}, **Fernando Albericio**^{2,3,*} and **Beatriz G. de la Torre**^{1,*}

¹ *KRISP, School of Laboratory of Medicine and Medical Science, College of Health Sciences, University of KwaZulu-Natal, Durban 4001, South Africa;
217078895@stuukznac.onmicrosoft.com (D.A.S.); 217078894@stuukznac.onmicrosoft.com (O.A.M.)*

² *School of Chemistry and Physics, University of KwaZulu-Natal, Durban 4001, South Africa*



³ *CIBER-BBN, Networking Centre on Bioengineering, Biomaterials and Nanomedicine and Department of Organic Chemistry, University of Barcelona, 08028 Barcelona, Spain*

[†] *These authors contributed equally to this work.*

* *Correspondence: albericio@ukzn.ac.za, Tel.: +27-614009144 (F.A.); garciadelatorreb@ukzn.ac.za, Tel.: +27-614047528 (B.G.d.l.T.)*

Review

2018 FDA Tides Harvest

Danah Al Shaer ^{1,2,†}, Othman Al Musaimi ^{1,2,†}, Fernando Albericio ^{2,3,*}  and Beatriz G. de la Torre ^{1,*} 

¹ KRISP, School of Laboratory of Medicine and Medical Science, College of Health Sciences, University of KwaZulu-Natal, Durban 4001, South Africa; 217078895@stuukznac.onmicrosoft.com (D.A.S.); 217078894@stuukznac.onmicrosoft.com (O.A.M.)

² School of Chemistry and Physics, University of KwaZulu-Natal, Durban 4001, South Africa

³ CIBER-BBN, Networking Centre on Bioengineering, Biomaterials and Nanomedicine and Department of Organic Chemistry, University of Barcelona, 08028 Barcelona, Spain

* Correspondence: albericio@ukzn.ac.za (F.A.); garciadelatorreb@ukzn.ac.za (B.G.d.l.T.); Tel.: +27-614009144 (F.A.); +27-614047528 (B.G.d.l.T.)

† These authors contributed equally to this work.

Received: 12 March 2019; Accepted: 3 April 2019; Published: 5 April 2019



Abstract: In 2018, the United States Food and Drug Administration (FDA) approved a total of 59 new drugs, three of them (5%) are TIDES (or also, -tides), two oligonucleotides and one peptide. Herein, the three TIDES approved are analyzed in terms of medical target, mode of action, chemical structure, and economics.

Keywords: dotatate; drugs; inotersen; Lutathera; oligonucleotides; Onpattro; patisiran; peptides; pharmaceutical market; Tegsedi

1. Introduction

Drug discovery is a unique transdisciplinary activity involving a wide range of interconnected parameters, thus posing a challenge for the pharmaceutical industry and related fields. The mission of this industry is to improve or restore health and wellbeing. Indeed, the administration of an appropriate treatment can very often save lives. Although the pharmaceutical industry was devoted mainly to research and development after the second world war, over the years economics has increasingly gained relevance. Between 12 and 20 years can lapse from the time a discovery has been made in a research laboratory and a product reaching the market, and this development pipeline carries with it an associated cost of up to US \$ 1–2 billion. What are the main reasons behind these long development times and high costs? There is probably no single answer. However, the main causes can be attributed to the increasingly stricter requirements of the corresponding agencies, mainly the federal Food and Drug Administration (FDA) in the USA, and the European Medicines Agency (EMA) in Europe, regarding toxicity and safety profiles, and the need for new drugs to show superior performance to that of those already on the market.

Drugs can be roughly divided into two main categories, namely biologics and chemical entities, the former being prepared by means of biotechnological techniques, and the latter by chemical synthesis. Figure 1 shows the 127 new drugs approved by the FDA in the last three years (2016–2018) (59 in 2018), classified on the basis of chemical structure [1–6]. In this period, 36 biologics (17 in 2018) and 91 chemical entities (42 in 2018) were endorsed by the FDA. In the biologics field, the predominance of monoclonal antibodies (mAbs) is remarkable (28 in 2016–2018, and 12 in just the last year). As chemical entities, the so-called small molecules continue to account for a considerable proportion of new drugs. Natural product-based drugs and TIDES (oligonucleo- and pep-TIDES) each represent approximately

10% of new drugs [7]. Indeed, there are currently 14 drugs (10 in 2018) inspired in natural products, and 13 TIDES (three in 2018) on the market.

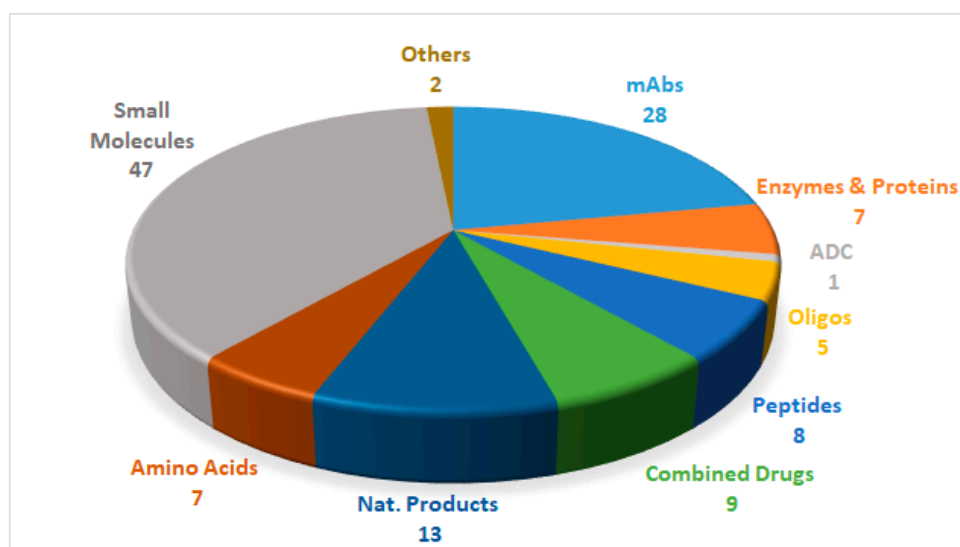


Figure 1. 127 new drugs approved by the United States Federal Food and Drug Administration (FDA) from 2016 to 2018, and classified on the basis of chemical structure [2,4,6].

Although only one peptide received FDA approval in 2018—a significant drop from the previous year in which six were approved—2018 has been extremely important for oligonucleotides, with two approvals. In support of this statement, only six oligonucleotide drugs have received FDA approval to date (three in 2016).

Herein, the three TIDES (one peptide and two oligonucleotides) with FDA approval are analyzed in terms of therapeutic use, mode of action, and chemical structures.

2. Oligonucleotides

The two oligonucleotides in the 2018 harvest, patisiran (Onpattro™) and inotersen (Tegsedi™), are prescribed for the treatment of polyneuropathy hereditary transthyretin mediated amyloidosis (hATTR) in adults.

Transthyretin (TTR or TBPA) is a transport protein that carries the thyroid hormone, thyroxine (T4), and the retinol-binding protein when it is bound to retinol (vitamin A) [8]. The liver is the main secretor of TTR into the bloodstream, and the choroid plexus secretes it into the cerebrospinal fluid. TTR is formed by four monomers of 127 amino acids, rich in β -sheet structures. Its final quaternary structure is a result of the association of two dimers in a face to face arrangement, creating a central channel that is responsible for two binding sites [8].

Individuals with hATTR show a mutation in the TTR gene, which in the protein is translated by replacing Val for Met at position 30 [9]. The mutation leads to an altered TTR protein structure [10], thus causing more dissociation at the dimer-dimer interface than in the wild-type. This dissociation results in the accumulation of the misfolded protein as insoluble amyloid fibrils in multiple organs, including nerves, heart, and gastrointestinal tract [11], and ultimately causes the disorder.

Previous treatments for this disease involved orthotopic liver transplantation (OLT) [10] and the use of some drugs, such as tafamidis [12] and diflunisal [13]. These act as TTR protein stabilizers, and thus delay the deposition of fibrils.

2.1. Patisiran (Onpattro™)

The approval of patisiran (Onpattro™) is probably the most impressive breakthrough in the drug discovery field in recent years. Patisiran is a double strand small interfering RNA (siRNA). Formulated

as patisiran sodium, and with a molecular weight of 14,303.6 Da, this drug is encapsulated within a liposome nanoparticle for better delivery to the liver, where TTR is produced [14].

Patisiran is the first siRNA drug to use RNA interference (RNAi) to downregulate protein expression. The RNAi pathway was first described in 1998 by Fire and Mello [15], who were awarded the Nobel Prize in Medicine in 2006 for their work. Twenty years after the seminal publication, approval for patisiran was granted to Alnylam Pharmaceuticals, Inc. [16]. Patisiran had previously been granted Fast Track, Priority Review and Breakthrough Therapy, and Orphan Drug designations to facilitate its final approval. Figure 2 shows the patisiran sequence.

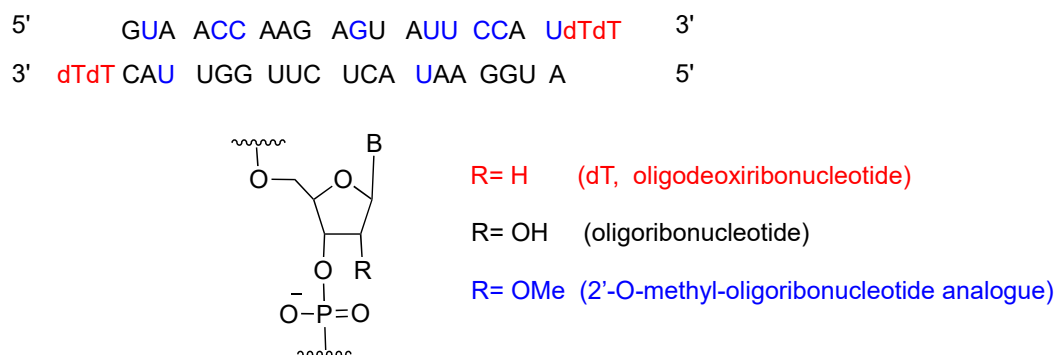


Figure 2. Patisiran sequence and chemical composition.

Patisiran is administered intravenously once every three weeks, and it has a demonstrated average knockdown of 87% and maximum of 96% of the TTR protein. Although, studies have shown that it is relatively well tolerated, it can cause some side effects, including tract infections, infusion-related reactions [13], and a decrease in vitamin A levels [13,17]. An important drawback of patisiran is the high cost of the treatment, which is calculated to be approximately \$450,000 [18].

2.2. Inotersen (TegsediTM)

Inotersen is a single stranded 20-mer phosphorothioate antisense oligonucleotide with 10 central 2'-deoxyribonucleotides flanked by five 2'-O-methoxyethyl (MOE)-modified ribonucleotides at each of the 5'- and 3'-termini (5-10-5 gapmer structure) [19] (Figure 3). All pyrimidines (cytosine C and uracil U) are 5-methylated, thereby increasing affinity for the complementary chain. Once inotersen is hybridized to mRNA, the complex is degraded by RNaseH, reducing the total amount of TTR secreted by the liver [20].

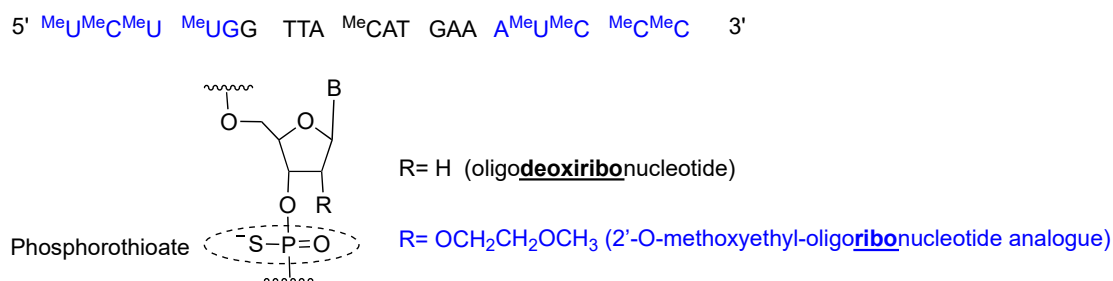


Figure 3. Inotersen sequence and chemical composition.

Inotersen is formulated as sodium salt, with a molecular weight of 7600.8 Da [19]. Tegsedi was developed by Ionis Pharmaceuticals, Inc. and was approved by the FDA in October 2018 [21]. It was produced using solid-phase synthesis [19].

Inotersen is administered subcutaneously once a week, and it does not show major toxicity. However, it does cause some side effects, such as abnormally low levels of platelets (thrombocytopenia)

and abnormal renal function (glomerulonephritis) [20]. Treatment with inotersen has a similar cost to that of patisiran [22].

2.3. Comments

Of the 59 drugs approved by the FDA in 2018, patisiran deserves to be named “Drug of the Year”. It is an oligonucleotide, where only six have been approved to date by the FDA, it shows a double strand, and requires a nanoformulation for its administration. From all points of view, patisiran could be considered a “tour de force” or in another context a “piece of art”. However, the main drawback is the investment needed for its development (some analysts are estimating this to be about US \$ 2 billion) and the cost of treatment (US \$ 450,000) [18]. Taking into account that its target is the same as that of inotersen, which has a similar treatment cost, these two drugs will compete for the same market, and are therefore unlikely to make a return on investment.

3. Lutathera®

[¹⁷⁷Lu]Lu-DOTA-TATE ([¹⁷⁷Lu]Lu-DOTA⁰, Tyr³]-octreotate) belongs to an emerging treatment called Peptide Receptor Radionuclide Therapy (PRRT) [23]. PRRT involves the combination of a chelating agent holding the radionuclide and a peptide, which binds to receptors overexpressed by tumor cells. This mechanism facilitates localized treatment, and can therefore be considered a targeted therapy. [¹⁷⁷Lu]Lu-DOTA-TATE is the first PRRT to have received FDA approval. It contains ¹⁷⁷Lu as radionuclide and DOTA (also known as tetraxetan) as a chelator, the latter bound to [Tyr³]-octreotate (Figure 4). This peptide is a strong somatostatin receptor antagonist that is overexpressed in tumor cells [24]. The trivalent radiometal ¹⁷⁷Lu has optimal β- and γ-emission characteristics, making it suitable to be used in theranostic radiopharmaceuticals as compared with other radionuclides: ¹¹¹In for diagnostic and ⁹⁰Y for therapy [25].

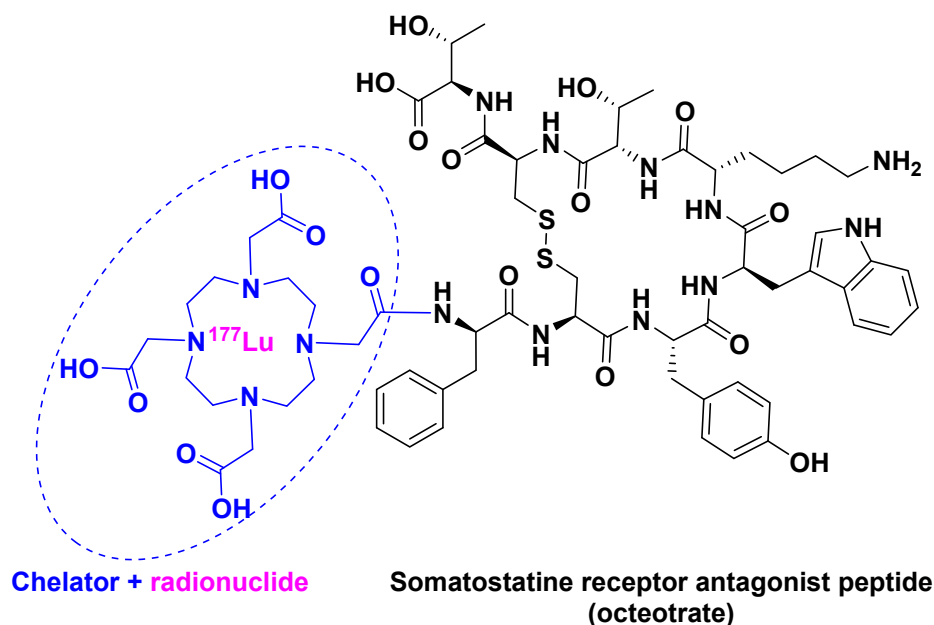


Figure 4. [¹⁷⁷Lu]Lu-DOTA-TATE chemical structure.

[¹⁷⁷Lu]Lu-DOTA-TATE is administered intravenously, and has mild side effects, especially if kidney-protective agents are used during the therapy, in comparison to other PRRTs in development [23]. In addition, as a result of lower whole-body retention, [¹⁷⁷Lu]Lu-DOTA-TATE has a lower risk for bone marrow toxicity [23].

[¹⁷⁷Lu]Lu-DOTA-TATE is used for the treatment of gastroenteropancreatic neuroendocrine tumors (GEP-NETs). It was developed by Advanced Accelerator Applications USA, Inc. and then approved by the FDA in January 2018 [26].

In the case of PRRTs, as well as other similar radionuclide constructs used just for imaging, the main challenge is to widen the use of targeting peptides beyond somatostatin analogs. Research efforts should be channeled into more peptides from diverse families, with the aim of broadening the use of this kind of therapy.

4. Conclusions

The three TIDES approved by the FDA in 2018 can be considered unique. [¹⁷⁷Lu]Lu-DOTA-TATE is the first drug of the PRRT family, patisiran is the first siRNA drug, and inotersen shows a distinctive gapmer structure. The acceptance of these drugs undoubtedly paves the way for the authorization of others with the same mode of action.

Finally, it is important to highlight that these and other drugs approved by the FDA in 2018 have a cost in the range of a six-digit figure, thus making them unaffordable for a large segment of the population.

Author Contributions: All authors have participated in searching for information, in writing the manuscript, and have approved the final version.

Funding: This research received no external funding.

Acknowledgments: The work in the laboratory of the authors was funded in part by the following: National Research Foundation (NRF) (CSUR # 105892 and Blue Sky's Research Programme # 110960) and the University of KwaZulu-Natal (South Africa); the Spanish Ministry of Economy, Industry and Competitiveness (MINECO) (CTQ2015-67870-P); and the Generalitat de Catalunya (2017 SGR 1439) (Spain).

Conflicts of Interest: The authors declare no conflict of interest.

References

- Mullard, A. 2016 FDA drug approvals. *Nat. Rev. Drug Discov.* **2017**, *16*, 73–76. [CrossRef] [PubMed]
- Torre, B.G.; Albericio, F. The pharmaceutical industry in 2016. An analysis of FDA drug approvals from a perspective of the molecule type. *Molecules* **2017**, *22*. [CrossRef] [PubMed]
- Mullard, A. 2017 FDA drug approvals. *Nat. Rev. Drug Discov.* **2018**, *17*, 81–85. [CrossRef] [PubMed]
- De la Torre, B.G.; Albericio, F. The pharmaceutical industry in 2017. An analysis of FDA drug approvals from the perspective of molecules. *Molecules* **2018**, *23*. [CrossRef] [PubMed]
- Mullard, A. 2018 FDA drug approvals. *Nat. Rev. Drug Discov.* **2019**, *18*, 85–89. [CrossRef] [PubMed]
- De la Torre, B.G.; Albericio, F. The pharmaceutical industry in 2018. An analysis of FDA drug approvals from the perspective of molecules. *Molecules* **2019**, *24*. [CrossRef] [PubMed]
- Al Musaimi, O.; Al Shaer, D.; de la Torre, B.G.; Albericio, F. 2017 FDA peptide harvest. *Pharmaceuticals* **2018**, *11*. [CrossRef] [PubMed]
- Butler, J.S.; Chan, A.; Costelha, S.; Fishman, S.; Willoughby, J.L.; Borland, T.D.; Milstein, S.; Foster, D.J.; Goncalves, P.; Chen, Q.; et al. Preclinical evaluation of rna1 as a treatment for transthyretin-mediated amyloidosis. *Amyloid* **2016**, *23*, 109–118. [CrossRef] [PubMed]
- Rowczenio, D.M.; Noor, I.; Gillmore, J.D.; Lachmann, H.J.; Whelan, C.; Hawkins, P.N.; Obici, L.; Westermarck, P.; Grateau, G.; Wechalekar, A.D. Online registry for mutations in hereditary amyloidosis including nomenclature recommendations. *Hum. Mutat.* **2014**, *35*, E2403–E2412. [CrossRef] [PubMed]
- Chakradhar, S. A protein puzzle. *Nat. Med.* **2017**, *23*, 266–269. [CrossRef] [PubMed]
- Adams, D.; Suhr, O.B.; Dyck, P.J.; Litchy, W.J.; Leahy, R.G.; Chen, J.; Gollob, J.; Coelho, T. Trial design and rationale for apollo, a phase 3, placebo-controlled study of patisiran in patients with hereditary attr amyloidosis with polyneuropathy. *BMC Neurol.* **2017**, *17*. [CrossRef] [PubMed]
- Vieira Simoes, C.J.; Lourenco de Almeida, Z.C.; Vasconcelos Dias de Pinho EMelo, T.M.; Pontes Meireles Ferreira de Brito, R.M.; Silva Costa, D.C.; Cabral Cardoso Lopes, A.L. Bis-Furan Derivatives as Transthyretin (TTR) Stabilizers and Amyloid Inhibitors for the Treatment of Familial Amyloid Polyneuropathy (FAP). 2018. Available online: <https://patents.google.com/patent/WO2016203402A1/ko> (accessed on 22 March 2019).

13. Hawkins, P.N.; Ando, Y.; Dispenzeri, A.; Gonzalez-Duarte, A.; Adams, D.; Suhr, O.B. Evolving landscape in the management of transthyretin amyloidosis. *Ann. Med.* **2015**, *47*, 625–638. [CrossRef] [PubMed]
14. Yang, J. Patisiran for the treatment of hereditary transthyretin-mediated amyloidosis. *Exp. Rev. Clin. Pharmacol.* **2019**, *12*, 95–99. [CrossRef] [PubMed]
15. Fire, A.; Xu, S.; Montgomery, M.K.; Kostas, S.A.; Driver, S.E.; Mello, C.C. Potent and specific genetic interference by double-stranded rna in caenorhabditis elegans. *Nature* **1998**, *391*, 806–811. [CrossRef] [PubMed]
16. FDA Approval Letter of Patisiran 2018. Available online: https://www.accessdata.fda.gov/drugsatfda_docs/appletter/2018/210922Orig1s000ltr.pdf (accessed on 22 February 2019).
17. FDA Label of Patisiran 2018. Available online: https://www.accessdata.fda.gov/drugsatfda_docs/label/2018/210922s000lbl.pdf (accessed on 22 February 2019).
18. Jarvis, L.M. The new drugs of 2018. *Chem. Eng. News* **2019**, *97*, 33–37. [CrossRef]
19. European Medicine Agency: Tegsedi Assessment Report 2018. Available online: https://www.ema.europa.eu/documents/assessment-report/tegsedi-epar-public-assessment-report_en.pdf (accessed on 22 February 2019).
20. European Medicine Agency: Tegsedi Label. Available online: https://s3-us-west-2.amazonaws.com/drugbank/cite_this/attachments/files/000/001/938/original/tegsedi-epar-product-information_en.pdf?1539980614 (accessed on 22 February 2019).
21. FDA Approval Letter of Tegsedi 2018. Available online: https://www.accessdata.fda.gov/drugsatfda_docs/nda/2018/211172Orig1s000Approv.pdf (accessed on 22 February 2019).
22. Fidler, B. FDA Oks Akcea Rare Disease Drug, Setting Up Market Clash with Alnylam 2018. Available online: <https://xconomy.com/boston/2018/10/05/fda-oks-akcea-rare-disease-drug-setting-up-market-clash-with-alnylam/> (accessed on 22 February 2019).
23. Kam, B.L.; Teunissen, J.J.; Krenning, E.P.; de Herder, W.W.; Khan, S.; van Vliet, E.I.; Kwekkeboom, D.J. Lutetium-labelled peptides for therapy of neuroendocrine tumours. *Eur. J. Nucl. Med. Mol. Imaging* **2012**, *39*, S103–S112. [CrossRef] [PubMed]
24. Lutathera FDA Label 2018. Available online: https://www.accessdata.fda.gov/drugsatfda_docs/label/2018/208700s000lbl.pdf (accessed on 22 February 2019).
25. Banerjee, S.; Pillai, M.R.; Knapp, F.F. Lutetium-177 therapeutic radiopharmaceuticals: Linking chemistry, radiochemistry, and practical applications. *Chem. Rev.* **2015**, *115*, 2934–2974. [CrossRef] [PubMed]
26. FDA Approval Letter of Lutathera 2018. Available online: https://www.accessdata.fda.gov/drugsatfda_docs/appletter/2018/208700Orig1s000ltr.pdf (accessed on 22 February 2019).



© 2019 by the authors. Licensee MDPI, Basel, Switzerland. This article is an open access article distributed under the terms and conditions of the Creative Commons Attribution (CC BY) license (<http://creativecommons.org/licenses/by/4.0/>).

Chapter 6. 2018 FDA Tides Harvest

Danah Al Shaer^{1,2,†}, **Othman Al Musaimi**^{1,2,†}, **Fernando Albericio**^{2,3,*} and **Beatriz G. de la Torre**^{1,*}

¹ *KRISP, School of Laboratory of Medicine and Medical Science, College of Health Sciences, University of KwaZulu-Natal, Durban 4001, South Africa;
217078895@stuukznac.onmicrosoft.com (D.A.S.); 217078894@stuukznac.onmicrosoft.com (O.A.M.)*

² *School of Chemistry and Physics, University of KwaZulu-Natal, Durban 4001, South Africa*

³ *CIBER-BBN, Networking Centre on Bioengineering, Biomaterials and Nanomedicine and Department of Organic Chemistry, University of Barcelona, 08028 Barcelona, Spain*

[†] *These authors contributed equally to this work.*

* *Correspondence: albericio@ukzn.ac.za, Tel.: +27-614009144 (F.A.); garciadelatorreb@ukzn.ac.za, Tel.: +27-614047528 (B.G.d.l.T.)*



Review

2017 FDA Peptide Harvest

Othman Al Musaimi ^{1,2,†} , Danah Al Shaer ^{1,2,†} , Beatriz G. de la Torre ^{3,*}
and Fernando Albericio ^{2,4,5,*}

¹ College of Health Sciences, University of KwaZulu-Natal, Durban 4000, South Africa; musamiau@gmail.com (O.A.M.); danah.shaer@gmail.com (D.A.S.)

² School of Chemistry, University of KwaZulu-Natal, Durban 4001, South Africa

³ KRISP, College of Health Sciences, University of KwaZulu-Natal, Durban 4001, South Africa

⁴ CIBER-BBN, Networking Centre on Bioengineering, Biomaterials and Nanomedicine, University of Barcelona, 08028 Barcelona, Spain

⁵ Department of Organic Chemistry, University of Barcelona, 08028 Barcelona, Spain

* Correspondence: garciadelatorreb@ukzn.ac.za (B.G.d.I.T.); albericio@ukzn.ac.za (F.A.); Tel.: +27-614-009-144 (F.A.)

† These authors contributed equally to this work.

Received: 9 April 2018; Accepted: 3 May 2018; Published: 7 May 2018



Abstract: 2017 was an excellent year in terms of new drugs (chemical entities and biologics) approved by the FDA, with a total of 46. In turn, one of the highlights was the number of peptides (six) included in this list. Here, the six peptides are analyzed in terms of chemical structure, synthetic strategy used for their production, source, therapeutic use, and mode of action.

Keywords: pharmaceutical market; drugs; drug discovery; solid-phase peptide synthesis

1. Introduction

The financial investment associated with the pharmaceutical industry is one of the largest in the industrial sector—surpassed only by the telecommunications sector. However, the number of new products (drugs) entering the market each year is relatively low. In this context, 2017 was an exceptional year, in that 46 new drugs were approved by the US Food and Drug Administration (FDA) [1]—the highest figure in the last twenty-five years. Drugs can be broadly divided into two main groups. The first encompasses biologics (12 approved in 2017, accounting for 25% of the total number of drugs approved), which are prepared by means of biotechnological techniques. The second group comprises chemical entities (34 approved in 2017), which are prepared using chemical synthesis [2]. In turn, chemical entities can be grouped into two categories, the so-called small molecules, which also include some natural products, and TIDES (peptides and oligonucleotides). Figure 1 shows the drugs approved by the FDA in 2017 and classified on the basis of their chemical structure. Thus, in a clockwise direction, biologics (antibodies, enzymes, and antibodies drug conjugates) appear first, followed by peptides, modified amino acids, and more traditional small molecules.

Along a similar line, 2017 was an excellent year for peptides, with the FDA approving five peptides and one peptidomimetic, which together accounted for 13% of the drugs accepted that year.

However, the 2017 figures should be interpreted with care. They cannot be taken as a trend since the arrival of a drug onto the market involves many unpredictable variables.

From a structural point of view, the six peptides in the 2017 harvest show almost the full range of diversity, probably lacking only a homodetic cyclic peptide and/or a cyclodepsipeptide. In this regard, in addition to a peptidomimetic macimorelin (MacrilenTM), the 2017 harvest included two linear peptides angiotensin II (GiaprezaTM) and abaloparatide (TymlosTM) with 8 and 34 amino acids, respectively, and a peptide plecanatide (TrulanceTM) containing two disulphide bridges. It also

included the following two unique branched peptides: semaglutide (Ozempic™) with a chain pending at a Lys residue, which contains two mini-PEG amino acids, a Glu residue linked to the chain through the ω -carboxylic group, and a C18 diacid; and etelcalcetide (Parsabiv™), which is formed by a linear chain of seven D-amino acids with a disulphide bridge between a D-Cys with a single L-Cys. Interestingly, three of these peptides (macimorelin, abaloparatide, and semaglutide) contain a residue of the non-proteinogenic aminoisobutyric (Aib) acid, with the purpose of conferring stability against peptidases.

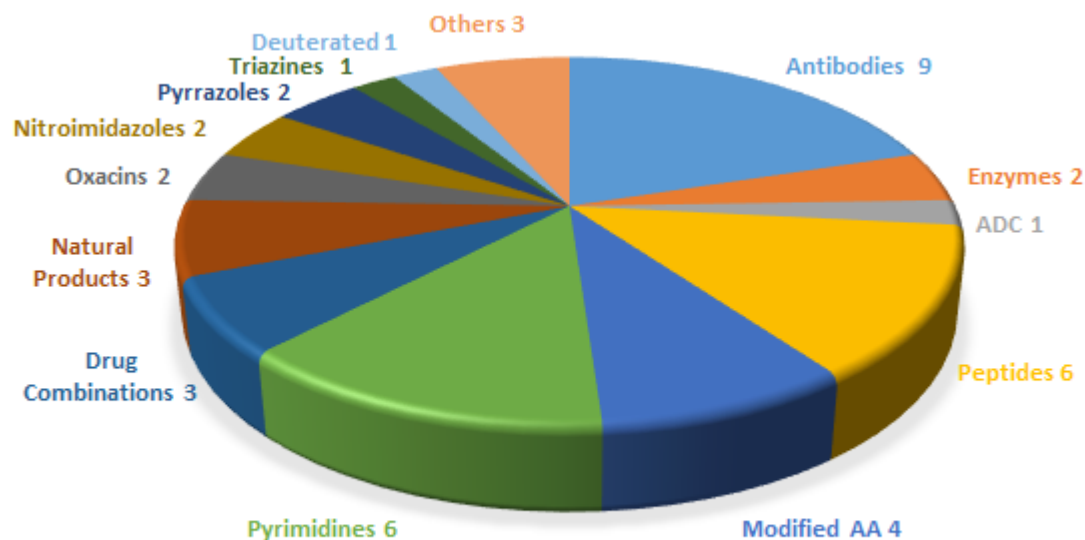


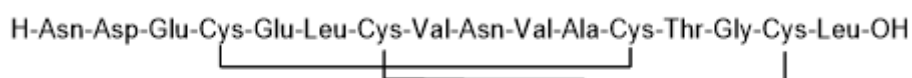
Figure 1. New drugs approved by the FDA in 2017 and classified on the basis of chemical structure.

Only one of these peptides have been developed by two so-called big pharmas (semaglutide by Novo Nordisk A/S) and the rest by biotech companies. Macimorelin had its roots in Fehrentz and Martinez's group at the University of Montpellier (France). The five peptides other than macimorelin were produced using the solid-phase technique.

2. Plecanatide (Trulance)

This peptide has a linear sequence of 16 amino acids with two disulphide bridges pairing Cys 4 with Cys12 and Cys7 with Cys15. Its C-terminal residue is in acid form (molecular weight of 1681.9 Da) (Figure 2a). It is manufactured using solid-phase technique.

(a) Plecanatide



(b) Linaclotide

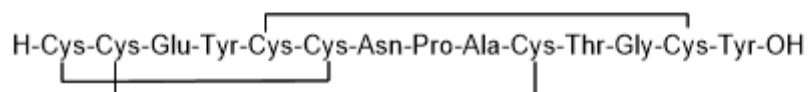


Figure 2. Structure of (a) plecanatide and (b) the related linaclotide.

Plecanatide differs from uroguanylin (the endogenous counterpart of plecanatide) only in the replacement of Asp3 by Glu3 [3].

It was developed by Synergy Pharmaceuticals (New York City, NY, USA) and was approved by the FDA on 7 January 2017 for the treatment of chronic idiopathic constipation (CIC) and irritable bowel syndrome with constipation (IBS-C) [4]. Plecanatide is an agonist of guanylate cyclase-C, it increases intestinal transit and fluid through a build-up of guanosine 3',5'-cyclic monophosphate (cGMP) [5] and has a similar mode of action as linaclotide (Constella-Linzess) (Figure 2b), which is a 14-amino acid peptide containing three disulphide bridges which are located between Cys1 and Cys6, between Cys2 and Cys10, and between Cys5 and Cys13. Linaclotide was approved by the FDA in 2012 [6].

Plecanatide draws water into the gastrointestinal (GI) tract, thereby softening stool and encouraging its natural passage. It activates guanylate cyclase-C (GC-C) on endothelial cells within the GI [7]. The pH-dependent activation of GC-C receptors by plecanatide (as it has the acidic residues Asp2 and Glu3) may promote bowel movements without causing severe diarrhea [3,7]. Furthermore, in molecular dynamics simulations, plecanatide showed optimal activity at pH 5, indicating that the proximal intestine (pH 5–6) is the ideal site of action [8].

The activation of GC-C catalyzes the production of the second messenger cGMP, which leads to the protein kinase A (PKA)- and protein kinase G II (PKGII)-mediated phosphorylation of the cystic fibrosis transmembrane conductance regulator (CFTR) protein [9]. Upon activation, CFTR secretes chloride (Cl⁻) and bicarbonate (HCO₃⁻) into the GI tract lumen, followed by the passive secretion of positively charged sodium ions into the lumen, and water follows by osmosis [10].

In the GI tract, plecanatide is metabolized by intestinal enzymes. The excretion of plecanatide has not been studied in humans [3].

Plecanatide is administered orally as is linaclotide. These two examples showcase the feasibility of the oral administration of peptides.

3. Etelcalcetide (Parsabiv)

This is an octapeptide formed by a linear chain of seven D-amino acids containing a D-Cys, which is linked through a disulphide bridge to an L-Cys. The C-terminal residue is in amide form (molecular weight of 1048.3 Da), and it is manufactured using a solid-phase technique (Figure 3). The presence of amino acids in D configuration confers the peptide chain resistance to proteolytic degradation. The presence of disulphide bonds facilitates the biotransformation process, especially with endogenous thiols in blood, and this is considered a main metabolic pathway of etelcalcetide [11–13].

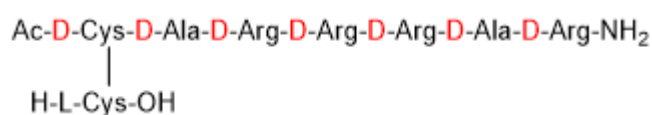


Figure 3. Structure of etelcalcetide. Amino acids of D configuration are shown in red.

Etelcalcetide was developed by KAI Pharmaceuticals Inc. (South of San Francisco, CA, USA), a wholly subsidiary of Amgen Inc. (Thousand Oaks, CA, USA) and approved by the FDA on 7 February 2017 [14]. It is used for the treatment of secondary hyperparathyroidism (SHPT) in chronic kidney disease (CKD) in adult patients on hemodialysis [11,12,15–18]. Cardiovascular calcination is common in CKD patients, and it occurs as a result of impaired mineral homeostasis and secondary hyperparathyroidism [16]. As a calcimimetic agent, etelcalcetide binds to the calcium-sensing receptor (CaSR) through a disulphide bridge between the D-Cys of the etelcalcetide molecule and L-Cys of the CaSRs, thereby enhancing activation of the receptor by means of extracellular calcium. Accordingly, activation of CaSRs on parathyroid chief cells decreases the secretion of parathyroid hormone (PTH), as well as fibroblast growth factor-23 (FGF23), which is stimulated by PTH [12,13,15–21]. Furthermore, etelcalcetide decreases phosphorus in the blood. Interestingly, high blood phosphorus occurs in vascular calcification [16].

A serious side effect of etelcalcetide is that it reduces serum calcium levels, which might lead to hypocalcemia. Therefore, monitoring serum calcium (after etelcalcetide dosing is initiated), as well as PTH, is deemed necessary [13,15,21]. Etelcalcetide can cause vomiting and nausea [11,13,20,21].

4. Abaloparatide (Tymlos)

This is a linear C-terminal amide peptide that contains 34 amino acids. The C-terminal residue is in amide form (molecular weight of 3960.7 Da) (Figure 4a). It is manufactured by a hybrid solution–solid phase approach.

Abaloparatide can be considered a second generation teriparatide (Forteo) (Figure 4b), which is a recombinant form of PTH (84 amino acids), formed by the N-terminal fragment (34 amino acids) of PTH. Abaloparatide contains exactly the same number of amino acids as teriparatide but has multiple substitutions. It has 41% homology with teriparatide [22]. Interestingly, abaloparatide has an Aib residue at position 29.

(a) Abaloparatide

H-Ala-Val-Ser-Glu-His-Gln-Leu-Leu-His-Asp-Lys-Gly-Lys-Ser-Ile-Gln-Asp-
Leu-Arg-Arg-Arg-Glu-Leu-Leu-Glu-Lys-Leu-Leu-Aib-Lys-Leu-His-Thr-Ala-NH₂

(b) Teriparatide

H-Ser-Val-Ser-Glu-Ile-Gln-Leu-Met-His-Asn-Leu-Gly-Lys-His-Leu-Asn-Ser-
Met-Glu-Arg-Val-Glu-Trp-Leu-Arg-Lys-Lys-Leu-Gln-Asp-Val-His-Asn-Phe-OH

Figure 4. Structure of (a) abaloparatide and (b) teriparatide. The residues modified are shown in red. The non-proteinogenic amino acid Aib is shown in bold.

Abaloparatide was developed by the biotech company Radius Health, Inc. (Waltham, MA, USA) and approved by the FDA on 28 April 2017 [23].

Abaloparatide works as an anabolic (bone-growing) agent through the selective activation of the parathyroid hormone 1 receptor (PTH1R), a G protein-coupled receptor (GPCR) expressed in osteoblasts and osteocytes [22]. This receptor can be present in two distinct conformation states (R0 and RG), which differ in their signaling response. Ligands that bind selectively to the RG state result in a shorter signaling response, whereas those that bind selectively to the R0 state lead to a prolonged response [24]. Abaloparatide preferentially binds to the RG state of PTH1R, which in turn elicits a transient downstream cyclic AMP signaling response towards a more anabolic signaling pathway [22,24].

Abaloparatide outperforms teriparatide as an anabolic agent, as shown by the increased messenger ribonucleic acid (RNA) expression level for the receptor activator of nuclear factor kappa-B ligand (RANKL) and macrophage colony-stimulating factor in a human osteoblastic cell line. Although the molecular mechanisms underlying the differences between abaloparatide and teriparatide are not well understood, they may be related to conformational differences that determine the affinities of the drugs for PTHR1 [22].

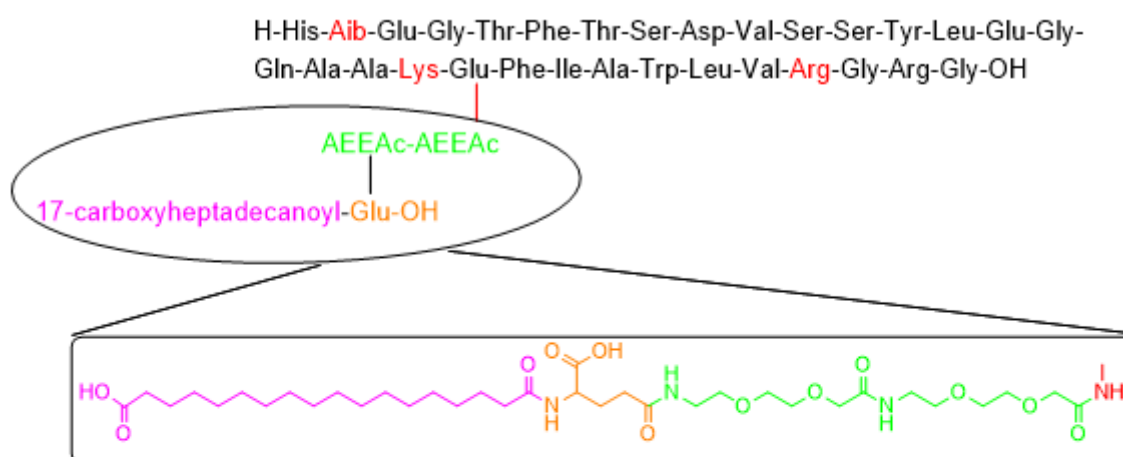
5. Semaglutide (Ozempic)

Semaglutide contains a linear sequence of 31 amino acids, with a moiety pending from the ϵ -amino function of Lys20 (the numeration of the amino acids in semaglutide is done by taking as reference the numeration in the parent peptide GLP-1), which contains a Glu residue linked to the ϵ -amino group of Lys side-chain through the γ -carboxylic group, two mini-PEG amino acids [8-amino-3,6-dioxaoctanoic

acid (ADO)] and a C18 diacid (Figure 5a). The C-terminal is in the form of a carboxylic acid (molecular weight of 4113.6 Da). It is manufactured using a solid-phase approach.

Semaglutide is a member of the glucagon like peptide-1 (GLP-1) family, derived from the GLP-1 (sequence 7-37), and can be considered the second generation of liraglutide (Figure 5b), which was accepted by the FDA in 2010 [25]. Liraglutide differs from GLP-1 (7-37) (Figure 5b) in the presence of Arg in position 34 instead of Lys and of a moiety at Lys20, which is a reduced version of the one in semaglutide. When comparing the structures of semaglutide and liraglutide, in addition to the pending moiety, semaglutide has Aib instead of Ala in position 8, thereby reducing the susceptibility of semaglutide to degradation by dipeptidyl peptidase-4 [26–28]. Both semaglutide and liraglutide were developed by Novo Nordisk A/S (Måløv, Denmark). Semaglutide was approved by the FDA on 21 December 2017 [29].

(a) Semaglutide



(b) Liraglutide

H-His-Ala-Glu-Gly-Thr-Phe-Thr-Ser-Asp-Val-Ser-Ser-Tyr-Leu-Glu-Gly-Gln-Ala-Ala-Lys-Glu-Phe-Ile-Ala-Trp-Leu-Val-Arg-Gly-Arg-Gly-OH

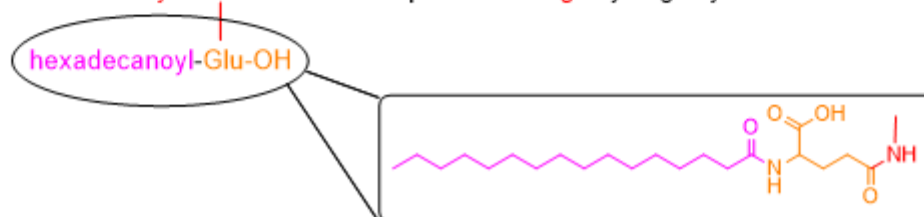


Figure 5. Structure of (a) semaglutide and (b) its related liraglutide. Changes in structure with respect to GLP-1 (7-37) are shown in color.

The GLP-1 family stimulates insulin and decreases glucagon secretion. However, GLP-1 has a short half-life (1–2 min) as a result of proteolytic degradation, thus hindering its use as a potential treatment for type 2 diabetes [27]. Liraglutide is the first once-daily glucagon-like peptide-1 analogue designed to resist enzymatic degradation and thus have a longer half-life [26,27,30]. The presence of the 17-carboxyheptadecanoyl fatty acid moiety results in its binding to human albumin, which is responsible for the longer-acting activity of liraglutide in comparison with other members of the same family. The rationale behind the design of semaglutide, which allows once-weekly administration, is to increase the affinity of the pending fatty acid moiety for albumin. Moreover, semaglutide has no serious adverse effects, only some mild gastrointestinal disorders [27].

6. Macimorelin (Macrilen)

Macimorelin is a small pseudopeptide formed by three residues: Aib as N-terminus, D-Trp at the central position, and a mimetic of D-Trp—a gem diamino moiety—which is formylated at its N-terminus (Figure 6) (molecular weight of 474.6 Da). It is prepared by solution synthesis.

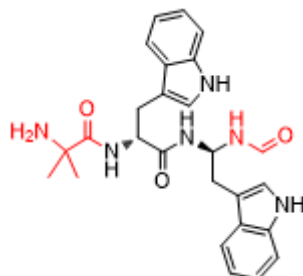


Figure 6. Structure of macimorelin. Modifications with respect to a tripeptide are shown in red.

Macimorelin was discovered by Fehrentz and Martinez's group at the University of Montpellier [31] and developed by the biotech company Aeterna Zentaris GmbH (Frankfurt, Germany). It was approved by the FDA on 20 December 2017 [32]. Administered orally, it is used for the diagnosis of adult growth hormone deficiency (AGHD).

Macimorelin acts as a growth hormone secretagogue (GHS) mimicking ghrelin, which is a 28-amino acid peptide produced by the stomach and is the endogenous ligand for this GHS receptor [31,33–36]. In addition to being orally bioavailable, macimorelin is selective, tolerable, and also safe, with only mild adverse effects—such as an unpleasant taste—being reported [34,35,37].

By acting in an almost identical manner to ghrelin [37], macimorelin outperforms other GHS such as the expensive recombinant human GH.

7. Angiotensin II (Giapreza)

Angiotensin II is a simple linear octapeptide formed by natural amino acids of the L series and its structure is identical to the human hormone of the same name. The C-terminal is in the form of carboxylic acid (molecular weight of 1046.2 Da) (Figure 7). It is manufactured using the solid-phase approach.

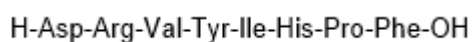


Figure 7. Structure of angiotensin II.

Angiotensin II was developed by a biotech company, La Jolla Pharmaceutical Company (San Diego, CA, USA), and approved by the FDA on 21 December 2017 [38]. It is recommended as a vasoconstrictor to increase blood pressure in adults with septic or other distributive shock. It is administered intravenously because its half-life is approximately 30 s.

Angiotensin II is related to the renin–angiotensin System (RAS). From a drug discovery perspective, it can be considered unique among the drugs approved by the FDA in recent years. Its roots can be found in the last part of the XIX century, when Tigerstedt and Bergman discovered the effect of renal extracts on arterial pressure [39]. In the 1930s, two independent groups, one in Argentina with Leloir, Houssay, Fernandez Braun, among others, and that of Page in the US, discovered that RAS is the hormone system that regulates blood pressure and fluid balance [40]. In 1957, again two groups—one in the US (Schwarz and colleagues) [41] and the second in Switzerland (GIBA Geigy) [42]—described the first synthesis of angiotensin II. Seventy years after its first synthesis, this octapeptide reached the market.

Angiotensin II is formed after the removal of two C-terminal residues of angiotensin I by the angiotensin-converting enzyme (ACE). In turn, angiotensin I is the N-terminal part of angiotensinogen, an α -2-globulin produced constitutively and released into the circulation mainly by the liver.

As a summary, Table 1 shows the six peptides approved by the FDA in 2017 highlighting several parameters (chemical modification, source, therapeutic use, mode of action, and administration) that have been key to their development.

Table 1. Summary of the peptides approved by the FDA in 2017.

Generic Name (Trade Name)	Company	Mode of Action	Therapeutic Use	Administration
Plecanatide (Trulance)	Synergy Pharmaceuticals, Inc.	Activation of guanylate cyclase-C	Gastrointestinal laxative	Oral
Etelcalcetide (Parsabiv)	KAI Pharmaceuticals, Inc. *	Activation of CaSR on parathyroid chief cells	Secondary hyperpara-thyroidism in adult patients with chronic kidney disease on hemodialysis	IV
Abaloparatide (Tymlos)	Radius Health, Inc.	Selective activation of the parathyroid hormone 1 receptor	Osteoporosis	SC
Semaglutide (Ozempic)	Novo Nordisk, Inc.	Acts as a Glucagon-like Peptide-1 agonist	Treatment of type 2 diabetes mellitus	SC
Macimorelin (Macrilen)	Aeterna Zentaris, Inc.	Mimic the endogenous ligand for the secretagogue (Ghrelin)	For the diagnosis of adult growth hormone deficiency	Oral
Angiotensin II (Giapreza)	La Jolla Pharm Co.	Acts on the CNS to increase ADH production	Control of blood pressure in adults with sepsis or other critical conditions	IV

* Wholly owned subsidiary of Amgen, Inc.; IV: intra venous; SC: subcutaneous.

Finally, it is important to recall the trend of the peptide market. This market was worth US\$5.3 billion in 2003, rising to US\$8 billion in 2005 and US\$14.1 billion in 2011, and it is expected to reach a value of US\$25.4 billion and US\$46.6 billion by the end of 2018 and 2024, respectively [43–45]. Furthermore, there are currently hundreds of peptides in preclinical testing stages and around 150 peptides in clinical development. Many of these molecules are showing a promising therapeutic impact [36,43,46–48].

It is to be hoped that the coming years will bring about the approval of a similar number of peptides to those accepted by the FDA in 2017 and that the trends of the market in terms of peptide development continue, thus making these molecules one of the best options to treat many diseases.

Author Contributions: All authors have participated in searching for information, in writing the manuscript, and have approved the final version.

Acknowledgments: The work in the laboratory of the authors was funded in part by the following: National Research Foundation (NRF) (CSUR # 105892 and Blue Sky's Research Program # 110960) and the University of KwaZulu-Natal (South Africa); the Spanish Ministry of Economy, Industry and Competitiveness (MINECO) (CTQ2015-67870-P); and the Generalitat de Catalunya (2014 SGR 137) (Spain).

Conflicts of Interest: The authors declare no conflict of interest.

References

- De la Torre, B.G.; Albericio, F. The pharmaceutical industry in 2017. An analysis of fda drug approvals from the perspective of molecules. *Molecules* **2018**, *23*, 533. [CrossRef] [PubMed]
- Mullard, A. 2017 fda drug approvals. *Nat. Rev. Drug Discov.* **2018**, *17*, 81–85. [CrossRef] [PubMed]
- Al-Salama, Z.T.; Syed, Y.Y. Plecanatide: First global approval. *Drugs* **2017**, *77*, 593–598. [CrossRef] [PubMed]
- FDA. Plecanatide (Trulance) Approval Letter. 2017. Available online: https://www.accessdata.fda.gov/drugsatfda_docs/appletter/2017/208745orig1s000ltr.pdf (accessed on 3 May 2018).

5. Thomas, R.H.; Luthin, D.R. Current and emerging treatments for irritable bowel syndrome with constipation and chronic idiopathic constipation: Focus on prosecretory agents. *Pharmacotherapy* **2015**, *35*, 613–630. [CrossRef] [PubMed]
6. Góngora-Benítez, M.; Tulla-Puche, J.; Albericio, F. Constella™(eu)-linzess™(USA): The last milestone in the long journey of the peptide linaclotide and its implications for the future of peptide drugs. *Future Med. Chem.* **2013**, *5*, 291–300. [CrossRef] [PubMed]
7. Shailubhai, K.; Comiskey, S.; Foss, J.A.; Feng, R.; Barrow, L.; Comer, G.M.; Jacob, G.S. Plecanatide, an oral guanylate cyclase c agonist acting locally in the gastrointestinal tract, is safe and well-tolerated in single doses. *Dig. Dis. Sci.* **2013**, *58*, 2580–2586. [CrossRef] [PubMed]
8. Brancale, A.; Shailubhai, K.; Ferla, S.; Ricci, A.; Bassetto, M.; Jacob, G.S. Mo1316 structural and dynamic features of plecanatide: Insights from molecular dynamics simulations. *Gastroenterology* **2016**, *150*, S695. [CrossRef]
9. Hamra, F.K.; Forte, L.R.; Eber, S.L.; Pidhorodeckyj, N.V.; Krause, W.J.; Freeman, R.H.; Chini, D.T.; Tompkins, J.A.; Fok, K.F.; Smith, C.E.; et al. Uroguanylin: Structure and activity of a second endogenous peptide that stimulates intestinal guanylate cyclase. *Proc. Natl. Acad. Sci. USA* **1993**, *90*, 10464–10468. [CrossRef] [PubMed]
10. Gadsby, D.C.; Vergani, P.; Csanady, L. The abc protein turned chloride channel whose failure causes cystic fibrosis. *Nature* **2006**, *440*, 477–483. [CrossRef] [PubMed]
11. Subramanian, R.; Zhu, X.; Kerr, S.J.; Esmay, J.D.; Louie, S.W.; Edson, K.Z.; Walter, S.; Fitzsimmons, M.; Wagner, M.; Soto, M.; et al. Nonclinical pharmacokinetics, disposition, and drug-drug interaction potential of a novel d-amino acid peptide agonist of the calcium-sensing receptor amg 416 (etelcalcetide). *Drug Metab. Dispos.* **2016**, *44*, 1319–1331. [CrossRef] [PubMed]
12. Edson, K.Z.; Wu, B.M.; Iyer, A.; Goodman, W.; Skiles, G.L.; Subramanian, R. Determination of etelcalcetide biotransformation and hemodialysis kinetics to guide the timing of its dosing. *Kidney Int. Rep.* **2016**, *1*, 24–33. [CrossRef] [PubMed]
13. Cozzolino, M.; Galassi, A.; Conte, F.; Mangano, M.; Di Lullo, L.; Bellasi, A. Treatment of secondary hyperparathyroidism: The clinical utility of etelcalcetide. *Ther. Clin. Risk Manag.* **2017**, *13*, 679–689. [CrossRef] [PubMed]
14. FDA. Etelcalcetide (Parsabiv) Approval Letter. 2017. Available online: https://www.accessdata.fda.gov/drugsatfda_docs/nda/2017/208325Orig1s000Approv.pdf (accessed on 3 May 2018).
15. Baker, D.E. Formulary drug review: Etelcalcetide. *Hosp. Pharm.* **2017**, *52*, 669–674. [CrossRef] [PubMed]
16. Yu, L.; Tomlinson, J.E.; Alexander, S.T.; Hensley, K.; Han, C.Y.; Dwyer, D.; Stolina, M.; Dean, C., Jr.; Goodman, W.G.; Richards, W.G.; et al. Etelcalcetide, a novel calcimimetic, prevents vascular calcification in a rat model of renal insufficiency with secondary hyperparathyroidism. *Calcif. Tissue Int.* **2017**, *101*, 641–653. [CrossRef] [PubMed]
17. Li, X.; Yu, L.; Asuncion, F.; Grisanti, M.; Alexander, S.; Hensley, K.; Han, C.Y.; Niu, Q.T.; Dwyer, D.; Villasenor, K.; et al. Etelcalcetide (amg 416), a peptide agonist of the calcium-sensing receptor, preserved cortical bone structure and bone strength in subtotal nephrectomized rats with established secondary hyperparathyroidism. *Bone* **2017**, *105*, 163–172. [CrossRef] [PubMed]
18. Martin, K.J.; Bell, G.; Pickthorn, K.; Huang, S.; Vick, A.; Hodsmann, P.; Peacock, M. Velcalcetide (amg 416), a novel peptide agonist of the calcium-sensing receptor, reduces serum parathyroid hormone and fgf23 levels in healthy male subjects. *Nephrol. Dial. Transplant.* **2014**, *29*, 385–392. [CrossRef] [PubMed]
19. Lavi-Moshayoff, V.; Wasserman, G.; Meir, T.; Silver, J.; Naveh-Many, T. PTH increases fgf23 gene expression and mediates the high-fgf23 levels of experimental kidney failure: A bone parathyroid feedback loop. *Am. J. Physiol. Renal Physiol.* **2010**, *299*, F882–F889. [CrossRef] [PubMed]
20. Block, G.A.; Bushinsky, D.A.; Cheng, S.; Cunningham, J.; Dehmel, B.; Druke, T.B.; Ketteler, M.; Kewalramani, R.; Martin, K.J.; Moe, S.M.; et al. Effect of etelcalcetide vs cinacalcet on serum parathyroid hormone in patients receiving hemodialysis with secondary hyperparathyroidism: A randomized clinical trial. *JAMA* **2017**, *317*, 156–164. [CrossRef] [PubMed]
21. Eidman, K.E.; Wetmore, J.B. Managing hyperparathyroidism in hemodialysis: Role of etelcalcetide. *Int. J. Nephrol. Renovasc. Dis.* **2018**, *11*, 69–80. [CrossRef] [PubMed]
22. Tella, S.H.; Kommalapati, A.; Correa, R. Profile of abaloparatide and its potential in the treatment of postmenopausal osteoporosis. *Cureus* **2017**, *9*, e1300. [CrossRef] [PubMed]

23. FDA. Abaloparatide (Tymlos) Approval Letter. 2017. Available online: https://www.accessdata.fda.gov/drugsatfda_docs/nda/2017/208743Orig1s000Approv.pdf (accessed on 3 May 2018).
24. Yang, L.; Morriello, G.; Pan, Y.; Nargund, R.P.; Barakat, K.; Prendergast, K.; Cheng, K.; Chan, W.W.-S.; Smith, R.G.; Patchett, A.A. Tripeptide growth hormone secretagogues. *Bioorg. Med. Chem. Lett.* **1998**, *8*, 759–764. [[CrossRef](#)]
25. FDA. Liraglutide Approval Letter. 2010. Available online: https://www.accessdata.fda.gov/drugsatfda_docs/label/2017/022341s027lbl.pdf (accessed on 3 May 2018).
26. Lau, J.; Bloch, P.; Schaffer, L.; Pettersson, I.; Spetzler, J.; Kofoed, J.; Madsen, K.; Knudsen, L.B.; McGuire, J.; Steensgaard, D.B.; et al. Discovery of the once-weekly glucagon-like peptide-1 (glp-1) analogue semaglutide. *J. Med. Chem.* **2015**, *58*, 7370–7380. [[CrossRef](#)] [[PubMed](#)]
27. Jensen, L.; Helleberg, H.; Roffel, A.; van Lier, J.J.; Bjornsdottir, I.; Pedersen, P.J.; Rowe, E.; Derving Karsbol, J.; Pedersen, M.L. Absorption, metabolism and excretion of the glp-1 analogue semaglutide in humans and nonclinical species. *Eur. J. Pharm. Sci.* **2017**, *104*, 31–41. [[CrossRef](#)] [[PubMed](#)]
28. Pratley, R.E.; Aroda, V.R.; Lingvay, I.; Lüdemann, J.; Andreassen, C.; Navarria, A.; Viljoen, A. Semaglutide versus dulaglutide once weekly in patients with type 2 diabetes (sustain 7): A randomised, open-label, phase 3b trial. *Lancet Diabetes Endocrinol.* **2018**, 1–12. [[CrossRef](#)]
29. FDA. Semaglutide (Ozempic) Approval Letter. 2017. Available online: https://www.accessdata.fda.gov/drugsatfda_docs/applletter/2017/209637s000ltr.pdf (accessed on 3 May 2018).
30. Jacobsen, L.V.; Flint, A.; Olsen, A.K.; Ingwersen, S.H. Liraglutide in type 2 diabetes mellitus: Clinical pharmacokinetics and pharmacodynamics. *Clin. Pharmacokinet.* **2016**, *55*, 657–672. [[CrossRef](#)] [[PubMed](#)]
31. Guerlavais, V.; Boeglin, D.; Mousseaux, D.; Oiry, C.; Heitz, A.; Deghenghi, R.; Locatelli, V.; Torsello, A.; Ghé, C.; Catapano, F.; et al. New Active Series of Growth Hormone Secretagogues. *J. Med. Chem.* **2003**, *46*, 1196–1203. [[CrossRef](#)] [[PubMed](#)]
32. FDA. Macimorelin (Macimorelin) Approval Letter. 2017. Available online: https://www.accessdata.fda.gov/drugsatfda_docs/nda/2017/205598Orig1s000Approv.pdf (accessed on 3 May 2018).
33. Garcia, J.M.; Swerdloff, R.; Wang, C.; Kyle, M.; Kipnes, M.; Biller, B.M.; Cook, D.; Yuen, K.C.; Bonert, V.; Dobs, A.; et al. Macimorelin (aezs-130)-stimulated growth hormone (gh) test: Validation of a novel oral stimulation test for the diagnosis of adult gh deficiency. *J. Clin. Endocrinol. Metab.* **2013**, *98*, 2422–2429. [[CrossRef](#)] [[PubMed](#)]
34. Broglio, F.; Boutignon, F.; Benso, A.; Gottero, C.; Prodam, F.; Arvat, E.; Ghè, C.; Catapano, F.; Torsello, A.; Locatelli, V.; et al. Ep1572: A novel peptido-mimetic gh secretagogue with potent and selective gh-releasing activity in man. *J. Endocrinol. Investig.* **2002**, *25*, RC26–RC28. [[CrossRef](#)] [[PubMed](#)]
35. Kojima, M.; Hosoda, H.; Matsuo, H.; Kangawa, K. Ghrelin: Discovery of the natural endogenous ligand for the growth hormone secretagogue receptor. *Trends Endocrinol. Metab.* **2001**, *12*, 118–126. [[CrossRef](#)]
36. Varamini, P.; Toth, I. Recent advances in oral delivery of peptide hormones. *Expert Opin. Drug Deliv.* **2016**, *13*, 507–522. [[CrossRef](#)] [[PubMed](#)]
37. Piccoli, F.; Degen, L.; MacLean, C.; Peter, S.; Baselgia, L.; Larsen, F.; Beglinger, C.; Drewe, J. Pharmacokinetics and pharmacodynamic effects of an oral ghrelin agonist in healthy subjects. *J. Clin. Endocrinol. Metab.* **2007**, *92*, 1814–1820. [[CrossRef](#)] [[PubMed](#)]
38. FDA. Angiotensin II (Giapreza) Approval Letter. 2017. Available online: https://www.accessdata.fda.gov/drugsatfda_docs/nda/2017/209360Orig1s000Approv.pdf (accessed on 3 May 2018).
39. Tigerstedt, R.; Bergman, P.G. Niere und kreislauf. *Arch. Physiol.* **1898**, *8*, 223–271. [[CrossRef](#)]
40. Basso, N.; Terragno, N.A. History about the discovery of the renin-angiotensin system. *Hypertension* **2001**, *38*, 1246–1249. [[CrossRef](#)] [[PubMed](#)]
41. Schwarz, H.; Bumpus, F.M.; Page, I.H. Synthesis of a biologically active octapeptide similar to natural isoleucine angiotonin octapeptide. *J. Am. Chem. Soc.* **1957**, *79*, 5697–5703. [[CrossRef](#)]
42. Rittel, W.; Iselin, B.; Kappeler, H.; Riniker, B.; Schwyzer, R. Synthese eines hochwirksamen Hypertensin II-amids (L-Asparaginyll-L-arginyll-L-valyll-L-tyrosyll-L-isoleucyll-L-histidyll-L-prolyll-L-phenylalanin). *Helvetica Chim. Acta* **1957**, *40*, 614–624. [[CrossRef](#)]
43. Fosgerau, K.; Hoffmann, T. Peptide therapeutics: Current status and future directions. *Drug Discov. Today* **2015**, *20*, 122–128. [[CrossRef](#)] [[PubMed](#)]
44. Kaur, K.; Singh, I.; Kaur, P.; Kaur, R. Food and drug administration (fda) approved peptide drugs. *Asian J. Res. Biol. Pharm. Sci.* **2015**, *3*, 75–88.

45. Ghosh, S. Peptide therapeutics market: Forecast and analysis 2015–2025. *Oligos Pept. Chim. Oggi Chem. Today* **2016**, *34*, 5–7.
46. Albericio, F.; Kruger, H.G. Therapeutic peptides. *Future Med. Chem.* **2012**, *4*, 1527–1531. [[CrossRef](#)] [[PubMed](#)]
47. Lau, J.L.; Dunn, M.K. Therapeutic peptides: Historical perspectives, current development trends, and future directions. *Bioorg. Med. Chem.* **2017**. [[CrossRef](#)] [[PubMed](#)]
48. Henninot, A.; Collins, J.C.; Nuss, J.M. The current state of peptide drug discovery: Back to the future? *J. Med. Chem.* **2018**, *61*, 1382–1414. [[CrossRef](#)] [[PubMed](#)]



© 2018 by the authors. Licensee MDPI, Basel, Switzerland. This article is an open access article distributed under the terms and conditions of the Creative Commons Attribution (CC BY) license (<http://creativecommons.org/licenses/by/4.0/>).

Chapter 8. Conclusion and Future Perspectives

Here we have introduced the synthesis of 1,2-HOPO containing peptides on solid support. The peptide backbones were synthesized using the standard SPPS Fmoc/tBu strategy and all were having Lys residues to hold the HOPO chelating moieties. The 1,2-HOPO-4-COOH (or 1,2-BnOPO-4-COOH) was introduced via two routes, through an amide linkage to the ϵ -NH₂ of the Lys residues on the backbone. The use of the unprotected N-OH in HOPO succeeded in giving the desired product in good yields and purities. Also in case of using the benzyl protected HOPO in the synthesis, cleaving the peptide from resin by using the mixture TFA:TFMSA:TIS (8:3:1) resulted successfully in the removal of the benzyl protecting group in the same step. The second route was by conjugating two pre-synthesized peptides, one of them contain the 1,2-HOPO unit as well as a thiol function and the other having three maleimide moieties. Both synthetic routes allowed the preparation of 1,2-HOPO-peptides in good yields and purities.

On the other hand, spectrophotometric evaluation the thermodynamic constants of the bidentate ligands (Y and A) and their Fe(III) complexes showed that they were comparable to those reported in literature. Which gives an indication that the position of the carboxyl substituent on the pyridine ring has less effect on the overall stability of the complex, with pFe^{+3} about 14.59 and 14.19.

The hexadentate ligands B and C formed 1:1 complex with iron stable enough to stand against the well-known strong chelator EDTA at pH=7.4, with pFe^{+3} 26.91 and 28.58, respectively. The strongest ligand was the hexadentate (ligand C) with slightly higher formation constant than that of (ligand B). Making these two potent candidates to be used as biostatic agents, since for an ideal agent $pFe^{+3} > 20$ is required.

Finally, this type of easily synthesized chelators (peptide-HOPO combinations) can be used not only for Fe (III) chelation but can also be used for other hard metal ions by tuning the denticity to fulfil the metal electronic requirements, bearing into mind the advantage of the high water solubility of such compounds.



**Synthesis and physiochemical characterization of new siderophore-inspired peptide-chelators
with 1-hydroxypridine-2-one (1,2-HOPO)**

(Supplementary Material)

2020

Danah Mahdi AlShaer

Table of Contents

Chapter 2. Solid-Phase Synthesis of Peptides Containing 1-Hydroxypyridine-2-one (1,2-HOPO).....	3
Chapter 4. Synthesis of new peptide-based Ligands with 1,2-HOPO pendant chelators. Thermodynamic evaluation of their iron (III) complexes.....	13

SUPPLEMENTARY MATERIAL

Chapter 2. Solid-Phase Synthesis of Peptides Containing 1-Hydroxypyridine-2-one (1,2-HOPO)

Danah Al Shaer ^{a,b}, Fernando Albericio ^{b,c,d} and Beatriz G. de la Torre ^a

^aKwaZulu-Natal Research Innovation and Sequencing Platform (KRISP), School of Laboratory Medicine and Medical Sciences, College of Health Sciences, University of KwaZulu-Natal, Durban 4041, South Africa; ^bPeptide Science Laboratory, School of Chemistry and Physics, University of KwaZulu-Natal, Durban 4001, South Africa; ^cInstitute for Advanced Chemistry of Catalonia (IQAC-CSIC), 08034 Barcelona, Spain; ^dCIBER-BBN, Networking Centre on Bioengineering, Biomaterials and Nanomedicine, and Department of Organic Chemistry, University of Barcelona, 08028 Barcelona, Spain

General:

Analytical HPLC: Agilent 1100 system using a Phenomex Luna C₁₈ (3 μm, 4.6 × 150 mm) column, with flow rate of 1.0 mL/min, 30 °C, and UV detection at 220 nm. Buffer A: 0.1% TFA in H₂O; buffer B: 0.1% TFA in CH₃CN.

LCMS:

1) Shimadzu 2020 UFLC-MS. Buffer A: 0.1% formic acid in H₂O; buffer B: 0.1% formic acid in CH₃CN, Flow: 1.0mL/min., UV detection=220 nm, Column: YMC-TriartC₁₈ (5 μm, 4.6 × 150 mm) column, 30 °C.

2) Thermo Scientific™ UltiMate™ 3000 Standard Binary System, ISQ™ EC Single Quadrupole. Buffer A: 0.1% formic acid in H₂O; buffer B: 0.1% formic acid in CH₃CN, Flow: 1.0mL/min., UV detection=220 nm, Column: Phenomenex Luna C₁₈ 3.6 μm, 4.6 × 150 mm column, 30 °C.

Figure S1: HPLC chromatogram for Ac-FKA-NH₂. Method 5-95% B in A over 15 min

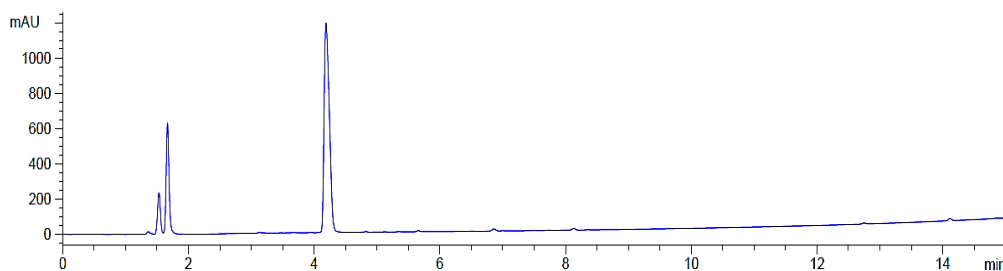


Figure S2: MS (LCMS 1) for Ac-FKA-NH₂.

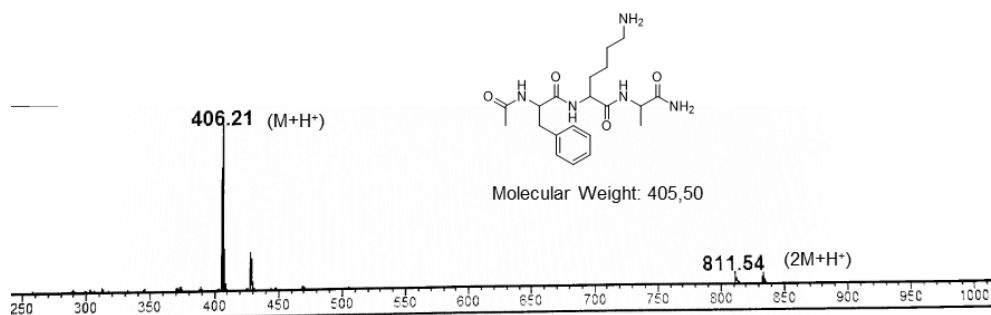


Figure S3: MS (LCMS 1) for unprotected 1,2-HOPO-4-COOH incorporated into Ac-FKA-NH₂. HPLC, Figure 2, main manuscript.

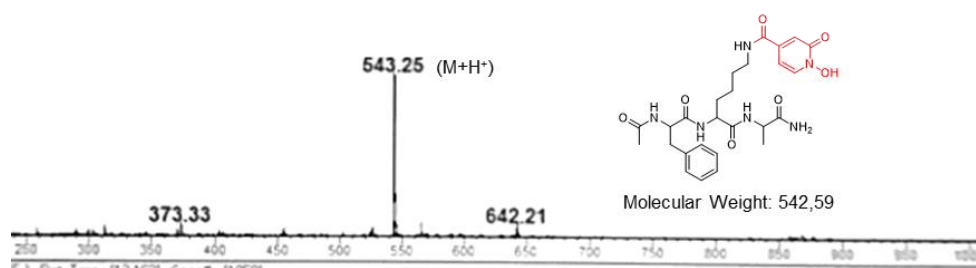


Figure S3 A,B,C,D Full integrated chromatograms of **Figure 2** in manuscript, Method 5-95% B in A over 15 min

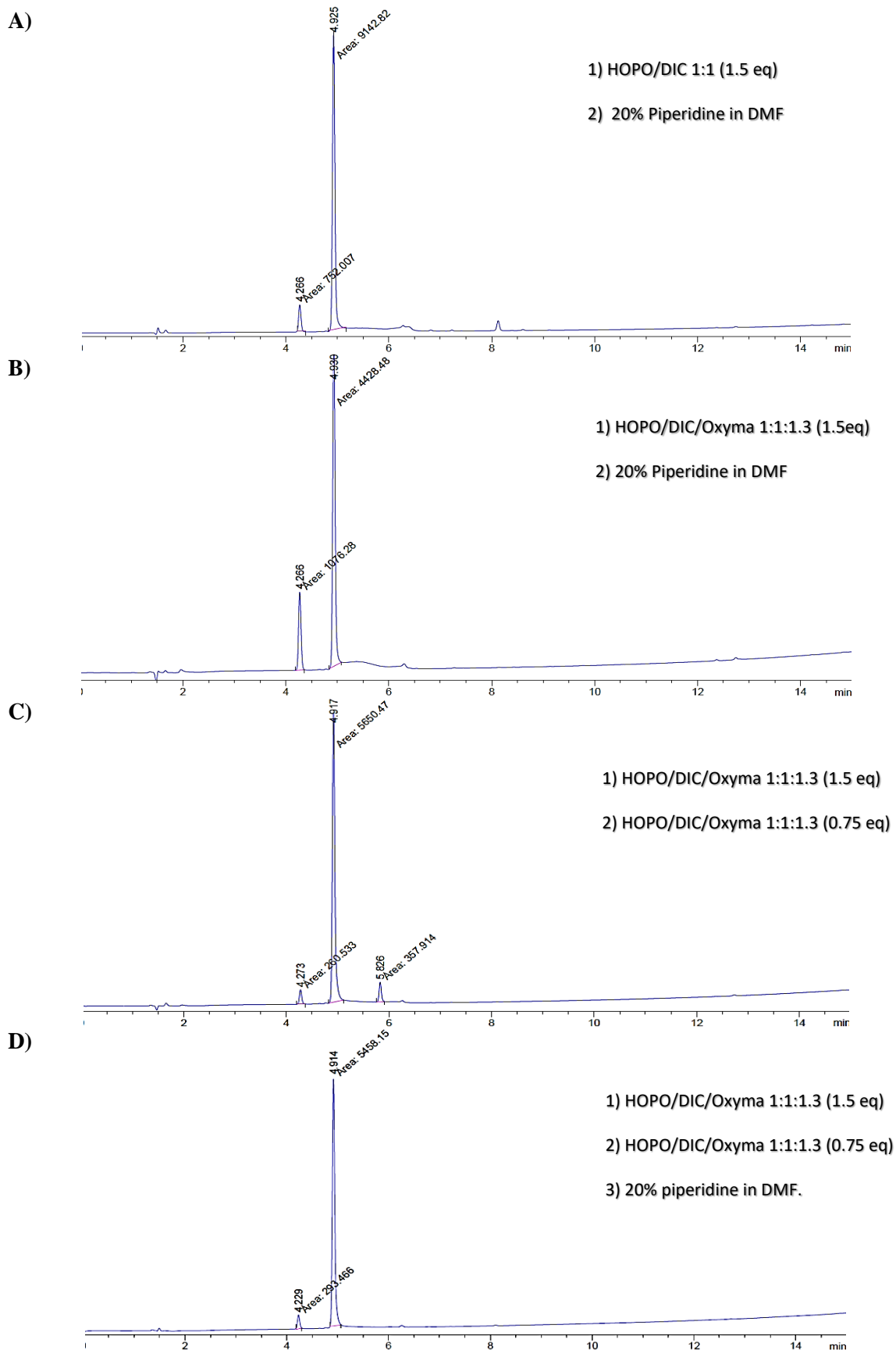


Figure S6. Expanded **Figure 3** (main manuscript). Comparison of the HPLC crudes after the incorporation of unprotected 1,2-HOPO-4-COOH to Ac-K-K-K-S(tBu)-S(tBu)-resin. Method 0-50% B in A over 15 min.

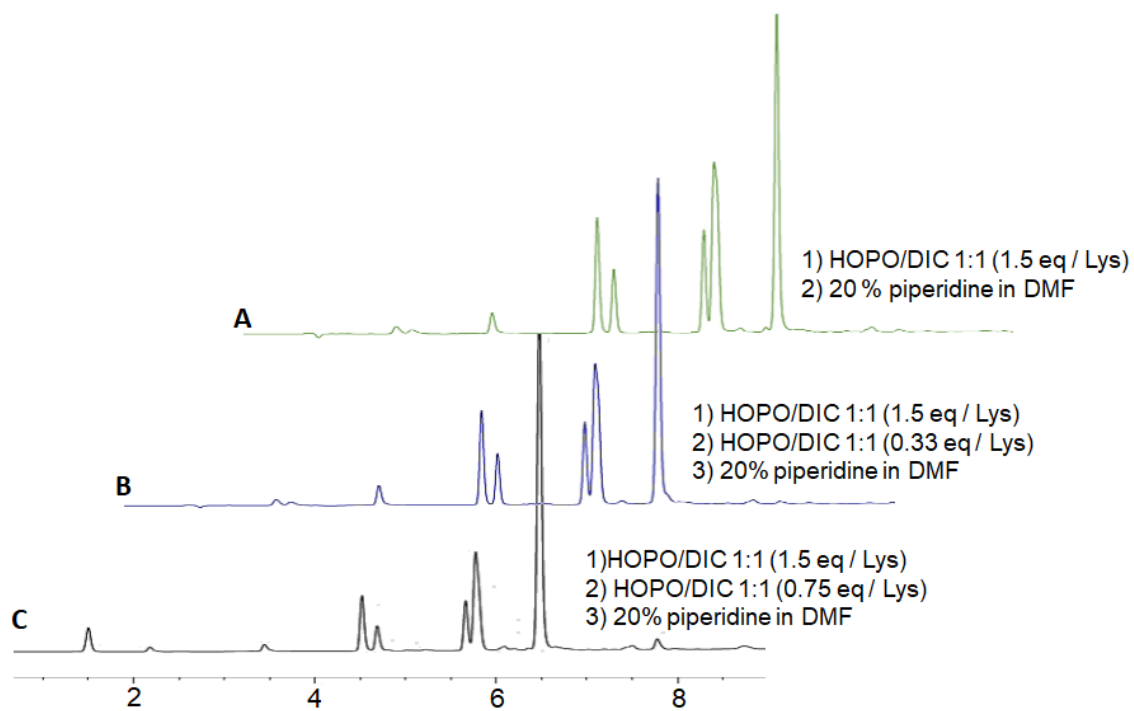
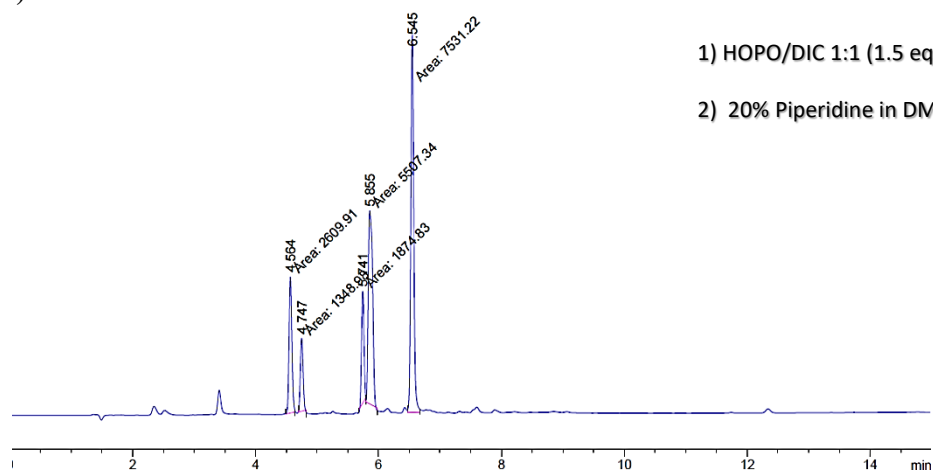


Figure S6 A-B-C: Full integrated chromatograms in Figure 3 in manuscript, Method 0-50% B in A over 15 min

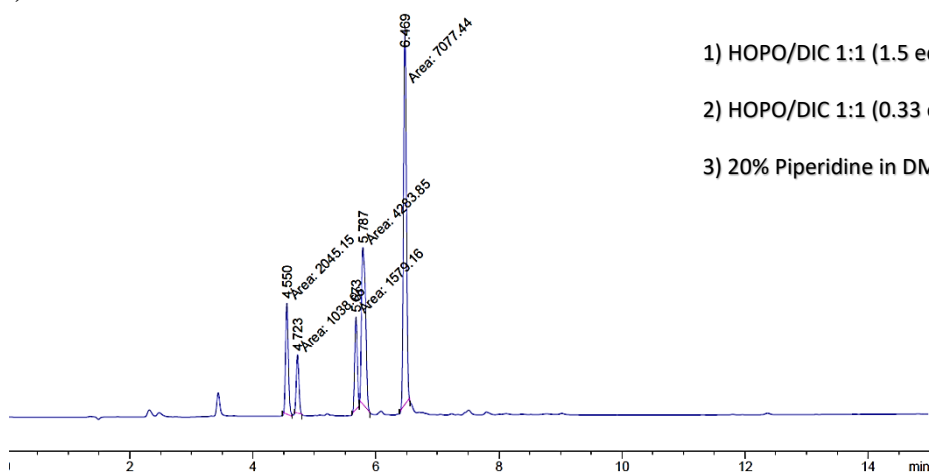
A)



1) HOPO/DIC 1:1 (1.5 eq / Lys)

2) 20% Piperidine in DMF

B)

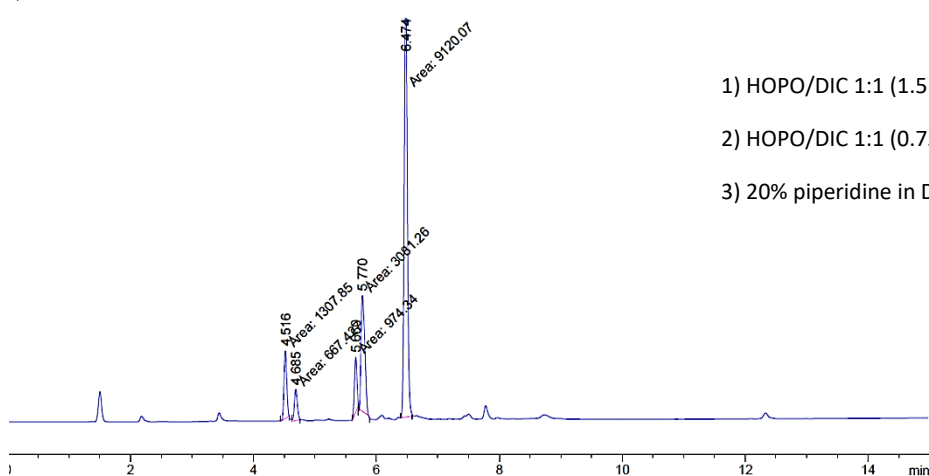


1) HOPO/DIC 1:1 (1.5 eq / Lys)

2) HOPO/DIC 1:1 (0.33 eq / Lys)

3) 20% Piperidine in DMF

C)



1) HOPO/DIC 1:1 (1.5 eq / Lys)

2) HOPO/DIC 1:1 (0.75 eq)

3) 20% piperidine in DMF

Figure S7: MS (LCMS 2) for unprotected 1,2-HOPO-4-COOH incorporated into Ac-KKKSS-NH₂. The 1,2-HOPO-4-CO- moiety could be incorporated in any of the three Lys. HPLC, **Figure 3**, peaks around 4.5 min, main manuscript

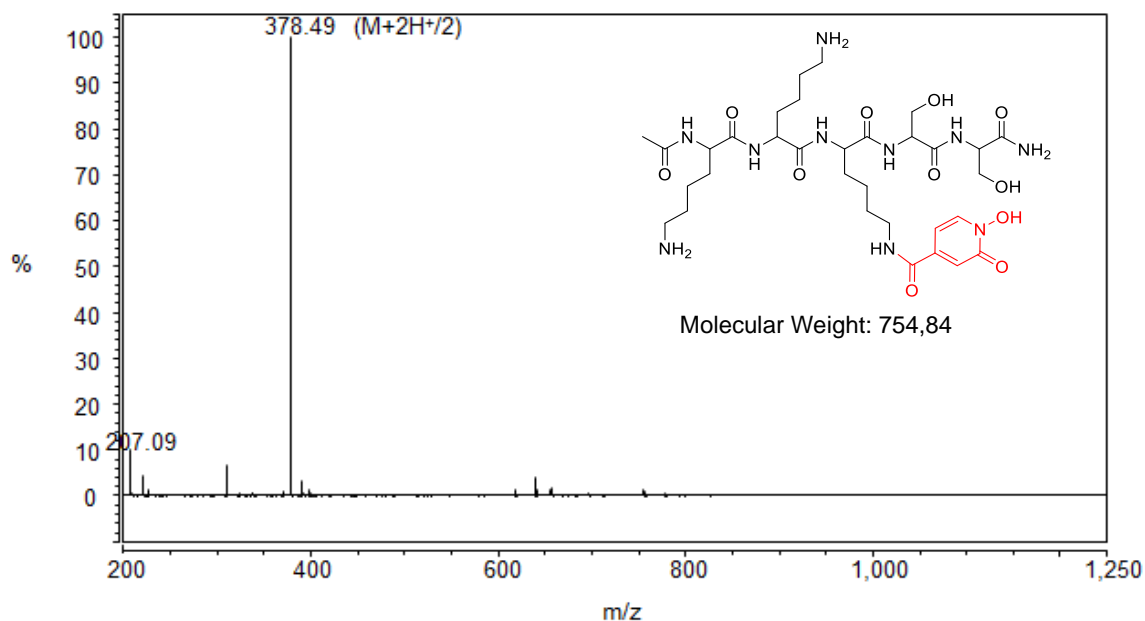


Figure S8: MS (LCMS 2) for two unprotected 1,2-HOPO-4-COOH incorporated into Ac-KKKSS-NH₂. The 1,2-HOPO-4-CO- moieties could be incorporated into any of the three Lys. HPLC, **Figure 3**, peaks around 5.7 min, main manuscript

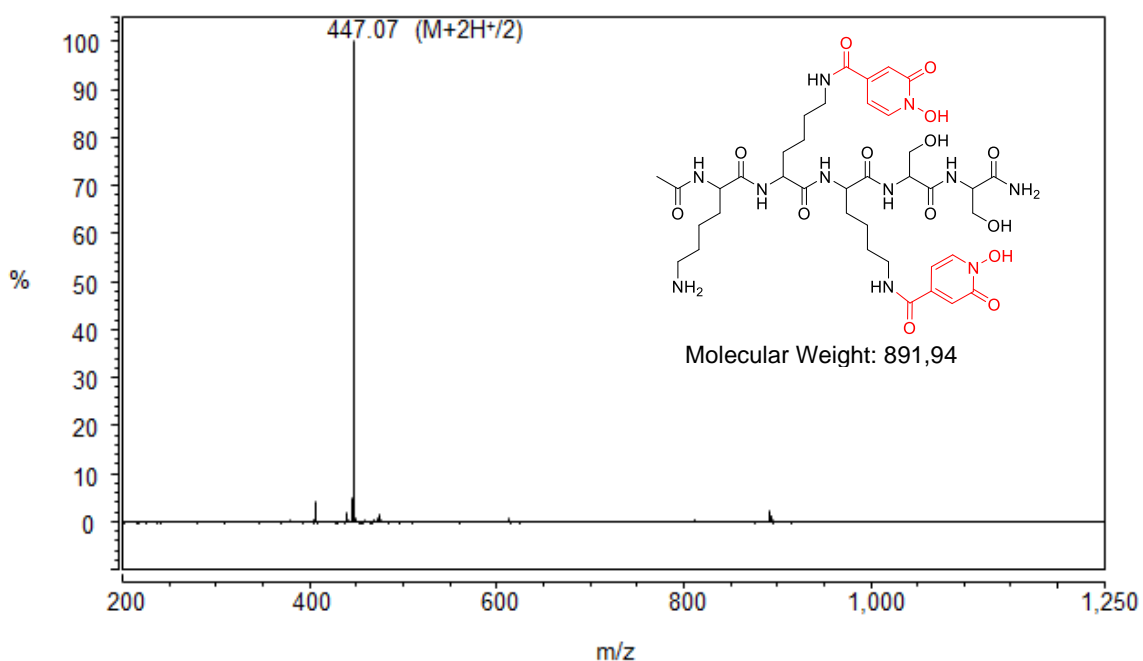


Figure S9: MS (LCMS 2) for three unprotected 1,2-HOPO-4-COOH incorporated into Ac-KKKSS-NH₂. HPLC, Figure 3, peak at 6.5 min, main manuscript

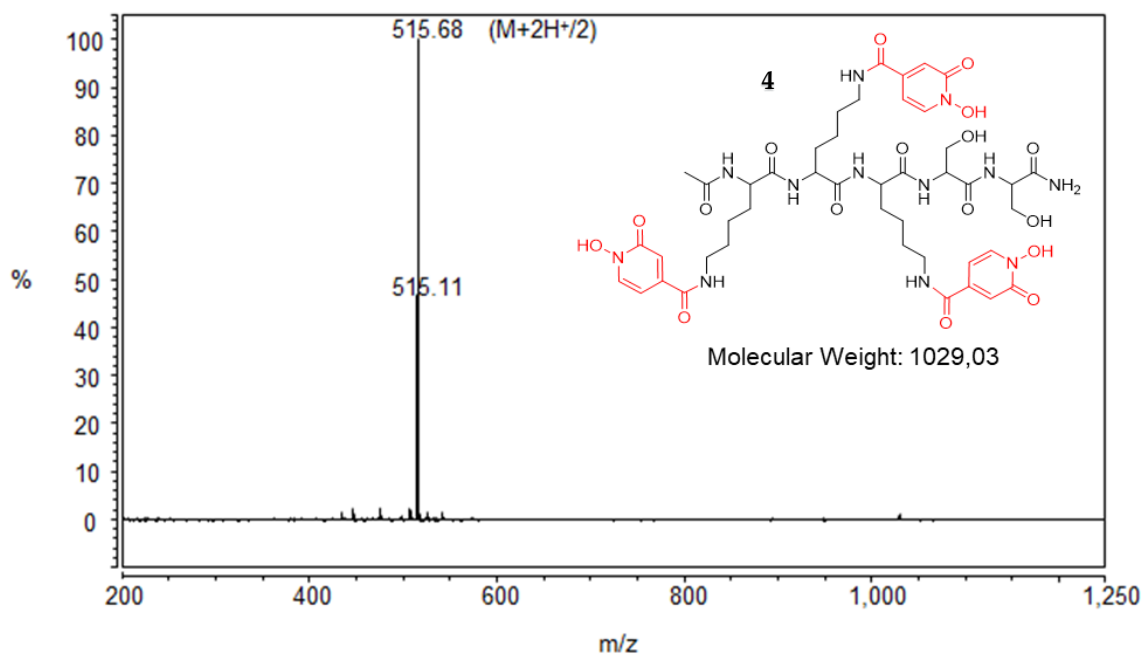
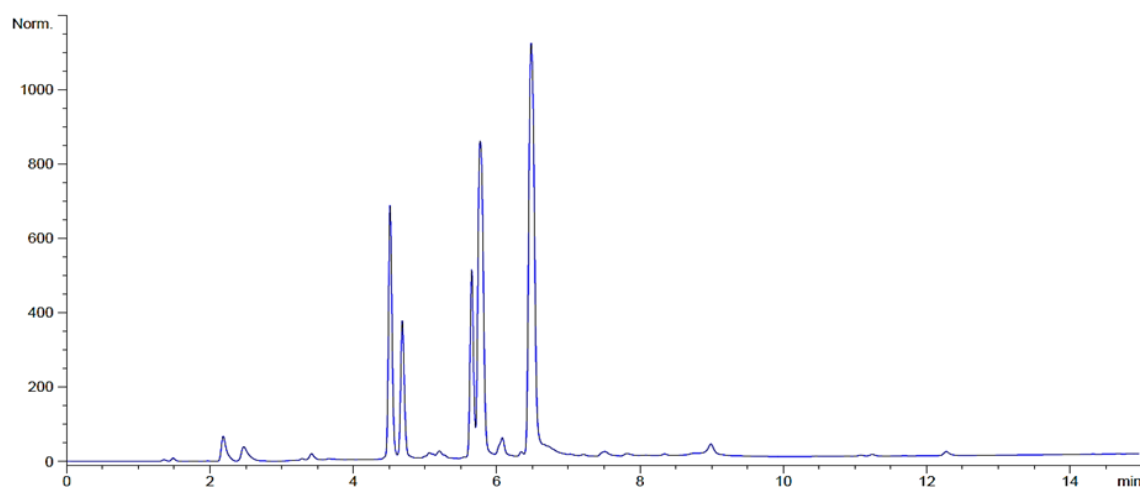


Figure S10: HPLC chromatograms (Method 0-50% B in A over 15 min) for different conditions of incorporation of unprotected 1,2-HOPO-4-COOH on Ac-KKKSS-resin. All the couplings were carried out using 1.5 eq of 1,2-HOPO-4-COOH per Lys residue

A) in DMF at 40 °C using sand bath, 4 h



B) in DMF-CH₃CN (1:1) at room temperature, 4 hrs.

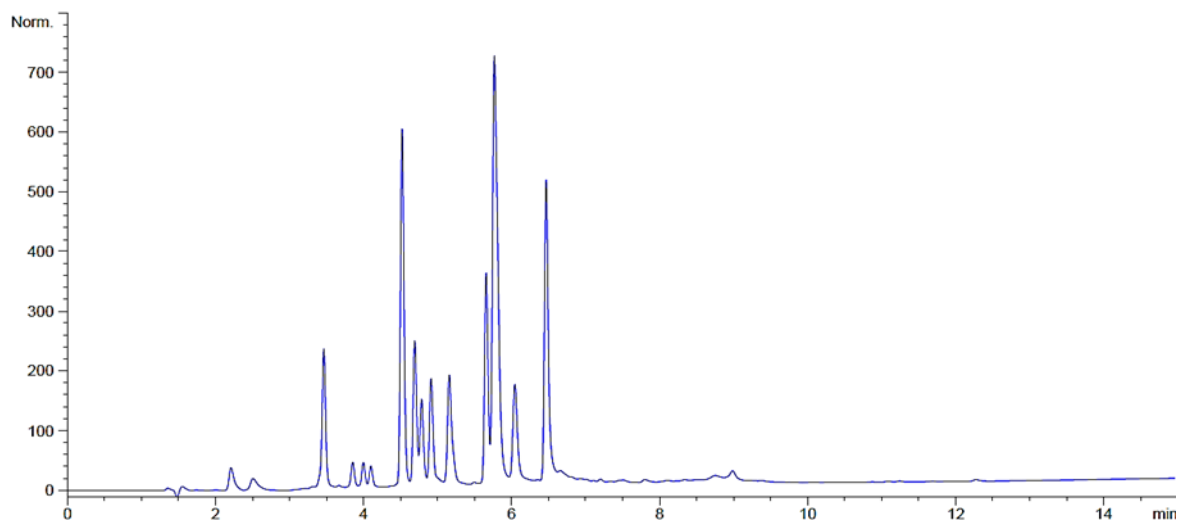


Figure S11 MS (LCMS 1) for one protected 1,2-HOPO-4-COOH incorporated into Ac-KKKSS-NH₂. The protected 1,2-HOPO-4-CO- moiety could be incorporated in any of the three Lys. HPLC, **Figure 4-A**, peaks around 8 min, main manuscript

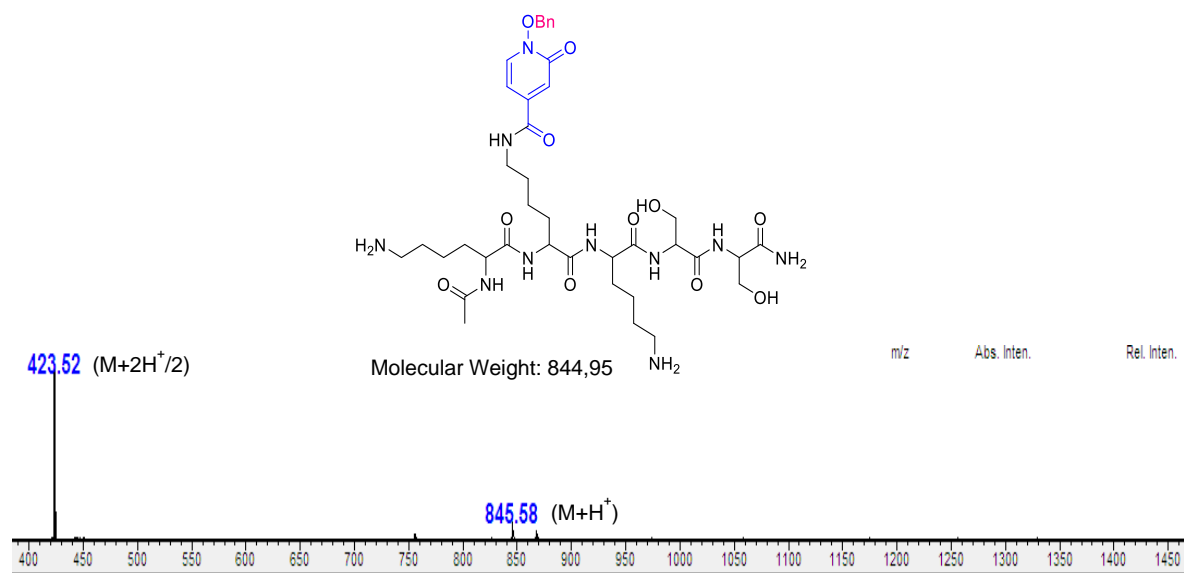


Figure S12 MS (LCMS 1) for two protected 1,2-HOPO-4-COOH incorporated into Ac-KKKSS-NH₂. The protected 1,2-HOPO-4-CO- moieties could be incorporated in any of the three Lys. HPLC, **Figure 4-A**, peaks around 11 min, main manuscript

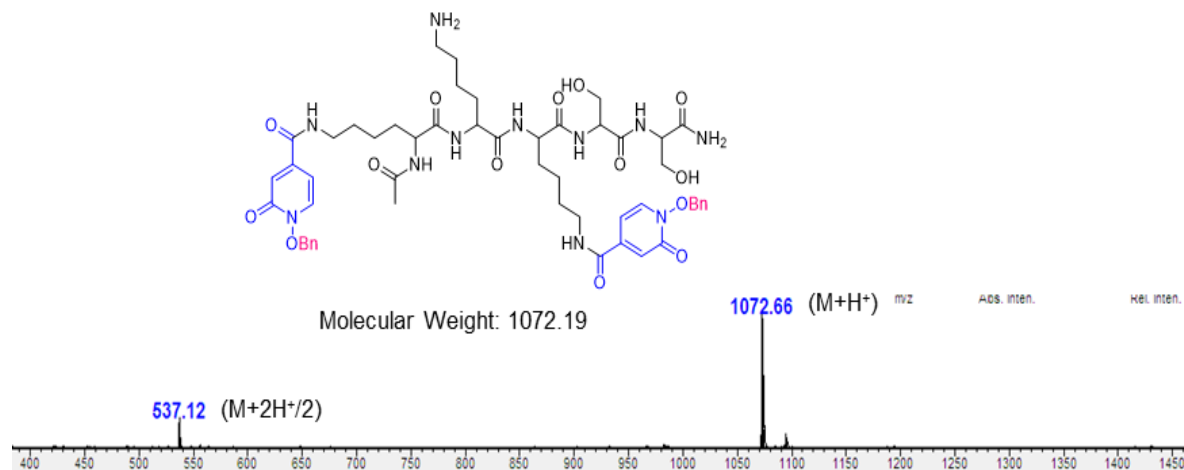


Figure S13 MS (LCMS 1) for three protected 1,2-HOPO-4-COOH incorporated into Ac-KKKSS-NH₂. HPLC, **Figure 4-A**, peaks around 13.8 min, main manuscript

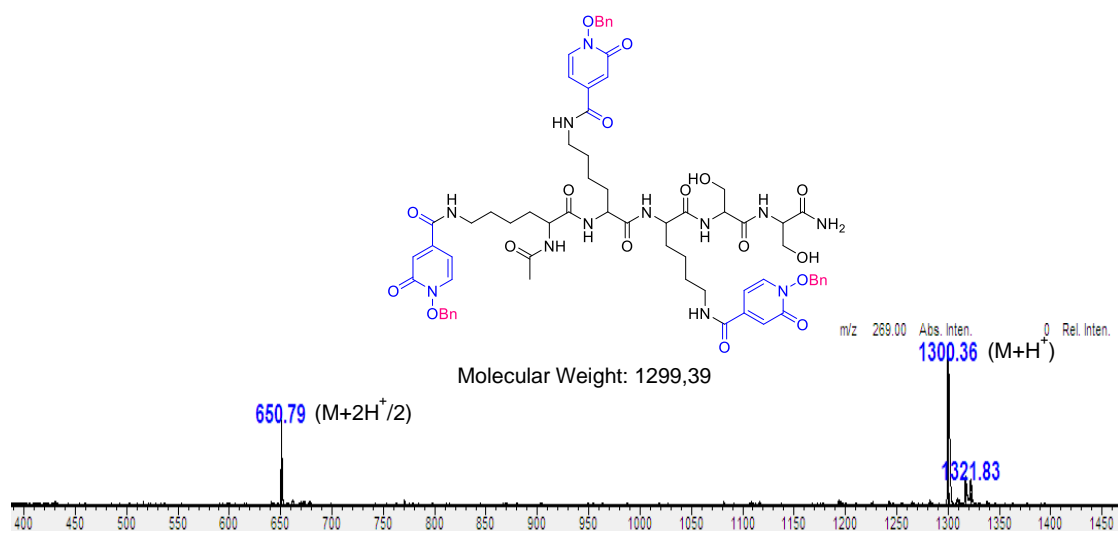


Figure S14: Comparison between **Figure 3-C** (using unprotected HOPO). figure 4-B (using protected HOPO then deprotection) in manuscript, Method 0-50% B in A over 15 min. (The slight shift of retention time is because using another HPLC instrument with all other conditions are the same)

Figure 3-C

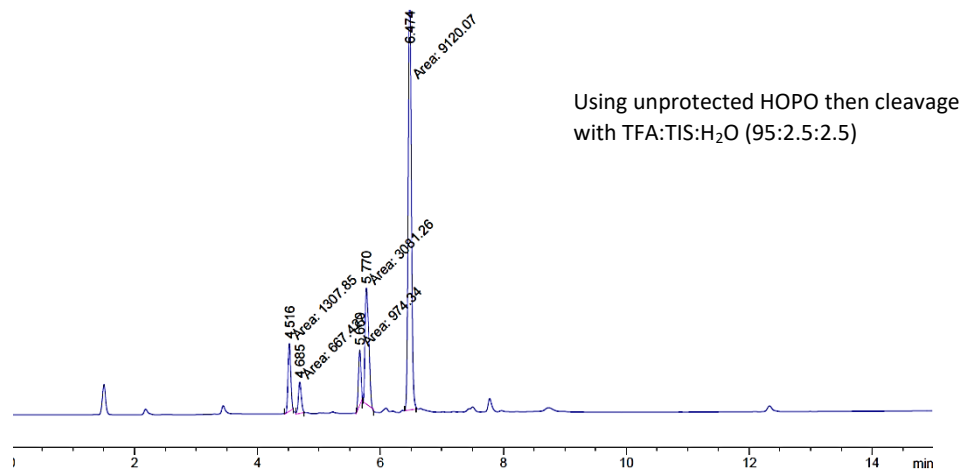
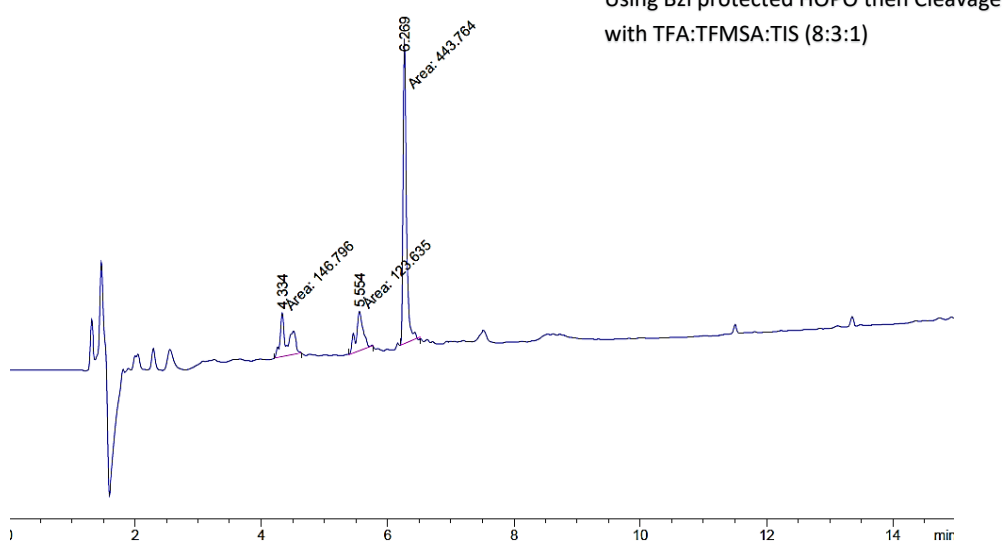


Figure 4-B



Chapter 4. Synthesis of new peptide-based Ligands with 1,2-HOPO pendant chelators and the thermodynamic evaluation of their iron (III) complexes

General:

Analytical HPLC: Agilent 1100 system using a Phenomex Luna C₁₈ (3 μm, 4.6 × 150 mm) column, with flow rate of 1.0 mL/min, 30 °C, and UV detection at 220 nm. Buffer A: 0.1% TFA in H₂O; buffer B: 0.1% TFA in CH₃CN.

LCMS:

Thermo Scientific™ UltiMate™ 3000 Standard Binary System, ISQ™ EC Single Quadrupole.

Buffer A: 0.1% formic acid in H₂O; buffer B: 0.1% formic acid in CH₃CN, Flow: 1.0mL/min., UV detection=220 nm, Column: Phenomenex Luna C18 3.6 μm, 4.6 × 150 mm column, 30 °C.

Figure S1: HPLC chromatogram for HOPO-βAC-NH₂. Method 0-30% B in A over 15 min

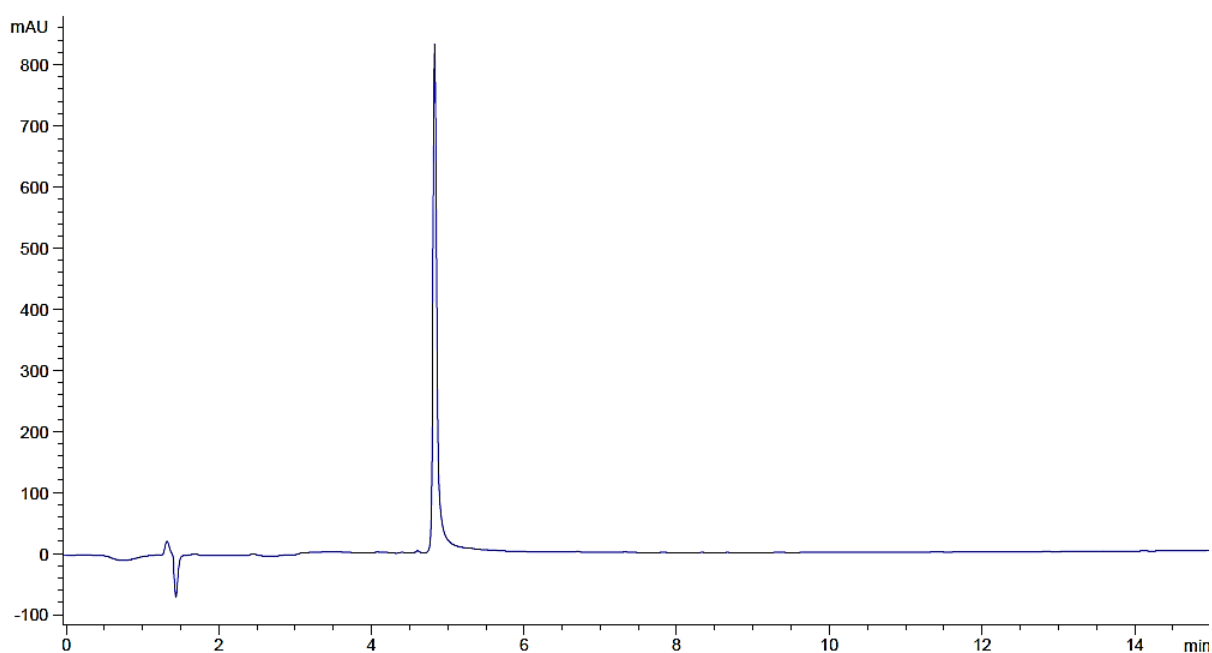
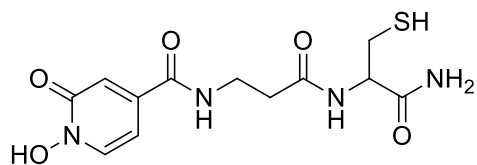
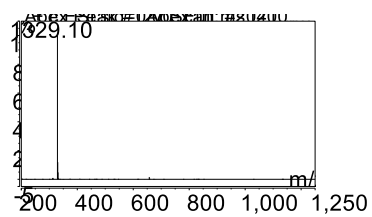


Figure S2: LCMS spectrum for HOPO-βAC-NH₂.



Exact Mass: 328,08

Figure S3: HPLC chromatogram for Ac-K(Mha)-K(Mha)-K(Mha)-βA-NH₂. Method 25-45% B in A over 15 min

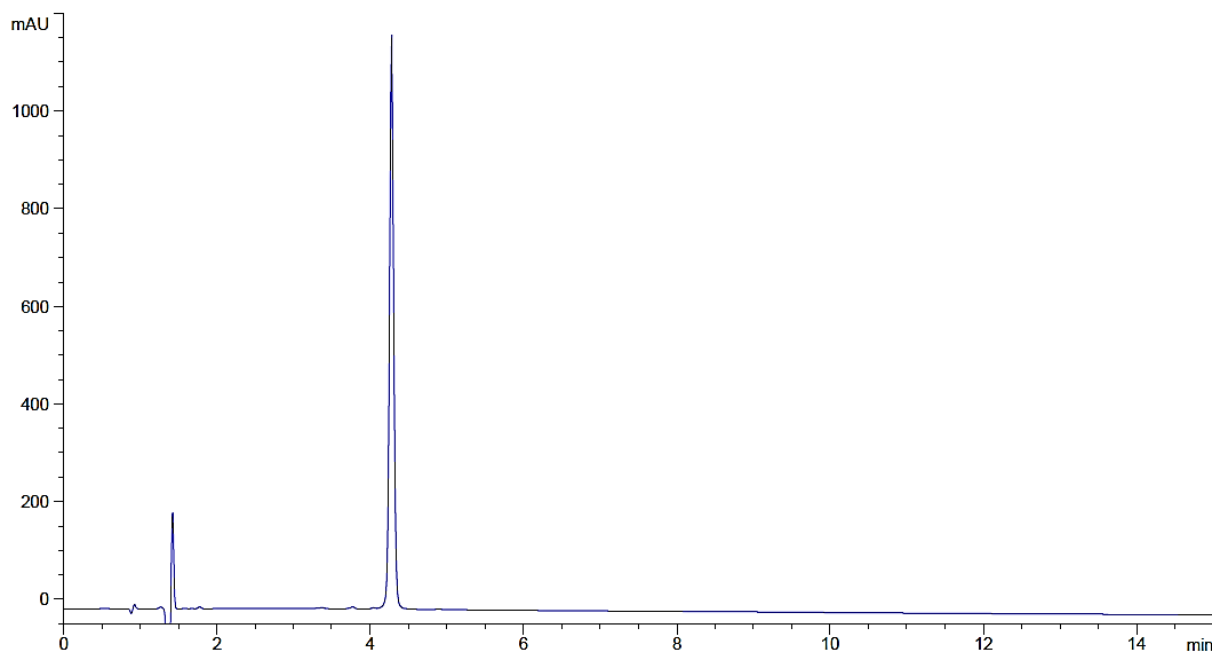


Figure S4: LCMS spectrum for Ac-K(Mha)-K(Mha)-K(Mha)- β A-NH₂

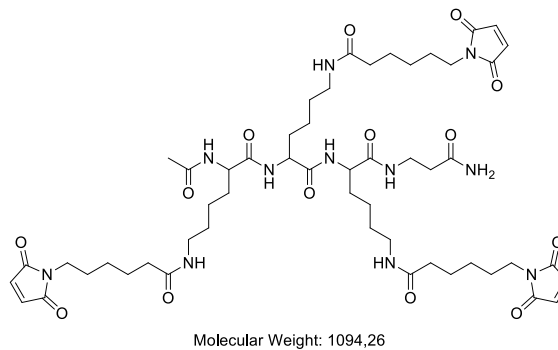
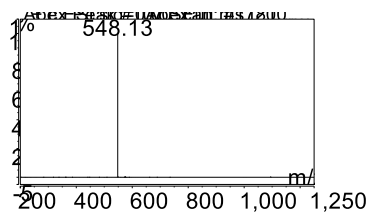


Figure S5: HPLC chromatogram for Ligand C. Method 10-60% B in A over 15 min

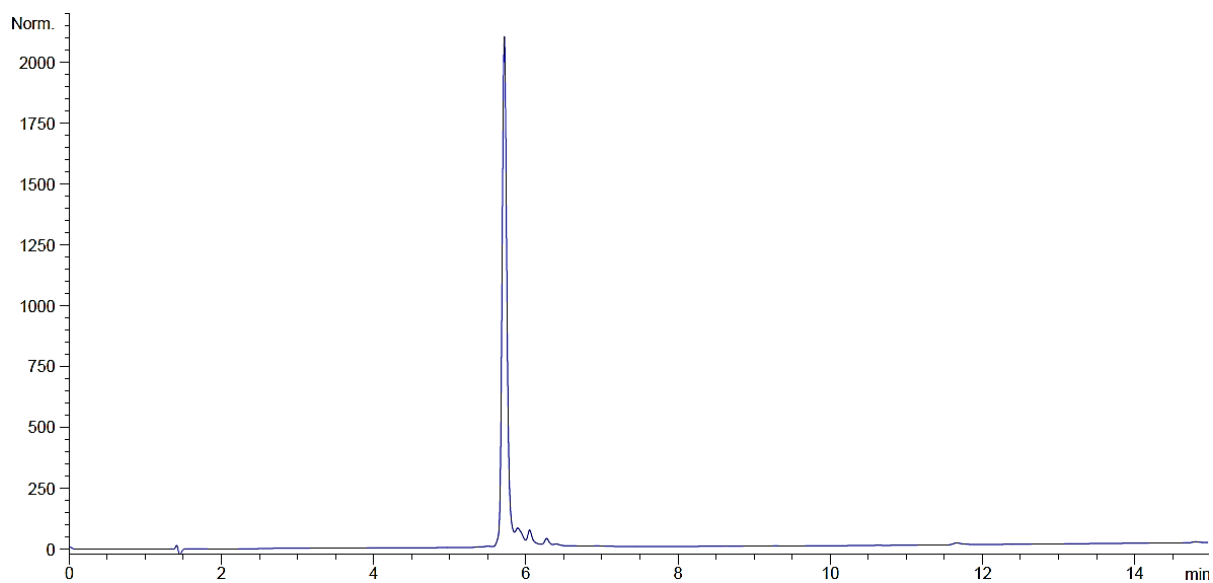


Figure S6: LCMS spectrum for Ligand C

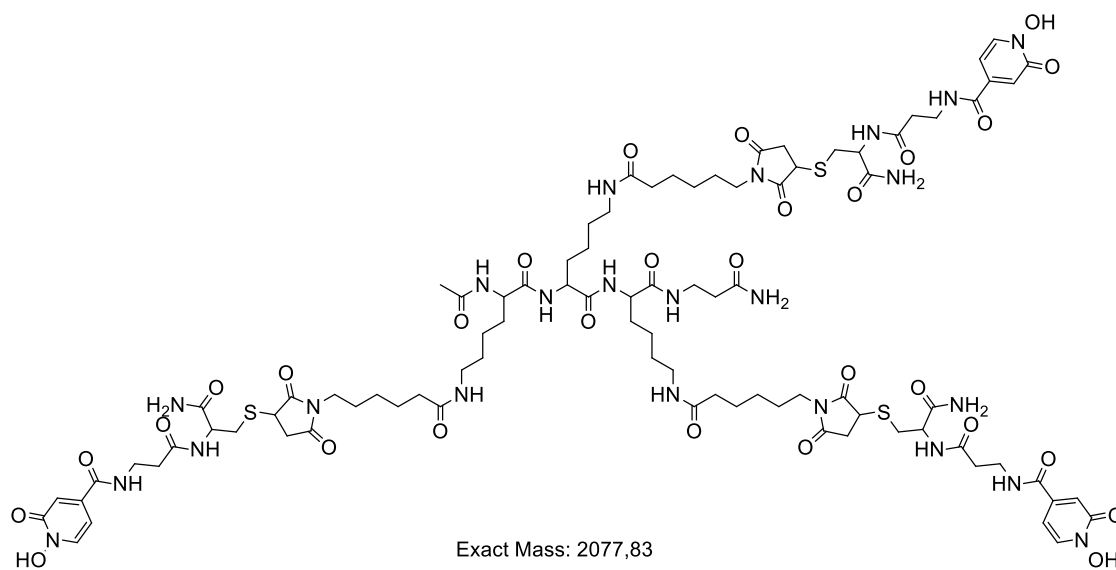
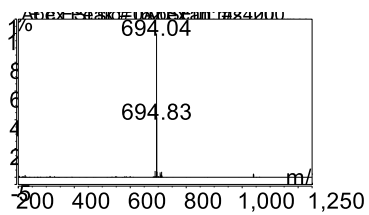


Figure S7: UV-visible spectra of Fe-L solutions in methanol around the chosen wavelength for stoichiometry determination for ligands: a) Y b) A c) B d) C. The highlighted spectra are for the ratios 1:3 for Y and A , 1:1 for B and C. Fig. 4 (main text)

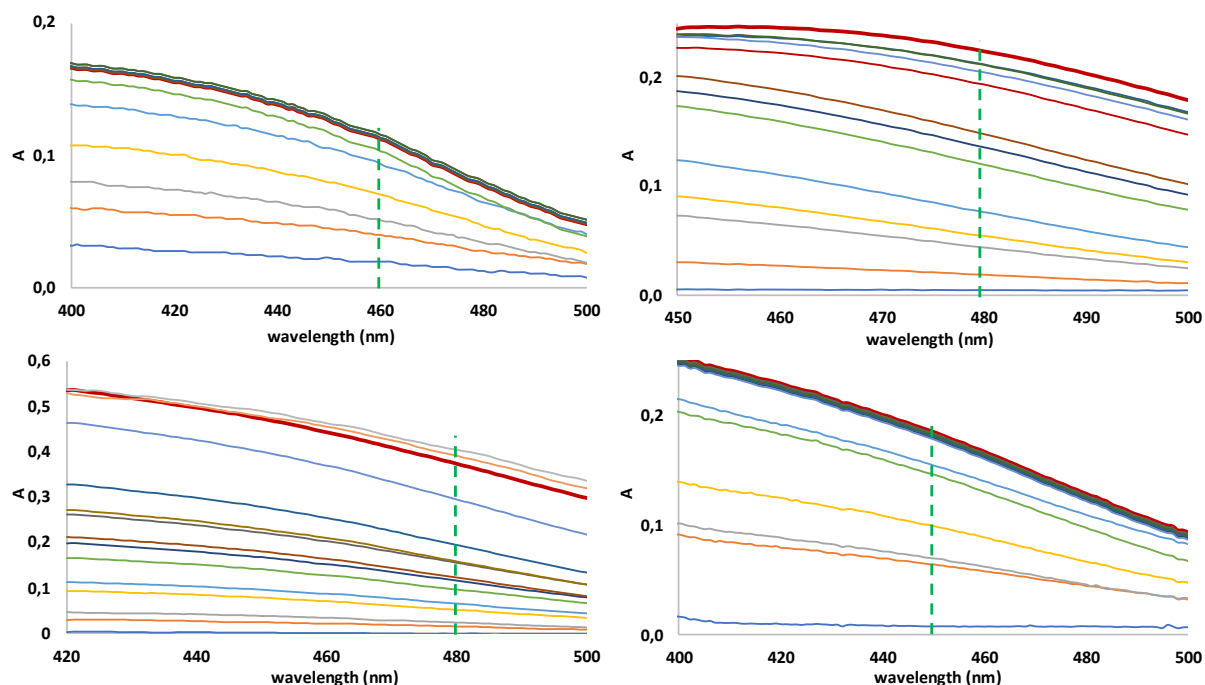


Figure S8: Dependence of UV spectra on pH ($I=0.1$ M KCl) of 5.2×10^{-5} M solutions of a) Ligand Y, b) Ligand A, c) Ligand B, and d) Ligand C. Full spectra of Fig. 5 (main text)

